University of New Hampshire
University of New Hampshire Scholars' Repository

Master's Theses and Capstones | Student Scholarship

Spring 2019

INFILTRATION CHARACTERISTICS OF SUBSURFACE GRAVEL FILTRATION SYSTEMS FOR STORMWATER MANAGEMENT

Ethan Ely
University of New Hampshire, Durham

Follow this and additional works at: https://scholars.unh.edu/thesis

Recommended Citation

Ely, Ethan, "INFILTRATION CHARACTERISTICS OF SUBSURFACE GRAVEL FILTRATION SYSTEMS FOR STORMWATER MANAGEMENT" (2019). *Master's Theses and Capstones*. 1272.
https://scholars.unh.edu/thesis/1272

This Thesis is brought to you for free and open access by the Student Scholarship at University of New Hampshire Scholars' Repository. It has been accepted for inclusion in Master's Theses and Capstones by an authorized administrator of University of New Hampshire Scholars' Repository. For more information, please contact Scholarly.Communication@unh.edu.

INFILTRATION CHARACTERISTICS OF SUBSURFACE GRAVEL FILTRATION SYSTEMS FOR STORMWATER MANAGEMENT

BY

ETHAN R. ELY
B.S. in Environmental Engineering
University of New Hampshire, 2015

THESIS

Submitted to the University of New Hampshire
in Partial Fulfillment of
the Requirements for the Degree of

Master of Science
in
Civil Engineering

May 2019

This thesis has been examined and approved in partial fulfillment of the requirements for the degree of Master of Science in Civil Engineering by:

Thesis Director, Thomas P. Ballestero
Associate Professor of Civil and Environmental Engineering

James J. Houle
Program Director, UNH Stormwater Center

John Matthew Davis
Associate Professor of Earth Sciences

Date

Original signatures are on file with the University of New Hampshire Graduate School.

ACKNOWLEDGEMENTS

While working on this thesis over the past several years, I have received help and support from many different people. First of all, I would like to thank those who were directly involved in the development my thesis. Thank you to my advisor, Dr. Thomas Ballestero, for all of his help and guidance both with my thesis and throughout my time at UNH. I would like to thank the other members of my thesis committee, Dr. James Houle and Dr. Matt Davis, for reviewing my paper and helping me improve my work.

I also greatly appreciate the help I received from Tim Puls of the UNH Stormwater Center and my fellow graduate students/friends, Daniel Macadam and David Tarushka, for their assistance with field work, lab work, and data collection. I learned a great deal from all of you and appreciate the time you spent helping me with my research. Additional thanks to Daniel for allowing me to bounce ideas off of you, tolerating my incessant whining about thesis issues, and joining me on hikes to de-stress.

Thank you to all of the people outside of UNH who helped support me during my time in grad school. I would not have made it without my two best friends, Nathan Krawczyk and Ben Bradbury-Koster, who always make me chuckle and were the best roommates a guy could ask for. Thank you to my family for their constant love, advice, and support (both mental and financial!). Additionally, I would like to thank Bob and Joyce Wood for letting me stay in their lovely home while I was in-between jobs and working on my paper. My final “thank you” goes to Allison Wood for her love, friendship, support, and for running away with me on an adventure to Colorado so that I could procrastinate finishing my thesis.

TABLE OF CONTENTS

LIST OF TABLES

LIST OF FIGURES

LIST OF EQUATIONS

ABSTRACT

INFILTRATION CHARACTERISTICS OF SUBSURFACE GRAVEL FILTER SYSTEMS FOR STORMWATER MANAGEMENT

By

Ethan R. Ely

University of New Hampshire, May 2019

Increased stormwater runoff due to the construction of impervious surfaces is a major issue in urban environments, causing combined sewer overflows, erosion in natural waterways, and damage to infrastructure. Subsurface gravel filter (SGF) system, a type of Green Stormwater Infrastructure (GSI), can effectively reduce stormwater runoff volumes and peak flows by infiltrating runoff. Current GSI design guidelines require that these systems be statically sized to store the 24-hour storm depth equaled or not exceeded approximately 90% of the days with rainfall. Across the United States, this design depth is roughly equal to 2.5 centimeters (1 inch) of rainfall. This sizing technique does not account for the dynamics of system performance such as horizontal infiltration through the sides of the systems, unsaturated soil conditions, or the dynamic nature of runoff generation. By neglecting these factors, subsurface infiltration systems may end up being oversized for desired runoff reduction objectives. For this study, the hydrologic performance of SGF systems was evaluated through a combination of monitoring data and computer modeling.

Monitoring data was collected for two SGFs in Dover, NH which are statically designed, according to NH stormwater regulations, to capture and treat the runoff from 1-inch of rainfall.

One system is located under Grove St and was found to infiltrate substantial volumes of runoff even though the soils surrounding the system were found to have a relatively low hydraulic conductivity (i.e. <0.5 inches per hour). On average, over the 1-year monitoring period, the Grove St SGF infiltrated 84% of the runoff it collected. The second system, which was located under the parking lot of the Seacoast Kettlebell workout center, did not meet design expectation as it infiltrated negligible volumes of runoff during each storm event. The extremely low hydraulic conductivity of the soils at the Kettlebell site, effects of high groundwater level, and close proximately of the system to Berry Brook appear to have severely limited infiltration.

Analysis of the systems with three computer-based infiltration models, including an unsaturated flow model, a Green-Ampt model, and a unit-gradient, saturated flow model, showed that system performance was highly dependent on horizontal infiltration. The unsaturated properties of soils appeared to have only minor effects on total infiltration volumes due to the rapid transition from unsaturated to saturated flow conditions. Statistical analysis of the model results for the Grove St SGF showed that the unit-gradient model was the most accurate of the three models. Together, monitoring and modeling results confirm that subsurface gravel filters and other infiltration-type GSI could be more accurately sized to meet runoff reduction objectives if horizontal and vertical infiltration are accounted for by incorporating the unit-gradient model into system design techniques.

CHAPTER 1: INTRODUCTION

1.1 Background

Stormwater runoff from impervious surfaces, such as roadways, rooftops, and parking lots, is a major source of pollution for natural waterways and the leading cause of receiving water impairment in the United States (EPA, 1996). For urban areas, some of the major stormwater pollutants of concern include oils, trash, sediment, nitrogen, phosphorous, and salt. However, the sheer volume of runoff produced during a storm event is also an issue, especially for communities with a combined sanitary and stormwater sewer, also known as a combined sewer (CS) system. According to the US Environmental Protection Agency (U.S. EPA), combined sewer systems are "sewers that are designed to collect rainwater runoff, domestic sewage, and industrial wastewater in the same pipe" (U.S. EPA, 2017). The various flows are usually separated by a knee wall structure to prevent mixing. During dry weather periods, these sewer systems transport domestic wastewater to a municipal wastewater treatment plant (MWTP) so that the water can be treated before releasing it into a receiving waterbody. When runoff is generated during rain events, the stormwater also drains into the CS system and discharges directly to nearby waterways. However, during large rain events, runoff flows may exceed the capacity of the sewer system knee wall, causing wastewater and stormwater flows to mix and discharge directly to the receiving waterbody without being treated by the MWTP. These combined sewer overflows (CSOs) can lead to severe pollution problems and are a major concern for around 772 municipalities through the US (U.S. EPA, 2008).

Even though new combined sewer systems are no longer being constructed in the U.S., these systems are fairly common in older cities, appearing in many urban areas throughout the northeast, including Boston, Philadelphia, and New York City. According to the EPA, current

combined stormwater and sanitary sewer systems discharge approximately 850 billion gallons of untreated wastewater into receiving waters each year (U.S. EPA, 2004). CSO events can severely degrade the water quality, leading to algal blooms and health problems for humans, especially if the receiving water is used for other purposes such as for swimming, fishing, or as a drinking water source (Evans, 2015). A study by Jagai et al. (2015) found that there was a statistically significant increase in emergency room visits for gastrointestinal issues during large rain events in areas where CSO outfalls discharged to drinking water sources.

Aside from CSO discharges, the large runoff volumes from impervious surfaces may cause issues such as stream channel erosion, flooding, and damage to roadways and public infrastructure (Konrad, 2016). The hydrologic effects of impervious cover on stream flow may be observed in Figure 1, which presents the hydrographs for two nearby streams in the state of Washington. Mercer Creek flows through an urban landscape, while Newaukum Creek has a more rural, undeveloped watershed. Flows in the urban stream spike more rapidly in response to a rain event, reach a much higher peak value, and recede more quickly compared to the rural stream.

The hydrologic and water pollution issue associated with impervious land cover may be expected to increase in frequency and severity as populations in the US become more centralized and urban. According to the US Census Bureau, between 2000 and 2010, urban populations grew at a rate of around 12.1 percent compared to the national growth rate of 9.7 percent (US Census Bureau, 2012). This rapid rate of urbanization is leading to increases in the percentage of land that is covered by paved and impervious surfaces, also referred to as impervious cover (IC). For example, a 2015 study conducted by the University of New Hampshire Stormwater Center (UNHSC and VHB) estimated that by 2040, the area of IC in the local Oyster River Watershed

could increase by as much as 40%, or 500 acres, due to commercial development and a forecasted population growth of 26% for the region.

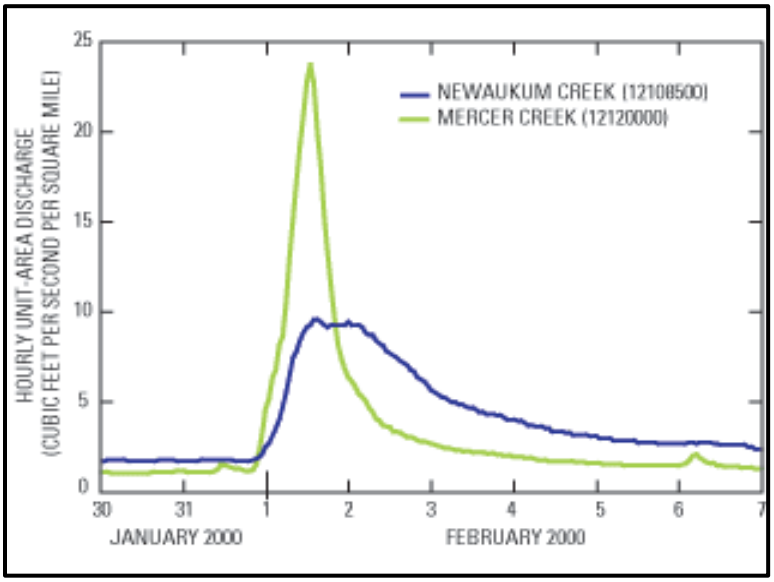

Figure 1: Comparison of urban and rural stream hydrographs from rain event on 02/01/2000 (Konrad, 2016)

In order to limit the hydrologic impacts of IC and the frequency of CSOs, stormwater runoff volumes and peak runoff flow rates must be reduced. This can be accomplished through the development and installation of Low Impact Development (LID) stormwater management systems, collectively referred to as Green Stormwater Infrastructure (GSI). GSI technologies are designed to not only remove pollutants from stormwater, but also reduce peak flows and runoff volumes through the storage and controlled release of runoff and through infiltration and/or evapotranspiration. Runoff volumes entering sewer systems and natural waterways can be effectively reduced by implementing GSI throughout urban environments (Graham et al., 2004).

Over the past few decades, since the implementation of the National Pollutant Discharge Elimination System's (NPDES) municipal separate storm sewer system (MS4) permit program, municipalities have started to incorporate GSI technologies into their regulatory requirements for

new developments and to retrofit older drainage systems to better manage stormwater runoff. Under the NPDES permit requirements, MS4 communities are required to develop stormwater management programs and obtain permits for their stormwater discharges. The push to meet permit requirements has helped spur efforts to reduce stormwater discharges through the use of GSI (Kwiatkowski et al., 2007).

Some examples of GSI stormwater controls include bioretention systems, raingardens, subsurface gravel wetlands, sand filters, and permeable pavement. One of the primary advantages of these systems is that they allow for on-site management of runoff. For new developments, these technologies may be used in place of the traditional stormwater management strategy of collecting runoff in catch basins and directing it with underground pipes to the nearest stream. However, for pre-existing developments, GIS must be retrofitted into existing infrastructure. When dealing with retrofits, land restrictions often strongly affect the location, size, and type of system that can be installed at a specific site. Systems which can be installed beneath paved surfaces are favorable as they allow the land aboveground to be used for other purposes, such as for parking or driving. One type of GSI that could be ideal for urban areas is the subsurface gravel filter.

1.2 Subsurface Gravel Filters

Subsurface gravel filter systems, or SGFs, are gravel filled excavations constructed underneath other surfaces. They fall into the category of GSI known as subsurface infiltration systems and function in a similar manner to permeable pavements and gravel infiltration trenches which provide storage for stormwater runoff in a porous gravel fill and allow the water to infiltrate into the surrounding native soils over time. The gravel can also provide some degree of filtration for the runoff, removing sediments and other pollutants from the water. Unlike

permeable pavements and infiltration trenches, for which runoff primarily enters the systems through their permeable surfaces, the surface of an SGF system is typically impervious. Runoff must enter the system through slotted and/or perforated distribution pipes which extend through the gravel layer between stormwater catch basins. Catch basins are the structural inlets to the SGF and provide some pretreatment for the stormwater, allowing larger solids to settle out of suspension before the water flows into the filter. Outflow from the systems may be directed back into the stormwater drainage network or may be conveyed directly to the nearest waterbody. A simple cross-sectional diagram of a subsurface gravel filter is presented in Figure 2.

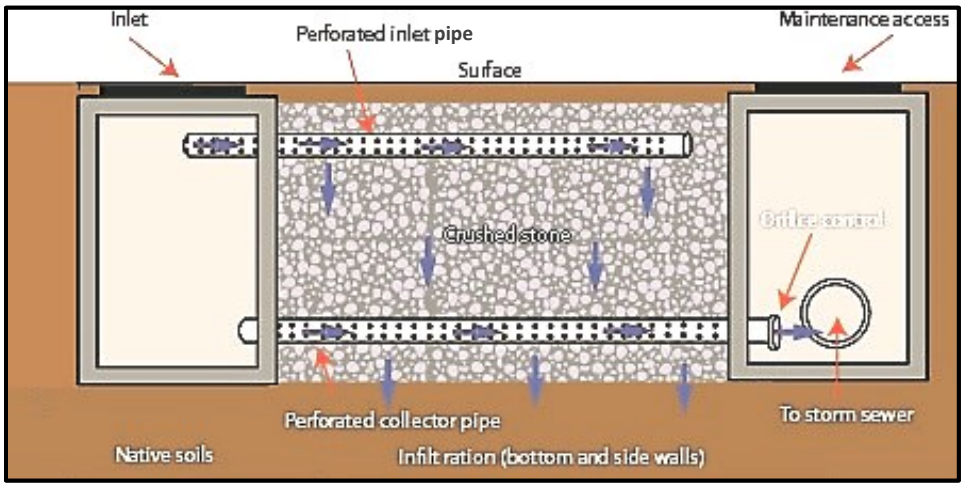

Figure 2: Cross-sectional diagram of a standard subsurface gravel filter system

Unlike most other GSI, subsurface infiltration systems may be constructed beneath roadways, parking lots, or other surfaces. This characteristic makes SGF systems an ideal option for stormwater management projects in space-limited urban environments. The systems take up minimal space aboveground and may be easily retrofitted into the catch basin-based drainage systems which are already in place. Additionally, SGFs are advantageous in term of maintenance, as the systems' catch basins may be cleaned out with the same jet/vacuum trucks

which are currently used in many towns for maintenance of conventional stormwater infrastructure.

With the support of Dover's Utilities Superintendent, Bill Boulanger, two SGF stormwater controls were installed in Dover, NH to help treat and reduce runoff volumes for several acres of urban watershed. These two controls are part of a much larger project entitle the "Berry Brook Watershed Restoration through Low Impact Development Retrofits in an Urban Environment", which aims to reduce the percentage of effective IC in the Berry Brook watershed in order to improve the water quality and restore the natural hydrologic conditions of the stream. The installation of the SGF stormwater controls and a number of other GSI controls was funded through this project. The two SGF system are located under Grove St, near the intersection of Grove St and Chesley St, and under the parking lot of the Seacoast Kettlebell fitness center. Each system was sized according to NH stormwater standards, which use static sizing methods based on the concept of the water quality volume, or WQV. The original designs for the Dover SGF stormwater controls were developed through collaboration between the UNH Stormwater Center (UNHSC) and the City of Dover's Community Services Department.

Based on the similarities between SGFs and other infiltration system, the SGF design has the potential to provide significant runoff volume reductions. Monitoring and modeling data for infiltration GSI, such as permeable pavement, infiltration trenches, and other subsurface infiltration system, shows that these systems can infiltrate significant water volumes under the right conditions. Some GSI have even been shown to surpass design expectations in terms of volume and peak flow reductions and pollutant removals (Roseen et al., 2006; Roseen et al., 2012; Houle et al., 2017). While higher performance is not a negative outcome, it does indicate that static sizing methods and current modeling techniques for GSI are not fully reflecting the

processes occurring in actual stormwater treatment systems and may be causing systems to be oversized.

1.3 Hypothesis and Research Objectives

While SGF systems and similar infiltration GSI are currently being constructed to help alleviate CSOs and the problems associated by impervious cover, limited performance data is available for these systems. One of the objectives of this research study was to measure the performance of SGF systems, specifically their ability to infiltrate water and reduce runoff volumes. The monitoring data collected from Kettlebell and Grove St. SGFs may be used to better understand how these systems operate in a developed, urban setting and how infiltration is affected by urban fill.

Another goal for this research was to determine what factors govern infiltration from SGF systems. Current sizing methods for GSI systems appear to overestimate how large a system must be to effectively treat the runoff from a specific catchment area. This oversizing is most likely due to the use of "static" sizing methods and an over simplification of infiltration processes when modeling GSI. Static sizing usually leads to larger system designs because the method relies on the assumption that no infiltration occurs while runoff is flowing into a system (MassDEP, 2008). For many stormwater system models, infiltration is assumed to be a constant value, under saturated flow conditions, and only occurring in the downward vertical direction (Freni et al., 2009). These assumptions tend to produce inaccurate models and oversized designs. By determining what variables have the greatest influence on infiltration in SGFs, sizing and design methods can be improved. The research described in this paper investigates the hypothesis that statically sizing subsurface gravel filters based on the WQV leads to the oversizing of systems. The rational for this hypothesis is that the design methods do not account

for the fact that hydrology is a dynamic (real-time) process, that infiltration occurs in both vertical and horizontal directions, and unsaturated soil conditions influence infiltration rates and system performance.

1.4 Outline of Research

The Kettlebell and Grove St subsurface gravel filters were monitored over a 1-year period (i.e. July 2016 to July 2017) to evaluate their performance. Precipitation, water depth, and flow data were collected in order to develop water balances for each system. Infiltration rates, volume reductions, and peak flow reductions were calculated from the water balances to determine how the SGFs compared to design predictions and determine if static sizing methods lead to oversizing of systems. The SGF systems were also analyzed using various mathematical infiltration models, including a unit-gradient saturated flow model, a Green-Ampt infiltration model, and a model for unsaturated flow based on Richard's equation. The results of the water balances and models were compared to investigate what factors have the greatest effect on infiltration in SGFs and to determine which model best describes system infiltration. Suggestions for how best to modify current design practices to reflect site infiltration characteristics were recommended based on this analysis.

CHAPTER 2: LITERATURE REVIEW

2.1 Design and Sizing Techniques for GSI Infiltration Systems

The design guidelines for GI-SWM systems vary between states, but usually focus on static sizing methods and a single, design rainfall event. Statically sized systems provide storage for the entire volume of runoff from a design event. Temporal aspects of runoff generation, collection, and treatment are not considered. The magnitude of the design event is selected based on the climate of a region and the desired degree of stormwater management. Selecting a large design rainfall depth helps ensure that a larger portion of annual runoff will be captured and treated by GSI systems.

Numerous studies have investigated the minimum amount of runoff that must be treated in order to effectively remove most stormwater pollutants. Initial studies of stormwater pollution, such as the study by Novotny (1995), found that common stormwater pollutants tend to be transported from impervious surfaces by the "first flush" of runoff at the beginning of rain events. The first flush refers to the concept that initial runoff flows, at the beginning of a storm, will have higher pollutant loads and transport the majority of stormwater pollution for an event (Taebi and Droste, 2004). Pollutant concentrations in the runoff have been found to decrease after the first flush, reaching fairly low concentration during the falling limb of the runoff hydrograph. Initial SWM regulations required systems to be sized to store and treat the runoff from the first 0.5 inches of rainfall (NH Stormwater Manual – Vol. 2). In more recent studies, such as those by the UNH Stormwater Center, it has been found that not all pollutants are first flush-weighted and that treating only the first half-inch of runoff becomes less effective as the amount of impervious cover increases.

To effectively manage stormwater pollution and reduce runoff volumes, many states have updated their GSI design guidelines so that systems will be sized to treat a larger portion of annual runoff. Current state stormwater regulations usually require systems to be sized to treat design precipitation depths between 0.75 and 1.5 inches (US EPA, 2011). These design depths are based on the "90% rule" whereby the depth is selected so that systems will be able to store and treat the runoff from 90% of rain events annually (Claytor and Schueler, 1996). For much of the Northeast United States, the 90th percentile rainfall depth is approximately 1 inch of rainfall (Roseen et al., 2006). Therefore, states such as New Hampshire, Maine, and Connecticut use a 1-inch design rainfall depth for calculating runoff volumes and sizing stormwater systems. Other states, such as Massachusetts, New York, and Vermont, simply require the 90% rule to be used to calculate a design depth instead of specifying a value for the entire state (US EPA, 2011). For Durham, NH, which is within a few miles from the two stormwater controls described in this paper, Roseen et al. (2006) found that the 1-inch design depth corresponded to the 92% non-exceedance rainfall depth based on 24-hour NOAA data.

The amount of runoff generated by the design storm is used to determine the required static storage volume for a stormwater control. The design runoff volume, referred to as the water quality volume or WQV, is a faction of the total rainfall depth and depends on the size of the system's drainage area and the percentage of impervious cover and soils within that area. As with the design depth, the equation used to calculate the WQV is state specific. For NH, the WQV is calculated using Equation 1 in which a runoff coefficient, based on the percentage of impervious cover (I), defines the portion of rainfall that will become runoff. NH and many other states also require that systems be able to recharge any additional runoff generated by new impervious surfaces when undeveloped land is being modified (i.e. redevelopment). This runoff

volume is referred to as the groundwater recharge volume (GRV), or just recharge volume (RV), and is calculated using some form of Equation 2, depending on state regulations. The groundwater recharge depth term is based on the NRCS Hydrologic Soil Groups and represents the amount of water that would have infiltrated if the land had not been converted to impervious cover.

Equation 1: Water quality volume calculation (2008 NH Stormwater Manual)

$$WQV = (P)(R_v)(A)$$

$$R_v = 0.05 + 0.9(I)$$

Equation 2: Groundwater recharge volume calculation (2008 NH Stormwater Manual)

$$GRV = (A_i)(R_d)$$

Where:

WQV = water quality volume (acre-inches)
GRV = groundwater recharge volume (acre-inches)
P = design precipitation depth (inches)
R_v = runoff coefficient (-)
A = drainage area (acres)
I = fraction of drainage area that is IC
A_i = effective impervious area created by new development (acres)
R_d = groundwater recharge depth based on the four NRCS Hydrologic Soil Groups

Infiltration systems that are statically sized, must be designed to store the larger of the entire WQV or GRV. This sizing method does not take into account the infiltration that occurs while a system is filling, outflows from the system, or the temporal aspects of runoff generation. While this design strategy can lead to designs which are larger than they need to be to treat the runoff from a design event, most states have incorporated this technique into their stormwater management guidelines. This "oversizing" can occur for infiltration GIs because runoff will immediately begin to infiltrate once it enters the systems. Dynamic sizing techniques produce smaller system designs as they can include some of the temporal aspects of stormwater runoff generation and management.

In addition to sizing with the WQV and GRV, many state regulations provide supplemental guidelines for the design of infiltration stormwater controls, such as infiltration basins, dry wells, infiltration trenches, and subsurface gravel filters. For example, the NH Stormwater Manual requires that infiltration systems are located no less than 3 ft above the seasonal high-water table (SHWT) and that systems drain within 72 hrs (NH Stormwater Manual – Vol. 2). In order to calculate the drain-down time, designers must measure the hydraulic conductivity of native soils at the project site using a Guelph permeameter, compact constant head permeameter, double-ring infiltrometer, or falling-head borehole infiltration test. All measurements are to be taken within the footprint of the proposed system, at or below the bottom elevation of the system. Designers are to use the lowest measured hydraulic conductivity, divided by a safety factor of 2, to calculate the length of time required for a system to fully drain. For this calculation, infiltration is assumed to operate under saturated, unit-gradient conditions, meaning that the infiltration rate is equal to the saturated hydraulic conductivity. Horizontal infiltration and the variability of infiltration rates due to changes in soil moisture are not considered. The regulations also require that infiltration systems have an underdrain if the measured infiltration rate is less than 0.5 in/hr. Infiltration rate measurements are therefore used to verify that an infiltration system is viable and to calculate the minimum bottom area needed to allow a system to drain within 72 hrs.

Other Northeastern states have similar regulatory guidelines for infiltration systems, requiring static sizing methods using the WQV and GRV, a maximum drain-down time of 24 to 72 hrs, a minimum height of 1 to 3 ft above the SHWT, and a minimum acceptable infiltration rate ranging from 0.17 to 0.5 in/hr. Massachusetts is one of the few states that provides alternative design methods to help reduce the size of GSI system. The Massachusetts Stormwater

Handbook outlines three methods for sizing infiltration BMPs: static, simple dynamic, and dynamic field sizing (MassDEP, 2008). As in NH, to meet both water quality and recharge standards, GSI systems are sized based of the larger of the GRV or WQV.

Massachusetts's static sizing method is similar to the previously described method used by most states and assumes that infiltration does not occur until system storage is filled. Statically size infiltration systems must store the entire design runoff volume and drain within the required drain-down time (i.e. 72 hrs for MA). This method is the most conservative of the three and leads to larger system designs. The two dynamic methods take into account the fact that water can flow out of or exfiltrate from the system while it is filling. Dynamically sized systems are smaller, as they are sized to store only a portion of the design runoff volume. The basal area of a dynamically sized system may be calculated using Equation 3. The primary difference between the simple dynamic and the dynamic field methods is the assumed length of time over which infiltration occurs. For the simple dynamic method, runoff is assumed to enter the system and infiltrate over a 2-hr period, while for the dynamic field method this process occurs over 12hrs. The methods also differ by how their design infiltration rates are calculated. For the static and simple dynamic methods, infiltration rates are selected by classifying the soils at the site of the proposed system and determining the hydraulic conductivities associated with that soil class from published values by Rawls et al. (1982). For the dynamic field method, the infiltration rate is measured along the base of the system using one of the approved measuring devices, including the Guelph permeameter, falling head permeameter, double ring infiltrometer, and Amoozemeter. The lowest measured hydraulic conductivity is divided by a safety factor of 2 before it is used to calculate the basal area of a system. The hydraulic conductivity estimate for the static and simple dynamic methods is not reduced with a safety factor because these methods

are already very conservative. In all three methods, infiltration rates are assumed to follow the saturated, unit-gradient flow model in which the rate equals the established saturated hydraulic conductivity value (MassDEP, 2008).

Equation 3: Calculation for dynamic sizing methods (MassDEP 2008)

$$A = \frac{RV}{D + KT\left(\frac{1ft}{12in}\right)}$$

$$V = (A)(D)$$

Where:

A = minimum required basal area of the system (ft^2)
D = depth of the system storage (ft)
RV = larger of the GRV or WQV (ft^3)
K = saturated hydraulic conductivity (in/hr)
T = inflow/infiltration period (2 hrs for the simple dynamic method, or 12hrs for the dynamic field method)
V = minimum require storage volume (ft^3)

The use of dynamic sizing methods, such as those described in the MA Stormwater Handbook, reduces the size of systems through a slightly more realistic representation of infiltration processes. Static sizing neglects all of the time-dependent aspects of stormwater systems, while the simple dynamic and dynamic field methods attempt to account for some of the infiltration which occurs while a system is filling. However, all of these design methods still neglect horizontal infiltration, surface runoff hydrographs, and the variability of infiltration due to soil moisture. GI, especially those system designed for infiltration, could potentially be more accurately sized by incorporating some of these other factors into design methods.

2.2 Performance of GSI Systems

GSI systems are designed for the purpose of removing pollutants from stormwater, lowering peak runoff flows, and reducing the total volume of runoff entering drainage systems and natural waterways. Design guidelines for GSI usually require that the systems capture a

specific volume of runoff, such as the runoff from 1 inch of rainfall, in order to treat the majority of the runoff pollutant load. However, the actual performance of a system depends on a variety of factors and can be difficult to plan for. Over the years, research studies have been conducted to quantify the performance of GSI and determine what factors are affecting perform.

Roseen et al. (2006) evaluated the performance of GSI, conventional, and manufactured stormwater treatment systems in terms of their capacity to remove stormwater pollutants, such as total suspended solids (TSS), petroleum hydrocarbons, zinc, and dissolved inorganic nitrogen. In the study, eight systems at the UNH Stormwater Center were monitored over the course of 11 storm events. Water samples were taken from the systems' influent and effluent flows to determine pollutant removal efficiencies. Systems were designed to treat the equivalent runoff volume from the 90th percentile rainfall event. Results from the study showed that the GSI systems had the highest removal efficiencies, performing markedly better than the conventional systems (i.e. the retention pond and rip-rap swale). The study also found that of the eight systems, those which allowed for filtration and/or infiltration had the highest pollutant removals.

Retrofit GSI (i.e. systems constructed at currently developed sites) are frequently constrained by space limitations and cannot be fully sized for the WQV. However, numerous studies have shown that undersized, retrofit systems can still provide significant volume reduction and water quality improvement benefits and frequently perform at a higher level than what is expected from design. Luell et al. (2011) compared the performance of an undersized bioretention system to that of a fully sized system and found that both systems significantly reduced pollutant loads. Although the undersized system was designed to contain only 25% of the total WQV, the system's nitrogen and TSS load removals were 84% and 50%, respectively, of the larger system's removals.

Houle et al. (2017) observed a similar trend for two undersized, retrofit GSI, which could not be fully sized due to space constraints. The first stormwater control, a subsurface gravel wetland (SGW), was statically sized to contain only 10% of the WQV, or 0.1 inches of runoff, while the second control, a modified bioretention system (IBSC) with an anaerobic storage reservoir, was dynamically sized for 23% of the WQV, or 0.23 inches of runoff. Both systems were monitored by the UNH Stormwater Center for two years to determine their performance in terms of water quality improvements. Results showed that the SGW and IBSC had removal efficiencies of 86% and 75%, respectively, for TSS, which are only slightly lower than the removal efficiencies for fully-sized bioretention and SGW systems monitored in a previous study. The systems also achieve high total phosphorous removals that were even greater than those of a fully-sized bioretention system due to the addition of water treatment residuals to the soil amendments use in the retrofits. Houle et al. (2017) concluded that GSI performance is not linearly related to system size and that undersized systems perform at a much higher level than what contemporary design and modeling practices estimate.

The hydrologic performance of GSI, which refers to a system's ability to reduce runoff volumes and peak flows, can also be difficult to predict. For example, Roseen et al. (2006) found that many of GSI system were hydrologically more efficient than what could be expected from design calculations. During the monitoring period of the study, GSI systems only bypass flows once, even though four of the measured storm events were larger than the design rainfall depth. Volume and peak flow reductions are dynamic processes which cannot be accounted for with simple static sizing and design methods.

Hydrologic performance of GSI is best measured using a water balance technique, which takes into account the various flow paths runoff takes as it moves through a system (Graham et

al., 2004). These paths may include inflows, infiltration, outflows from underdrains, and the bypass of high flows. By developing a water balance for a GSI, one can quantify the flows on each path and determine the volume reduction of a system on a per-event or annual basis. In the past, conventional stormwater management systems were primarily designed to control peak flows and manage large runoff events (Sørup et al., 2016). GSI systems are designed instead to manage the runoff from smaller, more common rain events and a portion of the runoff from larger events. The water balance technique is a better measure of hydrologic performance as it accounts for the full range of storm events that a system must manage (Graham et al., 2004).

Large water balances may be used to evaluate networks of GSI positioned throughout a watershed and can account for runoff generation, flow through the GSI, and the final discharges into the drainage network or waterways. Graham et al. (2004) used the LIFE water balance model, by CH2M HILL (2004) to evaluate the performance of several GSI systems throughout an urban watershed in Seattle, Washington and examine how stream flow in Venema Creek would change in response to proposed construction. The study found that infiltration GSI were an effective technique for managing and reducing runoff volumes and could be designed based on water balance modeling to achieve specific goals, such as a 10% reduction in peak stream flow. Sørup et al. (2016) used water balance modeling to evaluate the impact of distributing GSI throughout an urban environment and ranked system performance using the Three Point Approach (3PA). This approach looks at system performance for three types of rain events: 1) small rain events which make up approximately 75% of annual rainfall, 2) medium, or design, events which have a return period between 0.2 and 10 years and can cause CSOs, and 3) major events which can cause flooding and have a return period greater than 10 years. GSI sized for the small, 0.2-year rain events and medium, 10-year events were evaluated, using water balance

modeling, in terms of their capacity to reduce water volumes and CSOs during each type of rain event. Model results showed that both systems were able to manage over 83% of runoff annually and could significantly reduce CSO events by 31 to 38%. The performance of the smaller GSI is especially notable as these systems are three times smaller than the medium GSI, yet were able to manage 21% less runoff (i.e. 83% of annual runoff compared to 99.5%).

Another proven infiltration GSI that may be used for both pollutant removal and runoff volume reduction is permeable pavements. These systems are an alternative to impervious, paved surfaces and allow rain and runoff to drain down through the pavement into a gravel sub-base, where the water can either infiltrate into the surrounding soils or slowly drain to an outlet through an underdrain. Roseen et al. (2012) evaluated the performance of porous asphalt pavements in the cold-weather climate of NH. The pavement system was monitored over a 4-year period to assess its ability to reduce water volumes, lower peak flows, and improve water quality. Results showed that the pavement reduced peak flows by 90% on average and water volumes by 25% over the study period, even though the system was installed over fairly restrictive, hydrologic soil group (HSG) C soils. The unexpectedly high reductions agree with the results from numerous other studies of porous asphalt that have shown reductions between 50 and 100% (Stenmark, 1996; Legret and Colandini, 1999; Dempsey and Swicher, 2003).

Long-term performance studies have also been performed on infiltration GSIs, supporting their usage in urban environments for runoff volume reduction and CSO mitigation. Warnaars et al. (1999) and Bergman et al. (2011) each analyzed a pair of infiltration trenches over differing periods of time and found that the system effectively reduced runoff volumes even though the measured infiltration rates of the native soils were on the order of 10^{-6} m/s, or 0.14 in/hr. The trenches were constructed in Copenhagen in 1993 and were designed to capture the runoff from a

600m^2 drainage area. Warnaar et al. (1999) evaluated the performance and infiltration rates of the system over the first three years after construction, while Bergman et al. (2011) evaluated the system after 15 years of operation. During the first few years, Warnaar et al. found that the trenches infiltrated the runoff from the majority of rain events, bypassing flows during only 7 of the 89 recorded rain events. However, the infiltration rate for the trenches decreased slightly over the monitoring period.

Bergman et al. (2011) confirmed this observation by comparing the system's performance after 15 years of operation to the performance measurements taken during the first three years. Changes in water surface elevation in the system were used to determine field-saturated hydraulic conductivity (K_{fs}), which is the hydraulic conductivity of a soil which has been thoroughly wetted and is near-saturation, but still contains entrapped air. The decrease in K_{fs} for the soils surrounding the stormwater system was found to be statistically significant, dropping from average values of 0.28×10^{-6} m/s and 0.89×10^{-6} m/s for the bottom and sides of the systems, respectively, to values of 0.075×10^{-6} m/s and 0.29×10^{-6} m/s. Bergman et al. proposed that the decrease in performance was most likely due to clogging of the soil material along the circumference of the trenches. Overall, the results of both studies confirm that subsurface infiltration systems can significantly reduce runoff volumes, even when installed in urban areas where compacted urban fill may limit infiltration rates. The studies also found that the K_{fs} values for the sides of the systems were significantly larger than those of the bottom and contributed to the volume reduction capabilities of the infiltration trenches.

Overall, research has shown that the performance of GSI systems is not linearly related to storage volume and depends on a variety of factors. However, systems are still sized using simple static sizing methods that do not account for the dynamics of stormwater runoff and the

complex process of infiltration. The research describe in this paper will explore how these and other factors influence the hydrologic performance of subsurface gravel filters.

2.3 Modeling Infiltration in GSI Stormwater Systems

Modeling infiltration processes in GSI systems is an important step when designing GSI for management of runoff volumes. Models allow designers to better understand how a system will perform before it is constructed. Infiltration models are frequently incorporated into larger, watershed-scale models, which can help guide stormwater management planning. Numerous models have been developed to simulate infiltration. Some of these models were specifically designed for simulating infiltration in GIs, while many are more general models developed for calculating surface runoff generation or for use in the wastewater, solid waste, and remediation industries to calculate subsurface flows and contaminant transport rates. Overall, infiltration models can be classified according to four categories: 1) flow type, 2) soil uniformity, 3) dimensionality of flow, and 4) the type of mathematical model.

Models can simulate infiltration as either a saturated or unsaturated flow, depending on the moisture content of the modeled soil. Soil moisture content refers the amount of water contained within the pore spaces of a soil. When a soil media is saturated, its pores are entirely filled with water and the soil moisture content (θ) equals the soil's porosity (φ). Under these conditions, hydraulic conductivity is constant and matric potential (ψ), which is the negative pressure created by the capillarity of a porous media, equals zero. Darcy's saturated flow model is primarily used to simulate infiltration when saturated conditions exist. Unsaturated soils are those which contain both air and water in their pore spaces. Models for unsaturated soils are more complex as they must account for the effects of soil moisture on matric potential and hydraulic conductivity. Unsaturated flow models, most of which are based on Richards equation,

can only be solved numerically without making several simplifying assumptions. Richards equation (Richards, 1931) is a non-linear, partial differential equation which relates the infiltration rate to total hydraulic head (i.e. matric potential and hydrostatic head) and hydraulic conductivity (Ravi and Williams, 1998). Matric potential and hydraulic conductivity change in relation to soil moisture for Richards equation. As soil moisture conditions approach saturation, the Richards models can be simplified to Darcy's equation. The Green-Ampt infiltration model (Green-Ampt, 1911) is another interpretation of infiltration where water moves through the soil as plug flow, with a sharp, well defined wetting front, behind which the soil is saturated. This model is based on a one-dimensional, non-linear equation that relates the infiltration rate at the surface of a soil to the cumulative infiltration depth and reduces to the saturated flow equation when the cumulative infiltration depth is large (Ravi and Williams, 1998).

Soil uniformity affects the rate and flow path which water takes as it infiltrates. Natural soils can be highly heterogeneous, containing mixtures of different soil types and textures. This is especially true for urban environments, where compacted fill material can influence infiltration. Warnaar et al. (1999) found that K_{fs} values measured along one side of an infiltration trench ranged by six orders of magnitude. Additionally, the average K_{fs} value for one of the trenches was 10 times larger than that of the other trench located only 7 m away. Soil heterogeneity can be difficult to model and usually requires the use of simplifying assumptions. One strategy is to assume soils are homogenous and use average values for hydraulic conductivity, soil moisture, porosity, and other soil parameters. Many models rely on the assumption of homogeneity, such as the original Green-Ampt model (Green-Ampt, 1911), the Philip's two-term model (Philip, 1957), and numerous versions of Richards model (Philip, 1969; Warrick et al., 1991; Huang and Wu, 2012), even though soils are rarely uniform. Other models

assume a layered system of soils, each with their own specific properties. This strategy may be a more realistic interpretation of soil structure as soils frequently form as composition of individual layers, called horizons (Ouyang et al., 1998). Several variations of the Green-Ampt and Richards models have been developed for modeling layered soil systems, including Flerchinger et al.'s (1988) Green-Ampt model for layered systems (GALAYER), the constant ponding depth model by Bower (1969), and quasilinear Richards model for heterogeneous soils developed by Philip (1972).

The complexity of an infiltration model is strongly impacted by the dimensionality of the model. One-dimensional (1-D) models are some of the simplest, as they only consider flows in one direction. For infiltration of rainfall at the soil surface, 1-D models are usually an accurate interpretation of flows, as water depths are insignificant compared to infiltration area and most water flows downward into the soils (Ravi and Williams, 1998). However, in the subsurface storage zones of infiltration GIs, water can also infiltrate horizontally when ponding occurs. To accurately simulate infiltration from subsurface storage, models must be multi-dimensional (i.e. 2- or 3-D) and account for flows through both the sides and bottom of a system (Freni et al., 2009; Finch et al., 2008). This drastically increases the complexity of the infiltration calculations, the run time of simulations, and the amount of effort needed to set up a model (Browne et al., 2008; Freni et al., 2009).

Many models rely on the assumption that flows through the sides of a system are insignificant and that infiltration primarily occurs through the base of a system. Most state design guidelines (U.S. EPA, 2011) also rely on the assumption of 1-D, vertical infiltration for calculation of the drain-down time for a filled system. 1-D models, such as Green-Ampt and the 1-D form of Richards equation, can be valid for scenarios where the soils along the sides of a

system have a much lower hydraulic conductivity than those at the bottom or if a significant ponding depth does not develop during storm events. Some 1-D models attempt to include horizontal infiltration through the calibration of variables that account for both vertical and horizontal flows. For example, Heasom et al. (2006) modelled infiltration from bioinfiltration BMPs using a version of the Green-Ampt equation, but calibrated the hydraulic conductivity values from system monitoring data so that infiltration from all directions was accounted for.

Aside from dimensionality, model complexity also depends on the type of mathematical model used to simulate physical processes. The simplest models are developed by fitting basic equations, such as linear or power functions, to measured infiltration data using calibrated coefficients that do not have a physical basis. These empirical models, as they are named, disregard the physics of infiltration, but are usually easy to use and can be solved analytically (Ravi and Williams, 1998; Browne et al., 2008). Two of the most commonly used empirical infiltration models are the National Resource Conservation Service's (NRCS) rainfall-runoff relationship (USDA-SCS, 1957), which is primarily used for runoff calculations, and Horton's infiltration equation (Horton, 1940). In contrast, physically based models, such as Richards model, are developed from the hydraulic principals describing the flow of water through a porous media (Ouyang et al., 1998). Model parameters in physically based infiltration models relate to specific soil and water properties which can be measured in the field or from soil samples (Freni et al., 2009). This allows physically based models to be used more broadly compared to empirical models, which are restricted by the limited data sets used for parameter calibration. Models can also be somewhere in-between physical and empirical, such as the Green-Ampt model which is based on physical principles, but also relies on parameters which can be empirically determined. While physically based models are usually more complex than

their empirical counterparts, they allow the user to analyze the various factors affecting system performance and can therefore be a valuable tool for GSI system design (Heasom, 2006).

As described by numerous studies of infiltration modeling (Heasom, 2006; Assouline et al., 2007; Browne et al., 2008, Freni et al., 2009), most models used for simulating infiltration in GSI systems are either too complex for widespread use and design purposes or are too simplified and neglect important factors that influence infiltration. The more complex models are primarily based on some form of the Richards equation. These models are ineffective for incorporation into larger hydrologic models, as they must be solved numerically, leading to long run times and the high potential for mass balance errors (Celia and Bouloutas, 1990; Huang and Wu, 2012). A Richards-based model can also be data intensive, requiring the measurement and calculation of site-specific variables such as soil moisture, hydraulic conductivity, matric potential, and the soil-water retention curve (Browne et al., 2008).

Simpler models often assume constant infiltration rates or saturated conditions, even though subsurface infiltration systems are usually located in the vadose, or unsaturated, zone (Freni et al., 2009). These models may neglect horizontal flows, anisotropic conditions, variable ponding depths, and the dynamic nature of runoff generation (Elliott and Trowsdale, 2007; Browne et al., 2008). Even the more complex Richards models are frequently simplified by either assuming a constant ponding depth, constant flux of water at the soil surface, or some other boundary condition that is unrealistic for subsurface infiltration systems (Huang and Wu, 2012).

The three models selected for simulation of subsurface gravel filters in this study were chosen based on their specificity toward modeling subsurface infiltration systems, their usefulness as a tool for design, and because they are either fully or semi-physically based. While

each of the models use a different technique to estimate infiltration rates, they are all designed to simulate infiltration in systems that receive variable inflows and water depths, and are simple enough to be incorporated into larger stormwater models. The first model, developed by Browne et al. (2008), is unique as it has the ability to simulate saturated and unsaturated soil conditions, a mobile wetting front, variably ponded infiltration, and clogging due to the buildup of fines at the bottom of a system. Browne et al.'s model, referred to as the saturated/unsaturated flow model, divides infiltration GIs into four distinct zones: 1) a gravel storage zone, 2) an optional clogging zone, 3) a saturated soil zone, and 4) an unsaturated soil zone. The saturated and unsaturated zone are further divided into discrete layers in order to model how moisture spreads through the soils below a system. During rain event simulations, runoff enters the storage zone and moves downward through the various model layers. Flow into and through the saturated zone is calculated using Darcy's equation, while flows between the saturated and unsaturated zones and lower unsaturated layers are calculated from the 1-D, soil moisture-based form of Richards equation. While this model does not account for horizontal infiltration, it is more advantageous for simulating stormwater infiltration than many other models as it accounts for the complex movement of water through unsaturated soils and is much more efficient than multidimensional models.

The second model is based on the Green-Ampt equation for infiltration and was developed by Freni et al. (2009) for simulating infiltration trenches. The Green-Ampt model has been widely used for modeling infiltration as it considers changes in the infiltration rate due to the cumulative infiltration depth, while being more user-friendly than Richards equation. Freni et al.'s modification to the model is the addition of an effective infiltration area term (A_{eff}), which is used to account for horizontal infiltration through the sidewalls of a system even though the

Green-Ampt equation is one-dimensional. The A_{eff} term is based on a power-function relationship that relates the base area of a system to the total area of infiltration and is soil specific, but does not change in relation to water depth. Freni et al.'s modified Green-Ampt model was shown to produce similar results when compared to a more sophisticated VSF-MODFLOW 2000 model (Freni et al., 2009).

While the two previous models account for unsaturated flows and variable infiltration rates, the third model used for this research study is a simple unit-gradient, saturated flow model developed by Mikkelsen (1995). The model accounts for both horizontal and vertical infiltration because it assumes water infiltrates through the entire wetted area of the system, which changes based on the water level in the trench. The sides and bottom of the system are given unique hydraulic conductivities, obtained from soil measurements of infiltration or calibrated from monitoring data using linear regression equations to relate water depth to infiltration rate. Hydraulic conductivities are assumed to remain constant throughout the infiltration process, but were found to change over time due to the clogging of soil pores by suspended sediments (Warnaars et al., 1999; Bergman et al., 2011). This model is much simpler than the unsaturated infiltration models because it uses a unit-gradient driving force and neglects the effects of soil moisture. However, the model has been found to produce similar results to the more complex, unsaturated flow models (Mikkelsen, 1995). Warnaars et al. (1999) and Bergman et al. (2011) used the model to simulate infiltration in two infiltration trenches in Copenhagen and found that the linear relationship between infiltration and water depth in the systems is acceptable when a one-hour time step is used for calibration.

2.4 Infiltration Characteristics of Soil

A variety of soil-water characteristics must be evaluated in order to accurately design and model GSI infiltration systems. The one parameter which is needed for almost all modeling and design techniques, whether saturated or unsaturated, is hydraulic conductivity (K). It describes the ease at which water passes through a soil media when a hydraulic gradient is present. The value varies in relation to soil moisture, but is frequently assumed to be constant. Saturated models and most design techniques for calculating drain-down time use a constant value for K, specifically either the saturated hydraulic conductivity (K_s) or field-saturated hydraulic conductivity (K_{fs}). K_s is theoretically the maximum value for K for a specific soil and occurs when soils are fully saturated. Under most field conditions, vadose zone soils do not become fully saturated, instead reaching a condition called "field-saturation" where a wetted soil still contains a small amount of entrapped air that can only be removed by dissolution (ASTM D5126/D5126M; Elrick et al., 1989). In the field, K_{fs} is realistically the maximum value of K for a soil, but has been found to be only about half the value of K_s on average (Bouwer, 1966).

The hydraulic conductivity of a soil can be measured using a number of different field and laboratory techniques. Some of the most commonly used field techniques for measuring K_{fs} in the vadose zone include the Guelph permeameter, double-ring infiltrometer, single-ring infiltrometer, borehole test, and air-entry permeameter (ASTM D5126/D5126M; ASTM D6391-11; Reynolds and Elrick, 1985; Lee et al., 1985). Laboratory techniques include the falling-head and constant-head permeameter tests (Lee et al., 1985) and require the excavation of soil cores.

Field and lab methods have different strengths and weaknesses relating to their accuracy, ease of use, and time requirement. For example, laboratories methods have the advantages of being fairly quick and are performed in controlled environments where soil moisture can be

precisely controlled (USDA-SCS, 1991). However, due to the likelihood of disturbing and/or compacting the soil cores during extraction, laboratory measurements of K have been found to produce artificially lower K-values (Gallichand et al., 1990). The falling and constant head methods also produce lower K-values because the effects of macropores on permeability cannot be properly accounted for with small soil cores. Macropores are the cracks, holes, and passages in natural soil media which are larger than the pore spaces between soil particles. Studies involving soil permeability have found that the presence of macropores can significantly increase the hydraulic conductivity of a soil beyond what would be expected based solely on soil texture (Reeves et al., 1951; Lee et al., 1985; Gallichand et al., 1990; USDA-SCS, 1991). Field methods can do a better job of accounting for macropores and can be performed without significantly disturbing the soil or changing its compaction. Some disadvantages of field methods are that they usually take more time to perform, especially if the soils being tested are highly impermeable, and external variables (i.e. weather, temperature, soil moisture, etc.) cannot be readily controlled (USDA-SCS, 1991).

Of the seven techniques just mentioned, the Guelph permeameter is one of the most advantageous. The device uses a Mariotte siphon design to maintain a constant head of water in a small, cylindrical excavation. Once the soil surrounding the permeameter reaches field saturation, the steady-state rate of infiltration at a specific head can be measured and used to calculate K_{fs}. Different strategies can be used to calculate K_{fs} depending on how many rate measurements are taken at different hydraulic heads. Unlike most of the other methods, the Guelph measurements takes horizontal infiltration into account, producing K-values which are effectively an average of horizontal and vertical infiltration (Reynolds and Elrick, 1985). Another advantage of the Guelph methodology is that it does not assume saturated conditions,

making it ideal for vadose zone analyses. Depending on the permeability of a soil, accurate measurements with the Guelph permeameter can be made in a few hours.

Guelph permeameter rate measurements can be used to calculate K_{fs} using three different analysis approaches: the Laplace method, Richards method, and modified single-head method (Reynolds and Elrick, 1986; Elrick et al., 1989). The Laplace and modified single-head methods require only one infiltration rate and head measurement to calculate K_{fs}, while the Richards method requires two or more measurements. Of the three methods, the Laplace method is the easiest to perform but is also the least accurate as it neglects the effects of soil capillarity causing K_{fs} to be underestimated. The Richards analysis is the most accurate because it uses the variation between multiple infiltration rate measurement that are taken at different head values to quantify both the gravitational and capillary components of infiltration. The Richards method can therefore be used to not only estimate K_{fs}, but also matric flux (ϕ_m), sorptivity (S), and the relationship between K_{fs} and matric potential (ψ).

Unfortunately, the Richards analysis method has also been found to have a high failure rate and large standard deviation, most likely due to the sensitivity of the analysis to the steady-state flow measurements (Elrick et al., 1989). If flow measurements are taken before infiltration reaches steady-state, the Richards method can produce negative values for ϕ_m and α, which define the exponential relationship between K_{fs} and ψ. Elrick et al. (1989) developed a modified single-head approach, which utilizes an assumed value for the ratio between hydraulic conductivity and matric flux, to improve the K_{fs} estimate from a single rate measurement. This modified single-head technique has been found to produce statistically similar results when compared to the Richards analysis, but does not suffer from the same sensitivity to the flow measurements. For the purpose of most field investigations, Elrick et al. (1989) proposes that

while the Richards method may be slightly more accurate than the one-head method, the difference between the two is insignificant compared to the variability of K_{fs} at a field site. Due to the high heterogeneity of natural soils, numerous conductivity measurement must to be made to effectively characterize a site (Lee et al., 1985).

While K is required for all infiltration models and is the only measured parameter required for many saturated infiltration models, the more complex, unsaturated infiltration models require additional parameters to define soil-water characteristics. These parameters include, but are not limited to, soil porosity (φ), matric potential (ψ), and soil moisture content (θ). Soil porosity and initial moisture content (θ_i) are constants which can be measured from soil samples. Matric potential changes in relation to soil moisture according to specific soil-water retention curves. For the Green-Ampt equation, which assumes a piston-type wetting front, ψ is equal to the negative capillary pressure, or suction, along the edge of the wetting front (Green and Ampt, 1911). Similar to hydraulic conductivity, the wetting front matric potential (ψ_f) for the Green-Ampt model is a constant. Richards equation does not assume a constant ψ or K, requiring the relationship between these variables and soil moisture to be defined.

One of the major difficulties of using the Richards model is the inability to accurately measure or calculate equation parameters. Because each variable is a function of soil moisture, the values of each parameter change throughout the infiltration process. Measuring the parameters can be expensive and time-consuming and can usually only be best performed in a laboratory setting (Van Genuchten, 1980). This problem is further complicated by the effects of hysteresis, which occurs when the $K(\theta)$ and $\psi(\theta)$ curves vary depending on whether a soil is wetting or drying (Ravi and Williams, 1998). If the goal is primarily to analyze wetting soils, numerous studies have developed techniques for estimating the soil-water retention and

hydraulic conductivity relationships based on parameters that are easier to measure, such as initial, residual, and saturated soil moisture content; saturated hydraulic conductivity; air-entry matric potential; and pore-size index. Two of the most commonly used techniques are those proposed by Brooks and Corey (1964) and Van Genuchten (1980), both of which relate K to an empirical equation that is fit to a measured soil-water retention curve (Ravi and Williams, 1998).

Due to the frequent use of the Green-Ampt and Richards models for infiltration analyses and the difficulty of measuring site specific soil parameters, researchers have relate model parameters to qualitative soil properties, such as soil texture (Brakensiek et al., 1981; McCuen et al., 1981; Rawls et al., 1983; Rawls et al., 1992; Carsel and Parrish, 1988). By collecting soil data for over 1,000 different soil samples, Rawls et al. (1983) were able to calculate average values of the Green-Ampt model parameters for each of the 11 different soil textural classes. Other studies have tried to relate model parameters to the particle size distribution (PSD) of a soil (Rawls and Brakensiek, 1989; Wang et al., 2017). While the model parameters can be obtained based on soil texture relationship or calculated from particle size distributions, field or laboratory measurements are preferred because texturally similar soils from different sites can have unique hydraulic properties due to macropores, compaction, and other site-specific conditions (Ravi and Williams, 1998; Lee et al., 1985). This is especially true for parameters such as matric potential, residual soil moisture, and hydraulic conductivity, which have a large range within individual soil texture classes (Todd and Mays, 2005).

CHAPTER 3: MATERIALS AND METHODS

3.1 Site Descriptions

One of the subsurface gravel filters that was evaluated in this study is located under Grove St, near the intersection of Grove and Chesley St in Dover, NH. A picture of the SGF system after construction is presented in Figure 3. The system was statically designed according to NH stormwater guidelines to store and treat the runoff from its estimated drainage area, which consists of 1.44 acres of residential neighborhood with 22% impervious cover (Table 1). The second SGF evaluated for this study was constructed underneath the paved parking lot of the Seacoast Kettlebell workout facility off of Horne St in Dover, NH (Figure 4). The system was designed to treat the runoff from a 2.09-acre residential/commercial watershed of which 72% is impervious cover (Table 1). Due to spatial constraints, the Kettlebell system is undersized and designed to store and treat 30.5% of its WQV, or approximately 1620 ft^3 of runoff. The Grove St SGF was fully sized to store its entire WQV of 1320 ft^3 of runoff. The design procedure and associated sizing calculations for each system are provided in the Appendices.

Figure 3: Post-construction picture of Grove St subsurface gravel filter, Dover, NH

When the systems were originally designed, their watershed areas were roughly estimated based site assessments and the AutoCAD shapefiles provided by the City of Dover Community Services Department (CSD). After construction, the watershed areas for both systems were reassessed using a 1-meter resolution digital elevation map (DEM) from the NH GRANIT website and elevation data collected from site survey. The Grove St SGF's watershed was found to be over twice the size of the original estimate, with an area of approximately 4.10 acres. The watershed for the Kettlebell SGF was also calculated to be larger than the original estimate, with an area of 2.67 acres. Even though the Grove St system was sized to fully store and treat its WQV, these new drainage area estimates show that both systems are undersized for their actually watersheds. The Grove St and Kettlebell gravel filters both provide storage for just under 30% of their respective WQVs, based on their actual watersheds. The updated watershed characteristics for each system are presented in Table 1.

Figure 4: Post-construction picture of Kettlebell subsurface gravel filter, Dover, NH

Table 1: Original and updated watershed characteristics for the Grove St and Kettlebell SGF systems

Parameters	Grove St SGF		Kettlebell SGF	
	Original Values	**Updated Values**	**Original Values**	**Updated Values**
Drainage Area (acres)	1.44	4.10	2.09	2.67
Time of Concentration (min)	8.3	13.7	12.2	11.4
Weighted Curve Number (-)	88	83	92	92
Potential Maximum Retention (in)	1.36	2.05	0.87	0.87
Initial Abstraction (in)	0.27	0.41	0.17	0.17
% Impervious Area	22%	31%	72%	61%
WQV (Ac-In)	0.36	1.35	1.46	1.59
WQV (ft^3)	1307	4910	5296	5771
Constructed Storage Volume (ft^3)	1320	1320	1620	1620
% of WQV	101%	27%	31%	28%

The Grove St system design includes four catch basins, referred to as CB #1-4, located at the four corners of the system's rectangular, gravel filtration layer. Horizontal, perforated and slotted, HDPE pipes are embedded within the gravel layer and run along the perimeter of the system, connecting the catch basins. The whole system is approximately 60 feet long by 25 feet wide with a 2.2-foot deep layer of ¾-inch crushed stone. Figure 5 presents a simplified diagram of the stormwater control measure. Figure 59, Figure 60, and Figure 61 in the Appendix, are the original design diagrams for the system. Various changes to the system design, which occurred during and after construction, will be discussed in Section 3.4 of this report.

During rain events, runoff flows into the system's four catch basins. The water can then enter the SGF's stone layer through the five perforated and slotted inlet pipes which run between the catch basins. CB #1 and 2 are connected by a 6-inch diameter, slotted lower pipe and a 12-inch diameter, perforated upper pipe; CB #1 and 4 are connected by a single 6-inch diameter, slotted pipe; and CB #3 and 4 are connected by upper and lower 6-inch diameter, slotted pipes.

The lower pipes allow water to enter the gravel filter, filling the system from the bottom up, during low flow conditions. In the gravel layer, runoff water filters through the media and can infiltrate into the native soils surrounding the system. If the inflow rate exceeds the infiltration rate, water will pond in the gravel layer, filling the pore spaces of the stone media.

The two lower inlet pipes between CB #1, 3, and 4 also act as underdrains which drain the gravel filter layer to CB #4. Water can then flow out of the system though a 12-inch diameter pipe that discharges to a rip-rap lined swale draining towards Berry Brook. According to the design, outflows are regulated by the tee fitting on the outlet pipe in CB #4. Low flows are controlled by 1-inch orifice hole in the restrictor plate at the bottom of the tee fitting, while high flows are controlled by the open top of the tee. If the system's gravel layer fills, excess runoff will bypass the filter layer and flow directly the CB #4 through the 6-inch diameter, slotted pipe connecting CB #3 to CB #4. Due to the elevation of the outflow pipe in relation to the system's other pipes, the system will drain between rain events, even if the permeability of native soils limits infiltration.

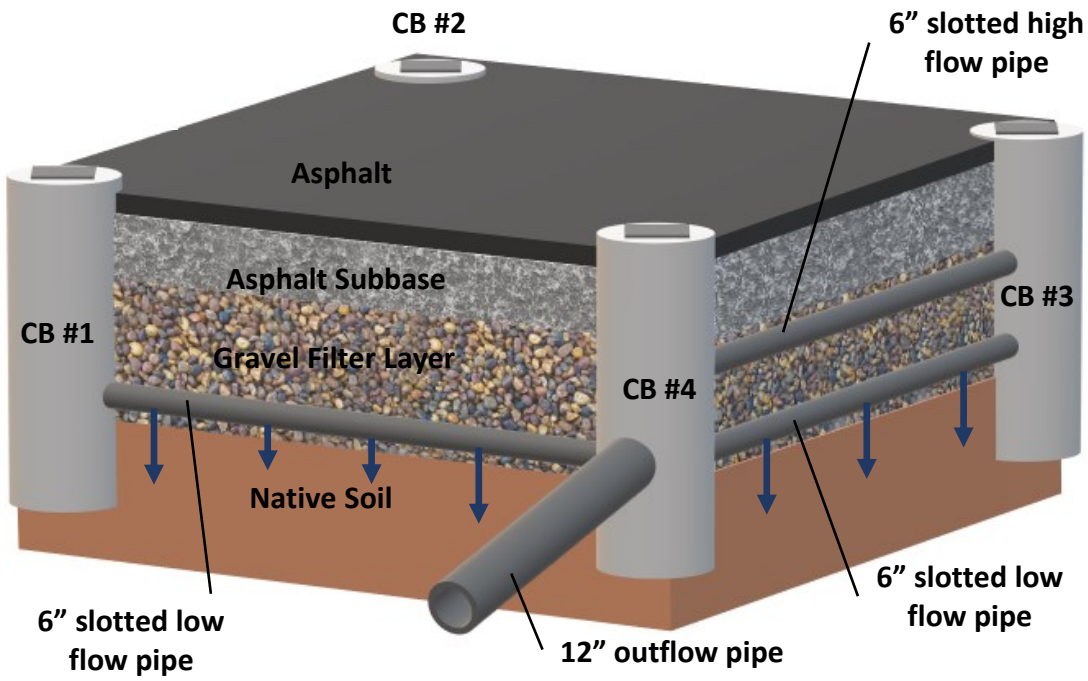

Figure 5: Diagram of the Grove St subsurface gravel filter

The Kettlebell System, presented in Figure 6, has a simpler design with a single 12-inch diameter, slotted, HDPE pipe running through the center of the gravel filtration layer between a catch basin (CB #1) and a manhole (MH). According to the design, surface runoff drains to CB #1 from the surrounding parking lot and an inline network of three other catch basins located throughout the paved portion of the watershed. The runoff then enters the slotted inlet pipe and drains down through the gravel layer, where it may be temporarily stored until it can infiltrate into the surrounding native soils underneath the parking lot. The Kettlebell SGF’s filtration layer is approximately 60 feet long by 30 feet wide and consists of a 2.5-foot deep layer of ¾-inch crushed stone. When the system’s storage fills, water bypasses the gravel filter layer and flows directly to Berry Brook through the 12-inch diameter, corrugated metal, outlet pipe attached to CB #1. Detailed design diagrams for the system are presented in Figure 62 and Figure 63 in the Appendix.

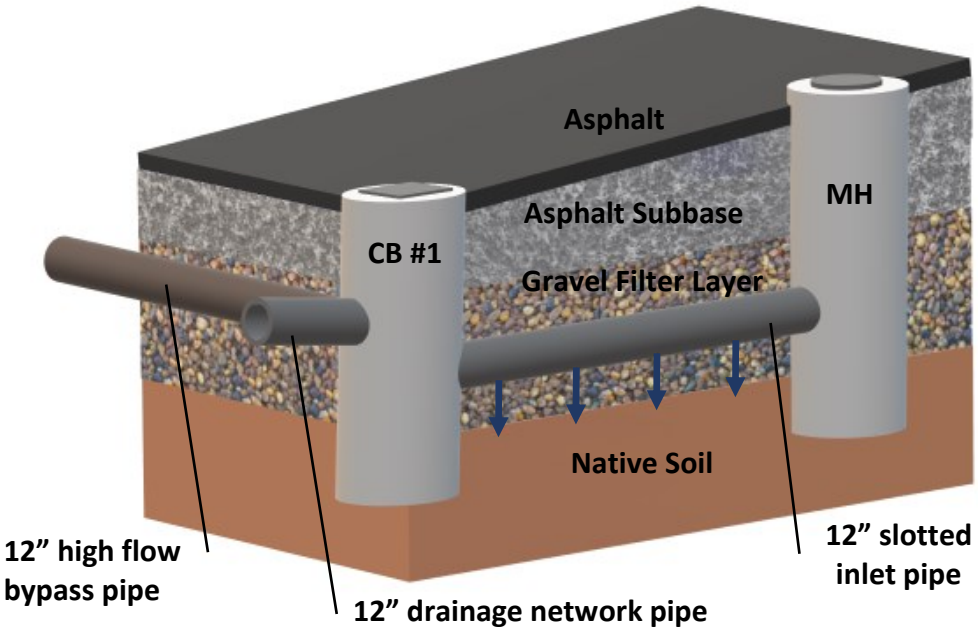

Figure 6: Diagram of Kettlebell subsurface gravel filter

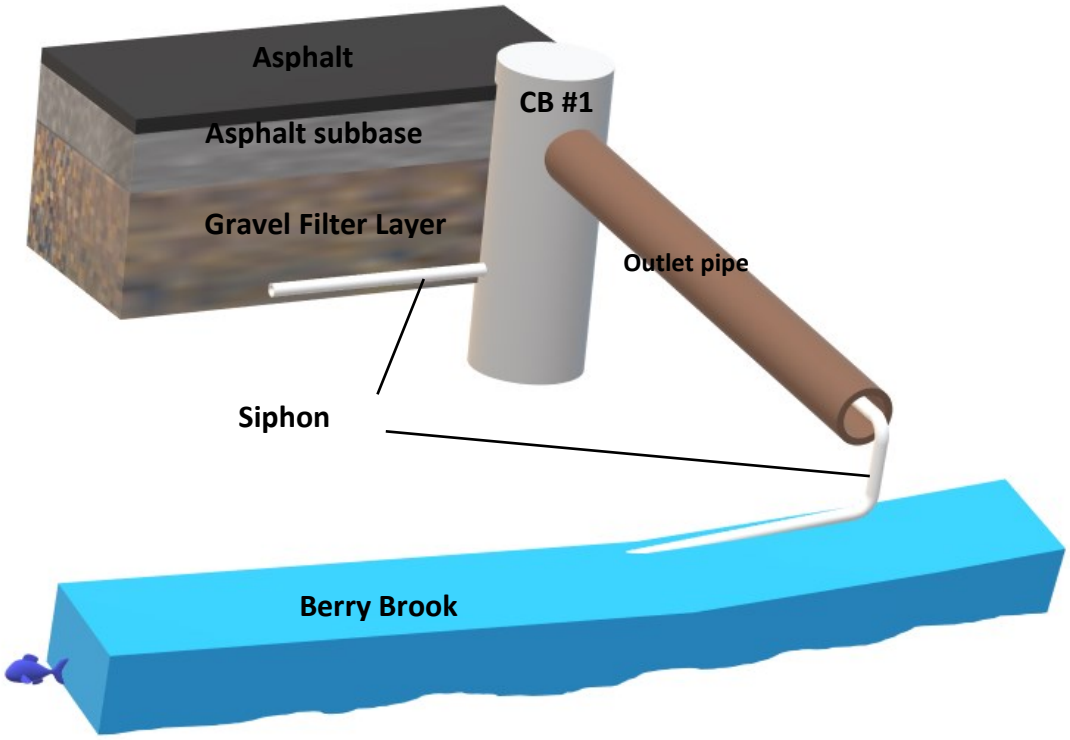

Figure 7: The siphon in the Kettlebell SGF

Unlike the Grove St SGF, the Kettlebell system can only drain by infiltration because the invert of the system's outlet is at a higher elevation than the inlet pipe. The elevation of the outlet could not be lowered due to the small elevation difference between the outlet and the water surface elevation (WSE) of Berry Brook. If the outlet were to be lowered, it would be below the WSE of the Brook during high flows and could allow water to back up into system. In order to drain the system between rain events, a 1-inch diameter, PVC pipe was installed along the base of the gravel layer, run up through the outlet pipe to the brook, and extended approximately 40 feet downstream to a location where the water level is significantly lower than the bottom elevation of the gravel layer (see Figure 7). The pipe is designed to act as a siphon for draining the water level down between storms. When the water surface in the system rises above the top of the PVC pipe, water starts to flow through the pipe and out of the system. Theoretically, as the water level drops below the top of the pipe, the system will continue to drain because the difference in elevation between the bottom of the gravel storage zone and the downstream outlet of the PVC pipe should create a positive suction head to maintain flow through the siphon.

3.2 Performance Evaluation based on Water Balance Calculations

The benefits of using SGF technology (i.e. lowering peak flows, removing stormwater pollutants from runoff, reducing stormwater runoff volumes, etc.) are related to the system's ability to store and infiltrate runoff. The primary mechanisms for pollutant removal are sedimentation in the systems' catch basins, filtration by the gravel layer and surrounding soils, surface reactions on the gravel media, and biological activity in the soils. The research described in this report focuses on the hydrologic and hydraulic performance (i.e. the infiltration capacity) of the systems rather than their capacity to remove pollutants. While pollutant removal is an important aspect of stormwater management, it largely depends on the technology's infiltration

capacity. By evaluating infiltration, one can gage a system's ability to remove stormwater pollutants. Additionally, SGFs are proposed to help alleviate CSO discharges by reducing runoff flows that enter combined sewer systems. With this goal in mind, the infiltration and peak flow reduction capabilities are the most important aspects of performance. System performance was examined by conducting water balances for the Grove St and Kettlebell SGFs and determining their infiltration capacity.

The basic water balance equations, Equation 4 and Equation 5, describe how water passes through the SGF systems. These equations are based on the principle of continuity and show that water flowing into the system can either go into storage or leave the system by means of the outlet pipe or by infiltrating into the soil. Runoff may only enter the system from the inlet catch basins due to the impervious asphalt surfaces overlaying the filters. The paved surface also prevents water from being lost to evaporation and transpiration processes, although these processes may be considered negligible during a runoff event. When analyzing a system's ability to infiltrate water, the water balance equation may be rearranged to solve for infiltration rates or infiltration volumes as long as inflow, outflow, and water storage are known.

Equation 4: Water balance equation in terms of flows

$$Q_{in} = Q_{out} + I \pm \frac{\Delta S}{\Delta t}$$

Equation 5: Water balance equation in terms of volumes

$$V_{in} = V_{out} + V_{infil} \pm \Delta S$$

Where:

Q_{in} = inflow (L^3/T)
Q_{out} = outflow (L^3/T)
I = infiltration rate (L^3/T)
ΔS = change in storage (L^3)
Δt = change in time (T)
V_{in} = inflow volume (L^3)
V_{out} = outflow volume (L^3)
V_{infil} = infiltrated volume (L^3)

Water balances were developed for individual storm events to assess performance. For each water balance, incremental flow measurements were integrated over time to calculate total inflow, outflow, and infiltration volumes. Infiltration rates were also calculated in order to analyze how the rates changed throughout a storm and evaluate the relationship between water depth and infiltration rate. Equation 6 was used to calculate the infiltration rates over a specified time interval. While most of the flow and depth measurements were collected with 1- or 5-minute intervals, infiltration rates were calculated using a longer 1-hour time interval due to fluctuations in depth over short time periods. When using similar methods to calculate the infiltration rates for two gravel infiltration trenches, Bergman et al. (2010) found that a 1-hour time interval effectively reduced variability while accurately describing the general relationship between infiltration rate and stored water depth.

Equation 6: Infiltration rate equation based on changes in WSE in system storage

$$I = \frac{V_{in} - V_{out}}{\Delta t} - \left(l * w * \Phi * \frac{h_{before} - h_{after}}{\Delta t} \right)$$

Where:

I = infiltration rate (L/T)
V_{in} = total inflow volume over the time interval (L^3)
V_{out} = total outflow volume over the time interval (L^3)
l = system base length (L)
w = system base width (L)
Φ = porosity of the gravel layer (L^3/L^3)
h_{before} = average WSE at start of time interval (L)
h_{after} = average WSE at end of time interval (L)
Δt = time interval (1-hour)

Infiltration rates were only calculated for those events which produced measurable ponding depths and only when water levels were receding near the end of those events. If ponding did not occur during a rain event, the infiltration capacity of the soil cannot be measured because the infiltration rate was supply limited and all water entering the system infiltrated.

Additionally, calculations of the infiltration rate were only based on the falling water levels near the end of rain events because large fluctuations in the water depth, which may occur during the beginning of a storm, can lead to the calculation of negative infiltration rates. By using data from the end of a storm event, one can insure that inflows are low compared to changes in the water level and will have less of an effect on the infiltration rate calculations.

3.3 Instrumentation and Monitoring

In order to measure flow rates and calculate the infiltration capacity of the Grove St and Kettlebell SGFs, a variety of sensors were installed throughout the systems. Information pertaining to the instrumentation at each monitoring site is provided in Table 2. At the Grove St site, Onset HOBO water level loggers were installed in each catch basin and were used to monitor water levels. The HOBO loggers are sealed, non-vented sensors that measure absolute pressure and temperature according to a set logging interval. The sensors were hung from the catch basin grates using nylon string, as displayed in Figure 8, to keep the sensors at a consistent elevation and allow for easy access throughout the monitoring period. A fifth HOBO water level logger was installed near the end of the lower perforated pipe which runs between CB #3 and CB #4 (see Figure 8). The sensor was used to monitor the water level inside the gravel layer when ponding occurred.

In order to convert the HOBOs' absolute pressure data to water levels, the data was first converted to gauge pressures by means of barometric compensation. An additional HOBO sensor (PTT-BARO) was set up at the UNH Stormwater Center field site, only 5.5 miles from the monitoring sites, to collect barometric pressure data for the correction. According to the HOBO U20 manual, the barometric compensation sensor is within the acceptable usage range of 10 miles. Details regarding PTT-BARO are provided in Table 2. After performing barometric

compensation, the gauge pressures were then divided by the specific weight of water (approximately 62.4 lbf/ft^3 at 4°C) to obtain values for the depths of water above the sensors. Water surface elevations were calculated by adding the depths to the known relative elevations of the sensors (see Table 2).

An Aqua TROLL data logger was installed at the end of the outlet pipe at the Grove St site to measure the depth of water flowing through the pipe. The Aqua TROLL is a vented sensor that can measure a variety of different parameters including pressure, water level, temperature, and conductivity. For the purposes of the research described in this report, the Aqua TROLL logger was only used to collect pressure and temperature data. Unlike the HOBOs, the pressure data collected by the Aqua TROLL is automatically corrected for barometric pressure. This data, along with the water level data collected for each of the catch basins, was used to determine inflows and outflows based on calibrated rating curves. Development of the rating curves will be described in the Section 3.4.

At the Seacoast Kettlebell site, a HOBO water level logger was installed in the systems inlet catch basin (CB #1) to collect pressure and water temperature data. The absolute pressure data was converted, as described previously, to elevations which were then used to calculate flows. No other sensors were installed at this site as monitoring data showed that the water level within CB #1 never dropped below the invert of the outlet pipe. This indicated that the system's gravel storage layer remained completely full throughout the majority of the monitoring period. Possible reasons for this observation will be discussed in Section 4.1.

Table 2: Information for sensors installed at each monitoring site

System	Type of Sensor	Manufacturer/ Model	Raw Pressure Accuracy	Relative Elevation (ft)	Description of the Location	Unique Name
Grove St	Water level logger	Onset HOBO / U20-001-04	± 0.3% FS (0.063 psi)	95.929	Suspended in CB#1; Dover, NH	GSt-1
Grove St	Water level logger	Onset HOBO / U20-001-04	± 0.3% FS (0.063 psi)	95.717	Suspended in CB#2; Dover, NH	GSt-2
Grove St	Water level logger	Onset HOBO / U20-001-04	± 0.3% FS (0.063 psi)	95.323	Suspended in CB#3; Dover, NH	GSt-3
Grove St	Water level logger	Onset HOBO / U20-001-04	± 0.3% FS (0.063 psi)	94.775	Suspended in CB#4; Dover, NH	GSt-4
Grove St	Water level logger	Onset HOBO / U20L-04	± 0.3% FS (0.063 psi)	96.545	Inside lower pipe connecting CB#3 & CB#4; Dover, NH	GSt-4_PrP3
Grove St	Data logger	Win-Situ Aqua TROLL / 200	± 0.05% FS (0.015 psi)	95.985	Downstream end of outlet pipe; Dover, NH	GSt_Outlet
Kettlebell	Water level logger	Onset HOBO / U20-001-04	± 0.3% FS (0.063 psi)	95.098	Suspended in CB#1; Dover, NH	KB-1
-	Water level logger	Onset HOBO / U20-001-04	± 0.3% FS (0.063 psi)	-	UNH SC field site, Durham, NH	PTT-BARO
Horne St Bioretention	Rain gauge	Campbell Scientific, TE525MM	± 1% at 1 in/hr (Resolution: 0.004 in)	-	Horne St, Dover, NH	D3BA1HB2

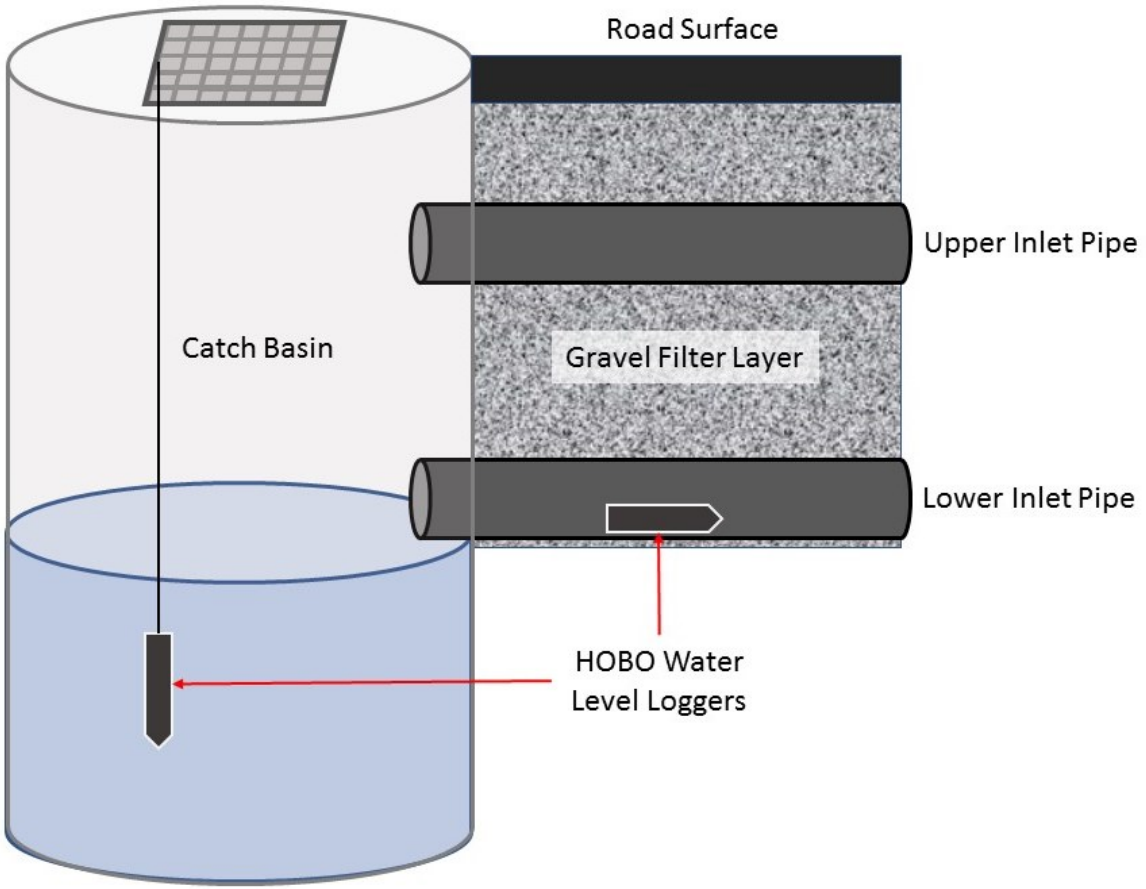

Figure 8: Diagram showing the general location of instrument installation

Rainfall data was collected using a tipping-bucket rainfall gauge, located at a bioretention system along Horne St in Dover, NH. The data from the rainfall gauge was applied to the two SGF monitoring sites because their locations were close enough (i.e. less than 2,000 ft away) that rainfall could be considered reasonably consistent for both sites. As a backup, rainfall data was also obtained from the weather station maintained by UNH at Kingman Farm in Durham, NH. Gaps in the gauge data from Horne St were filled in with data from the UNH weather station.

For this project, all sensors at the monitoring sites were set to either 1 or 5-minute logging intervals. Due to the limited size of the systems' watersheds and high percentage of impervious area, the time of concentration for the stormwater runoff is very short (Table 1). Runoff flows can therefore change quickly during rain events. A short logging interval was used in order to capture the rapid changes in the runoff hydrographs. The HOBO logger used for barometric compensation was set to a slightly longer logging interval of 15 minutes because changes in barometric pressure were more gradual than changes in runoff and the longer interval helped preserve device memory and battery life.

During the 1-year monitoring period, each sensor was periodically checked to verify the accuracy of the device. Accuracy checks were performed by analyzing the sensor reading for a known depth of water in a graduated cylinder. The Aqua TROLL data logger was also calibrated periodically for pressure if the accuracy check showed the sensor's measurements were shifting. The HOBO sensors were all factory calibrated and could not be recalibrated without being sent to Onset for maintenance. None of the HOBO sensors showed any significant reading drifts during the monitoring period that required the sensors to be recalibrated.

3.4 Development of Inflow and Outflow Rating Curve

In order to estimated infiltration rates using the water balance equations, values for inflows, outflows, and changes in water storage had to be obtained. Without a mechanism to directly measure flows, a strategy had to be developed to determine the flow from the water level data. Hydraulic rating curves and stage-storage curves were created to relate water level data to flow rates and storage volumes, respectively.

The water storage volume in the SGFs is linearly related to the depth of water in the systems' stone layer and can be calculated using the stage-storage relationship described by Equation 7. Incremental changes in water storage for the Grove St system were calculated using the depth data from the HOBO water level logger located in the lower pipe connecting CB #3 and #4. A sensor was not needed to measure the change in storage for the Kettlebell system as the filter remained full throughout the monitoring period.

Equation 7: Stage-storage function for gravel storage layer

$$\Delta V = \Delta d \times A_s \times \varphi$$

Where:

ΔV = change in stored water volume (ft^3)
Δd = change in depth (ft)
A_s = surface area of filter bed (ft^2)
φ = porosity of gravel (-) ≈ 0.40

3.4.1 Rating curves for the Grove St system

Unlike the stage-storage curve, flow calibration tests were required to relate water levels and flow rates. For the Grove St system, water can only enter through the system's four catch basins and leave through the system's outlet pipe or by infiltrating into the soil. To calculate flows through the outlet pipe, a rating curve (Equation 8) was developed, which relates the water surface elevation (WSE) in CB #4, measured with sensor GSt-4, to the outflow rate from the

system. The decision was made to use the rating curve developed from the HOBO water level data for all outflow calculations because this sensor was more reliable and produced a more complete data set than the Aqua TROLL sensor (GSt_Outlet) installed in the outlet pipe. The Aqua TROLL data and the rating curve, presented in the Appendices, were primarily used to validate the data from GSt-4.

Equation 8: Rating curve based on HOBO water level data

$$Q_{out} = 448.376 \times (h_{CB\#4} - h_{out})^{2.449}$$

Where:

Q_{out} = Outflow (cfm)
d_{outlet} = depth of flow in the outlet (ft)
$h_{CB\#4}$ = WSE in CB #4 (ft)
h_{out} = 96.227ft = relative elevation of the outlet pipe invert in CB #4 (ft)

The outflow rating curve was developed using a bucket-and-stopwatch technique. During rain events, water flowing from the outlet pipe at the Grove St site was collected with a 5-gallon bucket over a measured period of time. The collected water volume was divided by the collection time to produce a flow rate which could then be paired with the water level measurement taken at the time of collection. By repeating this procedure for a variety of different flows, each of the associated flow and water level measurements were then graphed on a coordinate plot to define the relationship between water level and flow (i.e. the rating curve). A power function was then fitted to the data points to produce the outflow rating curves. Figure 9 present the measured water level and flow data along with the associated power function.

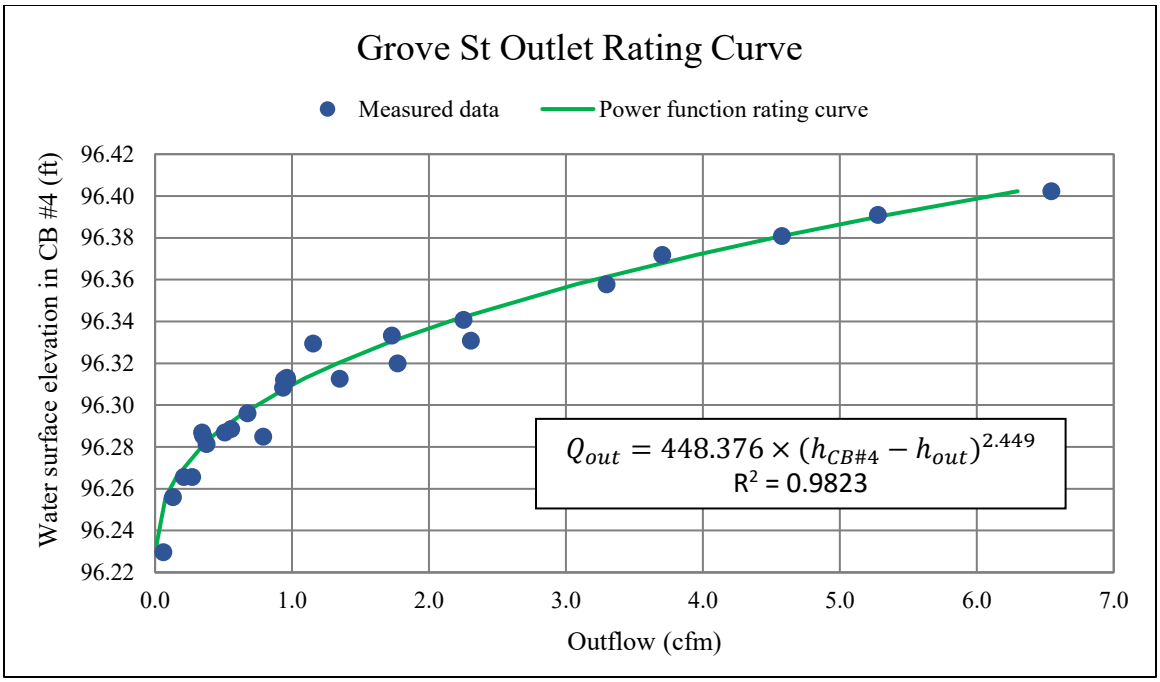

Figure 9: Outflow rating curve for the Grove St system, based on water surface elevation ($h_{CB\#4}$) in CB #4

Inflows into the Grove St SGF were more difficult to determine due to the type and number of inlets. Water can only flow into the filter from the perforated inlet pipes that connect the systems four catch basins. Each end of the pipes is another potential inlet for water to enter the gravel filter bed. Several modifications were made to the Grove St system during and after construction in order to simplify the system for monitoring purposes and improve system performance. For example, according to the original design drawings (see Figure 60 and Figure 61), the underdrain pipes were supposed to have hooded inlets to allow water to enter while preventing floating debris from flowing in and clogging the pipes. However, during construction the hoods were replaced with caps in order to force the majority of the runoff to flow into the system through the upper pipes, increasing the amount of filtration provided by the gravel layer. The caps restrict inflow without completely stopping it because water can still flow into the lower pipes through the slots around the protruding ends of the pipes.

The original design also specified that some of the pipes, specifically the underdrains connected to CB #4, were supposed to have their ends sealed with caps. The caps had 1-inch holes drilled in them to allow the system to drain, while also helping to restrict outflows. During the monitoring phase of this research project, these drilled caps were replaced with solid ones and the protruding ends of the lower pipes in CB #4 were completely sealed. This modification prevented water from draining into CB #4 from the underdrain pipes and forced water to leave the gravel layer by infiltration or by means of the overflow bypass. CB #4 was further modified when perforations in the walls of the catch basin were discovered early in the monitoring phase. These holes were allowing water to flow out of the catch basin without going through the outlet and made it difficult to actually measure outflows and inflows during storm events. These perforations were sealed with expanding foam and quick-drying concrete to force water to leave the catch basin through the outlet pipe. After the perforations were sealed, the outlet started producing a constant baseflow due to seepage into the catch basin from the ground water table. When calculating the flows due to stormwater runoff, a net outflow was calculated by subtracting the baseflow from the total outflow.

Another modification made to the system design was to leave off the tee fitting at the opening to the outlet pipe (see CB #4 in Figure 60). This fitting included a restrictor plate with a small 1-inch orifice to throttle outflow and force water to fill the stone layer before flowing out of the system. By sealing up the ends of the lower slotted pipes in CB #4, as described above, the tee was no longer needed to restrict outflows and fill the system. Any water that enters CB #4, immediately leaves through the outlet and does not enter the system. This modification, and those previously described, significantly simplified the flow paths through the system so that flows could be more easily measured.

Rating curves were developed for each of the seven inlets to relate water levels in the catch basins to inflow rates. For low flows, the water level in the catch basins stays below the upper pipe inlets and enters the system through the slots in the protruding ends of the lower pipes. During larger runoff events, water fills the catch basins until all of the inlet pipes are flowing. Consequently, rating curves were separated into two categories: low flow curves and high flow curves.

The high flow rating curves were developed using a bucket-and-stopwatch technique, but at a much larger scale. For each catch basin, water was pumped into the basin at a constant flow rate causing the water level to rise and flow into the system. Once the water level became constant, the flow rate and measured water level were recorded. This process was repeated numerous times at different flow rates for each of the system's catch basins. The flow and water level data were then graphed and a regression curve was fit to the data points. With some assistance from the Dover CSD and one of their sewer/catch basin cleaning trucks, high flow rating curves were developed for CB #1-3. The truck had a 1500-gallon water tank and a water jet that could produce flows ranging from 3.5 to 6.5 cubic feet per minute (cfm). Flows were measured with the bucket-and-stopwatch technique using a 50-gallon rain barrel and a stop watch. Water depths were measured with the hanging HOBO water level loggers that were already installed in the catch basins and with an additional HOBO logger that was mounted to the inside a makeshift, stilling well. The stilling well was used to minimize pressure fluctuations caused by the water jet and was made from a 10-foot long, 2-inch diameter PVC pipe with 10-20 quarter inch holes drilled in it. During inflow calibration, the stilling well sensor was set to a 10-second logging interval. The high flow rating curves are presented in Figure 10, Figure 11, and Figure 12. Their corresponding power functions are presented in Equation 9.

Equation 9: High flow rating curves for inflow

$$Q_{HF1} = 7.3103 \times (h_1 - h_{U1})^{0.5967}$$

$$Q_{HF2} = 7.0800 \times (h_2 - h_{U2})^{0.5154}$$

$$Q_{HF3} = 54.4076 \times (h_3 - h_{U3})^{1.8222}$$

Where:

Q_{HF1} = inflow into upper pipe from CB #1 (cfm)
Q_{HF2} = inflow into upper pipe from CB #2 (cfm)
Q_{HF3} = inflow into upper pipe from CB #3 (cfm)
h_1 = water surface elevation in CB #1 (ft)
h_2 = water surface elevation in CB #2 (ft)
h_3 = water surface elevation in CB #3 (ft)
h_{U1} = Elevation of upper pipe invert in CB #1 (ft) = 98.775ft
h_{U2} = Elevation of upper pipe invert in CB #2 (ft) = 98.605ft
h_{U3} = Elevation of upper pipe invert in CB #3 (ft) = 98.735ft

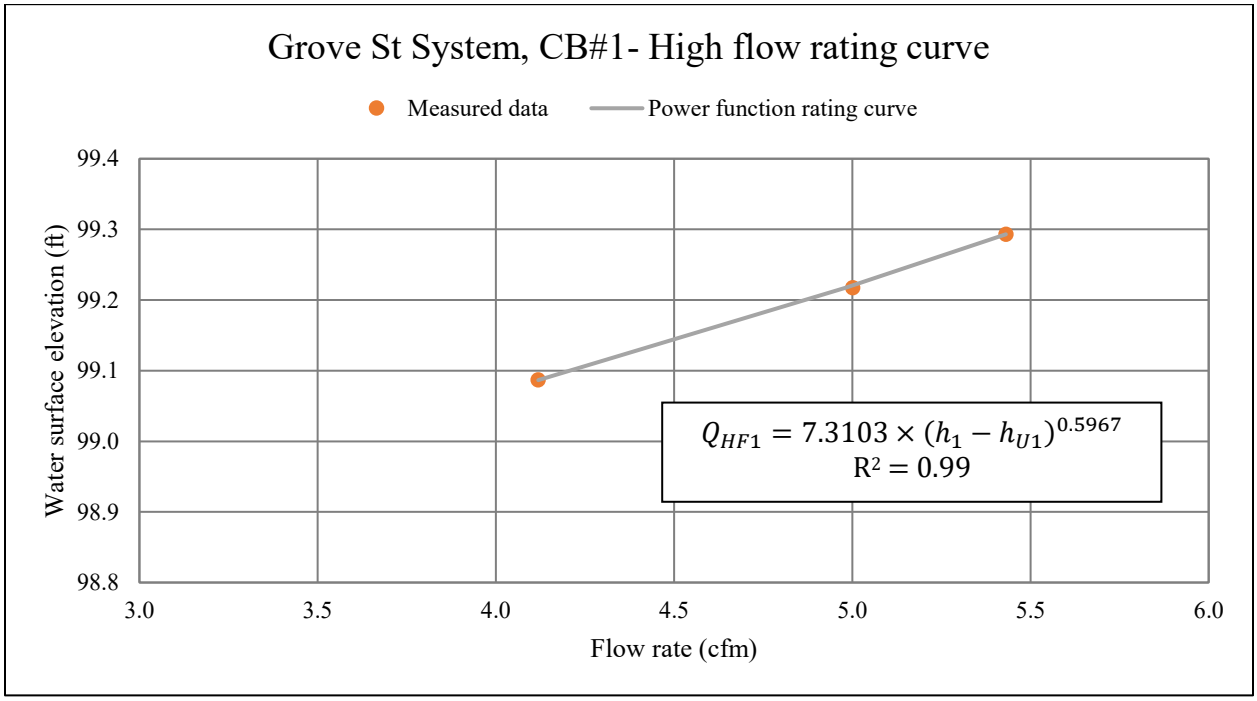

Figure 10: High flow rating curve for CB#1

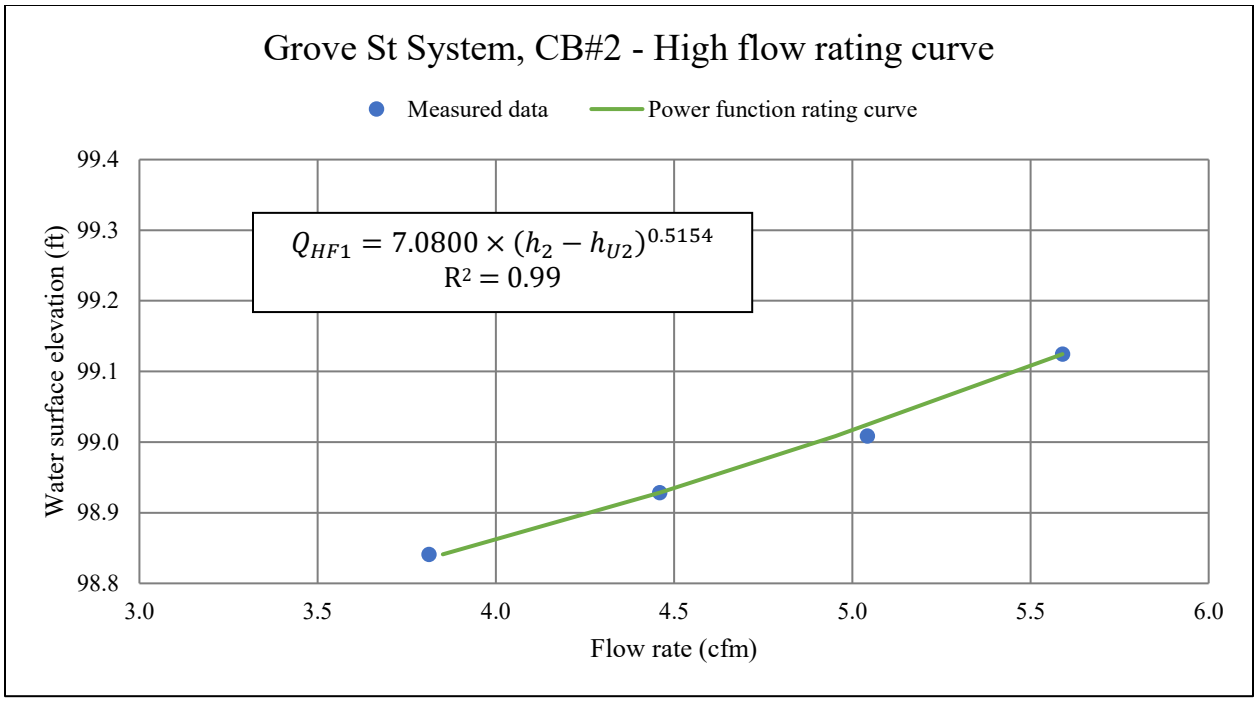

Figure 11: High flow rating curve for CB #2

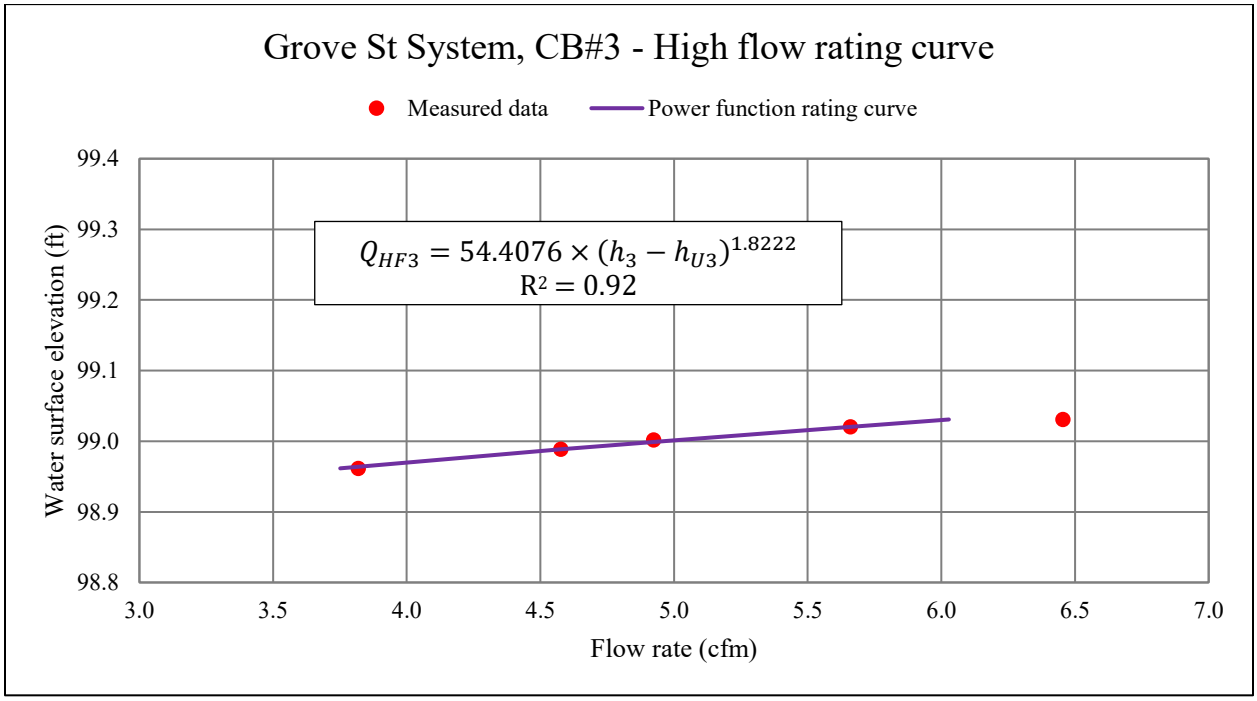

Figure 12: High flow rating curve for CB #3

The water jet on the catch basin cleaning truck was not suitable for developing the low flow rating curves because the truck's water jet was only operable for a small range of flows. Low flow curves were developed by monitoring the recession rate of the water level in each of the catch basins after they were filled. Figure 13 shows how the WSE decreased in CB #3 after the flow calibration testing.

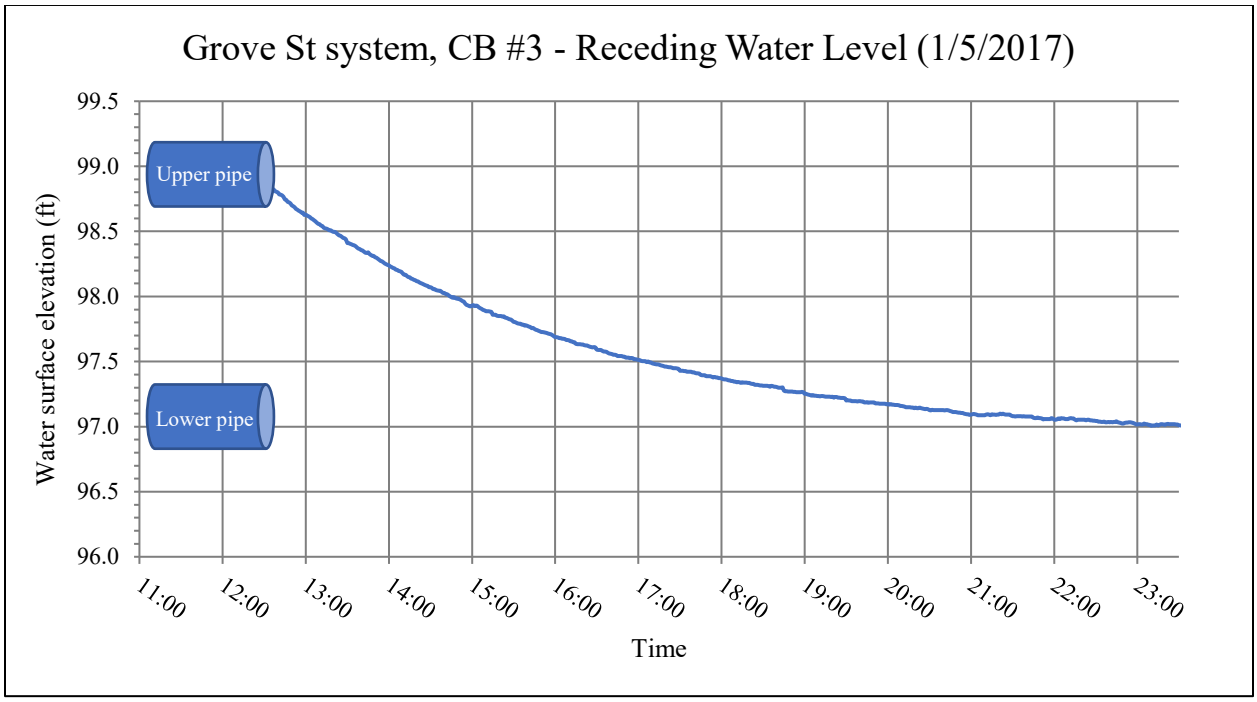

Figure 13: Receding water surface elevation in CB #3

When inflows are negligible, the rate at which the water level recedes in a catch basin corresponds to the flow rate into the gravel storage layer through the lower inlet pipes. As the water level decreases, the flow rate into the system decreases due to the reduction in hydraulic head. By calculating the incremental flow rate using Equation 10, one can construct a rating curve that relates WSE and inflow. Once the water level dips below the invert of the upper pipe, the flow into the stone layer is entirely controlled by the lower inlet pipe. The low flow rating curve can therefore be derived from the changing water level. However, this is only valid if the water level in the system does not affect inflows. Incremental flow rates were calculated by

dividing incremental changes in water depth by the amount of time it took that change to occur and then multiplying by the cross-sectional area of the catch basin, as shown by Equation 10. Each incremental flow rate was then paired with the average WSE for the time period over which the water level dropped. This flow and WSE pair are a single point for one of the low flow rating curves. By repeating the flow calculation and WSE averaging over a long period of time, a full rating curve was developed from the values.

Equation 10: Equation for inflow based on incremental change in WSE

$$Q_{in} = \frac{\Delta h}{\Delta t} * A_x$$

Where:

Q_{in} = inflow (cfm)
Δh = change in WSE (ft)
Δt = change in time (min)
A_x = cross-sectional area of the catch basin (ft) ≈ 4ft

A variety of incremental time steps (Δt) were analyzed to see how long the time step needed to be in order to create a well-defined hydraulic rating curve. Due to the restrictive openings of the lower inlets, the flow rate through these pipes is fairly miniscule (i.e. < 0.5 cfm). If a short Δt is used, tiny random variations in the flow rate are amplified due to the limited change in the WSE that occurred over the time step. Longer Δt values help to smooth out the random variation; however, with longer the time steps more information is lost to averaging and changes in flow rate become more linear. Δt value between 10 and 60 minutes were used depending on how slow the inflow rates were for each catch basin. In some instances, two different time steps were used: a shorter Δt for when the WSE was higher and dropping more rapidly and a longer Δt when the WSE was lower and dropping more slowly. Figure 14 demonstrates how the various times steps affected the spread of the data for CB #1's low flow rating curve. The figure also shows how the low flow rating curves for CB #1 and 2 have a distinct shift when the water level approaches the tops of the lower inlet pipes. This shift was accounted for using a piecewise function to describe the low flow rating curve in each basin. All of the power functions that were fitted to the flow data are presented in

Equation 11. Figure 15, Figure 16, and Figure 17 present the final rating curves with their fitted power function for catch basins 1, 2, and 3, respectively.

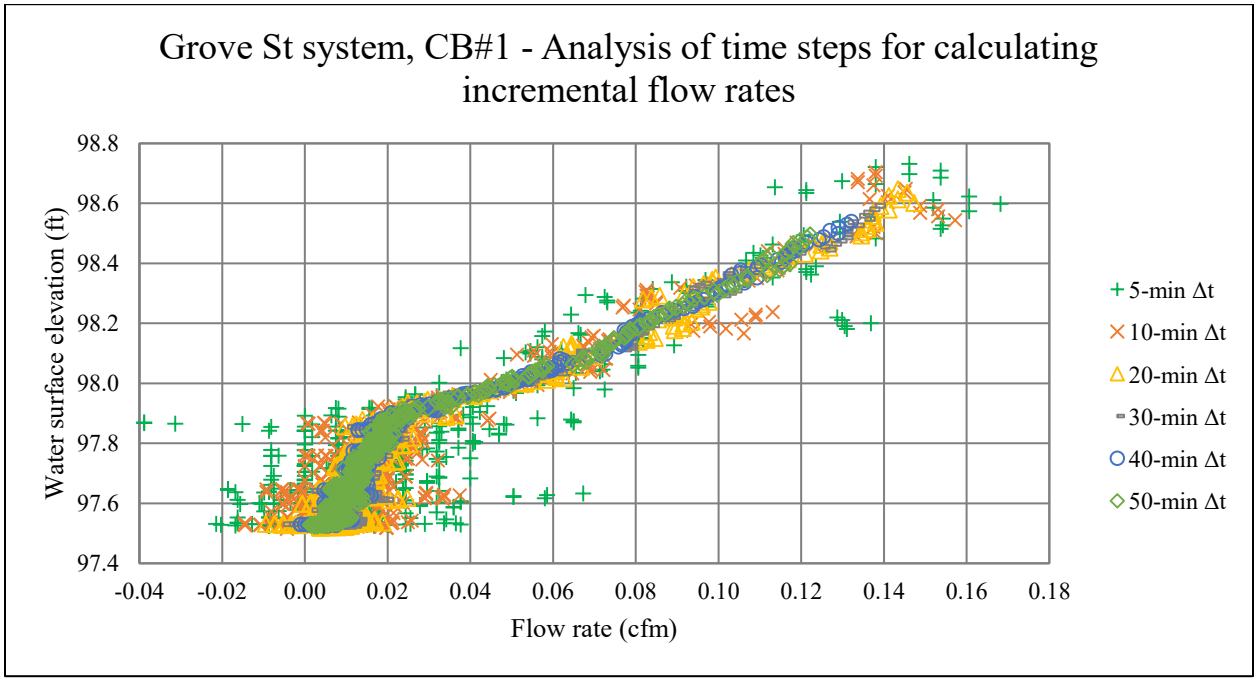

Figure 14: The calculation of incremental flow rates (Q_{LFI}) based on various time steps (Δt) for CB #1 - Grove St SGF

Equation 11: Low flow rating curves for inflows in the Grove St system

$$h_1 > 97.865, \quad Q_{LF1} = 0.1714 \times (h_1 - 97.865)^{0.6273}$$

$$h_{L1} \leq h_1 < 97.865, \quad Q_{LF1} = 0.0353 \times (h_1 - h_{L1})^{2.2681}$$

$$h_2 > 97.677, \quad Q_{LF2} = 0.2938 \times (h_2 - 97.677)^{0.6688}$$

$$h_{L2} \leq h_2 < 97.677, \quad Q_{LF2} = 0.2281 \times (h_2 - h_{L2})^{2.6690}$$

$$h_3 \geq h_{L3}, \quad Q_{LF3} = 0.0515 \times (h_3 - h_{L3})^{1.0548}$$

Where:

Q_{LF1} = inflow through lower inlet in CB #1 (cfm)
Q_{LF2} = inflow through lower inlet in CB #2 (cfm)
Q_{LF3} = inflow through lower inlet in CB #3 (cfm)
h_1 = WSE in CB #1 (ft)
h_{L1} = Elevation of the lower inlet pipes in CB #1 = 97.075ft
h_2 = WSE in CB #2 (ft)
h_{L2} = Elevation of the lower inlet pipe in CB #2 = 97.185ft
h_3 = WSE in CB #3 (ft)
h_{L3} = Elevation of the lower inlet pipe in CB #3 = 96.850ft

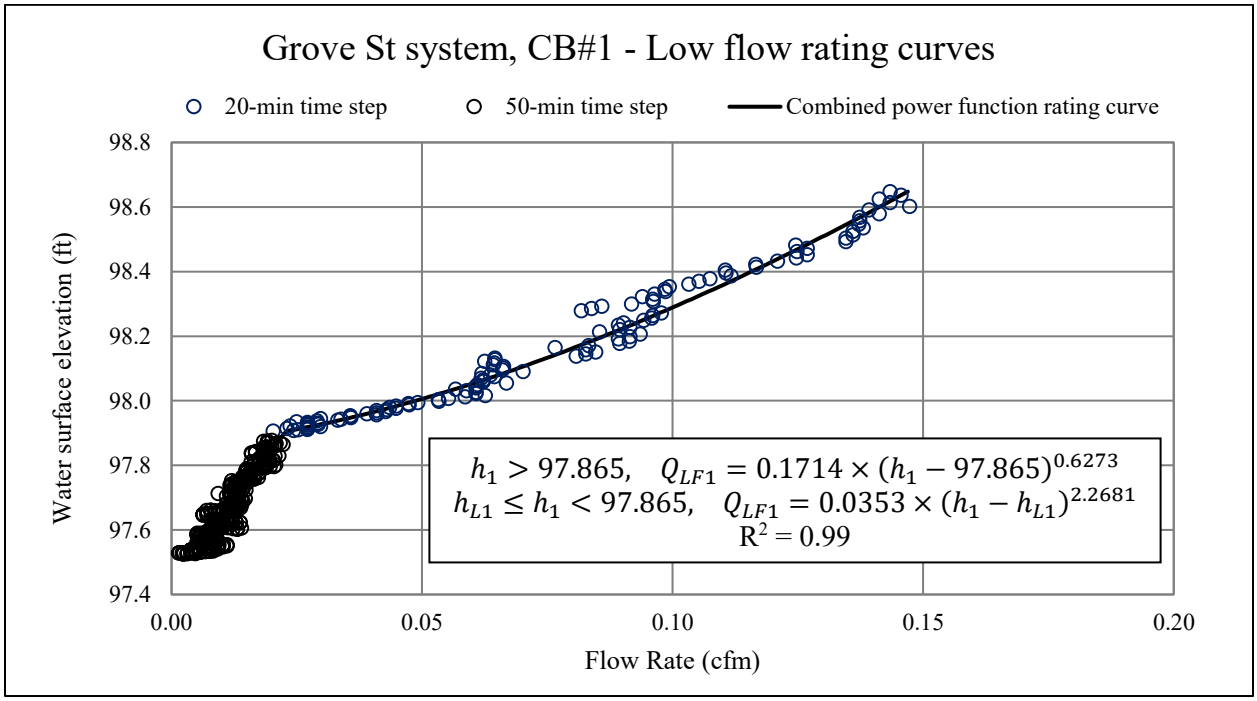

Figure 15: Low flow rating curve and fitted power function for CB #1 - Grove St SGF

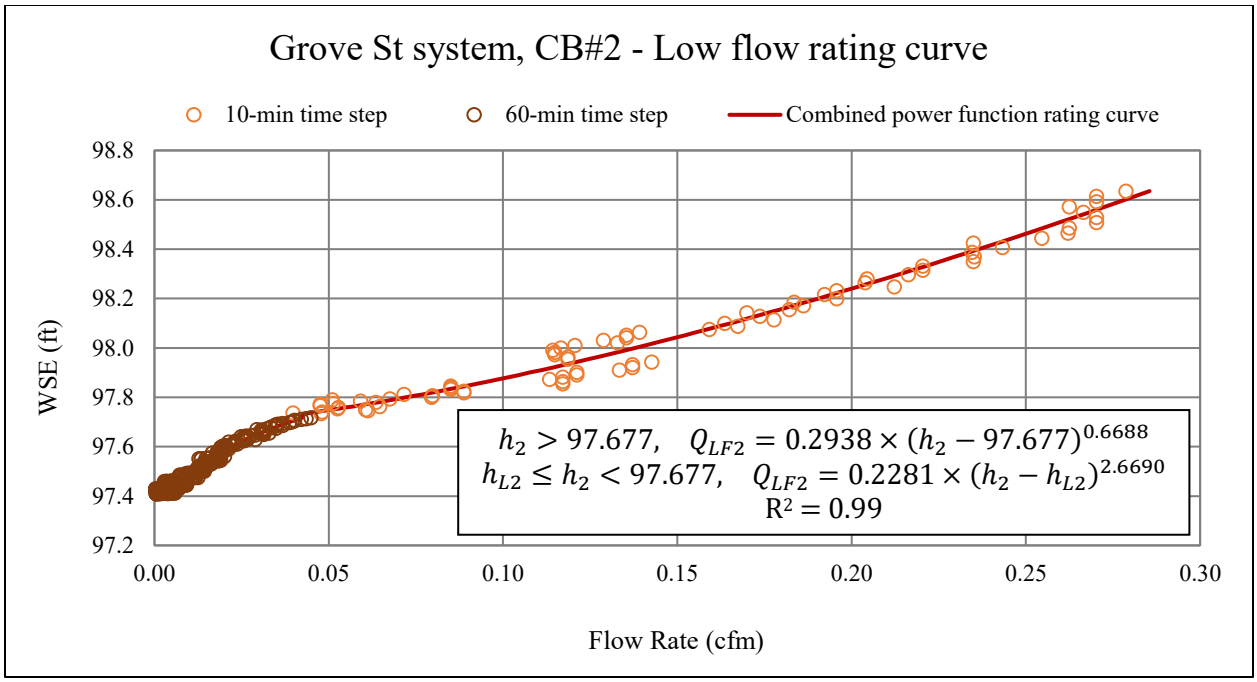

Figure 16: Low flow rating curve and fitted power function for the CB #2 - Grove St SGF

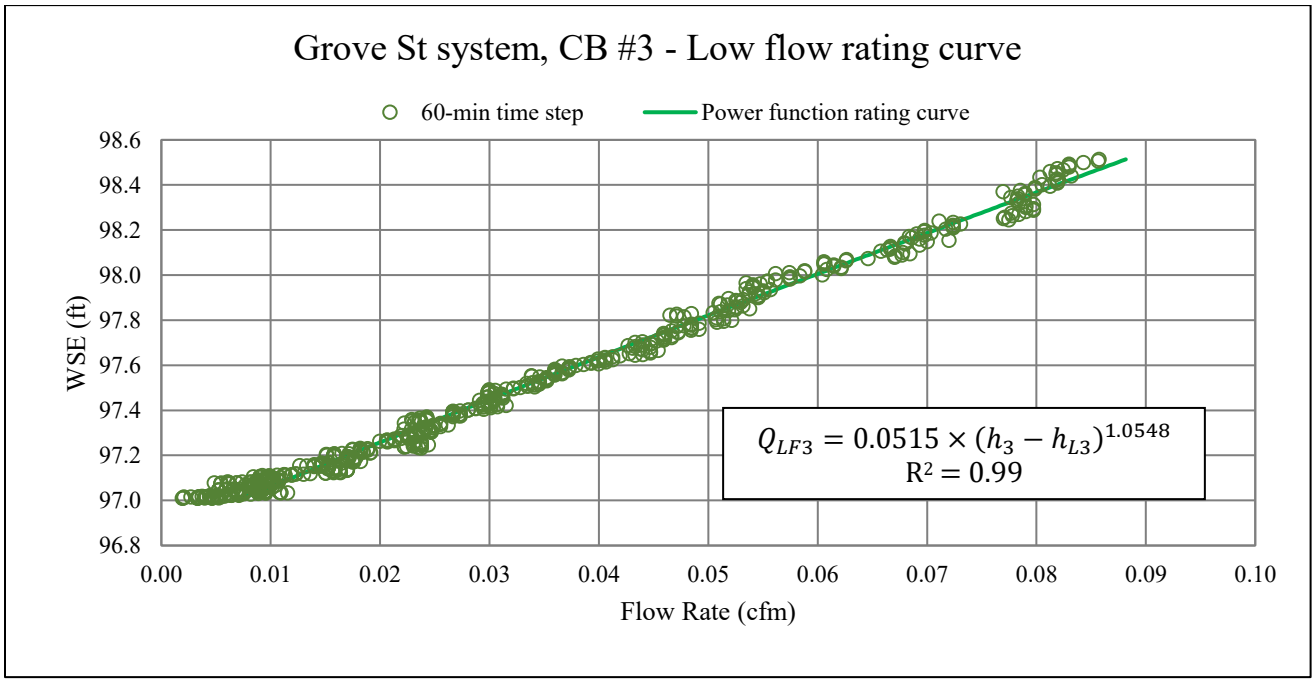

Figure 17: Low flow rating curve and fitted power function for CB #3 - Grove St SGF

The validity of the high and low flow rating curves relies on several of assumptions. One is that the perforated/slotted inlet pipes provide high enough drainage rates that water cannot flow from one catch basin into another unless the system storage is completely filled. This means that all of the water entering the inlet pipe flows into the gravel storage layer and that each catch basin can be calibrated separately since the flow out of one basin should not influence the amount of water in another. Therefore, the rate of flow into the storage layer is equal to the flow rate out of a catch basin. This assumption should be valid if the perforated/slotted pipe have similar drainage rates to those which were measured in a laboratory experiment performed by the UNHSC (UNHSC, 2015). Details of the results of this experiment will be discussed in Section 3.6 of this report.

Another assumption is that drainage through the inlet pipes is not influenced by the water level in the storage layer unless the system is full. The rating curves could potentially change if the water level inside the system were to rise, thereby reducing the total driving head for inflow. For the high flow curves, this assumption should be valid because the water is entering the upper pipes, draining through the slots or perforations, and then trickling down through the gravel layer until it reaches the underlying native soils or the ponded water in the stone. However, this assumption may not be preserved for the low flow curves, as the system's lower pipes are positioned just above the bottom of the gravel layer. If the water level in the system rises above the inverts of the pipes, the low flow rating curves may be inaccurate. However, the effect on the total system water balance should be miniscule because the amount of water that can pass through the slots in the protruding ends of the lower pipes is very small in comparison to the amount of flow being passed by the upper pipes.

The last major assumption is that the rating curves do not change over time. When the system was first constructed in 2015, the pipes were new and clear of debris and probably had drainage rates very close to those measured by UNHSC in a laboratory setting (UNHSC, 2015). Over time, as dirty runoff flows through the system, sediment, leaf litter, and other debris can clog the perforations and slots in the inlet pipes, restricting the flow rates. The system's catch basins provide some pretreatment, settling out large sediments and debris, while the caps at the ends of the lower pipes and the hooded attachments on the upper pipe help reduce the amount of floating debris that enter the pipe. However, suspended fine sediments cannot be completely removed from the water and appear to have settled on the bottom of the inlet pipes as the runoff drains into the gravel storage layer. When sensors were first installed in July of 2016, little was known about the condition of the perforated and slotted inlet pipes. However, during one of the initial flow calibration tests, it was discovered that there was a small layer of sediment along the bottoms of the pipes which reduced their drainage capacity. Assuming this layer did not significantly increase, or was not removed, during the monitoring period, the rating curves developed for each catch basin should not have change significantly. In order to maintain the drainage capacity of the pipes and overall systems performance, periodic maintenance should be conducted to remove sediment from the pipe and clean large sediments from the catch basins. Maintenance will be discussed further in Section 5.1.

In addition to altering the drainage rates of the inlet pipes, the sediment in the pipes affected how water moved through the system during runoff events. This, in turn, had an effect on how the rating curves could be used to calculate inflows into the gravel layer because the assumption that water could not pass from one basin into another was invalid. The sediments had clogged the bottom of the upper pipes to the point where water could flow between CB #1 and 2

and from CB #3 to CB #4 during high flows. Due to this phenomenon, use of the high flow rating curves was modified, as described next, to account for the connectivity of flow between the catch basins.

For CB #1 and 2, the flow calibration tests were altered so that both catch basins were filled to almost the same water level before data was collected. The catch basins therefore share a high flow rating curve when the water level in each basin reaches the same level above the invert of the perforated high flow pipe. Figure 18 illustrates this concept. Both catch basins were still tested separately and were found to have similar rating curves, yet not quite similar enough to be considered the same. This may be due to minor differences in the water level between the basins and drainage rates of various sections of the inlet pipe. To make up for this difference, water balance calculations were performed using whichever curve corresponded to the basin with a higher WSE.

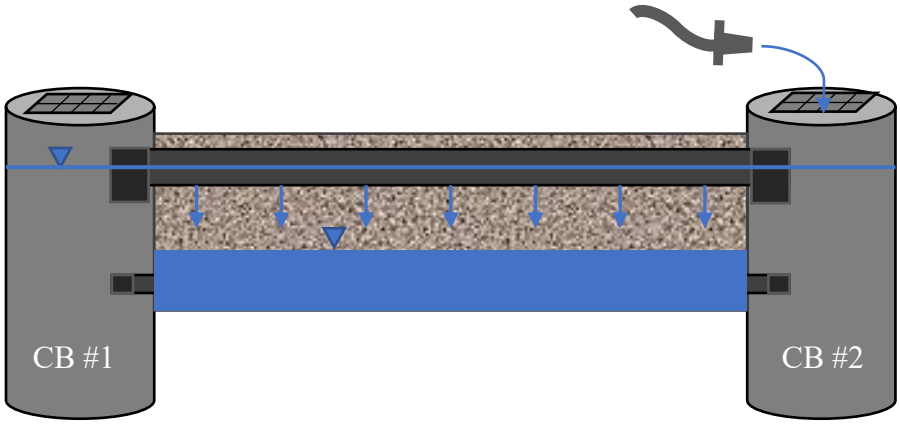

Figure 18: Development of combined inflow rating curve for CB #1 and 2, Grove St system

For example, if the WSE was slightly higher in CB #2, the high flow rating curve developed for this basin was used to calculate the combined inflow from CB #1 and 2. If the opposite was true, the rating curve developed for CB #1 was used. Overall, this strategy enabled

the curves to be used for the system even though the two basins are not completely independent of each other. The power function rating curves that were fitted to the measured data are presented in Equation 9.

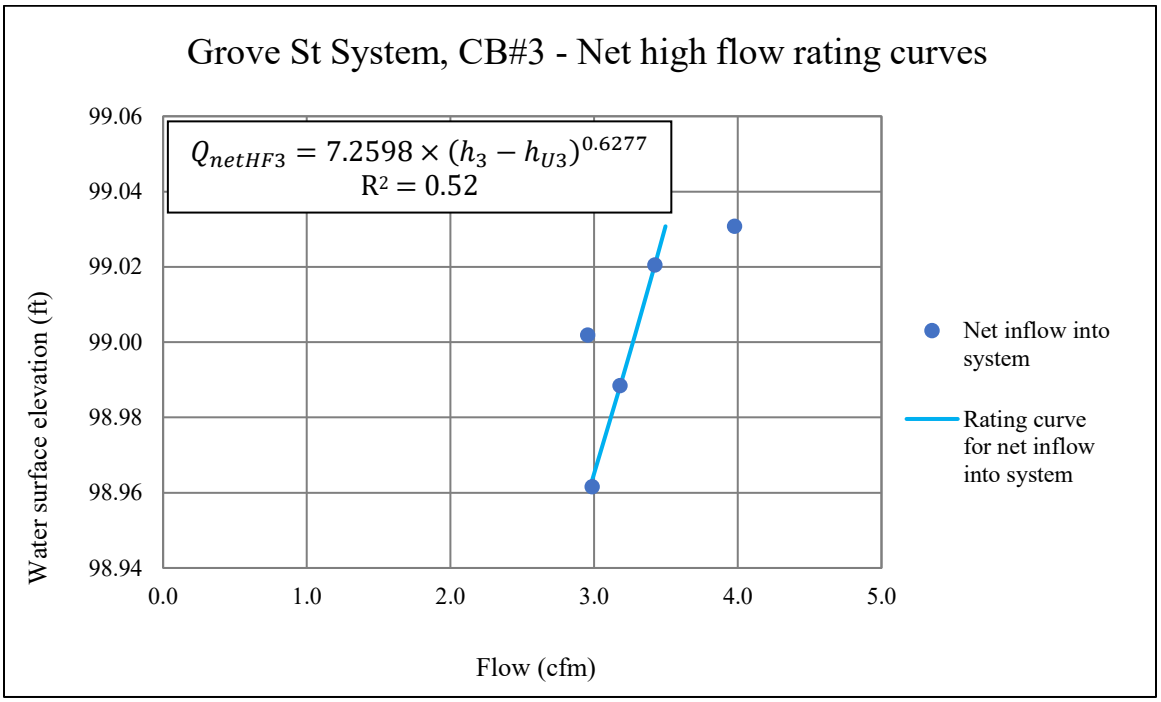

Figure 19: Rating curves describing high flows from the fourth catch basin (CB #4)

For CB #3 and 4, the flow calibration did not have to be redone; however, multiple rating curves needed to be combined in order to account for the amount of water bypassing the gravel storage layer. During the high flow calibration testing for CB #3, the water level in CB #4 was monitored. The rating curve for the flow out of CB #4 was used to calculate how much water was flowing into CB #4 from CB #3. This flow rate was then subtracted from the total inflow rate of CB #3 to produce the net inflow of water draining into the gravel layer. Figure 19 displays the net high flow rating curve for CB #3 and the fitted power function (i.e.

Equation 12).

Equation 12: Power function for net high flow rating curve of CB #3 in Grove St system

$$Q_{netHF3} = 7.2598 \times (h_3 - h_{U3})^{0.6277}$$

Where:

Q_{netHF3} = net inflow into system from CB #3 (cfm)
h_3 = WSE in CB #3 (ft)
h_{U3} = Elevation of upper pipe invert in CB #3 = 98.735ft

3.4.2 Rating curves for the Kettlebell system

Flow rate calculations for the Seacoast Kettlebell SGF were far simpler than those required for the Grove St system. Due to the elevation of the outlet pipe above the system inlet and the extremely low permeability of the surrounding native soils (see Section 3.5), the system remained completely filled through the entire monitoring period. All of the runoff entering CB #1 flowed directly to Berry Brook through the outlet pipe without entering the system. As discussed in Section 3.1, a siphon was installed in the Kettlebell SGF to help drain the system between storms. However, due to a lack of hydraulic head, entrapped air, and/or potential air leaks in the connections between the PVC pipes, the siphon was ineffective at draining the filter.

For flow calculations, inflows were equal to outflows and only one rating curve was needed to calculate flow rates. The sewer or catch basin cleaning truck was used to develop the rating curve as described in the previous section of this report. A power function (Equation 13) was fitted to the data points and used to calculate flows into and out of CB #1 based on the WSE in the catch basin. A graph of the rating curve and power function are presented in Figure 20.

Equation 13: Power function rating curve for CB #1 in the Kettlebell system

$$Q_{Kb} = 49.679 \times (h_{Kb1} - h_{out})^{0.731}$$

Where:

Q_{Kb} = Kettlebell system flows (cfm)
h_{Kb1} = WSE in CB #1 (ft)
h_{out} = Elevation of the outlet pipe in CB #1 (ft) = 97.06ft

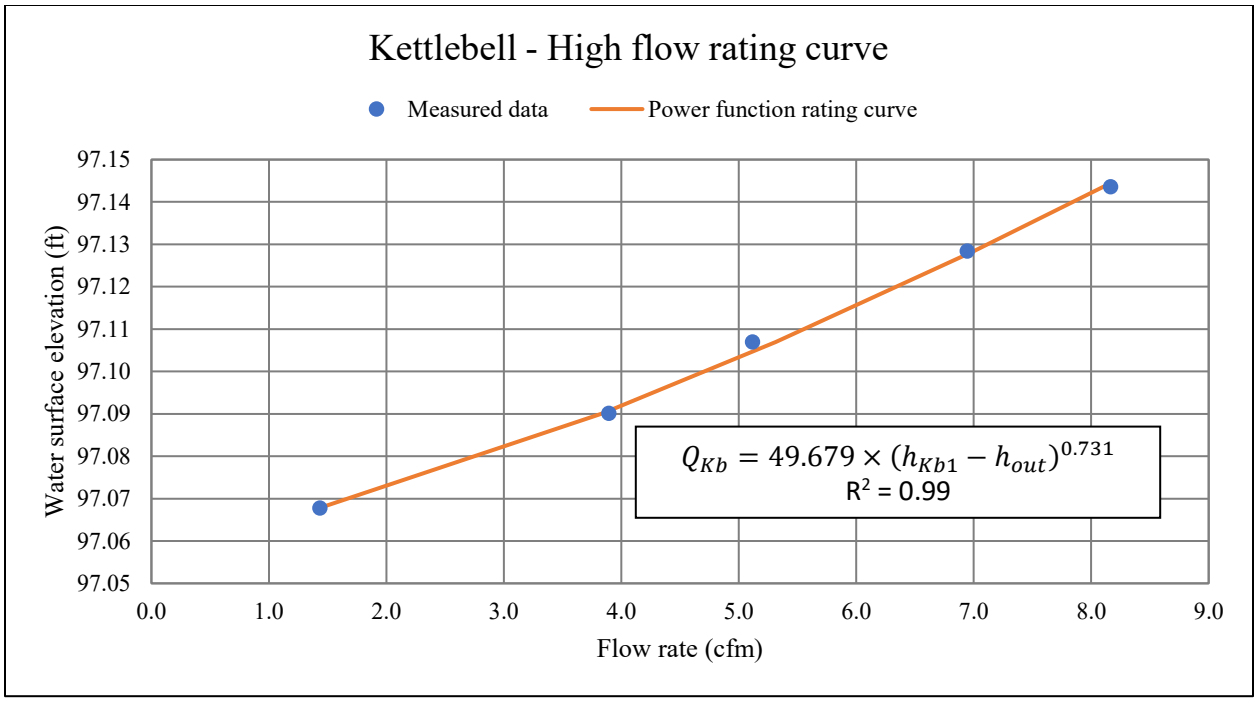

Figure 20: Rating curve and power function for CB #1 in the Kettlebell system

3.5 Soil Analysis

The Kettlebell and Grove St subsurface gravel filters were originally sized using "static" methods due to the apparent low permeability of the native soils below the systems. Initial estimates of soil type and K were obtained from Web Soil Survey. According to the web-service, the native soils at the Grove St site consist primarily of Suffield silt loam, which is in Hydrologic Soil Group (HSG) C and has a saturated hydraulic conductivity (K_{sat}) between 0.00 to 0.20 in/hr. At the Kettlebell site, the primary soil type is Buxton silt loam, which is classified as an HSG C/D soil with a K_{sat} ranging from 0.06 to 0.20 in/hr. During the excavation phase of construction, the soils across the base of the Kettlebell system were determined by visual inspection to be hydraulically more restrictive than previously estimated.

In order to model infiltration in the SGF systems, more precise measurements of the native soil properties were needed. Some properties of interest include the particle size distribution (PSD), soil porosity, and saturated hydraulic conductivity. Both in situ and

laboratory measurement techniques were used to determine the desired soil properties for infiltration modeling. At the site of each system, hydraulic conductivity was measured using a Guelph permeameter (Reynolds and Elrick 1986). The PSDs for soil samples were determined in the lab using hydrometer test methods and sieve analysis (ASTM D7928-16). Additional soil properties, including porosity, matric potential, pore size index, and residual moisture content, were calculated using the PSDs. Horizontal and vertical hydraulic conductivity values for the unit-gradient flow model, which is discussed in Section 3.6.3, were also calibrated from the water balance analyses.

3.5.1 Guelph permeameter measurements

The Guelph permeameter is a constant-head permeameter that is used to obtain in situ measurements of the field-saturated infiltration rate. Guelph measurements can be used to calculate field-saturated hydraulic conductivity (K_{fs}), sorptivity (S), and the relationship between conductivity and soil-water pressure head ($K(\psi)$). The device operates according to the Mariotte Principle, releasing a constant rate of water into a narrow, cylindrical excavation while maintaining a constant head of water. Over time, the flow rate reaches steady-state and can be measured by monitoring the water level in the instruments reservoir. The head is then raised slightly and a new flow measurement is taken. This process may be repeated as many times as desired; however, at least two rate measurements are required for certain soil property analyses. For example, the Richards analysis method, which is used to calculate K_{fs}, S, and matric flux potential (Φ_m), requires two rate measurements, while the Laplace, Gardner, and modified one-ponded head analyses require only a single measurement. These analysis methods for the Guelph data are described by Reynolds and Elrick (1986) and Elrick et al. (1989).

At each of the field sites, the Guelph was used to measure the field-saturated hydraulic conductivity of the soils surrounding the SGF systems. Measurements were taken from 8 cm-diameter excavated holes at various depths relative to the elevation of the gravel infiltration layer. At least two sets of rate measurements were taken in each hole: one set at an elevation that corresponded to the middle of the gravel bed and a second set at an elevation near the bottom of the gravel bed. Four infiltration rate measurements were taken at each excavated elevation. The Richards, Laplace, Gardner, modified one-ponded head, and Least Squares Analysis methods were used to calculate the hydraulic conductivity and matric flux potential from the infiltration rate data. The equations, variables, and example calculations for the Guelph data analysis are presented in the Guelph Permeameter Analyses section of the Appendix.

For this study, measurements were taken from three different auger holes and at four soil depths. In one of the excavations, multiple steady-state infiltration measurements were taken in order to use the Richards and least squares methods. Single head measurements were taken for the other two excavations. Figure 21 presents the approximate location where each Guelph permeameter test was performed at the Grove St site. Measurements with the Guelph were also taken at the Kettlebell site (Figure 22), but did not produce usable results due to the extremely slow, if not negligible, rate of drainage from the excavations.

Figure 21: Guelph permeameter test locations at the Grove St site

Figure 22: Attempted Guelph permeameter test locations at the Kettlebell site

Although, the Guelph permeameter is a proven method for measuring K_{fs}, only three excavations produced usable results. These holes were located on both sides of Grove St, along the perimeter of the SGF. Numerous attempts were made to use the Guelph in other locations around both SGF systems, but were unsuccessful. During these attempts, water would initially drain into the soils at a reasonable rate. However, as the infiltration rate stabilized, the flow rate decreased until it was immeasurably slow for the device being used. This may be due to the highly impermeable native soils surrounding the systems, especially at the Kettlebell site. According to Reynolds and Elrick (1986), large well diameters and high head levels are needed when taking measurements in low permeability porous media with K_{fs} values less than 10^{-7} m/s (0.014 in/hr). The Guelph permeameter and hand-auger that were available for the tests restricted the hole diameter and hydraulic head that could be used. Additionally, most of the Guelph measurements were taken during the autumn months of 2016, when frequent heavy rain events kept the water content of the soils fairly high. When drilling the well-holes, the wet clayey soils tended to smear along the sides of the excavation. This has been shown to dramatically reduce infiltration rates from the wells (Reynolds and Elrick, 1985). The smear layer may have affected the test results, although an attempt was made to remove the layer using a wire brush. While the Guelph permeameter can be a useful tool for measuring unsaturated soil properties in the field, it may not be effective in all natural soils.

3.5.2 Particle Size Distribution (PSD) measurements

Native soil characteristics were determined from PSDs, which were calculated from soil samples using the ASTM hydrometer-based sedimentation method (ASTM D7928-16). This analysis technique was employed due to the relatively fine grain size of the soil media. In total, seven soil samples were analyzed from the SGF sites. Only two of the seven were collected from

Kettlebell because the majority of the land surrounding the SGF is paved, limiting access to the soils. As with the permeameter testing, samples were taken from a variety of depths in order to examine how the soil characteristics change in relation to the gravel infiltration beds. Table 3 provides information about the elevation and location where each sample was extracted.

Table 3: Relative elevations and locations of soil samples at SGF sites, Dover, NH

Sample number	Site location	Borehole location	Date collected	Elevation of sample (ft)	Notes
GS1	Grove St.	W side of street, S of outlet	8/24/2016	96.37	Elevations relative to system
GS2	Grove St.	W side of street, S of outlet	8/24/2016	98.37	Elevations relative to system
GS3	Grove St.	W side of street, S of outlet	8/24/2016	99.07	Elevations relative to system
GS4	Grove St.	W side of street, N of outlet	12/2/2016	97.35	Elevations relative to system
GS5	Grove St.	E side of street, next to GSt-3, 7ft from road	12/9/2016	97.82	Elevations relative to system
KB1	Kettlebell	W of KB-1, in grass next to garage door	11/2/2016	98.38	Elevation relative to top of KB-1 (assumed Elev. Of 100')
KB2	Kettlebell	E of KB-1, in grass next to garage door	11/2/2016	97.99	Elevation relative to top of KB-1 (assumed Elev. Of 100')

The particle size distribution analysis was conducted according to ASTM standard D7928-16, which consists of a sedimentation test followed by a sieve test. The sedimentation test is based on Stokes' Law and can be used to calculate the PSD for the finer portion of the soil samples (i.e. particles smaller than 0.075mm in diameter). The sieve test is used to calculate the PSD for the larger portion of the sediments. For the analysis, 50 to 70-gram soil samples were mixed with a solution of sodium hexametaphosphate (a dispersant) to prevent the finer particles from flocculating. The soil-dispersant mixtures were rinsed into 1000mL graduated cylinders, which were then filled to the 1000mL mark with distilled water. After mixing the solutions thoroughly, their specific gravities (SG) were measured at defined time intervals with an ASTM

151H-type soil hydrometer. The temperature of the solutions was kept between 20 to 22°C during the sedimentation process to minimize fluctuations in water density. As the suspended particles settled to the bottom of the graduated cylinders, the SG of the solutions decreased. These time-dependent changes in SG were monitored and used to calculate percent-finer values for specific particle sizes. Once the sedimentation tests were complete, the soil-dispersant mixtures were wet-sieved with a No. 200 sieve and rinsed, to separate the fines and dispersant chemical from the coarser sediments. Both soil-water mixtures were then dried and weighed. The coarser sediments were also sieved and weighed to determine the second portions of the soil sample PSDs. A more detailed description of the test procedure is provided in the referenced ASTM standard for the PSD analysis (ASTM D7928-16). Example calculations and test data are provided in Particle Size Distribution Analyses section of the Appendix.

The PSDs were used to calculate a variety of soil characteristics including soil texture classification, effective porosity, hydraulic conductivity, residual moisture content, and capillary pressure head. Texture classifications were calculated by determining the proportions of sand, silt, and clay in each sample and using the USDA textural classification chart (Figure 64 in the Appendix), which assigns soils to one of twelve textural classes. The other soil properties were either obtained from tables containing commonly used, statistically-derived values based on soil classification or calculated using empirical and physically-based equations.

It should be noted, that samples GS1 and GS2 were taken from the bore hole used for the multi-head Guelph permeameter tests. Sample #1 was taken at a relative elevation of about 96ft, while Sample #2 was taken from a relative elevation of approximately 98ft. The hydraulic conductivity values measured with the Guelph permeameter should theoretically be similar (i.e.

the same order of magnitude) to those obtained from the regression equations and the soil classifications.

3.5.3 Hydraulic conductivity calibration

Horizontal and vertical hydraulic conductivity (K) values were estimated for the sidewalls and base, respectively, of the Grove St SGF. The calibration process for these values and the unit-gradient flow model in which they are used are based on the work of Bergman et al. (2010), who used the model to evaluate the performance of a gravel infiltration system. Calibrated K values could not be obtained for the Kettlebell SGF because the water level inside the system did not fluctuate significantly between rain events.

Water balances were performed, as described in Section 3.2, for 27 different rain events, all of which produced measurable ponding depths within the Grove St system. Of these events, 8 were selected for calibration of the horizontal and vertical K-values as these events produced ponding depths greater than 10 cm. Infiltration rates were calculated over 1-hour intervals during the receding segment of ponding and then graphed against the average water depths during each time period. A linear regression line was fitted to the data and K-values were calculated according to Equation 14 through Equation 16, which are based on the unit-gradient model described in Section 3.6.3. The results of the calibration process are presented in Chapter 4 of this report.

Equation 14: Linear regression curve fit to the infiltration rate vs. water depth data

$$f = (\alpha * h) + \beta$$

Equation 15: Horizontal K equation based on slope of linear regression curve

$$K_{fs,H} = \frac{(\alpha * l * w)}{2 * (l + w)}$$

Equation 16: Vertical K equation based on y-intercept of linear regression curve

$$K_{fs,V} = \beta$$

Where:

f = infiltration rate (cm/hr)
α = slope of linear regression curve (1/hr)
β = y-intercept of linear regression curve (cm/hr)
h = average depth of water during a 1-hour interval (cm)
$K_{fs,H}$ = Horizontal field saturated hydraulic conductivity (cm/hr)
$K_{fs,V}$ = Vertical field saturated hydraulic conductivity (cm/hr)
l = system base length (cm)
w = system base width (cm)

Each calibrated K-value is thought to equal the unidirectional field saturated hydraulic conductivities of the native soils surrounding the Grove St system. One should keep in mind that the K-value developed from the water balance calculations and those measured using the Guelph permeameter were developed over very different spatial scales. The calibrated K-values from the water balance are averages that incorporate all of the variation of the soils surrounding the system. The Guelph permeameter measurements sample a much smaller volume of soil and may not account for the variations in soil texture and effect of macropores, which may influence infiltration rates from the system.

3.6 Modeling System Performance

Three infiltration models were used to evaluate system performance, including: 1) a one-dimensional saturated/unsaturated flow model, 2) a Green-Ampt model, and 3) a unit-gradient saturated flow model. The saturated/unsaturated model and Green-Ampt model are both deterministic models which use measured physical parameters to simulate the complex processes of infiltration and account for changes in soil-moisture. The unit-gradient model is semi-empirical and uses calibrated or measured hydraulic conductivities. Input parameters included the estimated inflow hydrographs and site-specific soil characteristics, discussed in the first

section of Chapter 4: Results and Discussion. While soils were assumed to be homogeneous for each model, a range of soil characteristics were initially used in order to calculate high and low estimates of infiltration and evaluate the degree to which each parameter affected infiltration. The models were run for individual storm events and did not account for the effects of soil drainage after infiltration, antecedent moisture conditions, or the seasonality of soil moisture. Various values for initial soil moisture were used depending on the soil texture classification. After running the models, the calculated water depths, infiltration volumes, and infiltration rates were compared to measured values in order to assess the effectiveness of the model and determine the factors influencing infiltration in SGF systems.

3.6.1 Saturated/Unsaturated Flow Model

The first model is based on the work of Browne et al. (2008) who developed a model for simulating stormwater infiltration systems, such as infiltration trenches and basins. The model is one-dimensional and assumes infiltration occurs in the vertical direction, through the base of a system. Flows passing through the system and into the underlying native soils are calculated by separating the system into three zones, as shown in Figure 23: 1) a porous storage zone, 2) a saturated soil zone directly beneath the storage, and 3) an unsaturated soil zone below the saturated zone. Each soil zone is further divided into discrete layers of constant soil moisture.

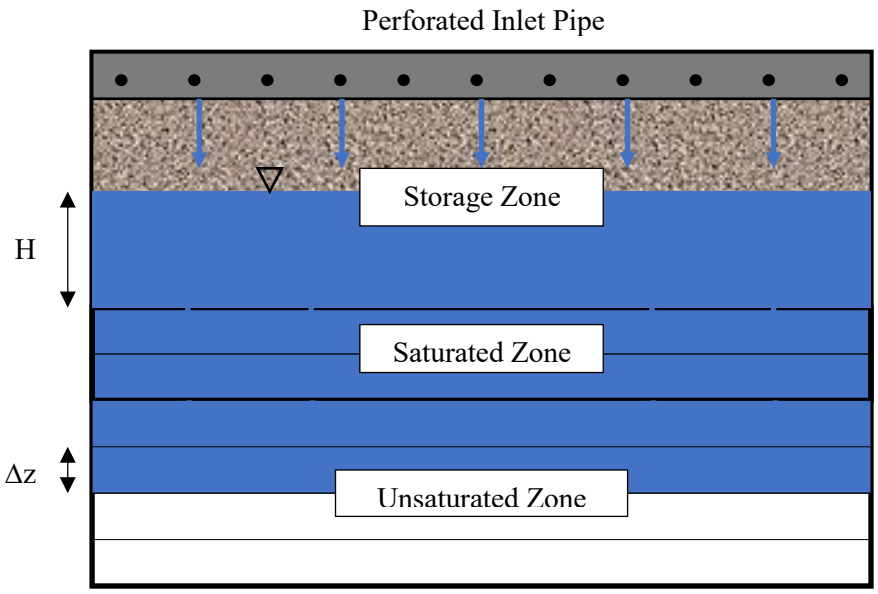

Figure 23: Diagram displaying the three zones of the saturated/unsaturated model

Initially, at the start of a simulation, the saturated zone is absent and the entire system is unsaturated. As runoff trickles down through the stone in the storage zone, it will start to infiltrate into the soil below. The moisture content (θ) of the top soil layer will then increase until it reaches saturation and the saturated zone is created. If water continues to infiltrate, the saturated zone will grow, extending downward layer by layer. In this way, the model is conceptually similar to the Green-Ampt model, except for the facts that the unsaturated zone does not have a constant θ-value and a more gradual wetting front can be simulated. The underlying unsaturated soil layers draw water away from the saturated zone's wetting front creating a gradual transition from saturated conditions to the initial soil moisture condition. The depth of soil below the system is assumed to be deep enough that water can drain freely from the system and is not influenced by a water table.

Flows through the saturated zone are calculated using Darcy's law (Equation 17), while flows through the unsaturated zone are based on the 1-D form of Richards' equation that is

solved for moisture content (Equation 18). The hydraulic conductivity (K), diffusivity (D), and matric potential (ψ) parameters in the Richards equation were calculated using the Brooks and Corey (1964) equations that relate these variables to soil moisture (see Equation 19 through Equation 21). Inflows from the storage zone into the top soil layer (Equation 25) are equal to the minimum of 1) the amount of water available for infiltration, 2) the infiltration capacity of the top layer, or 3) the amount of porous storage available for water in the soil layer. The infiltration capacity of the soil decreases as the moisture content of the soil increases until saturation is reached.

When the soil layer immediately under the storage zone is unsaturated, driving forces for infiltration include the depth of water in the storage zone (H) and the negative matric potential (i.e. soil suction) of the first soil layer. Once the layer reaches saturation, the flux of water through the layer is controlled by saturated inflows under hydrostatic pressure and unsaturated outflows into the soil layer below driven by matric suction. A layer is considered saturated when the θ value for the layer is greater than or equal to 99.9% of the θ_s value. Smaller percentages down to about 95% can be used to identify saturation, depending on the restrictiveness of the soils being evaluated. However, the soils surrounding each SGF system are hydraulically restrictive and necessitate the use of a fairly high percentage. As soil layers become saturated, the depth of the saturated zone (dz) increases, causing the hydraulic gradient $\left(\frac{dH}{dz}\right)$ to decrease. When the depth of the saturated zone is relatively large, the saturated flow rate approximately equals the saturated hydraulic conductivity (K_s) (see Equation 17). The water depth in the storage zone (H) is calculated with a reservoir equation (Equation 26) that accounts for the porosity of the gravel in the storage zone, runoff inflows into the system, and infiltration flows into the

native soils. Inflows into the storage zone were calculated from the actual flow data for the Grove St system and are assumed to be distributed evenly throughout the storage zone.

Equation 17: Continuous form of Darcy's Law for saturated flow with ponding in the storage zone

$$q_s = K_s\left(\frac{dH}{dz} + 1\right)$$

Equation 18: Continuous form of 1-D Richards equation for unsaturated flow

$$\frac{\delta\theta}{\delta t} = \frac{\delta\left[D(\theta)\frac{\delta\theta}{\delta z} + K(\theta)\right]}{\delta z}$$

Equation 19: Brooks and Corey equation for hydraulic conductivity in terms of soil moisture

$$K(\theta) = K_s(S_e)^n$$

Equation 20: Brooks and Corey equation for diffusivity in terms of soil moisture

$$D(\theta) = \frac{K_s}{\alpha\lambda(\theta_s - \theta_r)}(S_e)^{2+\frac{1}{\lambda}}$$

Equation 21: Brooks and Corey equation for capillary pressure head in terms of soil moisture

$$\psi(\theta) = \frac{\psi_b}{(S_e)^{\frac{1}{\lambda}}}$$

Where:

q_s = saturated flow rate (cm/hr)
K_s = saturated hydraulic conductivity (cm/hr)
H = depth of water in storage zone (cm)
z = relative elevation (cm)
t = time (hr)
θ = soil moisture content (-)
θ_s = saturated moisture content (-)
θ_r = residual moisture content (-)
D = diffusivity (cm^2/hr)
K = hydraulic conductivity (cm/hr)
ψ = negative capillary pressure head (cm)
ψ_b = bubbling capillary pressure (cm)
S_e = Effective saturation (-) = $\frac{\theta-\theta_r}{\theta_s-\theta_r}$
n = $3 + \frac{2}{\lambda}$
λ = pore-size index (-)
$\alpha = \left|\psi_b^{-1}\right|$

A finite volume methodology, that is explicit in time, is used to solve the model equations. The discretized forms of the equations, which use the variables k and i to indicate the time step and soil layer, respectively, are displayed in through Equation 25. For simplicity, constant temporal and spatial increments (i.e. Δt and Δz, respectively) were used, although variable time steps, such as those used by Browne et al. (2008), can be implemented. The soil characteristic parameters and Δt and Δz values used for the model are presented in Table 35. A soil depth of 200cm was selected for the model because it is deep enough that the boundary condition along the base of the system does not influence infiltration.

Due to the uncertainty in estimating soil characteristics from PSD and soil classification data, simulations were initially run for a range of different soil characteristics, including the K_{fs} values estimated from the Guelph permeameter measurements. From these initial simulation, the Guelph-based soil characteristics were select for further model analysis. The simulated water depths produce by the model were statistically closure to those measured during various storm events when the Guelph-based parameters were used as input. The results of the statistical comparison are presented in the Appendix. Based on the similarities between the simulated and measured water depths K-values measured with the Guelph permeameter appear to be closer to the actual soil characteristics at the Grove St site than the PSD-regression or texture-based soil parameter estimates. The Guelph measurements may be more accurate for simulating infiltration, especially at sites with anisotropic soils, because each measurement is an average of both horizontal and vertical infiltration.

Equation 22: Discrete form of Darcy's Law for saturated flow out of the i^{th} layer at time k

$$q_{s,i-1/2}^{k} = -K_s\left(\frac{H^k}{L_s^k} + 1\right)$$

Equation 23: Discrete equation for moisture content in the i^{th} layer at time k+1

$$\theta_i^{k+1} = \theta_i^k + \left[\frac{q_{i+1/2}^k - q_{i-1/2}^k}{\Delta z}\right]\Delta t$$

Equation 24: Discrete equation for unsaturated flow out of the i^{th} layer at time k

$$q_{i-1/2}^{k} = \left\{\left[\frac{D\left(\theta_i^k\right) + D\left(\theta_{i-1}^k\right)}{2}\right] \times \left[\frac{\theta_i^k - \theta_{i-1}^k}{\Delta z}\right] + \left[\frac{K\left(\theta_i^k\right) + K\left(\theta_{i-1}^k\right)}{2}\right]\right\}$$

Equation 25: Infiltration rate into native soils

$$q_{inf}^{k} = \min\begin{Bmatrix} q_{available}^{k} \\ q_{inf,pot}^{k} \\ q_{soil,cap}^{k} \end{Bmatrix}$$

$$q_{available}^{k} = \left(\frac{H^k \times \varphi}{\Delta t}\right) + q_{in}^{k}$$

$$q_{inf,pot}^{k} = K\left(\theta_N^k\right)\left[\frac{H^k - \psi\left(\theta_N^k\right)}{\frac{\Delta z}{2}} + 1\right] \; if \; \theta_N^K < (0.999)\theta_s \; or \; q_{inf,pot}^{k} = q_s^k \; if \; \theta_N^K \geq (0.999)\theta_s$$

$$q_{soil,cap}^{k} = (\theta_s - \theta_N^K) \times \frac{\Delta z}{\Delta t}$$

Equation 26: Discrete equation for calculating depth of water in storage layer

$$H^{k+1} = H^k + \left[\frac{q_{in}^k - q_{inf}^k - q_{overflow}^k}{\Delta t} \times \varphi\right]$$

Equation 27: Overflow from Grove St system storage based on regression equation for perforate pipe

$$q_{overflow}^{k} = \frac{L_{overflow} \times \left[4.6279\left(\frac{h^k}{0.5ft}\right)^{1.3782}\right]}{A} \times \left(\frac{60min}{hr}\right) \times \left(\frac{30.48cm}{ft}\right)$$

Where:

L_s = length of the saturated zone (cm)
$L_{overflow}$ = length of overflow pipe (ft)
H = depth of water in the gravel filter layers (ft)
h = H – 2.2ft = depth of water above overflow pipe invert (ft)
A = base area of system (ft^2)
k = time step index
i = soil layer index
N = number of soil layers
Δt = length of time steps (hr)
Δz =depth of layers (cm)
q_{in} = inflow rate (cm/hr)
q_{inf} = infiltration rate (cm/hr)
$q_{available}$ = available flow rate from storage zone (cm/hr)
$q_{inf,pot}$ = infiltration capacity of underlying soil layer (cm/hr)
$q_{soil,cap}$ = infiltration rate that will fill available pore space in underlying soil layer (cm/hr)
$q_{overflow}$ = flow out of system from overflow pipe (cm/hr)

The model was coded, setup, and run for individual rain events using Python 3 and the array functionalities of NumPy. Input values include the inflow hydrograph data developed from the inflow calibration curves (Section 3.4) and the site-specific soil characteristic parameters (Section 3.5). Soil layers below the system are assumed to be homogeneous and have a constant moisture content initially. Values for the initial soil water content (θ_i) were obtained from Rawls et al. (1992) and correspond to the θ-values of various soil textures at field capacity, which occur when water can no longer drain from a soil under the force of gravity alone (i.e. at a matric potential of approximately -33 kPa). This assumption may lead to slight overestimations of initial infiltration rates for rain events in short succession because field capacity conditions are usually achieved after 2-3 days of drying.

When running the model, the moisture content profile for the native soils below the system and the depth of water in the gravel storage zone are calculated for each time step. If the water surface elevation in the system reaches the top of the storage layer, the simulation will calculate an outflow term that represents excess flow leaving the system through an overflow

pipe. The equation used to calculate this outflow depends on the type of overflow pipe in use. For Grove St, the overflow pipe is a 6-inch perforated pipe that runs between CB #3 and 4 and was simulated using a regression equation (Equation 27) developed by the UNHSC for flow out of perforated pipes (UNHSC, 2015). The simulated water depths were compared to those measured during specific rain events in order to evaluate how well the model simulated the actual system performance. Because the Kettlebell system remained full throughout the monitoring period, the accuracy of the model could not be assessed for the Kettlebell SGF.

3.6.2 Green-Ampt Infiltration Model

The second model used for simulating infiltration in the SGF systems was an explicit Green-Ampt model based on the work of Freni et al. (2009). The original Green-Ampt model (Green-Ampt, 1911) conceptualizes unsaturated infiltration as a 1-dimensional flow of water that moves through soils as a saturated wave with a sharp transition between saturated and unsaturated conditions at its edge, or wetting front. For vertical infiltration, the model assumes that soils above the wetting front are under saturated conditions and the soils below the front are homogeneously unsaturated. While the model is technically 1-D, Freni et al. (2009) proposed the used of an effective infiltration area (A_{eff}) term to account for some of the effects of horizontal infiltration in stormwater infiltration trenches. The effective infiltration area includes the bottom area of a system and a portion of the area of the sides. Freni et al. estimated the term by performing numerous infiltration simulations in VSF-MODFLOW 2000 for trenches with different dimensions and soil types. Power-functions were developed to relate the bottom area of the trenches to the effective area of infiltration. For example, infiltration trenches surrounded by sandy loam soils were found to have effective infiltration areas equal to $5.336 \times A^{0.575}$, where A is the bottom area of a trench in square meters.

The modified Green-Ampt model used for this study (Equation 32) employs the effective infiltration area term to improve infiltration estimates. Unlike the work of Freni et al. (2009), A_{eff} was initially set to the bottom areas of the system so that the result could be compared to the monitoring data to determine if horizontal infiltration was significant. The model was then run using various functions (Equation 34) relating A_{eff} to the storage depth to determine if this factor could be altered to more accurately simulate infiltration in the systems. Driving forces for infiltration include the depth of water in the gravel storage zone (H) and the negative wetting front pressure head (ψ_f). The distance from the soil surface to the wetting front is equal to the cumulative infiltration depth (F) divided by the change is moisture content ($\Delta\theta$). Infiltration rates are calculated as the minimum of the infiltration capacity of the soil (Q_{GW}) and the flow of water available for infiltration ($q_{available}$) (see Equation 31). Because the Green-Ampt equation for infiltration capacity depends on the cumulative infiltration depth, the initial infiltration rate is theoretically infinite. The first incremental inflow is therefore assumed to infiltrate no matter how large the flow is. This assumption is acceptable if the first initial inflow is relatively small.

Equation 28: Differential equation for the depth of water in the system (H)

$$\frac{dV}{dt} = \frac{d(HA\varphi)}{dt} = (Q_{in} - Q_{inf} - Q_{out})$$

Equation 29: Discrete equation for the depth of water in the system (H)

$$H^{k+1} = H^k + \frac{\left(Q_{in}^k - Q_{inf}^k - Q_{overflow}^k\right)\Delta t}{A \times \varphi}$$

Equation 30: Overflow from the Kettlebell system storage

$$Q_{overflow}^k = (49.6786 \times (h)^{0.7306}) \times \left(\frac{60min}{hr}\right) \times \left(\frac{30.48cm}{ft}\right)^3$$

Equation 31: Discrete equation for the infiltration rate at time k

$$Q_{inf}^k = \min\begin{Bmatrix} Q_{GW}^k \\ Q_{available}^k \end{Bmatrix}$$

Equation 32: Discrete form of the modified Green-Ampt equation for the infiltration capacity at time k

$$Q_{GA}^k = K_s\left(1 - \left(\frac{(\psi_f - H^k)(\theta_s - \theta_i)}{F^k}\right)\right)A_{eff}$$

Equation 33: Discrete equation for the maximum potential flow rate based on the water volume available for infiltration

$$Q_{available}^k = Q_{in}^k + \left(\frac{H^k \times A \times \varphi}{\Delta t}\right)$$

Equation 34: Various functions relating effective infiltration area (A_{eff}) to water depth in the system

$$Linear\ function\text{:}\ \ A_{eff} = A + (P \times H)$$

$$Linear\ function\ with\ multiplier\text{:}\ \ A_{eff} = A + (P \times H \times C_1)$$

$$Power\ function\text{:}\ \ A_{eff} = A + aH^b$$

$$Piece - wise\ function\text{:}\ \ A_{eff} = \begin{Bmatrix} if\ H \le H_{pw} & A + (C_2 \times P \times H^c) \\ if\ H > H_{pw} & \left(A + (C_2 \times P \times {H_{pw}}^c)\right) + \left((H - H_{pw}) \times P \times C_2\right) \end{Bmatrix}$$

Where:

V = volume of water in the system (cm^3)
H = depth of water in the system (cm)
A_{eff} = effective infiltration area (cm^2)
A = area of the bottom of the system (cm^2)
C_1, C_2, a, b, c = constants for the function relating depth and A_{eff} (-)
H_{pw} = Depth of transition for piece-wise function relating depth and A_{eff} (ft)
P = perimeter of the system (cm)
φ = porosity of the gravel storage layers = 0.4
Δt = change in time (hr)
k = time step index
Q_{in} = inflow into system (cm^3/hr)
Q_{inf} = infiltration rate (cm^3/hr)
Q_{out} = outflow from system (cm^3/hr)
Q_{GA} = infiltration capacity of the soil (cm^3/hr)
$Q_{available}$ = available flow for infiltration (cm^3/hr)
K_s = saturated hydraulic conductivity (cm/hr)
ψ_f = wetting front soil suction (cm)
θ_s = saturated moisture content (-)
θ_i = initial moisture content (-)
F = cumulative infiltration depth (cm) = $\sum \frac{Q_{inf}^{k} \times \Delta t}{A}$

Python3 and the array functionalities of NumPy were used to solve the model for individual rain events. Input values include the inflow hydrograph data developed from the inflow calibration curves and the site-specific soil parameters. As mentioned in the previous section, simulations were initially run for a range of different soil characteristics, due to the uncertainty in estimating soil characteristics from PSD and soil classification data. The soil parameters and the Δt and A values used in the model are presented in the Model Input Parameters section of the Appendix. From the initial simulations, the Guelph-based soil characteristics were select for further model analysis. The simulated water depths produce by the model were statistically closure to those measured during various storm events when the Guelph-based parameters were used as input. The results of the statistical comparison are presented in the Appendix.

For each time step, the modified Green-Ampt model calculates the infiltration rate, cumulative infiltration depth, and the depth of water in the SGF system. As in the saturated/unsaturated model, overflows are simulated if the WSE reaches the top of the storage layer. For the Grove St system, Equation 27, described in the previous section, was used to calculate overflows. For the Kettlebell system, the rating curve developed for the system (Equation 30) was used to simulate outflow because the system's outlet pipe acts as its overflow.

For Grove St, the accuracy of the model was assessed by comparing the simulated water depths to that which were measured during an actual rain event. The accuracy of the Kettlebell model could not be evaluated because the system remained full throughout the monitor period. Results from the model were primarily used to see if the system should theoretically be draining.

3.6.3 Unit-gradient flow model

The third model used for simulating infiltration from an SGF system was a unit-gradient, saturated flow model based on the work of Bergman et al. (2010) and Warnaars et al. (1999). Both studies used the model to analyze the performance of a gravel infiltration trench and evaluate how infiltration rates from the system changed over the life of the system. Unlike the previous two models, the unit-gradient model, presented in Equation 35, accounts for both horizontal and vertical infiltration and is semi-empirical. The equation requires two values for hydraulic conductivity, one to describe infiltration through the sides of the system and the other to describe infiltration through the bottom. Hydraulic conductivity values can either be obtained through the calibration process described in Section 3.5.3 or obtained from field or lab measurements. As the name of the model implies, the gradient driving infiltration is assumed to be constant and equal to 1 unit of head applied over 1 unit of distance.

When simulating SGF performance, infiltration rates are calculated based on the depth of water in the system. Before ponding occurs, infiltration capacity of the native soil is equal to the vertical K_{fs} times the base area of the system. The modelled infiltration rate equals the lesser of the infiltration capacity and the maximum potential flow rate (Equation 36). When the inflow surpasses the infiltration capacity, ponding will commence and the infiltration rate will increase as horizontal infiltration now occurs. As shown in Equation 35, the horizontal infiltration rate is similar to the vertical rate, except that the area of infiltration is equal to the wetted area of the system's sides, which changes with the depth of water in the system. The water depth is calculated explicitly according to Equation 37.

Equation 35: Infiltration capacity of soil at time k based on unit-gradient field-saturated flow model

$$I_H^k = K_{fs,H}[2(l+w)]h^k$$

$$I_V^k = K_{fs,V}[l \times w]$$

$$I^k = I_H^k + I_V^k$$

Equation 36: Modeled infiltration rate at time k

$$Q_{inf}^k = \min\left\{ \begin{matrix} I^k \\ Q_{available}^k \end{matrix} \right\}$$

Equation 37: Function for the depth of water in the system during the subsequent time step

$$H^{k+1} = H^k + \frac{(Q_{in}^k - Q_{inf}^k)\Delta t}{A \times \varphi}$$

Where:

H^k, H^{k+1} = depth of water in the system at time step k and k+1 (cm)
φ = porosity of the gravel storage layers = 0.4
l = system base length (cm) = 1829 cm for Grove St.
w = system base width (cm) = 762 cm for Grove St.
A = area of the bottom of the system (cm^2) = 1,393,546 cm^2 for Grove St.
Δt = change in time (hr)
k = time variable
Q_{in} = inflow into system (cm^3/hr)
Q_{inf} = infiltration rate (cm^3/hr)
I_H^k = horizontal infiltration capacity of soil at time k (cm^3/hr)
I_V^k = vertical infiltration capacity of soil at time k (cm^3/hr)
I^k = total infiltration capacity of native soils at time k (cm^3/hr)
$Q_{available}$ = available flow for infiltration (cm^3/hr) – see Equation 33
$K_{fs,H}$ = horizontal field-saturated hydraulic conductivity (cm/hr)
$K_{fs,V}$ = vertical field-saturated hydraulic conductivity (cm/hr)

Python3 and the array functionalities of NumPy were used to run the model for individual rain events. Input values include the inflow hydrograph data and horizontal and vertical K values. Initially, the model was run using the K_{fs} estimate of 0.51 cm/hr from the Guelph permeameter for both the horizontal and vertical hydraulic conductivity values. Simulations were then performed using the calibrated K values (Section 4.1). For each time step, the unit-gradient model calculates the infiltration rate and the depth of water in the system. While this model can account for both horizontal and vertical infiltration, it does not account for soil moisture or its effects on infiltration rates.

CHAPTER 4: RESULTS AND DISCUSSION

4.1 Measured System Performance

During the 1-year monitoring period, 134 precipitation events occurred at the research sites in Dover, NH based on a minimum antecedent dry period of 6 hours (Figure 24). These events cumulatively produced 44 inches of rain with the largest event producing 2.71 inches. Using the SCS Curve Number method, it was estimated that approximately 93,200 cubic feet of runoff was produced at the Grove St site while around 152,000 cubic feet of runoff was produced at the Kettlebell site. Flow data was collected for approximately 110 of these events and may be found in the Monitoring Data section of the Appendices.

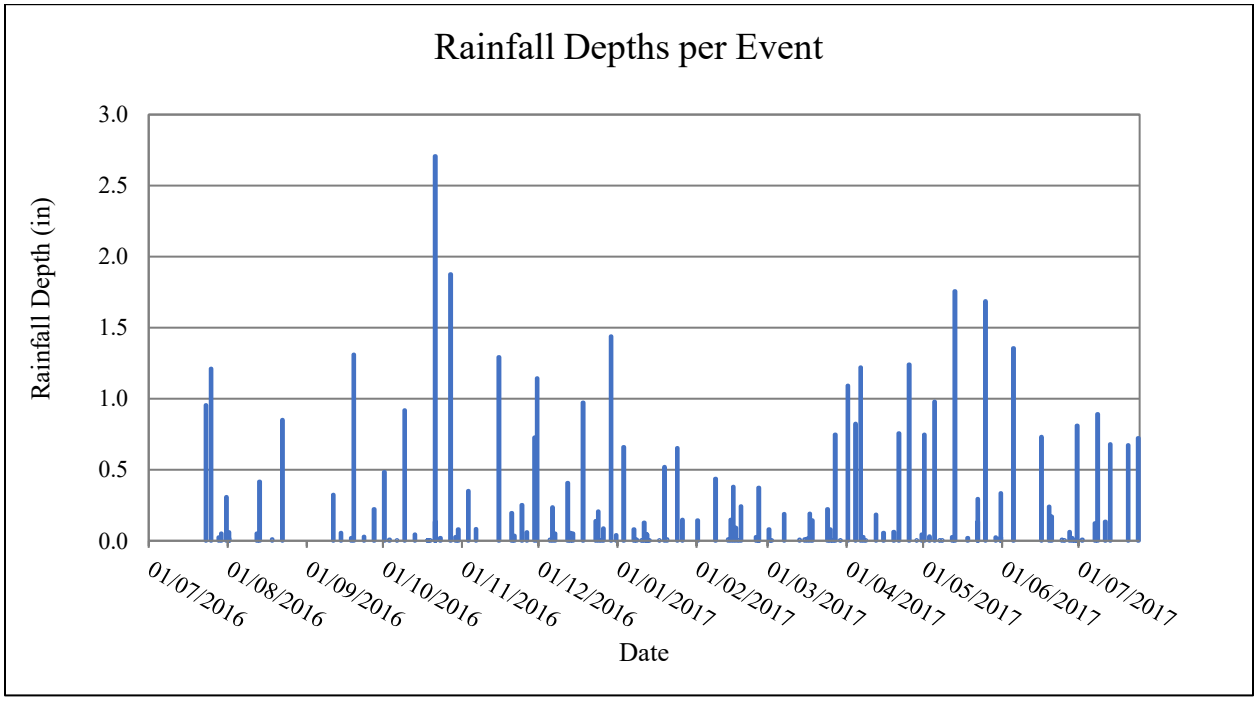

Figure 24: Total rainfall depths per storm event in Dover, NH

The monitoring data for each of the subsurface gravel filters was developed into long-term hydrographs in order to examine system performance. Figure 25 and Figure 26 present the long-term hydrographs for the Grove St and Kettlebell systems, respectively. When analyzing

the performance of Grove St system, it is important to distinguish between the runoff flows which were collected by the system's catch basins and the flows which actually entered the gravel filter layer. Due to the elevation of the system's outlet pipe, the runoff collected by the fourth catch basin (CB #4) could not enter the gravel layer and instead flowed directly to the outlet swale. Because these runoff flows completely bypass the filter layer, they were excluded from the water balances when analyzing system performance. Throughout this report inflows for the Grove St system refer to the runoff flows which entered CB #1, 2, and 3. Outflows refer to the runoff which flowed to CB #4 through the upper inlet pipe collected CB #3 and 4. The inflow and outflow hydrographs for the Grove St system are presented in Figure 25. Only one hydrograph is presented in Figure 26 for the Kettlebell system because the system did not fully drain throughout the monitoring period causing all inflows into the inlet/outlet catch basin (CB #1) to bypass the system and flow directly to Berry Brook.

The hydrographs show how inflows and outflows fluctuated over the entire one-year monitoring period. For each rain event that generated runoff, water levels would rise in the systems' catch basins and flow into the perforated inflow pipes running through the gravel storage layer. Flow estimates were calculated using the rating curves described in Section 3.4. At the Grove St system, the highest recorded inflow, excluding the runoff which was collected by CB #4, was 82 cfm, while the highest outflow was 59 cfm. The Kettlebell system, which had a smaller watershed but a much higher percentage of impervious cover, experienced a maximum flow of approximately 125 cfm. The peak flows for each storm event are reported in Table 42 in the Appendix.

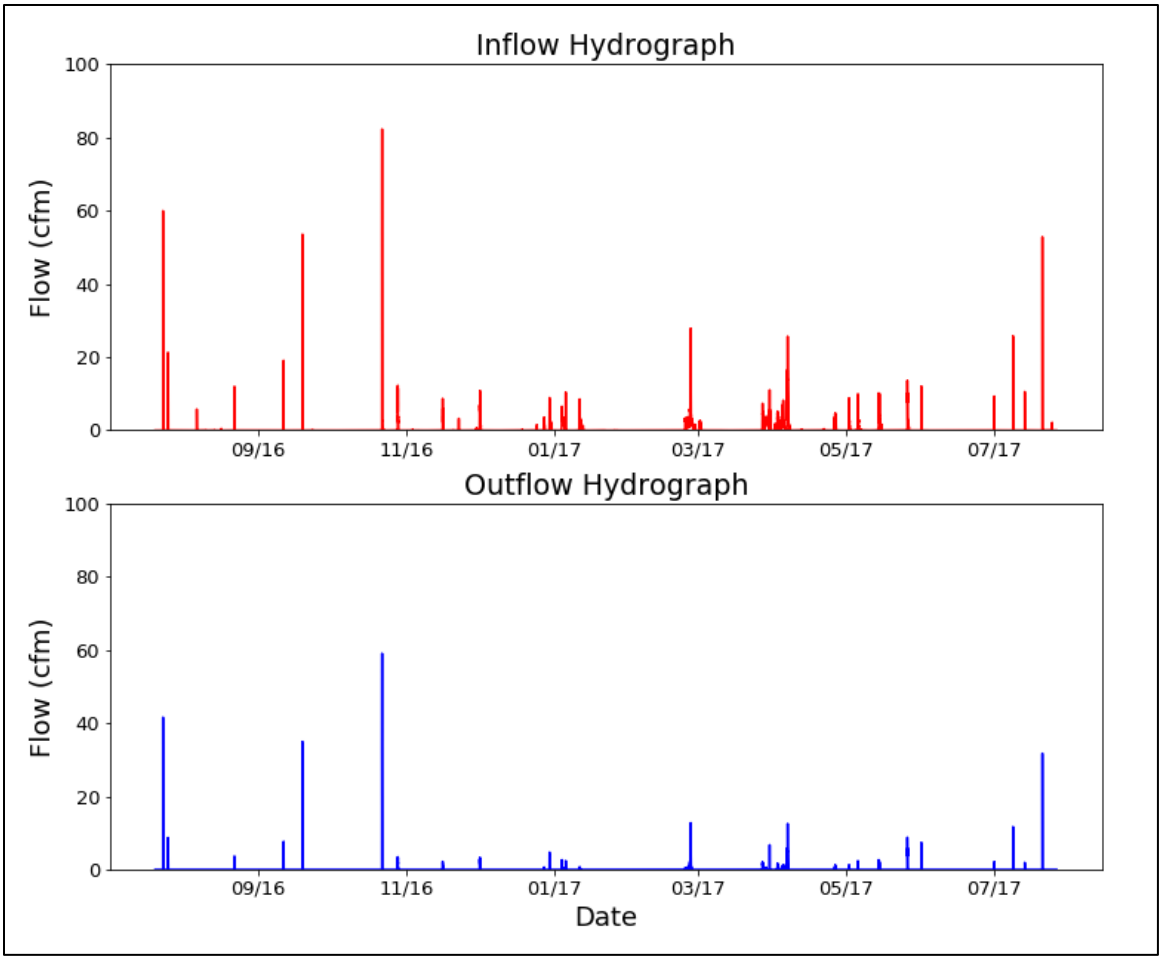

Figure 25: Long-term instantaneous inflow and outflow hydrographs for the Grove St SGF

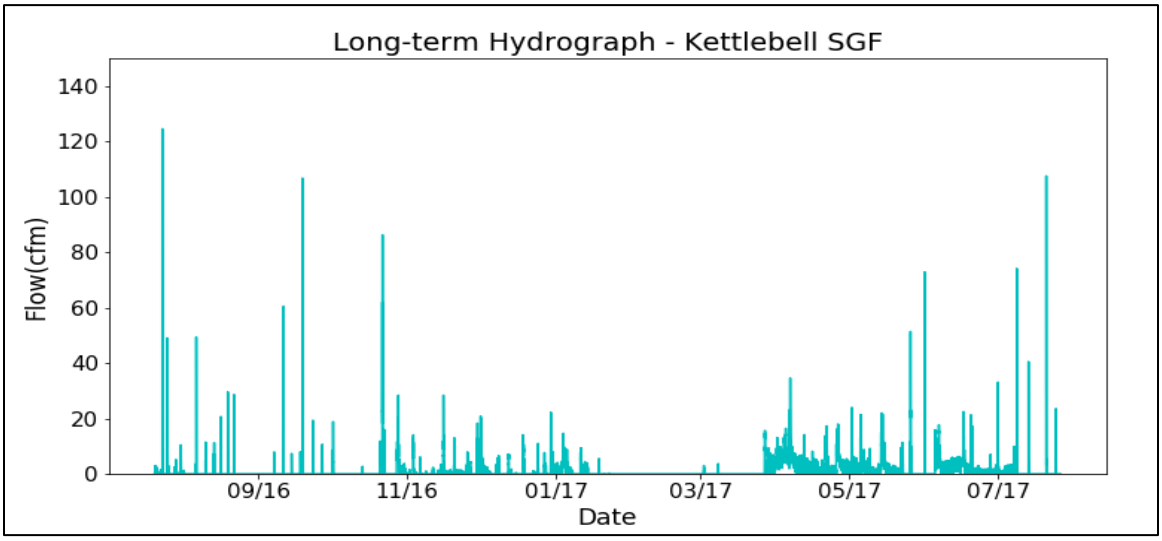

Figure 26: Long-term inflow/outflow hydrograph for the Kettlebell SGF

In between storms, inflows and outflows dropped back to around zero as the WSE in the catch basins and gravel filter layer receded. However, outflows from CB #4 did not completely stop because groundwater was continually flowing into CB #4 through perforations near the bottom of the catch basin. Because the Grove St SGF is located along the natural drainage path for a small ephemeral tributary of Berry Brook, the system may have been constructed over a high groundwater table, causing water to leak into the perforated catch basin. Additionally, the groundwater table beneath the system may be elevated (mounded) due to the infiltration of runoff from the system. Prior to November 20, 2016, baseflows from CB#4 were not recorded because water was flowing into the catch basin through perforations on one side of the structure and leaking out through perforations on the other side. The leaking water would surface in the riprap swale below the outlet pipe and flow down to Berry Brook. In order to measure these baseflows, most of the perforations underneath the outlet of CB #4 were filled and sealed with concrete and expanding foam. This restricted leakage, raised the water level in the catch basin, and forced most of the baseflow to pass through the outlet pipe, enabling flow measurement. These baseflows were not accounted for in the water balance analyses because the outflow from CB #4 were excluded.

Baseflows were also recorded at the Kettlebell site during some seasons. A foundation drain at one of the properties adjacent to the Kettlebell Fitness Center drains to the network of catch basins which collects water for the Kettlebell system. When sensors were first installed at the site in the summer of 2016, NH was experiencing a severe drought and the foundation drain remained dry. However, after a number of significant rain events during the fall, the drain started to flow consistently, releasing a small flow into the system throughout much of the monitoring period. This baseflow may be the reason why the hydrograph did not return to zero throughout

most of April and May 2017. Additionally, the baseflow may have prevented the system from fully draining. If infiltration from the gravel layer were less than the baseflow, the system would have remained full as long as the baseflow continued. Figure 27 shows the WSE in the Kettlebell system's inlet/outlet catch basin over the 1-year monitoring period. If water were infiltrating from the system, the water level in the catch basin should have fallen below the elevation of the outlet invert in between storms. However, this only occurred on four separate instances, all of which may be explained by external events.

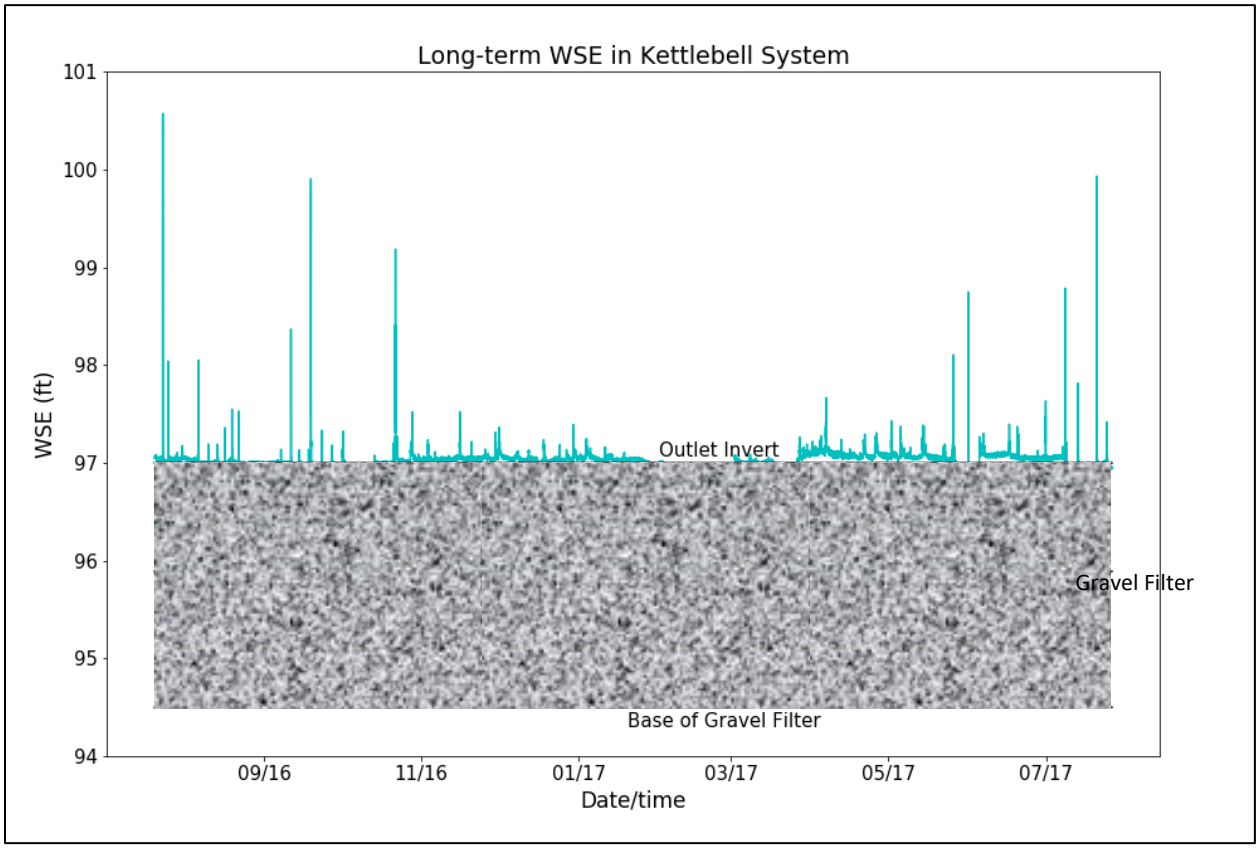

Figure 27: Water level in inlet/outlet catch basin of the Kettlebell SGF

The first instance where the water level appeared to dip below the outlet invert occurred on March 13, 2017 and was due to the catch basin being cleaned by a vacuum truck. The other three instances, which occurred on May 26th, June 1st, and July 9th may be due to the extension of the system's siphon and installation of a second siphon. On May 4th the original siphon, which

had been installed during construction of the SGF, was extended downstream with additional lengths of PVC pipe to increase the potential driving head for the device. A second, larger diameter PVC siphon was also installed to increase the available drainage capacity. In order for these siphons to start draining the system, the water level above the siphon inlet must be significantly greater than the water level above the siphon outlet. The rain events on May 26th, June 1st, and July 9th appear to have been large enough to significantly increase the water level in CB #1 and initiate the siphons. After the storms ended, the WSE in CB #1 continued to fall at a steady rate of approximately 9 inches per day. The siphons continued draining the system until the next storm event refilled the system storage. While the siphons appeared to be able to drain the system, they were only initiated during very high flow events where the WSE in CB #1 exceeded a relative elevation of approximately 98 ft (i.e. approximately 1 ft greater than the outlet invert).

Overall, due to the extremely low permeability of the soils at the Kettlebell site, the system did not significantly reduce runoff volumes through infiltration. Additionally, because system storage remains filled throughout most storm events, the system provided almost no benefit in terms of reducing and/or delaying peak flows. The siphons only allow the system to drain after very large rain events due to the limited difference in head between the system and Berry Brook.

Based on the hydrographs for the Grove St subsurface gravel filter, the system appears to have been functional and was infiltrating a large portion of the runoff being collected. For a more precise look at the performance of the Grove St system, hydrograph data was used to determine the inflow, outflow, and infiltration volumes for each of the rain events (Table 41). A graph of the inflow versus outflow volumes for each storm event is presented in Figure 28. As one would

expect, outflow volumes appear to increase as inflow volumes increase. According to the slope of the regression line that was fit to the data, outflow volumes equate to approximately 17% of inflow volume. The cumulative flow volumes for all of the rain events during the monitoring period are presented in Table 4. The measured inflow volume of approximately 76,700 ft^3 was lower than CN-based runoff volume estimate of 93,200 ft^3, but did not include the runoff flows collected by CB #4. If these flows are accounted for, the inflow volume increases to approximately 122,000 ft^3, which is significantly higher than the CN-based runoff estimate.

Table 4: Cumulative flow volumes for the Grove St system over the one-year monitoring period

Cumulative Flow Volumes (ft^3)	
Inflow Volume	76,695
Outflow Volume	12,272
Infiltrated Volume	64,423

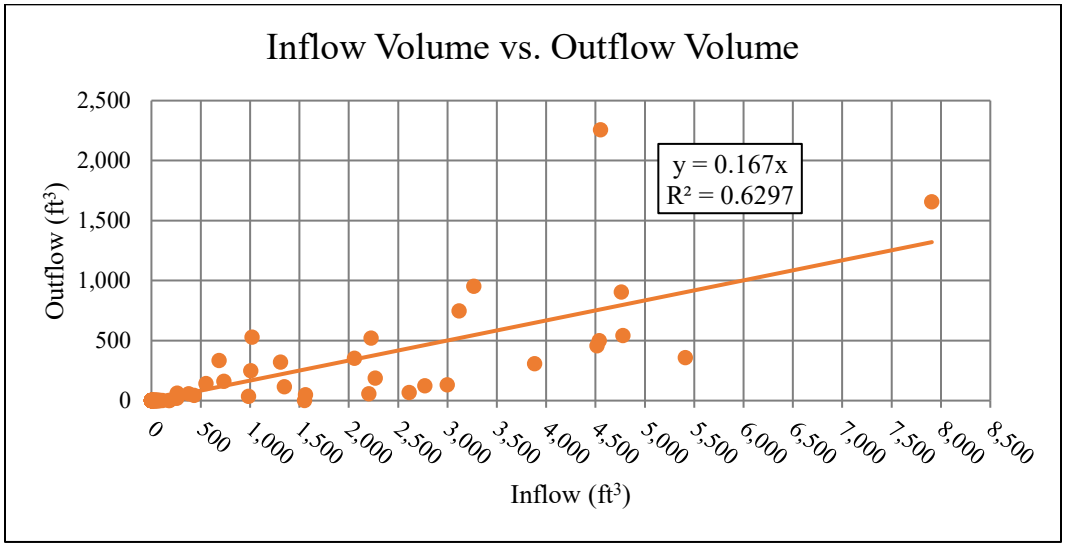

Figure 28: Inflow and outflow volumes per rain event for the Grove St system

The difference between these numbers could be related to the high flow rating curves used to calculate the flows for each catch basin. The curves were developed from very limited data and may be producing unrealistic flow estimates during very high flow events. This is

especially true for the curves relating to CB #3. The rating curve for CB#3 had to be modified to account for the runoff which bypassed the gravel filter and flowed directly to CB #4 due to clogging in the slotted high flow pipe by fine sediments. Due to this modification, the power function that was fitted to the flow and depth data had a low R^2 value of 0.52. Another potential reason for the discrepancy between the runoff and total inflow volume is that the CN-method underestimates runoff volumes. Because the initial abstraction value calculated for the watershed was 0.41 inches, all rain events which produce less than this depth of rain are assumed to not produce runoff. This is inaccurate as there is a substantial area of connected impervious cover surrounding the system which should produce some amount of runoff even during small rain events.

Runoff volume reductions (i.e. the percentage of the inflow volume that was infiltrated) were calculated by dividing the infiltrated runoff volumes by the inflow volumes. These values are presented in Table 41 in the Appendix. It should also be noted that the rainfall depths for the precipitation events which occurred throughout the winter may not be representative of the amount of runoff that was generated because snowmelt also may have contributed to flows. Over the entire monitoring period, the system reduced the runoff volume by approximately 84%. Of the 76,700 ft^3 of runoff which passed through the Grove St SGF system over the monitoring period, approximately 64,400 ft^3 infiltrated into the ground. While the system effectively reduced runoff volumes, a fairly large amount of the collected runoff bypassed the system's gravel layer due to the clogging in the upper pipe collecting CB #3 and 4 and because all of the runoff that was collected by CB #4 flowed directly to the outlet swale.

The percent runoff volume reductions for each storm event appear to be related to the cumulative rainfall depth of the storm events. As rainfall depths increase, volume reductions

decrease, potentially due to higher bypass flows through the upper pipe collecting CB #3 and 4. Figure 29 presents a comparison of cumulative rainfall depths versus percent volume reductions. A linear regression curve was fitted to the data set to highlight the general trend of the data. The distinct negative slope of the line emphasizes that volume reductions decreased as rainfall depths increased. A vertical line has been drawn on the graph at a rainfall depth of 0.27 inches to show how runoff reductions compare to the design storage volume, which is equivalent to this depth of rainfall over the system's watershed area. One can see that the majority of events which produced rainfall depths less than 0.27 inches had runoff volume reductions close to 100%.

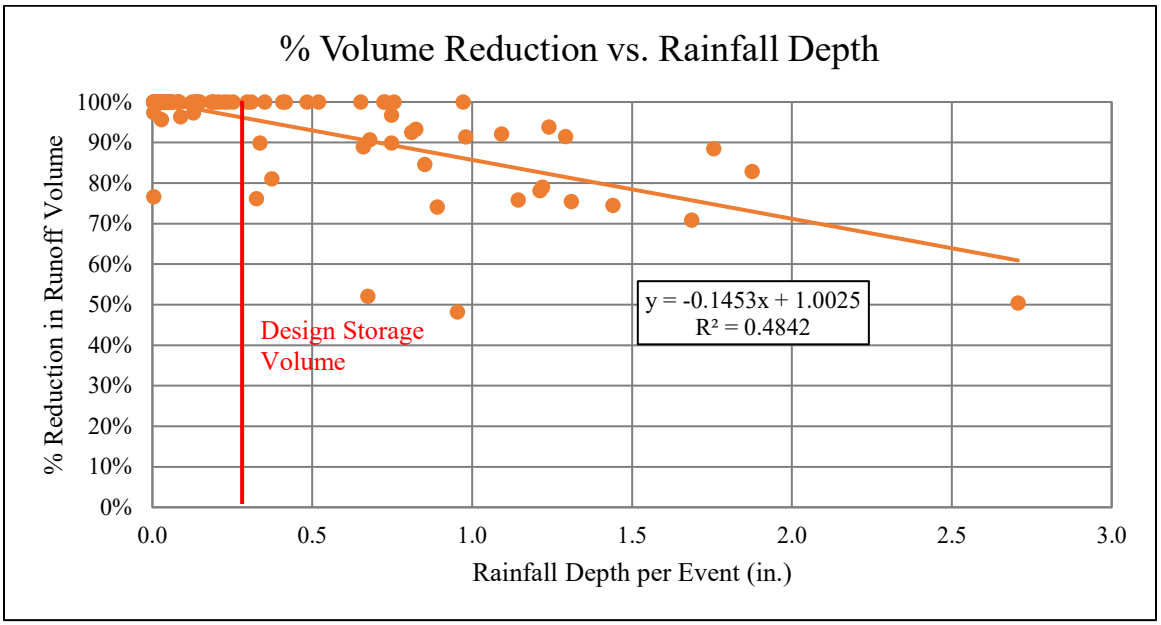

Figure 29: Percent runoff volume reductions vs rainfall depths for the Grove St SGF

A number of other factors, including rainfall intensity and duration, antecedent moisture conditions, and the occurrence of snowmelt, can affect runoff volume reductions. Those factors which increase runoff flow rates lead to a decrease in volume reductions because more of the runoff that enters CB #3 will flow through the upper pipe connecting CB #3 and 4 and bypass the gravel layer. The relationship between volume reductions and maximum inflow rates is

presented in Figure 30. The linear regression curve shows that volume reductions are negatively correlated to peak inflow rates with an R^2 value of 0.80.

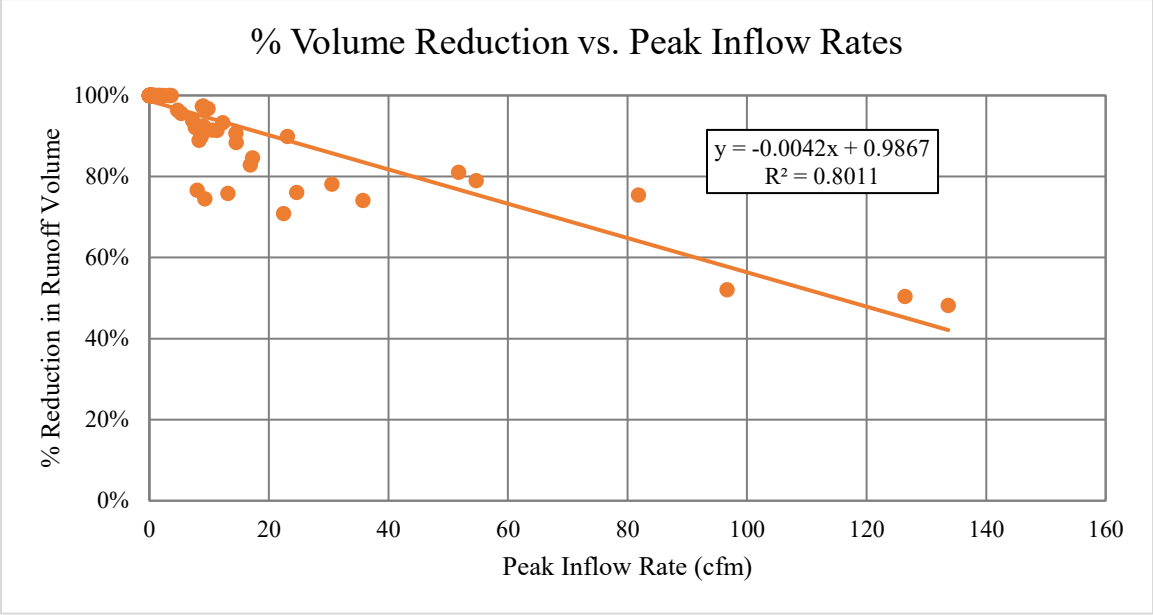

Figure 30: Percent runoff volume reduction vs peak inflow for the Grove St SGF

In addition to reducing runoff volumes, the subsurface gravel filters can reduce peak runoff flows by temporarily storing runoff and reducing runoff volumes. The Grove St system's impact on peak flows can be evaluated by comparing the maximum flow rates of the SGF's inflow and outflow hydrographs. Figure 31 shows how flows are reduced as they pass through the system for the rain event which occurred on 11/30/2016. The difference between the flows provides a quantitative measure of the system's ability to reduce peak flows. The flows presented in Figure 31 do not include the runoff which was collected by CB #4. One should also note that for monitoring purposes, the Grove St SGF was modified so that the gravel filter layer did not drain to the system's outlet, as described in section 3.4.1. Water could only flow from the gravel layer to CB #4 if the layer became completely filled and started to overflow into CB #4 through the upper pipe connect CB #3 and 4. Peak flow reductions are therefore simply a measure of how

much runoff drained through the slotted/perforated inlet pipes into the gravel layer versus how much bypassed due to the sediment clogging the inlet pipes.

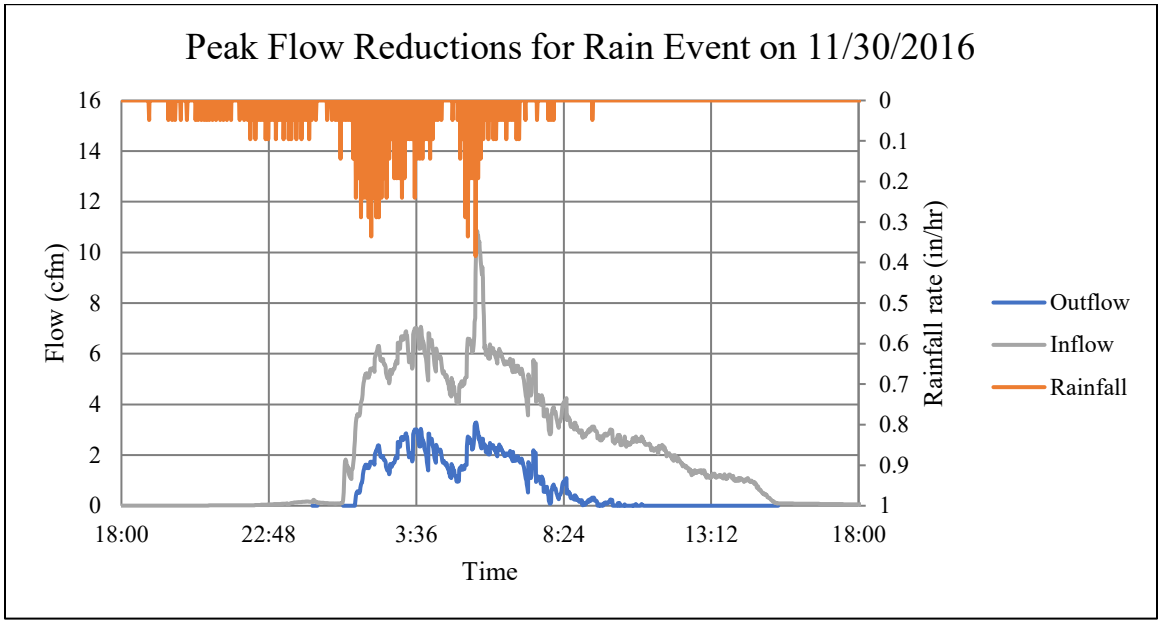

Figure 31: Comparison of inflow and outflow hydrographs for the Grove St system on 11/30/2016

The peak flow reductions for each event are provided in Table 42 in the Appendices. On average, the peak flows were reduced by 88%. For those events which exhibited more than 0.5 inches of rainfall, the average peak flow reduction for system flows decreases to approximately 70%. The graph of peak inflows versus peak outflows for each storm event (Figure 32) shows that as peak inflows increase, the amount of reduction the system provides decreases. This is demonstrated by the regression curve, which steepens as peak inflows increase suggesting a decrease is outflow reduction. Peak flow reductions and the percent of runoff infiltrated could have been further increased by cleaning out the perforated inlet pipes.

As with volume reductions, peak flow reductions appear to be higher for smaller rain events and frequently reached 100% when rainfall depths were less than 0.5 inches, as shown in Figure 33. This result is reasonable because when runoff flows are low, bypass flows are close to zero and almost all inflows drain into the gravel layer. Similarly, peak flow reductions appear to

decrease in relation to the maximum rainfall intensity during storm events, as show in Figure 34. Peak flow reductions are important for assessing system performance, especially when CSO reduction is a goal of stormwater management.

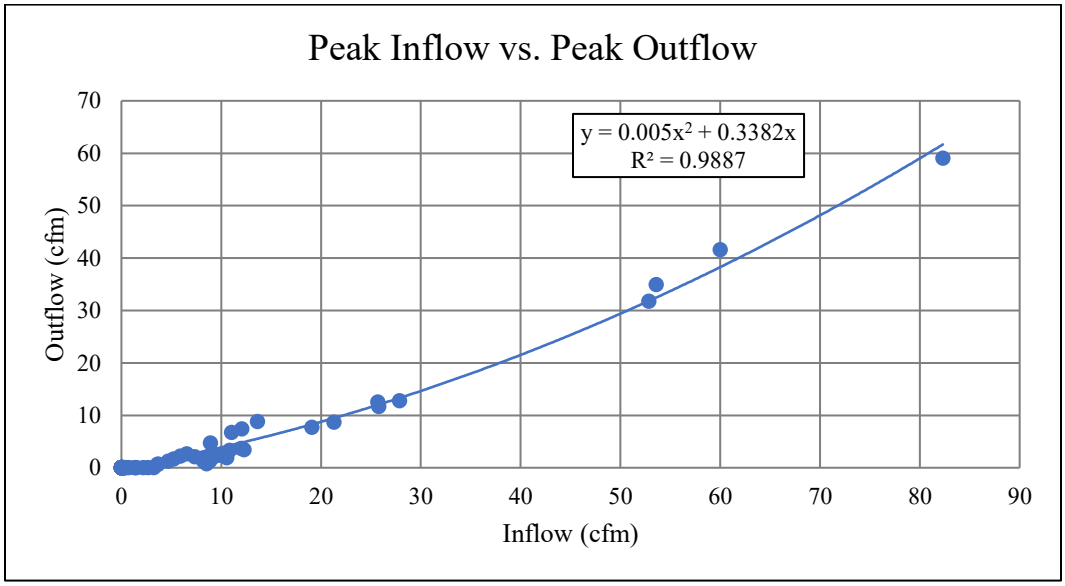

Figure 32: Peak inflows and outflows per rain event - Grove St SGF

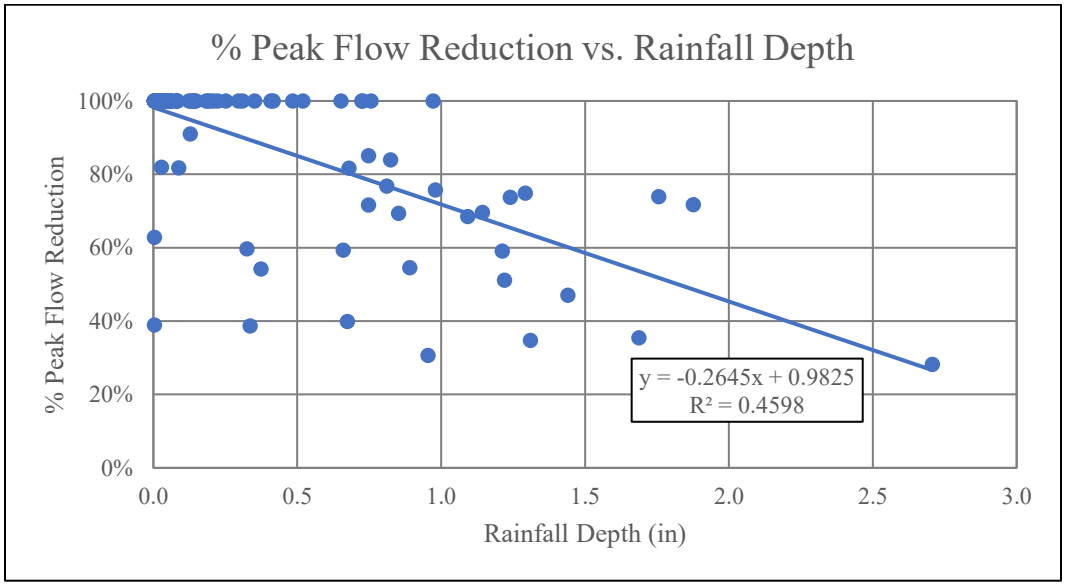

Figure 33: Percent peak flow reduction vs rainfall depth per storm event - Grove St SGF

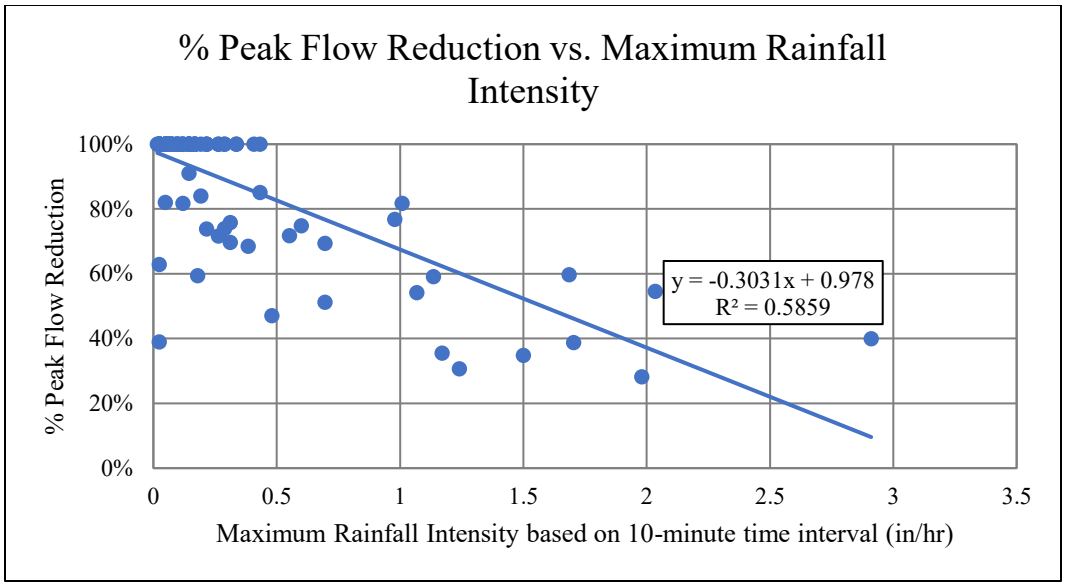

Figure 34: Percent peak flow reduction vs maximum rainfall depth per storm event - Grove St SGF

The maximum depth of water in the gravel filter during each rain event provides a measure of system performance and was used to assess the accuracy of the infiltration models used in this study. The HOBO sensor installed in the lower inlet pipe between CB #3 and 4 provided this information. However, the sensor was only installed partway through the monitoring period and had to be removed from the system intermittently in the winter due to issues with freezing. Therefore, depth data was only collected for 27 different storm events (see Figure 35). The maximum water depths measured during each event are presented in Table 39 in the Appendix.

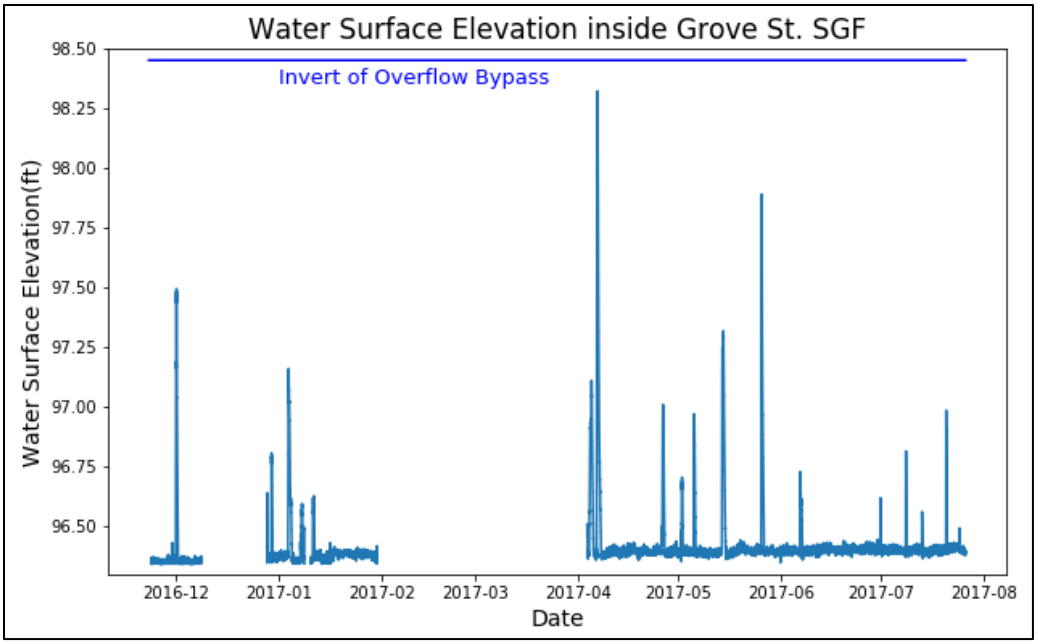

Figure 35: Water surface elevation in the gravel filter layer - Grove St System

Maximum water depth data shows that during each storm event, the system never reached capacity. Grove St's gravel layer is approximately 2.2 feet thick and can hold around 1,320 cubic feet of water, which represent the runoff from a 0.27-inch rain event. The closest the system came to completely filling was on April 6, 2017 when a 1.25-inch rain event filled the system to a maximum depth of 1.94 feet. Numerous other large rain storms, including the 1.76-inch event on May 13, 2017, were unable to raise the water level in the system more than a foot. The Grove St system appears to be able to handle the runoff from rain events that are larger than the 1-inch event for which it was originally designed.

The water depth data highlights the need for dynamic designs which account for infiltration and the temporal aspects of runoff. Static designs assume infiltration is negligible from HSG-C and D soils, but the runoff volume reduction and maximum water depth data from Grove St show that infiltration can still be a significant factor in fairly low permeability soils. For the 1.22 and 1.76-inch rain events, the Grove St system infiltrated a combined total of over

10,000 cubic feet of runoff, which is just over half of the runoff produced by these storms. If the Grove St SGF's perforated inlet pipes had been maintained and its fourth catch basin was able to drain into the gravel layer, the system would have been able to infiltrate even more water. The monitoring data for Grove St shows that neglecting infiltration in design may lead to underestimations of the amount of water that can be treated.

In addition to calculating total infiltration volumes, the instantaneous estimated infiltration rates (f) were estimated from the water balances. Rates were only calculated for the ponding portion of an event, specifically when water levels were receding. This ensured that infiltration rates were equal to the infiltration capacity of the soils and that infiltration was greater than the inflows. Of the 27 monitored rain events for which water depths were measured, only 9 produced significant ponded water depths. Figure 36 shows how the infiltration rates in the Grove St system decreased as the stored water receded during the event which began on April 6, 2017. The graph also displays the depth of water in the system over time to show how the infiltration rate changes in relation to water depth.

When the water level is near its peak, the estimated infiltration rate is at its maximum rate of around 7.7 cm/hr. Over time, both the infiltration rate and water level steadily decreased until the water dips below a depth of approximately 0.3 ft, or about 9 cm, and the infiltration rate levels off at around 0.5 cm/hr. At high water levels, the estimated infiltration rate appears to follow Darcy's Law, which maintains that the infiltration rate is linearly related to water depth. When the water level is low, the infiltration rate plateaus and seems to be only minimally affected by water level fluctuations. These observations may be a result of the occurrence of horizontal infiltration during ponding. When the water depth is high, more of the systems sides are submerged, creating larger infiltration areas and allowing for high horizontal infiltration

rates. As the water level drops, the wetted area is reduced and horizontal infiltration decreases. Once the water level drops to just 0.3 ft deep, only a small portion of the sides are submerged, making horizontal infiltration insignificant compared to vertical infiltration through the system's base. The relationship between water depth and infiltration rate lends credence to the hypothesis that horizontal infiltration accounts for a significant portion of the total infiltration volume when runoff ponds in the Grove St gravel filter.

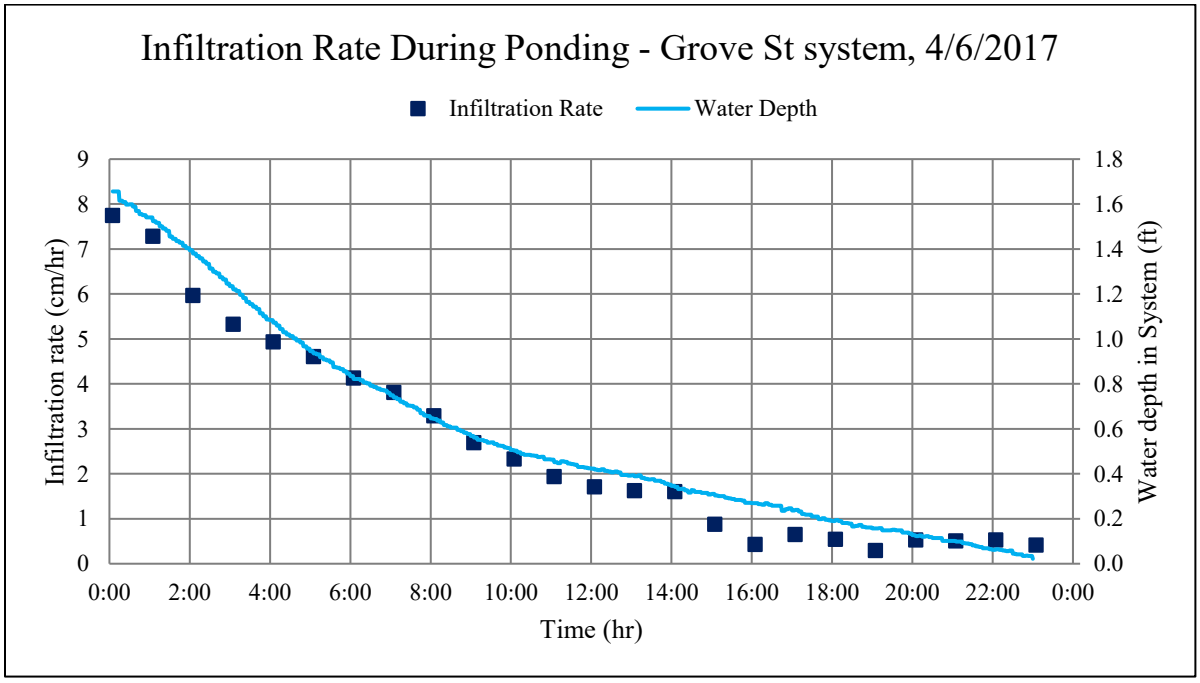

Figure 36: Estimated infiltration rate for the Grove St system during the rain event which occurred started on 4/6/2017.The infiltration rates were averaged over 1-hr intervals.

The average and maximum estimated infiltration rates and water depths for the 9 storm events are presented in Table 5. The Grove St system achieved infiltration rates greater than 5.0 cm/hr for the storm event which produced the largest water depths. Average infiltration rates during ponding ranges from about 0.8 to 3.4 cm/hr, with a median value of 1.8 cm/hr. All of these rates are much high than initial estimates based on soil type. On average, the rates are also larger than then K_{fs} values measured in the field using the Guelph permeameter, the maximum of

which was 1.11 cm/hr (Table 6). However, for storm events where the average water depth in the system remained fairly low, such as the events on 12/29/2016, 7/8/2017, and 7/20/2017, the average and maximum infiltration rates were fairly similar to the K_{fs} values measured using the Guelph permeameter. One should keep in mind that these estimated infiltration values were developed from a relatively small portion of the water balance data that was collected for the Grove St system and are representative of the infiltration rates which occurred after the water level had peaked and begun to recede. The maximum rates may be lower than those which occurred earlier in the storm events because initial infiltration rates in unsaturated soils can be higher than those of field saturated soils due to capillary effects.

Table 5: Average and maximum estimated infiltration rates (f) and water depths (H) during ponded infiltration, Grove St system

Storm #	Date	Antecedent Dry Period (days)	Average f (cm/hr)	Max f (cm/hr)	Average H (ft)	Max H (ft)
40	11/30/2016	0.6	2.39	5.49	0.38	0.91
52	12/29/2016	2.0	0.79	1.11	0.17	0.34
54	1/3/2017	2.4	3.37	3.86	0.50	0.64
92	4/4/2017	1.7	2.22	4.12	0.32	0.70
93	4/6/2017	1.4	2.66	7.75	0.59	1.65
105	5/5/2017	1.7	1.19	2.92	0.26	0.50
109	5/13/2017	1.6	1.80	3.95	0.40	0.84
130	7/8/2017	0.8	0.93	1.26	0.18	0.37
133	7/20/2017	7.1	0.98	1.27	0.22	0.48

In Figure 37, calculated infiltration rates were graphed versus the average water depths in the system during each 1-hour time interval to determine how ponding influenced infiltration. By fitting a regression curve to the data, one can see that there is a distinct linear relationship between the two variables. Excel's best-fit line attains a high R^2 value of just over 0.9 and shows that infiltration rates are positively related to the water depth in the system. These results agree with those of Bergman et al. (2010) and Warnaars et al. (1999), both of which found that a linear equation could be effectively used to relate infiltration rates to water depths in gravel infiltration

trenches. Even through soil moisture was not monitored, the apparent linear relationship between infiltration and depth indicates that infiltration may be occurring under saturated conditions when the ponded water level starts to recede.

Hydraulic conductivity values were obtained from the linear regression equation by assuming infiltration follows a unit-gradient flow model in which the horizontal and vertical hydraulic conductivities are related to the slope and y-intercept of the linear equation, respectively. Equation 14 to Equation 16 in Section 3.5.3, show how the K-values are calculated. Based on the linear regression curve in Figure 37, the horizontal and vertical K-values were determined to be 41.9 cm/hr and 0.2 cm/hr, respectively. The higher horizontal K shows that infiltration through the sides of the system is much more significant than vertical infiltration during ponding. The K-values calculated from the linear regression curve were used in the unit-gradient model to simulation infiltration in the Grove St system and estimate the ponded water depths throughout storm events.

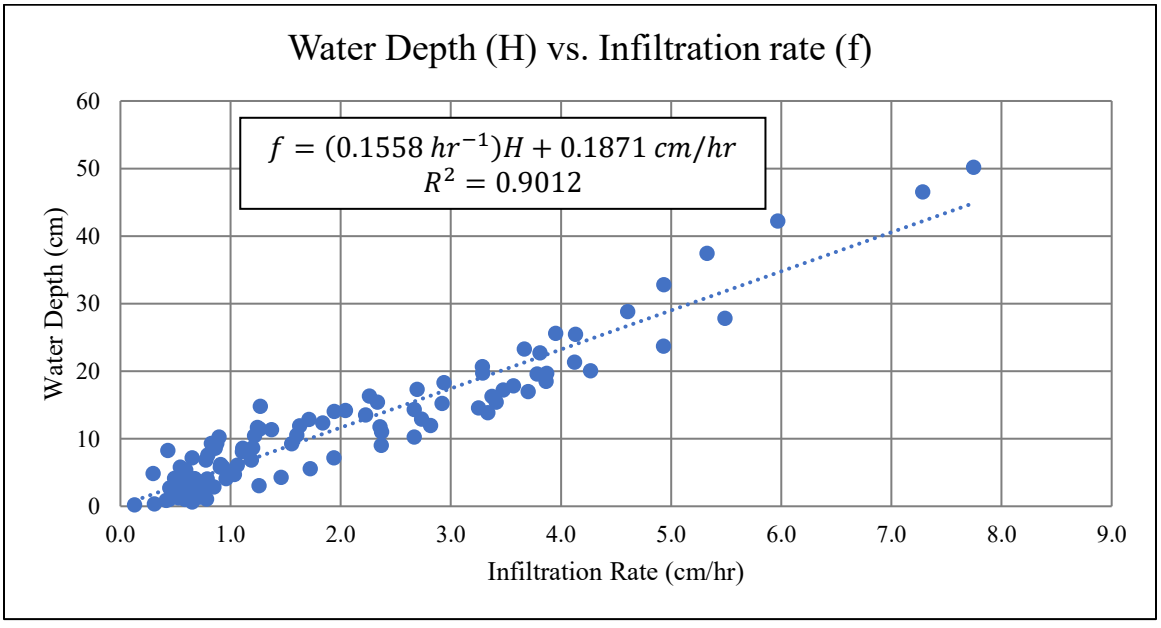

Figure 37: Linear relationship between estimated infiltration rate and water depth, Grove St system

4.2 Guelph Permeameter Results

The measured infiltration rates from the Guelph permeameter tests were used to calculate the field saturated hydraulic conductivity (K_{fs}) and matric flux potential (Φ_m) of the soils at the Grove St site. As stated earlier, measurements were not obtained for the Kettlebell site due to a number of potential issues during testing. Values for K_{fs} and Φ_m, presented in Table 6 and Table 7, were calculated using the one-ponded head, Laplace, Gardner, Richards, and least squares analysis methods. The geometric means for K_{fs} and Φ_m values from the single head and Richards methods are also presented in the table. According to Lee et al. (1985) and Gallichand et al. (1990), the geometric mean is a better measure of the average than the arithmetic mean because K_{fs} and Φ_m measurement for soils are usually log-normally distributed. The values in red in Table 6 and Table 7 are considered invalid because they are negative.

Table 6: K_{fs} estimates for the Grove St site calculated using single head, Laplace, Richards, and least squares methods

Auger Hole	Relative elevation (ft)	K_{fs} Values (cm/hr)					
		Single head method	Laplace method	Richards method	Least squares method	Geometric mean of Single head	Geometric mean of Richards
#1	98.12	0.02	0.08	0.84	0.49	0.06	0.53
		0.08	0.32	0.59	-	-	-
		0.09	0.30	0.56	-	-	-
		0.12	0.35	0.39	-	-	-
		-	-	0.39	-	-	-
		-	-	0.50	-	-	-
	96.17	1.06	5.38	2.38	0.51	1.06	1.11
		1.17	4.44	0.74	-	-	-
		1.02	3.35	0.85	-	-	-
		1.02	2.86	-1.68	-	-	-
		-	-	-0.05	-	-	-
		-	-	1.02	-	-	-
#2	98.19	0.02	0.11	-	-	-	-
#3	97.12	0.02	0.11	-	-	-	-

Table 7: Φ_m estimates for the Grove St Site calculated using single head, Gardner, Richards, and least squares methods

Auger Hole	Relative elevation (ft)	Φ_m Values (cm^2/hr)					
		Single head method	Gardner method	Richards method	Least squares method	Geometric mean of Single head	Geometric mean of Richards
#1	98.12	0.40	0.50	-4.67	-1.90	1.57	0.89
		2.12	2.88	-3.13	-	-	-
		2.31	3.31	-2.92	-	-	-
		3.08	4.77	0.89	-	-	-
		-	-	-0.61	-	-	-
		-	-	-2.15	-	-	-
	96.17	26.47	32.95	18.359	32.30	26.58	30.51
		29.22	39.68	28.432	-	-	-
		25.41	36.45	27.77	-	-	-
		25.41	39.42	54.70	-	-	-
		-	-	40.15	-	-	-
		-	-	25.35	-	-	-
#2	98.19	0.61	0.78	-	-	-	-
#3	97.12	0.58	0.75	-	-	-	-

While the Φ_m values presented in Table 7 were not directly used for further calculations, they provide useful information about the unsaturated properties of the soils and show how the soils change with depth. At a relative elevation of approximately 98 ft, which corresponds to the soils along the sides of the system's gravel layer, the Φ_m values from the one-ponded head method range from 0.40 to 3.08 cm^2/hr with a mean value of 1.57 cm^2/hr. In the soils near the bottom of the system (i.e. an elevation of approximately 96 ft), the Φ_m values increased to between 25.41 and 29.22 cm^2/hr with a mean value of 26.58 cm^2/hr. This shows that the soils near the bottom of the system may be different from those along the sides. However, this information is only from three excavations and many not reflect the native soils around the entire system. The multi-head methods (i.e. the Richards and least squares analyses) showed a similar trend with elevation; however, many of the Φ_m values calculated using these methods were invalid and could not be used for soil analysis. Reasons why the values might be negative were discussed in Section 2.4.

For the K_{fs} data, Table 6 shows that the soils at an elevation of approximately 96 ft may have a slightly higher hydraulic conductivity than those above 97 ft. The soils around 98.12 ft produced a mean K_{fs} values ranging between 0.06 cm/hr and 0.53 cm/hr, depending on the estimation method used, while soils at 96.17 ft produced a mean K_{fs} values between 0.51 cm/hr and 1.11 cm/hr. Another trend that can be observed from the values in Table 6 is that at 98.12 ft, the Richards method produced K_{fs} values that are significantly larger than those from the single head or Laplace methods. In contrast, K_{fs} values for soils around 96.17 ft were similar for the single head and Richards methods, and larger for the Laplace method. According to the theory behind these methods, the Laplace analysis should produce the largest K_{fs} values because the method assumes capillary forces are negligible (i.e. soils are under saturated conditions). Reynolds and Elrick (1985) suggest that measured values may be incorrect if the Richards analysis produces a larger K_{fs} than the Laplace analysis. The accuracy of the Richard's K_{fs} values measured at 98.12 ft is questionable.

One should keep in mind when looking at the Guelph permeameter test results that the instrument measures a combination of horizontal and vertical infiltration. The work of Reynolds and Elrick (1985) showed that the K_{fs} calculated from Guelph measurements was effectively an average of the horizontal and vertical K_{fs} of a soil. In an ideal isotropic soil, these values are fairly similar; but in many natural soils, anisotropy dominates. The horizontal and vertical hydraulic conductivities of a media can vary significantly. In an attempt to determine the horizontal conductivity of soils surrounding the Grove St SGF, the single head K_{fs} values were compared to the dimensionless ratios of borehole radius to ponded depth (i.e. a/H). Reeve and Kirkham (1951) found, while measuring saturated hydraulic conductivity (K_{sat}) using the piezometer, auger hole, and tube methods, that the permeability of soils decreased linearly in

response to increasing test hole diameter. The article proposed that this observation was due to the anisotropic properties of the test soils and that one could theoretically calculate the horizontal K_{sat} by fitting a linear regression curve to a/H vs. K_{sat} data and determining the K-value as the limit of the a/H ratio approached zero. Horizontal K_{fs} values were estimated for this study by extending Reeve and Kirkham's theory about anisotropy to the Guelph infiltration measurements. Figure 38 and Figure 39 present graphs of the single head K_{fs} values vs. the a/H ratios used for each test.

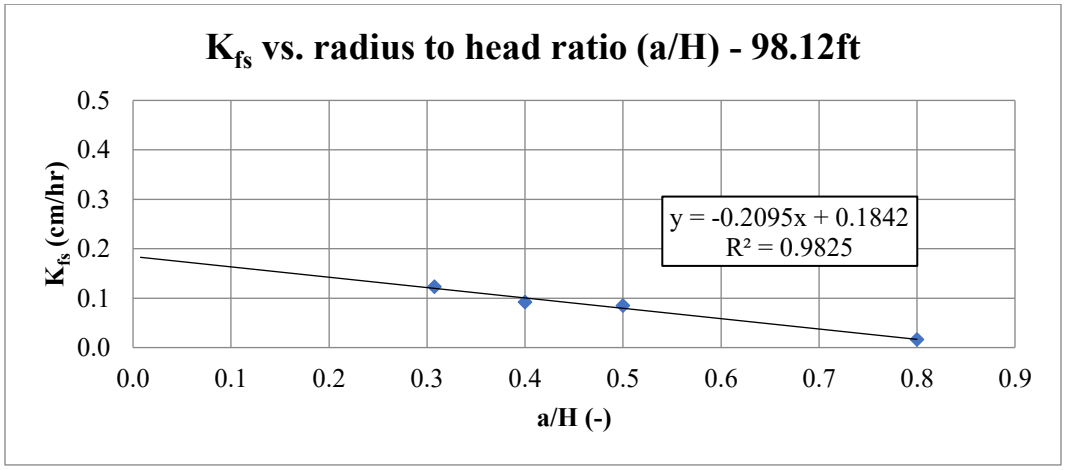

Figure 38: Single head K_{fs} vs. hole radius to head ratio (a/H) for soils at a relative elevation of 98.12 ft

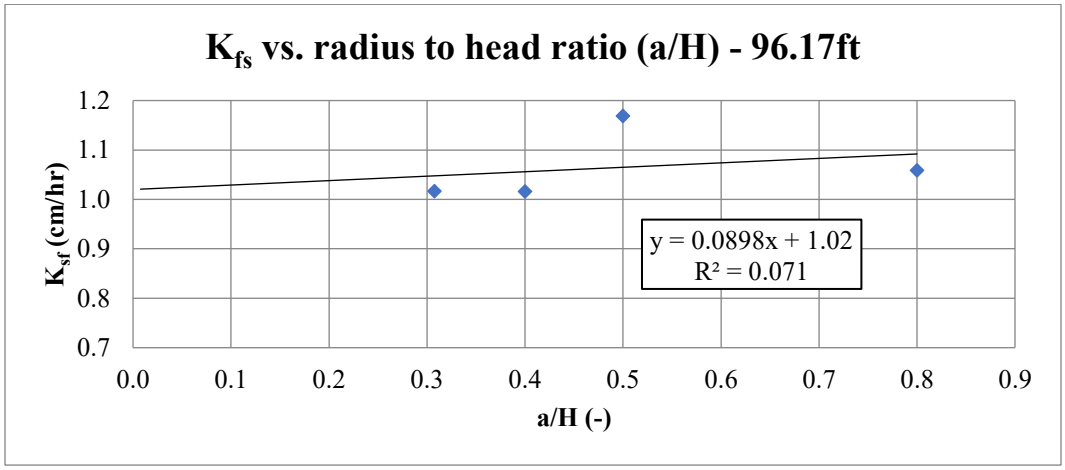

Figure 39: Single head K_{fs} vs. hole radius to head ratio (a/H) for soils at a relative elevation of 96.17 ft

As predicted, Figure 38 shows a fairly distinctive linear increase in conductivity as the a/H ratio decreases. The relationship between K_{fs} and a/H indicates that the soils being tested are anisotropic and have a greater horizontal K_{fs} than vertical K_{fs}. By fitting a regression line to the data and finding the value for K_{fs} as a/H approaches zero, it was estimated that the horizontal conductivity is approximately 0.2 cm/hr for the soils around 98 ft. Figure 39 indicates that the soils at around 96 ft are also anisotropic, but appear to have a slightly lower horizontal K_{fs} than vertical K_{fs}, as indicated by the positive slope of the regression line. As the a/H ratio approaches zero, the conductivity value decreases to approximately 1.0 cm/hr. The relationship between K_{fs} and a/H is not very distinct in Figure 39. While this method of calculating horizontal hydraulic conductivities has some theoretical support, more infiltration measurements are needed to obtain definitive results.

Overall, the data obtained from the Guelph permeameter tests provides some information about the hydraulic properties of the soils around the perimeter of the Grove St system. The relative elevations of measurements show that the soil properties change with depth. Additionally, the measurements provide some idea of the magnitude of the hydraulic conductivity of the soils at the site. However, due to the limited number of measurements and potentially high degree of heterogeneity of natural soils, additional data was obtained from soil samples taken from excavations at both the Grove St and Kettlebell sites. The results of the soil sample analyses are provided in the follow section.

4.3 Particle Size Distributions and Related Soil Characteristics

The results for the sedimentation and sieve tests were combined to produce complete particle size distributions for the seven soil samples. Figure 40 and Figure 41 present graphs of the PSDs for the Grove St and Kettlebell soil samples, respectively. The graphs are each divided

into four segments, which define the composition of the soil samples based on particle size according to the Wentworth Scale. Any sediments smaller than 0.00391 mm in diameter are considered clays, sediments between 0.00391 mm and 0.0625 mm are silts, sediments between 0.0625 mm and 2 mm are sands, and sediments larger than 2 mm are gravels. Larger particles (i.e. those with a diameter greater than 64 mm), such as cobbles and boulders, were not found within the soil samples or were removed before the PSD analysis. Table 8 provides the exact percentages of each sediment type in the soil samples.

Table 8: Composition of the soil samples based on particle size

Soil Sample Composition							
Sediment Type	**GSt #1**	**GSt #2**	**GSt #3**	**GSt #4**	**GSt #5**	**KB #1**	**KB #2**
Gravel	7.3%	5.9%	0.4%	5.7%	3.6%	0.2%	0.0%
Sand	54.3%	26.0%	8.5%	31.8%	24.2%	6.1%	7.7%
Silt	17.9%	30.2%	39.1%	30.9%	42.1%	48.2%	29.3%
Clay	20.6%	37.9%	52.0%	31.6%	30.1%	45.5%	63.0%

Table 9: Mean and median values for the composition of soil samples from each site

	Grove St			**Kettlebell**		
Sediment Type	**Median**	**Arithmetic Mean**	**Geometric Mean**	**Median**	**Arithmetic Mean**	**Geometric Mean**
Gravel	5.7%	4.6%	3.2%	0.1%	0.1%	0.0%
Sand	26.0%	28.9%	24.7%	6.9%	6.9%	6.9%
Silt	30.9%	32.0%	20.7%	38.8%	38.8%	37.6%
Clay	31.6%	34.5%	32.9%	54.2%	54.2%	53.5%

Table 10: Soil texture classifications for site samples

Sample #	**Texture classification**	
	Grove St Samples	**Kettlebell Samples**
1	Sandy clay loam	Silty Clay
2	Clay loam	Clay
3	Clay	-
4	Clay loam	-
5	Clay loam	-
Mean composition	Clay loam	Clay
Median composition	Clay loam	Clay

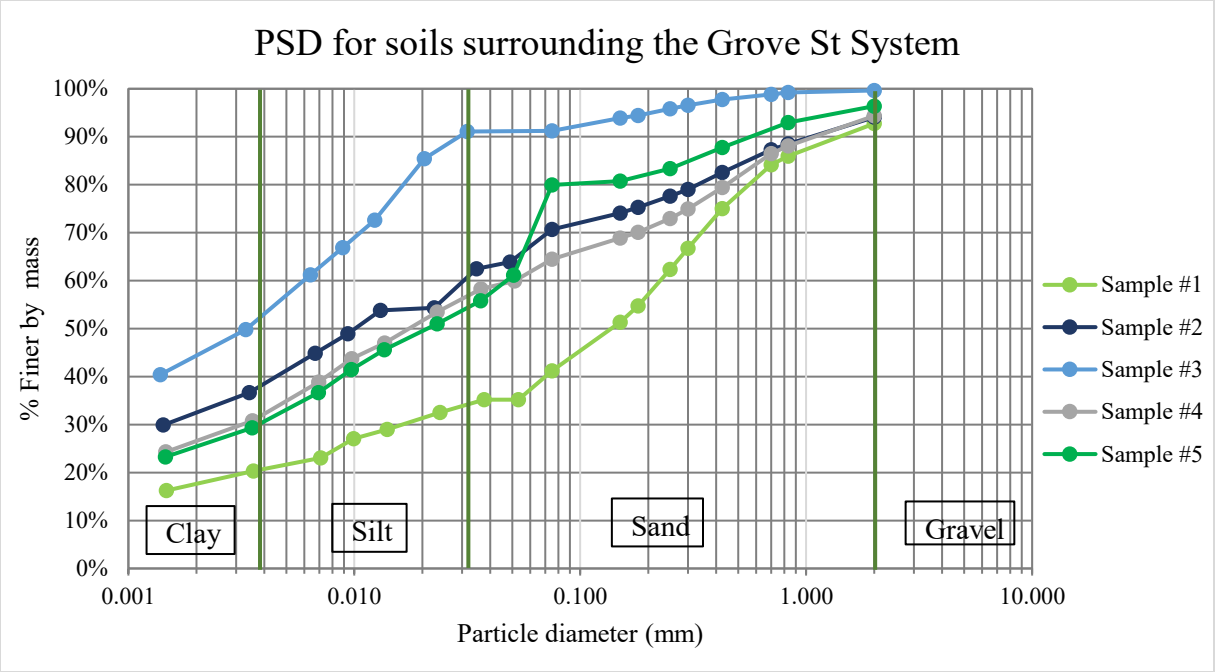

Figure 40: PSDs for the soil samples from the Grove St site

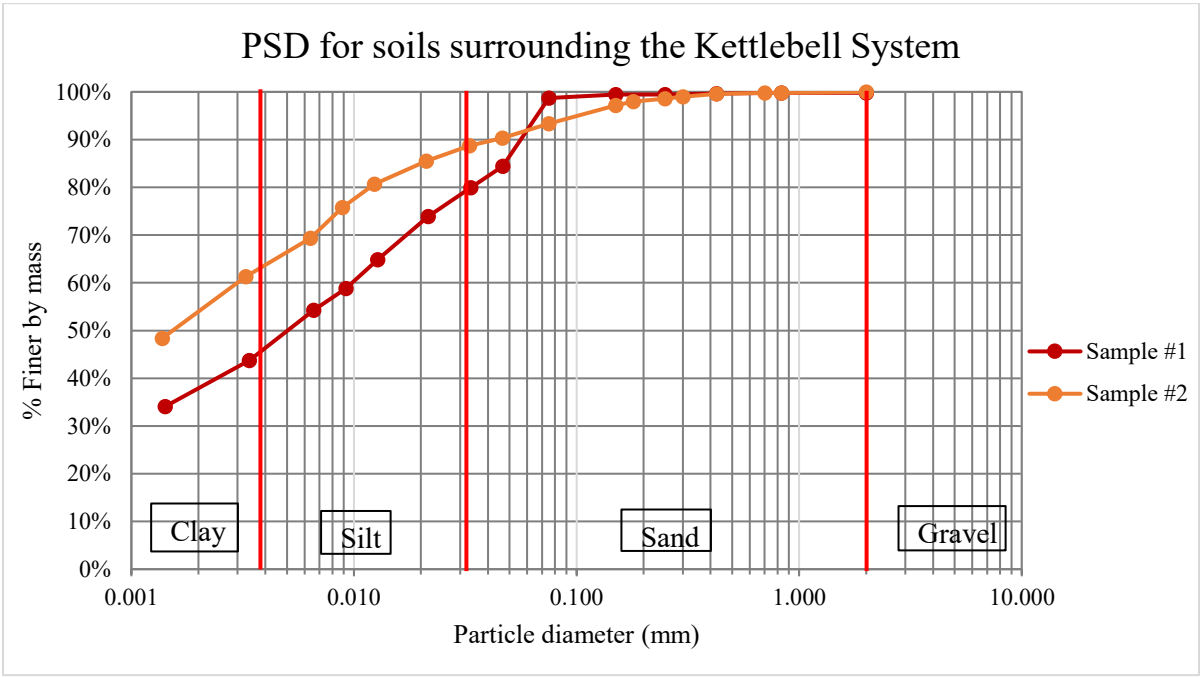

Figure 41: PSDs for the soil samples from the Seacoast Kettlebell site

The texture classifications for the soil samples, determined using the USDA Textural Classification chart (Figure 64), are presented in Table 10. Most of the soil samples from the Grove St site fell into the clay loams category, while the Kettlebell samples were classified as silty clay and clay. A variety of soil properties, including saturated hydraulic conductivity (K_s), porosity (φ), residual moisture content (θ_r), and wetting front matric potential (ψ_f), were determined based on these soil classifications. The procedures and sources used to obtain the values for each soil property are described in the Section 3.5.2 and Section 2.3, respectively. Mean values for each parameter and the sources from which they were obtained are presented in Table 11. The values highlighted in orange and yellow were calculated with equations from Rawls et al. (1983) and Brakensiek and Onstad (1977), respectively, using the other soil parameters as input.

Although many researchers have found correlations between soil classifications and various soil properties, there is a lot of variation within individual classes. Compaction, the presence/absence of organic matter, macropores, moisture content, and a number of other factors can have a large impact on the properties of a specific soil class. The standard deviations and median values provided in Table 11, offer some measure of the variability of the parameters. Based on these values, one can see that properties such as φ, θ_s, θ_r, and effective porosity (φ_e) are fairly consistent within soil classes and vary the least of all of the soil parameter. The other properties, including ψ_f, air-entry matric potential (ψ_b), pore-size distribution index (λ), K_s, and K vary significantly within soil classes. Panian's (1987) estimate of ψ_f is approximately 11 cm for silty clays, while Carsel and Parrish (1988) estimated a value of over 175 cm for the same soil class. While determining soil properties based on soil class requires minimal effort, the high variability of certain properties makes field measures a preferred alternative.

Table 11: Soil properties in terms of soil classification

Parameter	Soil Class	(Rawls et al. 1992)	(Rawls et al. 1983)	(Brakensiek et al. 1981)	(Panian 1987)	(Carsel and Parrish 1988)	(McCuen et al. 1981)	Median	Standard Deviation
K_s (cm/hr)	SCL	0.43	0.30	0.073	10.228	1.389	4.719	0.91	4.00
	CL	0.23	0.20	0.099	0.486	0.086	3.632	0.22	1.40
	SC	0.09	0.10	0.064	1.987	0.001	1.807	0.10	0.95
	C	0.06	0.06	0.020	3.641	0.002	1.071	0.06	1.45
φ_e (cm^3/cm^3)	SCL	0.330	0.330	0.222	0.387	0.290	0.331	0.33	0.06
	CL	0.389	0.389	0.295	0.363	0.315	0.388	0.36	0.04
	SC	0.423	0.423	0.298	0.388	0.290	0.39	0.39	0.06
	C	0.385	0.385	0.254	0.312	0.312	0.37	0.31	0.05
φ or θ_s (cm^3/cm^3)	SCL	0.398	0.398	0.41	0.48	0.39	-	0.40	0.04
	CL	0.464	0.464	0.48	0.47	0.41	-	0.47	0.03
	SC	0.479	0.479	0.48	0.49	0.36	-	0.48	0.06
	C	0.475	0.475	0.48	0.49	0.38	-	0.48	0.05
θ_r (cm^3/cm^3)	SCL	0.068	0.068	0.188	0.093	0.100	-	0.10	0.05
	CL	0.075	0.075	0.185	0.107	0.095	-	0.10	0.05
	SC	0.056	0.056	0.182	0.102	0.070	-	0.09	0.06
	C	0.090	0.090	0.226	0.178	0.068	-	0.13	0.07
ψ_b (cm)*	SCL	28.08	-	46.28	7.81	16.95	-	28.08	21.11
	CL	25.89	-	42.28	31.25	52.63	-	42.28	13.19
	SC	34.19	-	41.72	15.87	200.00	-	41.72	73.97
	C	37.30	-	63.96	10.00	125.00	-	63.96	44.20
λ (-)*	SCL	0.250	-	0.37	0.44	0.48	-	0.37	0.09
	CL	0.194	-	0.28	0.40	0.31	-	0.28	0.08
	SC	0.127	-	0.21	0.38	0.09	-	0.15	0.11
	C	0.131	-	0.21	0.41	0.09	-	0.17	0.12
ψ_f (cm)*	SCL	19.66	21.85	34.11	5.59	11.95	19.43	19.66	12.17
	CL	18.37	20.88	32.63	22.73	39.95	21.41	22.73	9.25
	SC	24.68	29.22	33.66	11.64	178.74	22.40	29.22	57.98
	C	26.89	31.63	51.60	7.24	111.71	27.11	31.63	34.17

Note: Value highlighted in orange and yellow were calculated with equation from Rawls et al. (1983) and Brakensiek and Onstad (1977), respectively
*Value based on geometric mean of samples

Some soil properties were also calculated with regression equations that used the PSD data as input. The equations were developed by Rawls and Brakensiek (1989) and account for the percentages of sand and clay in a soil sample. Median and mean percentages (Table 9) for the soil samples were used for the regression equations. The calculated soil parameters, presented in Table 12, agree with the values based on the soil classifications.

Table 12: Soil parameters calculated using regression equations from Rawls and Brakensiek (1989)

	Grove St		Kettlebell	
Parameter	**Median**	**Mean**	**Median**	**Mean**
(median) θ_s	0.47	0.47	0.48	0.48
ψ_b (cm)	45.08	42.07	125.33	125.33
λ (-)	0.25	0.23	0.13	0.13
θ_r (cm^3/cm^3)	0.10	0.11	0.10	0.10
K_s (cm/hr)	0.13	0.13	0.005	0.005
K (cm/hr)	0.064	0.064	0.0025	0.0025
ψ_f (cm)	31.54	29.55	90.39	90.39

4.4 Modeled System Performance

The water balance results and inflow/outflow hydrographs show how the two subsurface gravel filters systems in Dover, NH perform in terms of runoff volume and peak flow reduction. However, they provide limited information about the factors influencing infiltration within the systems and particularly the significance of horizontal infiltration. Infiltration models were developed to help analyze these factors and determine if system performance depends on horizontal infiltration, soil moisture, and the dynamics of stormwater runoff. By comparing the model results to the monitoring data, one can evaluate the accuracy of the models. Changes in the water depth were used as a proxy for infiltration rates because the water depth is controlled by the infiltration rate. Therefore, difference between the simulated and measured water depths imply that the simulated infiltration rates are different from the actual rates. The total infiltration volume for each storm event was also used to compare modeled and measured system performance.

4.4.1 Saturated/unsaturated model

The saturated/unsaturated model, which was only used to simulate the Grove St system, produced values for the moisture content of the soils below the system, the depth of water in the gravel layer, and the instantaneous infiltration rates. The model was initially run using four sets of soil parameters to determine how slight variations in the input parameters would affect the modeled infiltration rates. The results of these preliminary simulations, in terms of peak water depths in the gravel filter, time to peak water depth, and total infiltration volume, were compared to the monitored data using the root mean squared error (RMSE). The lowest values for RMSE were produced when the Guelph-based soil parameters were used, suggesting that these results were the closest to the measured values. Therefore, all further analyses with the saturated/unsaturated model used the Guelph-based soil parameters as input. The results from the preliminary simulations are presented in the Appendices.

Soil moisture (θ) values were calculated for each of the discrete soil layers below the system for every time step. By plotting θ for various soil layers versus time, one can analyze how infiltrated water spreads through the native soils over the course of a rain event. Figure 42 and Figure 43 each present four graphs of the simulated θ values during the rain events on 6/30/2017 and 4/4/2017, respectively. Each of the four graphs represent a different soil depth below the system gravel filter (i.e. 0, 20, 50, and 100 cm below the system). One can see that the soils directly below the system experience rapid increases in soil moisture at the start of the events. The soil moisture then plateaus as the soil approaches saturation; although, none of the soil layers actually reach saturation during any of the simulated events. Infiltration rates were therefore defined by Richards' unsaturated flow equation. Lower soil layers have a delayed response to infiltration because the water must first pass through the upper layers. For the

simulations of the 6/30/2017 event, increases in θ occurred down to almost 160 cm. Below these depths, the water content remained unaffected by the infiltrating water during the modeled time period, which means that the model's assumption of freely draining soils is not violated.

The rain event on 4/4/2017 lasted longer and produced more runoff than the one on 6/30/2017. Due to the extend modeling period, the infiltrated water reached even deeper soil depths. The moisture content of the deepest simulated soil layer, located around 200 cm below the system, still remained unchanged throughout the duration of the storm. In reality, soils may not be freely draining because the elevation of the groundwater table could be closer to the bottom of the system. The groundwater baseflows observed in CB #4 provide evidence to support the existence of a high groundwater table at Grove St. If this is true, horizontal infiltration rates may be contributing to an even larger portion of the total infiltration from the system.

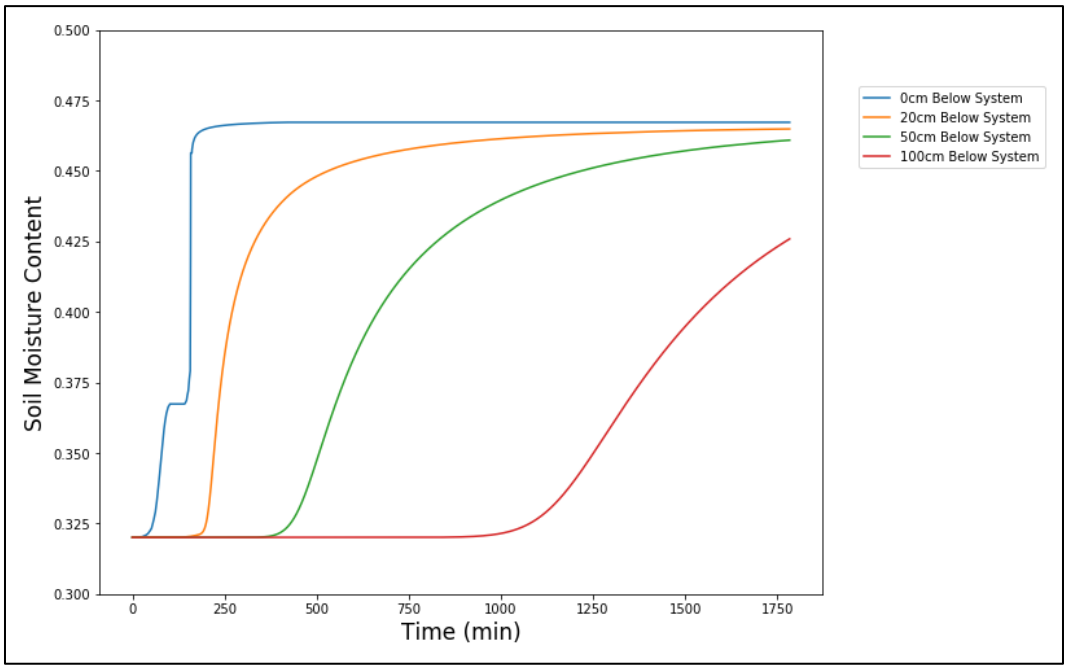

Figure 42: Simulated soil moisture content from the saturated/unsaturated model for specific soil layers below Grove St system for the rain event on 6/30/2017

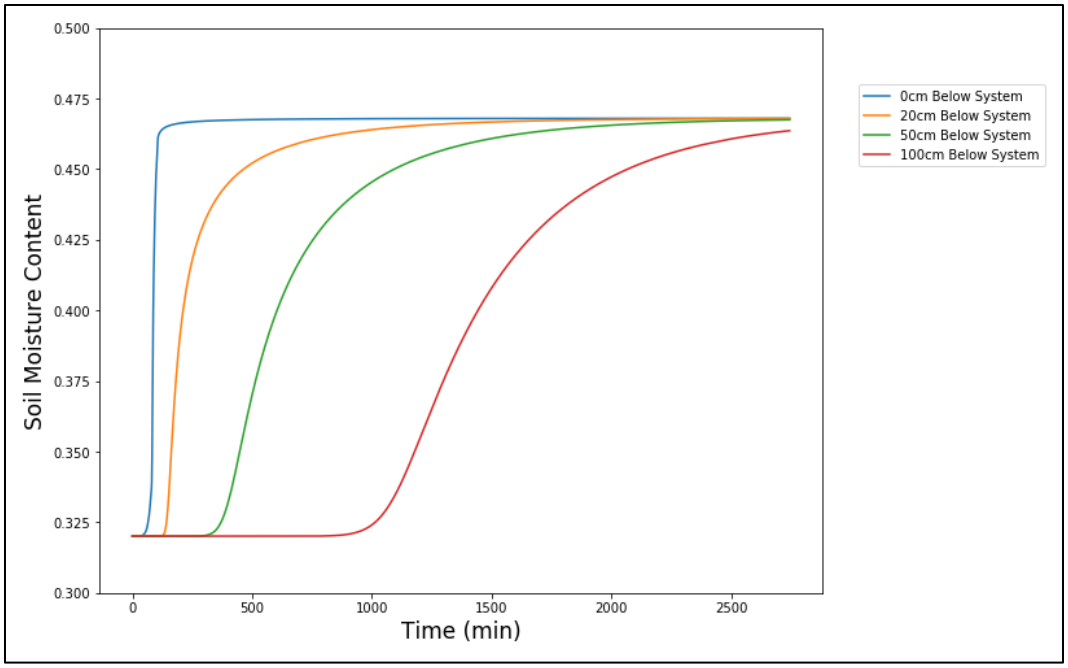

Figure 43: Simulated soil moisture content from the saturated/unsaturated model for specific soil layers below Grove St system for the rain event on 4/4/201

For most storm events, simulated infiltration rates are initially defined by the runoff inflow rates because the infiltration capacity of the soil is much higher than the amount of water available for infiltration. As inflow rates increase and approach the soil's infiltration capacity, the infiltration rate will spike. After peaking, water will begin to pond in the system storage and the infiltration rate becomes limited by the soil's infiltration capacity. Figure 44 displays a graph of the simulated infiltration rate and system water depth for the event on 11/30/2016. The graph shows that after peaking, the infiltration rate decreased at a rate defined by the increasing soil moisture, eventually approaching the value of the saturated hydraulic conductivity (i.e. 0.51 cm/hr for the Guelph-based soil parameters).

During "flashier" rain events (i.e. shorter, higher intensity events), such as that which occurred on 7/20/2017, the infiltration rate can sometimes spike after the water has already started to pond. Figure 45 shows that the simulated infiltration rate peaks just after the water level starts to rise. The delayed spike is most likely due to the rapid increase in inflow at the start

of the storm. Water enters the system and begins to pond before any significant infiltration can occur. By the time the water level starts the rise, the soils were still fairly unsaturated. During these flashier rain events, the infiltration rate spikes significantly higher than during the longer, low intensity events. The peak simulated infiltration rates for each storm ranged from about 2.45 cm/hr to over 10 cm/hr, with a median value of 3.88 cm/hr.

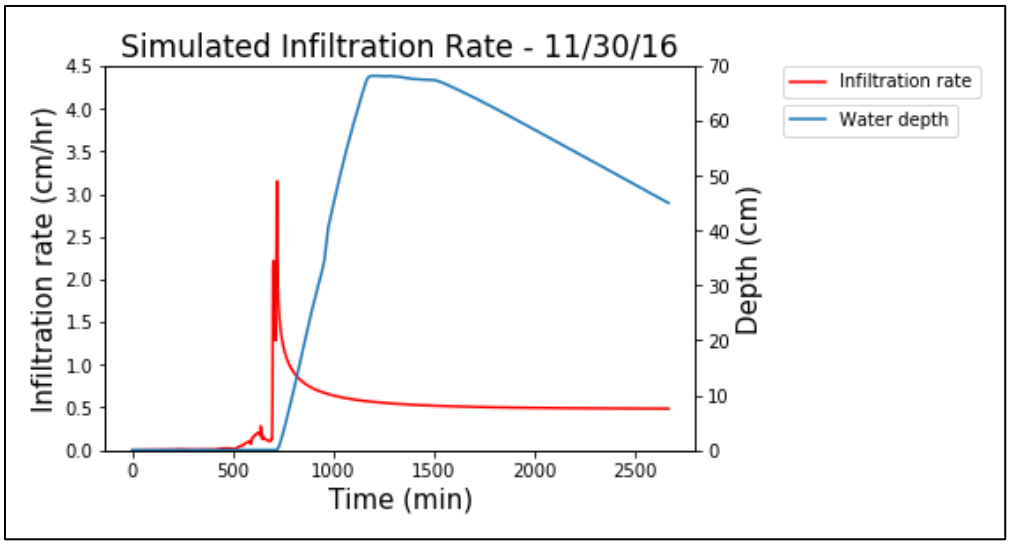

Figure 44: Simulated infiltration rate and water depth for the rainstorm on 11/30/2016

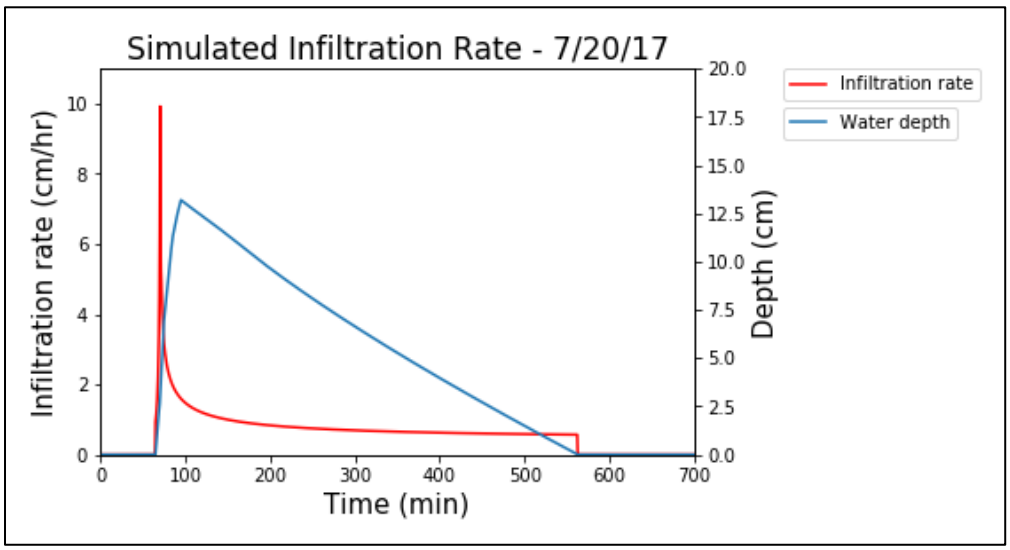

Figure 45: Simulated infiltration rate and water depth for the rainstorm on 7/20/2017

The peak rates calculated from the monitoring data should not be compared to the peak values from the model because infiltration rates based on the monitoring data were only calculated after peak ponding was reached and the water levels started to recede. For comparison purposes, the peak infiltration rates after maximum ponding were sampled from the models. The modeled rates are significantly lower, on average, than the estimated rates (Table 13). For most storm events, the modeled infiltration rates after peak ponding were less than 1.5 cm/hr (with the exception of the event where infiltration peaked after peak ponding), while the estimated rates are almost all greater than 2.0 cm/hr. The median peak infiltration rate of 3.84 cm/hr from the monitoring data was much greater than the median value of 0.60 cm/hr from the model. These differences may be attributable to the absence of horizontal infiltration in the model.

Table 13: Modeled and measured maximum infiltration rates after peak ponding

Maximum Infiltration Rates after Peak Ponding (cm/hr)		
Date	**Modeled Values**	**Measured Values**
11/30/2016	0.56	5.13
12/29/2016	0.82	1.33
1/3/2017	0.55	4.27
4/4/2017	0.50	4.64
4/6/2017	0.60	5.83
4/25/2017	0.51	3.4
5/5/2017	0.56	3.19
5/13/2017	0.53	4.28
7/8/2017	1.31	2.16
7/20/2017	1.59	2.53
Median	*0.60*	*3.84*

The simulated system water depths provide information about system performance and can be used to compare the model to the real system. Figure 46 and Figure 47 present graphs comparing the simulated water depths to the measured water depths for 13 of the 27 storm events which were modeled. Figure 46 contains all of the events in which the maximum simulated water depths completely fill the system's gravel storage layer, while Figure 47 presents events which produced simulated depths that only partially fill the storage.

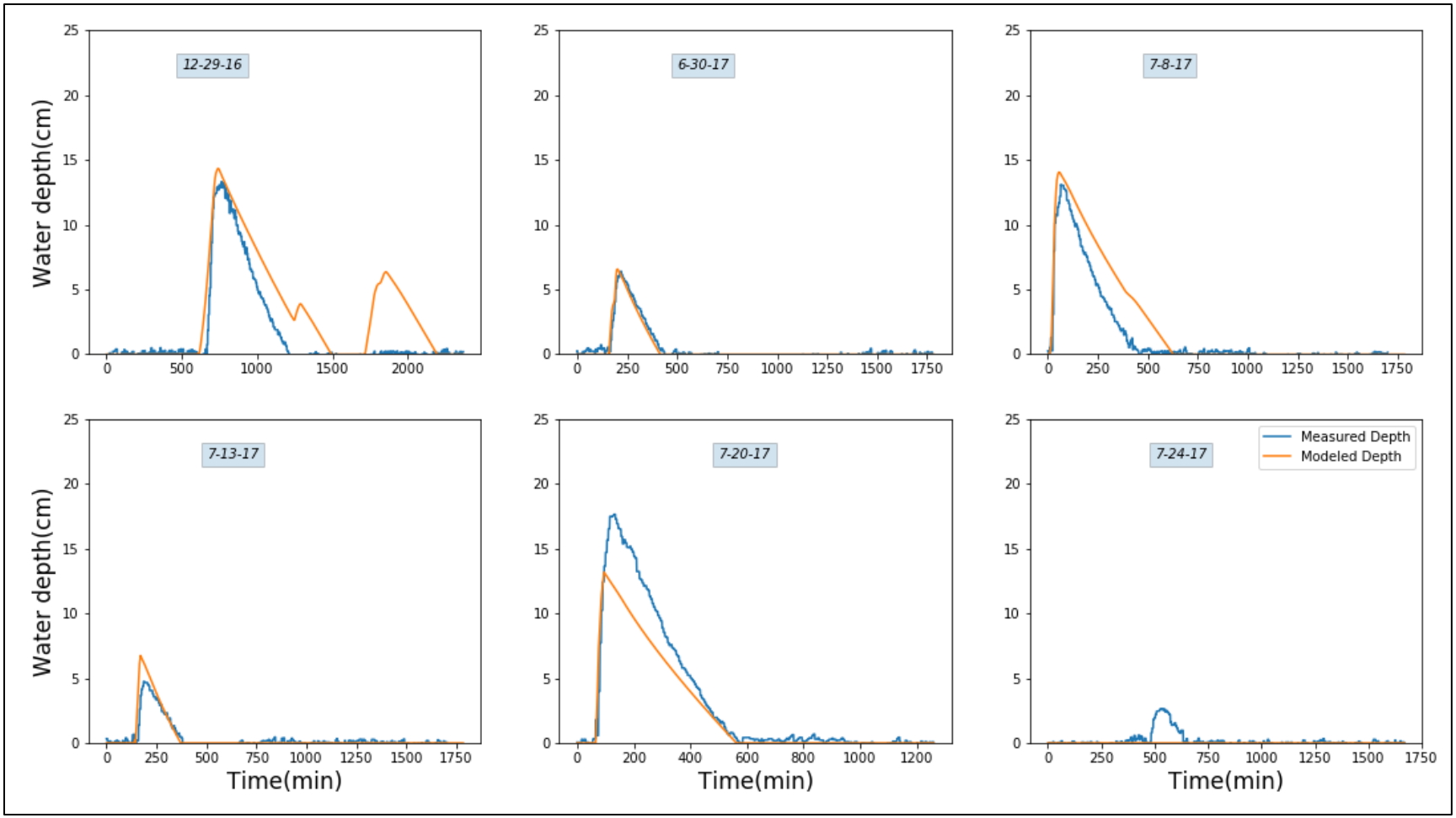

Figure 46: Comparison of simulated water depths from the Saturated/Unsaturated model to the measured water depths in the Grove St system during short duration precipitation events

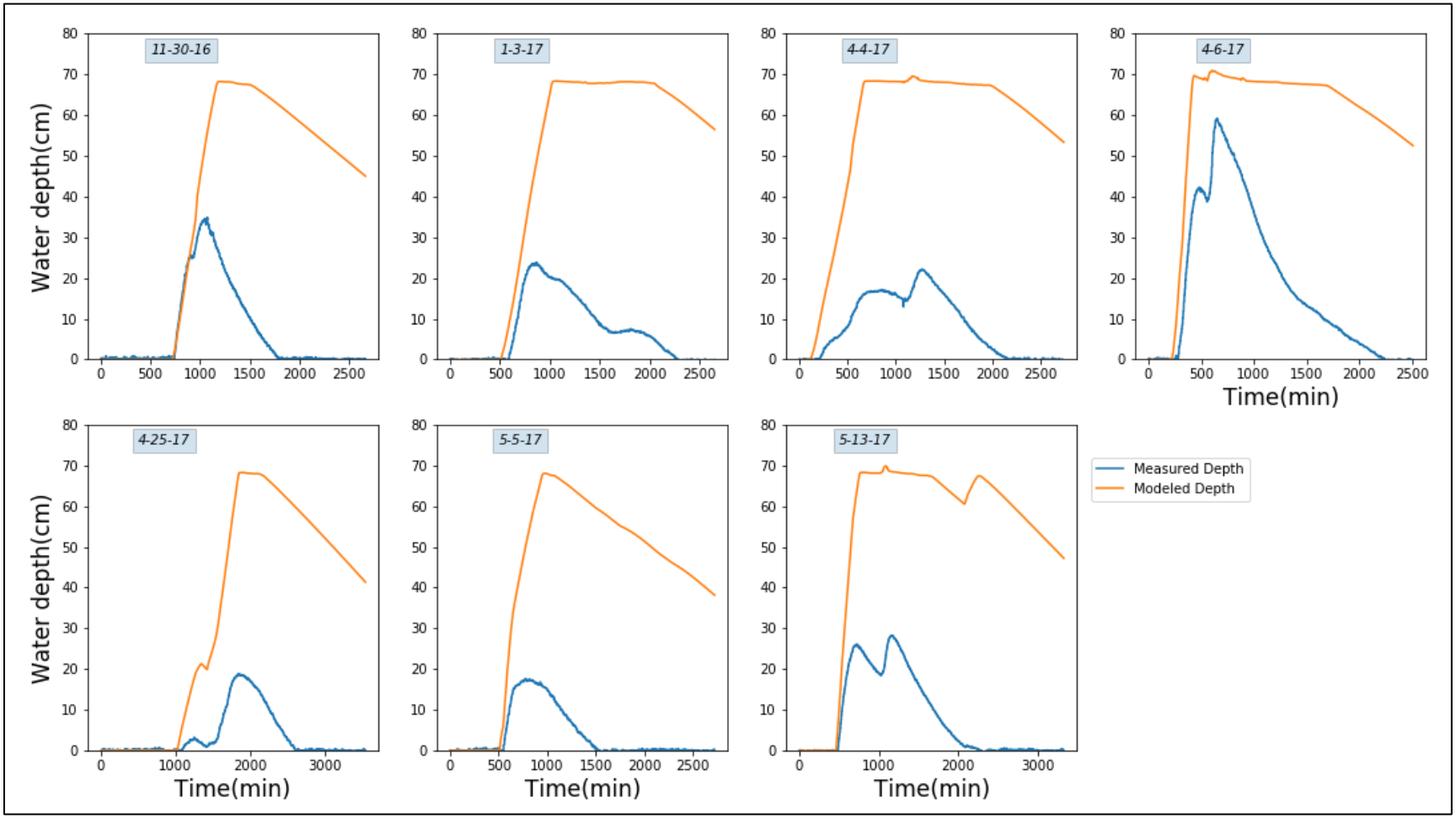

Figure 47: Comparison of simulated water depths from the Saturated/Unsaturated model to the measured water depths in the Grove St system during long duration precipitation event

By visually comparing the modeled water depths to the measured ones, it appears that the model does a fairly good job simulating infiltration processes for smaller precipitation events which produced water depths less than 20 cm (Figure 46). The simulations match the actual water depths especially well for the events between 6/30/2017 and 7/134/2017. The measured and simulated depths both appear to start rising at almost the same times, peak at about the same values, and recede at similar rates. Similarities between the depth curves support the idea that the model is effectively simulating infiltration processes within the SGF system. For the event on 12/29/2016, the modeling results appear to match the monitoring results for the first half of the event. However, the simulation shows a second water level spike during the second half of the event, which does not occur in the actual system. This inaccuracy may have occurred because the model did not account for the drainage that would occur in the soils after the first water level spike.

Differences between the simulated and measured water depths appear to be much larger for the storm events present in Figure 47, which produced water depths greater than 20 cm. While the simulated and measured water levels appear to start rising at approximately the same times, the simulated depths reach much higher peak values that only level off at the top of the gravel layer because of the overflow pipe. The closeness of the start times for the simulated and measured water level rises indicate that the model may be valid to simulate vertical infiltration rates and moisture contents, at least initially. The water levels also appear to rise at similar rates at first as shown by the graph for 11/30/2016. However, the differences in peak depths show that the model is drastically underestimating the infiltration rates after water levels begin to rise.

The accuracy of the model was assessed by performing two-sided T-tests for the mean value of the peak storage depths, time to peak, and total infiltration volume with a confidence

level of 95%. For each T-test, the mean of the measured data was compared to the mean of the model results. The mean values were derived from the modeling results for 27 different storm events for which measured water depth data was obtained. To calculate each T-statistic, the variance of the measured and modeled values was pooled. Table 14 present the results of the T-tests for the saturated/unsaturated model. The accuracy of the model was also assessed by calculating the root mean square error (RMSE) between specific modeled and measured values, including the peak storage depths, the time to peak depth, and the total infiltration volume for each storm event. The RMSE values are presented in Table 15 and will be discussed in Section 4.4.5.

Table 14: T-test comparing results of Saturated/Unsaturated model to measured data

	Data set	**n**	**t**	**α**	**$\pm t_{\alpha/2}$**	**Reject null hypothesis?**
Peak Water Depths (cm)	Full Data Set	27	2.94	0.05	±2.056	Reject
	Small Storm Events	18	-0.73	0.05	±2.11	Cannot Reject
	Large Storm Events	9	11.51	0.05	±2.306	Reject
Total Infiltration Volume (ft^3)	Full Data Set	27	-2.94	0.05	±2.056	Reject
	Small Storm Events	18	0.00	0.05	±2.11	Cannot Reject
	Large Storm Events	9	-6.00	0.05	±2.306	Reject
Time to Peak (hr)	Full Data Set	14	0.49	0.05	±2.056	Cannot Reject
	Small Storm Events	5	-0.23	0.05	±2.776	Cannot Reject
	Large Storm Events	9	0.89	0.05	±2.306	Cannot Reject

Table 15: SSE, MSE, and RMSE for the Saturated/Unsaturated model

	Peak Water Depth (cm)	Total Infiltration Volume (ft^3)	Time to Peak (hr)
SSE	17722	64597013	339045
MSE	656	2392482	24218
RMSE	26	1547	156

Based on the results of the T-tests, the peak water depths and the total infiltration volumes for the measured and model results are not statistically similar. For the larger storm events, the measured peak water depths are significantly smaller than the modeled peak depths. Additionally, the gravel filter becomes completely filled during seven of the modeled events causing some of the runoff to flow out through the overflow bypass. The total infiltration volume is reduced by the bypass flow and causes the modeled values to be statistically different from the measured ones for which the bypass did not occur. The modeled and measured data are statistically similar in terms of the amount of time it takes for the water depth to peak.

One of the most likely reasons for the differences between the results of the saturated/unsaturated model and measured data is that the model does not take into account horizontal infiltration. As the water level rises, the stored water comes in contact with a larger portion of the sidewall area, thereby accommodating horizontal infiltration, which may become a significant factor in the measured data. While the sidewall area is only about a quarter of the bottom area of the Grove St system, high horizontal K values may lead to large infiltration flows through the sidewalls.

Overall, the 1D saturated/unsaturated model appears to do a better job modelling shorter, lower magnitude rain events than the longer, higher magnitude event. When the T-tests are performed for the data from only the smaller storms, the peak water depths and total infiltration volumes of the measured and modeled data are no longer statistically different (i.e. the null hypothesis that the mean values are statistically similar cannot be rejected). Table 14 presents the

results of the T-tests when performed separately for the output of the smaller and larger storm events. During smaller, shorter duration rain events, system depths remain relatively low, indicating that vertical infiltration dominates and horizontal infiltration makes up a smaller proportion of the total infiltration rate. Longer duration events create and sustain higher water depths within the gravel storage layer for significantly longer periods of time. The events presented in Figure 47, which were ineffectively simulated, each produced measurable water depths for greater than 1500 minutes. The longer periods of water storage and higher water depths may increase the significance of horizontal infiltration causing the 1-D model to underestimated infiltration rates and overestimate water levels. For the larger storm events, the T-tests support the null hypothesis that the modeled results are significantly different from the measure data (see Table 14).

It is also important to note that most of the events which filled the system in the simulations occurred during the spring season, in the months of April and May. In contrast, the events which were more accurately modeled primarily occurred during the summer, in the months of June and July. This observation may be related to the seasonality of specific types of rain events (i.e. longer duration, lower intensity storms in the spring and shorter, more intense storms in the summer) or could involve some unknown factors affecting infiltration, such as antecedent moisture content.

4.4.2 Green-Ampt model – Grove St. System

The Green-Ampt model was used to simulate both the Grove St and Kettlebell systems. The traditional form of the model is one-dimensional and does not account for sidewall infiltration. Model output includes the resulting water depths within the gravel storage and the instantaneous infiltration rates throughout an event. Soil moisture content was not tracked

because the Green-Ampt model assumes that all soils above the wetting front have reached saturation. The results from the Grove St simulation were compared to the monitoring data to evaluate the effectiveness of the model.

The same events that were simulated with the saturated/unsaturated model, were also simulated with the Green-Ampt model for the Grove St system. Initially, the model was run using four different sets of soil parameters to determine how slight variations in the input parameters would affect the modeled infiltration rates. The results of these preliminary simulations, in terms of peak water depths in the gravel filter, time to peak water depth, and total infiltration volume, were compared to the monitored data using the root mean squared error (RMSE). As with the saturated/unsaturated model, the lowest values for RMSE were produced when the Guelph-based soil parameters were used, suggesting that these results were the closest to the measured values. Therefore, all further analyses with the saturated/unsaturated model used the Guelph-based soil parameters as input. The results from the preliminary simulations are presented in the Appendices.

For each storm event, the water depths from the model were visually compared to the measured water depths to help determine if the model effectively simulated infiltration. The accuracy of the model was also evaluated statistically through the use of two-sided T-tests and by calculating the RMSE between various modeled and measured values, including the peak storage depth, the time to peak depth, and the total infiltration volume for each storm event. The results of the T-test analyses and RMSE values for the Green-Ampt model are presented in Table 16 and Table 17, respectively.

Table 16: T-test comparing results of Green-Ampt model to measured data

	Data set	n	t	α	± $t_{\alpha/2}$	Reject null hypothesis?
Peak Water Depths (cm)	Full Data Set	27	2.73	0.05	±2.056	Reject
	Small Storm Events	18	-1.30	0.05	±2.11	Cannot Reject
	Large Storm Events	9	10.76	0.05	±2.306	Reject
Total Infiltration Volume (ft^3)	Full Data Set	27	-2.01	0.05	±2.056	Cannot Reject
	Small Storm Events	18	0.00	0.05	±2.11	Cannot Reject
	Large Storm Events	9	-4.32	0.05	±2.306	Reject
Time to Peak (hr)	Full Data Set	14	0.74	0.05	±2.056	Cannot Reject
	Small Storm Events	5	-0.18	0.05	±2.776	Cannot Reject
	Large Storm Events	9	1.30	0.05	±2.306	Cannot Reject

Table 17: SSE, MSE, and RMSE for the Green-Ampt model

	Peak Water Depth (cm)	Total Infiltration Volume (ft^3)	Time to Peak (hr)
SSE	15974	39060616	613340
MSE	592	1446689	43810
RMSE	24	1203	209

The results of the T-tests (Table 16) show that for a 95% confidence level, the measured and modeled peak water depths are not statistically similar. However, when performed for the simulation results from only the smaller, shorter duration events (Table 16), the T-tests can no longer prove that the values are significantly different between the modeled and the measured data. The mean time to peak and total infiltration volume for the full data set were not proven to be statistically different from the measured values. T-test results for the larger storm events (Table 16) suggested that the simulated peak water depths and total infiltration volumes are statistically different from the measured values. During these larger events, the simulated water depths surpassed the capacity of the gravel storage layer cause water to leave the system through

the overflow bypass and reducing the total infiltration volume. The T-test were unable to detect a statistical difference between the modeled and measured infiltration volumes for the whole data set because the model produced similar infiltration volumes for all of the smaller event where the gravel layer never filled. Overall, it appears that the model was significantly less accurate for longer duration storms, where ponded water depths rose to over 20 cm.

The RMSE values for the Green-Ampt model (Table 17) are slightly lower on average than those calculated for the saturated/unsaturated model (Table 15). This shows that the Green-Ampt model may be more accurate than the saturated/unsaturated model in terms of peak water depth, time to peak, and total infiltration volume. Further comparison of the various research models using RMSE is presented in Section 4.4.5.

Figure 48 and Figure 49 present graphs of the simulated and measured water levels for the Grove St system. The graphs in Figure 48 represent shorter duration storms which produced lower ponding depths. The model appears to be more accurate for these events than for the longer duration events presented in Figure 49 based on the similarity of the spike in water level. As with the saturated/unsaturated model, the Green-Ampt model underestimates infiltration rates as ponded water depth rise, causing the model to overestimates water depths for longer duration events and those which produced higher water levels.

From the graphs in Figure 48, one can see that the simulated and measure water levels start to rise at almost the same time and initially rose at similar rates. This shows that the model may effectively predict the time to ponding and the initial infiltration rates after ponding starts. The model appears to lose validity as the water level rises because only a few of the model runs produce similar peak water levels to the monitoring data. The maximum simulated water depths were only close to the measured ones for the storms on 6/30, 7/8, and 7/13/2017.

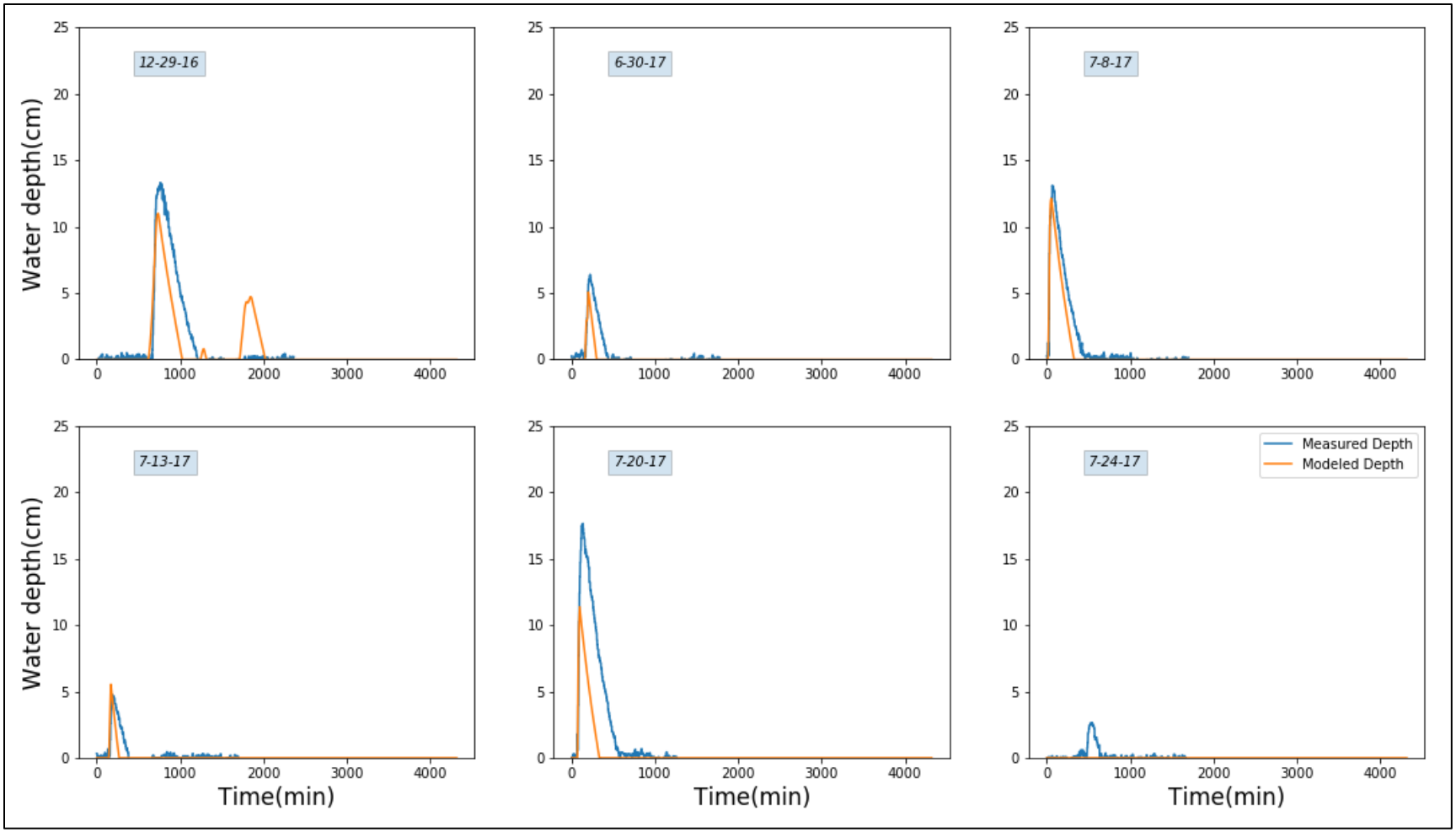

Figure 48: Comparison of simulated water depths from the Green-Ampt model to the measured water depths in the Grove St system during short-duration precipitation events

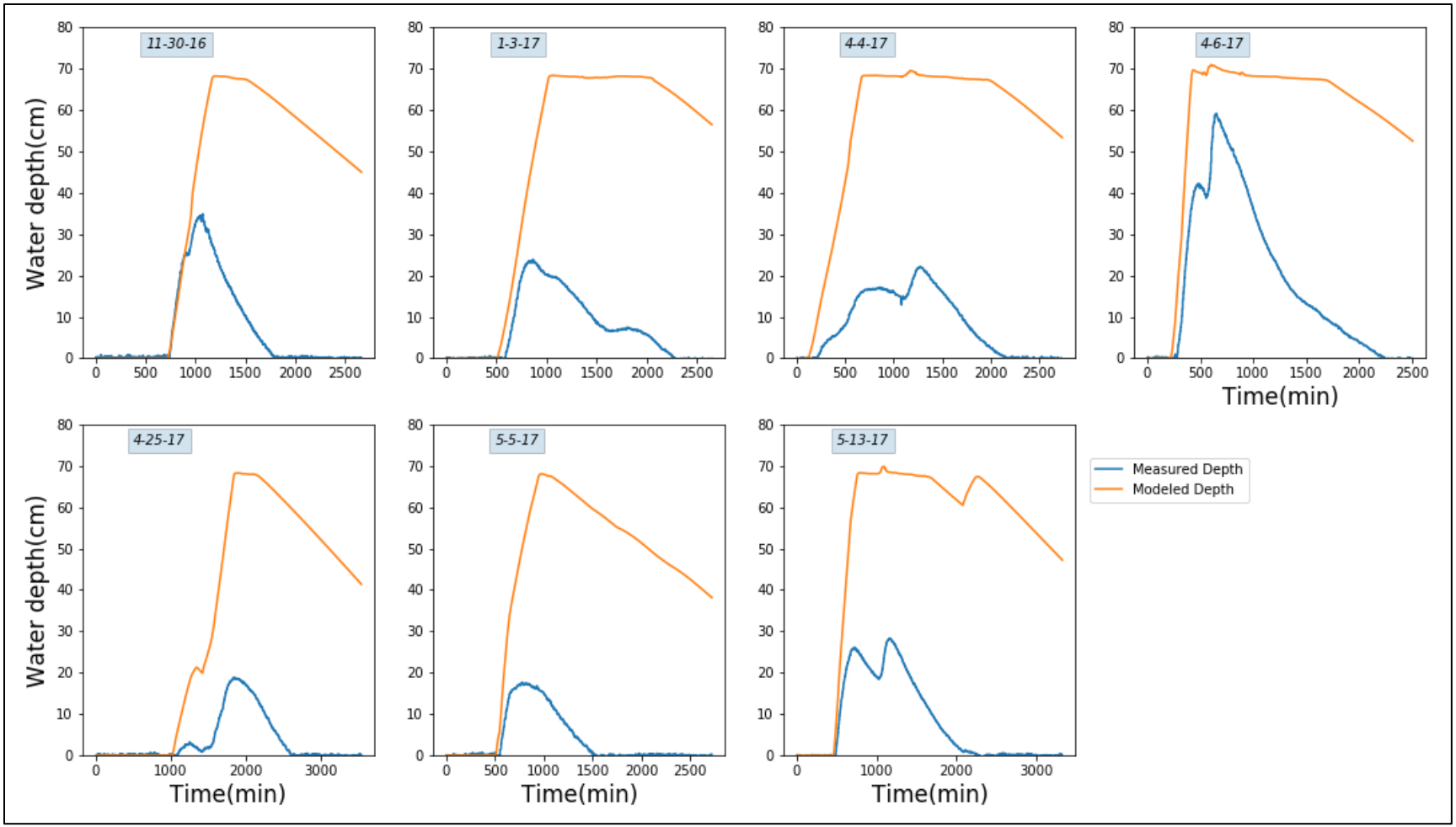

Figure 49: Comparison of simulated water depths from the Green-Ampt model to the measured water depths in the Grove St system during long-duration precipitation events

During the short duration rain events, the Green-Ampt model appears to overestimate infiltration rates, leading to lower peak depths than what was measured. One explanation for the model's lack of fit may be due to the inverse relationship between the Green-Ampt model and the cumulative infiltration depth, which causes the model to overestimate initial infiltration rates. If inflows at the start of a rain event increase rapidly in only a few time steps, the model determines that this water will infiltration because the infiltration capacity of the soil is very high when the cumulative infiltration depth is low. This model deficiency can lead to unrealistic results for 'flashy' events, such as thunderstorms, but this is not a problem for rain events which increase slowly. For example, on 7/20 and 7/24 inflows increased so rapidly that the modelled infiltration capacity was still very high when inflows became large. For the 7/20 event, inflows increased from about 3.0×10^{-3} cfm to 12 cfm in a single time step, causing the infiltration rate to jump to almost 15 cm/hr (see Figure 50). Using a smaller time step helps to reduce the initial infiltration rate spike.

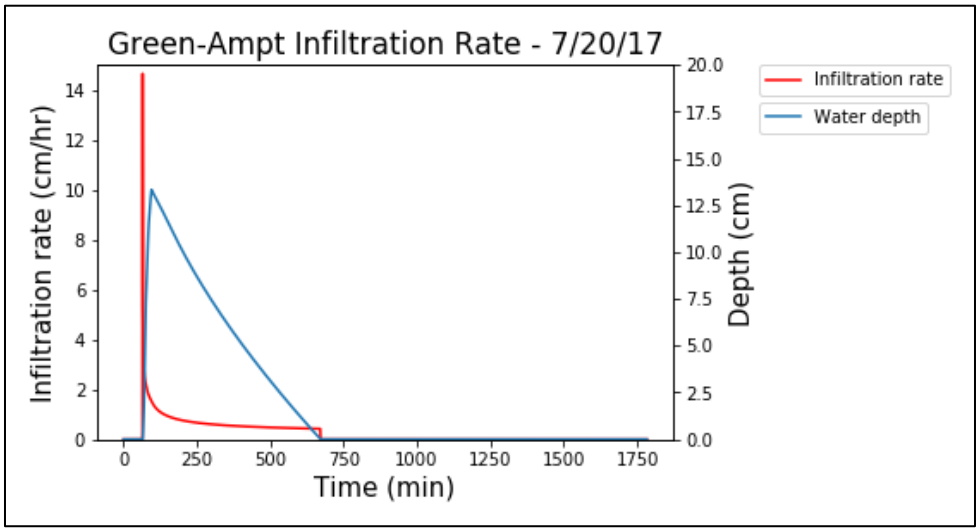

Figure 50: Simulated infiltration rate and water depth from the Green-Ampt model - 7/20/2017 rain event

In Figure 49, the maximum simulated water depths are all greater than the values measured during monitoring. However, the Green-Ampt model appears to be producing slightly

higher infiltration rates than those calculated with the saturated/unsaturated model. When comparing Figure 49 and Figure 47, one can see that the simulated water levels fall more rapidly for the Green-Ampt model. In order to compare modeled infiltration rates to those calculated from the monitoring data, the measured and modeled maximum infiltrate rates after peak ponding are presented in Table 18. The maximum simulated infiltration rates after peak ponding are all less than those calculated from the monitoring data. This helps explain why the Green-Ampt model overestimated the water depth for the longer, lower intensity rain events and why the modeled water levels dropped more rapidly for the Green-Ampt model than the saturated/unsaturated model. Overall, the 1-D Green-Ampt model appears to be ineffective when modeling SGF system performance for long duration events and those that produce significant ponding depths because the model does not account for sidewall infiltration.

Table 18: Maximum infiltration rates after peak ponding for Green-Ampt model for the Grove St system

Green-Ampt Model - Maximum Infiltration Rates after Peak Ponding (cm/hr)		
Date	**Modeled Rate**	**Measured Rate**
11/30/2016	1.08	5.13
12/29/2016	1.35	1.33
1/3/2017	0.84	4.27
4/4/2017	0.90	4.64
4/6/2017	1.25	5.83
4/25/2017	0.92	3.4
5/5/2017	1.05	3.19
5/13/2017	1.03	4.28
7/8/2017	2.10	2.16
7/20/2017	2.39	2.53
Median	*1.25*	*3.84*

4.4.3 Green-Ampt model – Kettlebell System

For the Kettlebell system, the Green-Ampt model was only used to simulate four precipitation events. The resulting depths from the Kettlebell simulations were not compared to those that were measured because the system remained full throughout most of the monitoring

period. Instead, the purpose of the model was to investigate why the Kettlebell system is not draining and determine the theoretical amount of time required for the system to drain.

Figure 51 presents graphs of the simulated water depths for each of the four storm events. Contrary to reality, the system was assumed to be empty at the start of each event. During the simulations, as runoff starts to enter the system, the water levels rise rapidly due to the highly restrictive nature of the native soils. Once the system is filled, water starts to flow through the outlet pipe, bypassing the gravel layer and flowing directly to Berry Brook. At the end of each storm event, the water levels slowly decrease as water infiltrates into the native soils. While the rates at which the WSE decreases in each model run are very small, they still exceed that which was observed from the monitoring data and show that the Green-Ampt model is overestimating the infiltration rate in the system.

One potential explanation for the disagreement between the model and the monitoring data is that the soils are actually saturated around the base of the system due to a high groundwater level. The original design drawings for the Kettlebell system, presented in Figure 63 in the Appendix, show that the WSE of Berry Brook is at almost the same elevation as the invert of the system's slotted inlet pipe. Due to the system's close proximity to Berry Brook, the groundwater table may be very close to, if not above, the base of the system, causing soils around the gravel storage area to remain saturated. Therefore, by assuming that the soils are freely draining below the system, the Green-Ampt model may be overestimating infiltration.

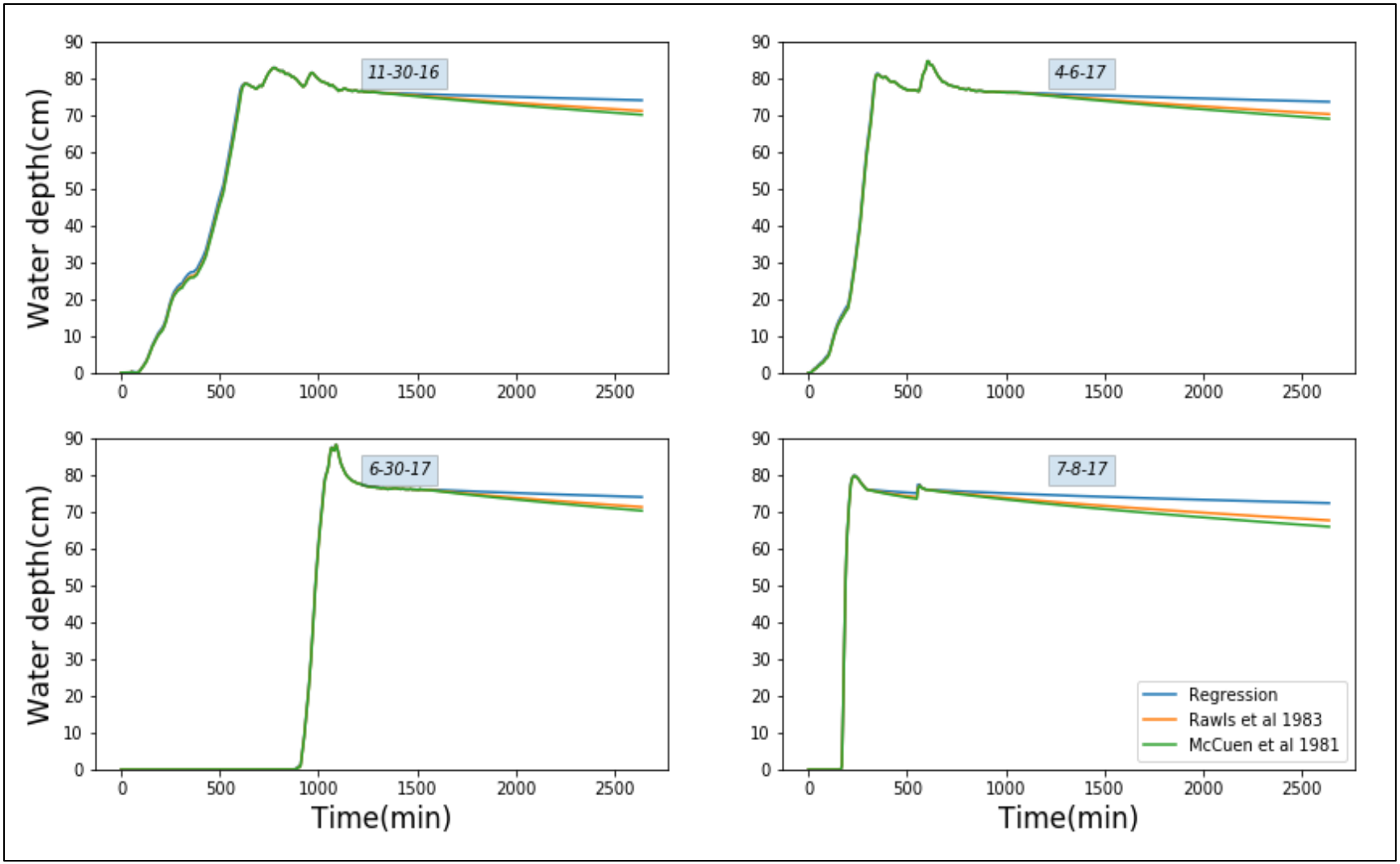

Figure 51: Simulated water depths for the Kettlebell system during various precipitation events

To test this theory and evaluate model fit for longer simulated time periods, the Green-Ampt model was used to simulate infiltration in the Kettlebell SGF over an extended 37-day period between 11/15/2016 to 12/22/2016. Figure 52 presents the water depths produced by the model and those measured at the Kettlebell site. The system was assumed to be empty at the start of the simulation and soil moisture conditions were set close to saturation with an initial θ-value of 0.46 cm^3/cm^3. The regression-based soil parameters from Rawls and Brakensiek (1989) were used in the model because they were more restrictive, in terms of permeability, than the other sets of parameters.

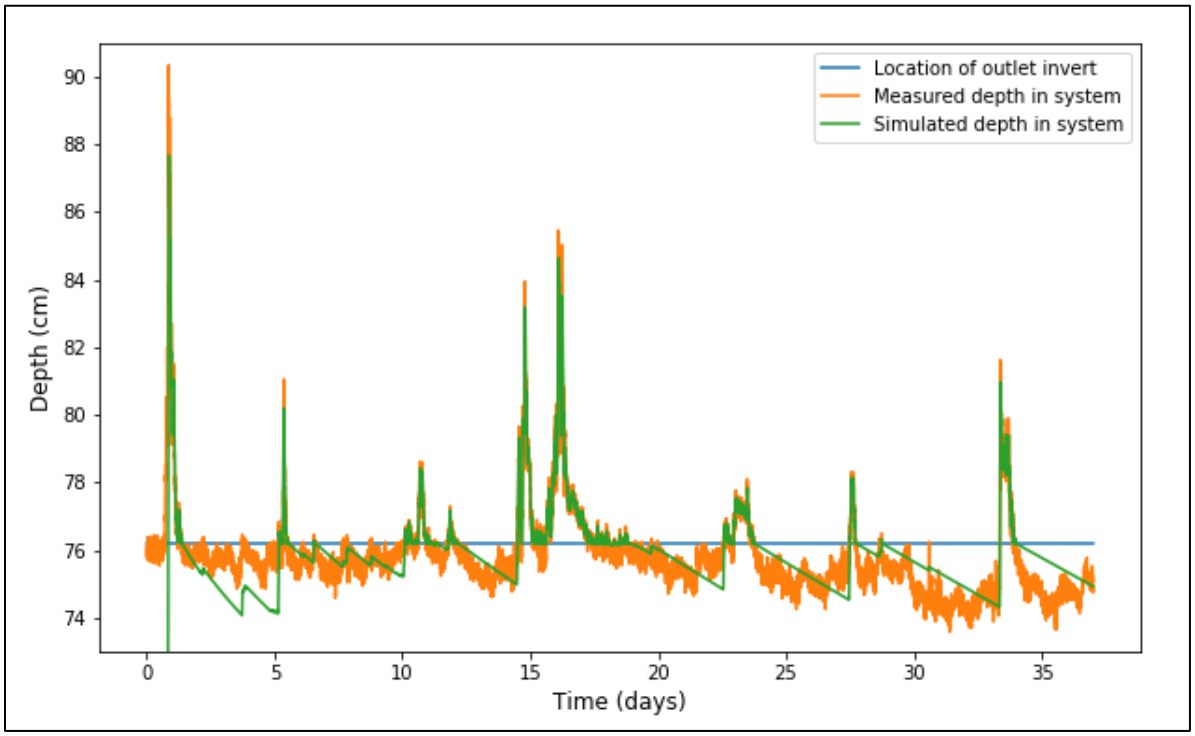

Figure 52: Water depths from the monitoring data and an extended simulation of the Kettlebell system using the modified Green-Ampt model

The first few days of the simulation acted as a "ripening" period where the model ran until the effects of the initial model conditions were no longer influential. During this time period the system filled with water, the extended downward into the soils, and the infiltration rate

decreased until it equaled the saturated infiltration rate. For the first five days, the model overestimates the infiltration rate causing the simulated water level to drop more rapidly than the measured WSE. After this ripening period, the model appears to accurately replicate the water level fluctuations in the Kettlebell system. Both water levels rise to almost the same depths during rain events and then drop back down at similar rates after the events are over. One should note that the flow through the outlet pipe was calculated using the rating curve developed from the jet-truck flow calibration tests. The rating curve is system specific and is not a physically based equation. To compare the actual infiltration rates to the modeled rates, one must examine how the water levels change once they drop below the invert of the outlet pipe. Between storm events, the water level dips below the outlet pipe and fluctuates by only a few centimeters. While these fluctuations are small, the model appears to replicate the measured WSE fairly accurately after the initial calibration period.

During no point in the simulation was the system able to drain completely. This provides evidences as to why the Kettlebell system did not drain down during the monitoring period. The infiltration rates appear to be so low that the water level can only drain down by a few centimeters on average between storms. For example, when running the model with the least restrictive soil parameters (i.e. those from McCuen et al. (1981)) and assuming an initial cumulative infiltration value of 6.5 cm, the system would require over 23 days to completely drain. If the more restrictive parameters from the regression equations are used in the model, the drain time increases to over 160 days. These extremely slow drain times have created a constant state of ponding in the system and are most likely preserving saturated conditions in the soils surrounding the SGF.

4.4.4 Modified Green-Ampt model

One of the biggest simplifying assumptions that the saturated/unsaturated and Green-Ampt models rely on is that infiltration only occurs in the vertical direction through the basal area of the systems. In order to help capture the effects of horizontal infiltration, an effective infiltration area term (A_{eff}) was used in a modified Green-Ampt model. As discussed in the Section 3.6.2, Freni et al. (2009) used MODFLOW to developed texture-specific, power-functions to relate A_{eff} to the base dimensions of a gravel infiltration trench system. The A_{eff} parameter is assumed to be constant for all storm events no matter the depth of ponding in the system because the time required for the system to fill is considered insignificant compared to the variation in effective area (Freni et al., 2009).

For continuous modeling, where the total infiltration volume is more important than the instantaneous infiltration rate, or when modeling smaller systems which can fill rapidly during rain events, it may be reasonable to assume A_{eff} is independent of the instantaneous water depth in the system. However, for the short time step, event-based models used for this research, the water depth varies considerably between individual storm events and can have a significant effect on the rate of exfiltration from an SGF system. Additionally, the systems being analyzed in this paper are almost an order of magnitude larger than those assessed by Freni et al. (2009). A constant value for A_{eff} oversimplifies the infiltration process and produces unreliable results in terms of how well the Green-Ampt model fits the measured data. This is demonstrated by the results of the traditional Green-Ampt model where the infiltration area is equal to the base area of the system. When modeling an SGF, the A_{eff} term needs to account for changes in water depth in order to effectively estimate horizontal infiltration.

For this study, various equations were developed to relate A_{eff} to water depth. Four types of functions, presented in Section 3.6.2, were considered for calculating A_{eff}: 1) a linear function for total wetted area, 2) a linear function with a multiplier to account for higher horizontal infiltration rates, 3) a power function, 4) and a piece-wise function that combined both the linear and power functions. After a process of trial-and-error, it was found that combining the power and linear functions together as a piece-wise function, significantly improved infiltration estimates for most of the modeled storm scenarios.

The piece-wise function (see Equation 34) is in the form of a power function until the water depth rises above 12 cm (0.4 ft) after which the function becomes linear with a constant multiplier. The transition depth was selected based on observed changes in the infiltration when the water depth in the system drops below this level, shown in Figure 36. The constant multiplier for the power and linear function portions of the piece-wise function was calculated by dividing the horizontal hydraulic conductivity estimated for the unit-gradient model (41.9 cm/hr) by the hydraulic conductivity measured with the Guelph permeameter (0.51 cm/hr). The ratio of hydraulic conductivities was used to help account for the higher rate of infiltration through the system's sidewalls. If the modified Green-Ampt model were to be used for design, the horizontal and vertical hydraulic conductivities could potentially be measured in the field so that the constant could be developed. Figure 53 shows the improved fit of the model, in terms of simulated and measured water depths for four different storms, including two smaller events (i.e. <20 cm of ponded water depth) and two larger ones. By visually comparing the measured and model water depths in Figure 53, one can see that the modified Green-Ampt model fairly accurately simulates the infiltration processes within the Grove St SGF.

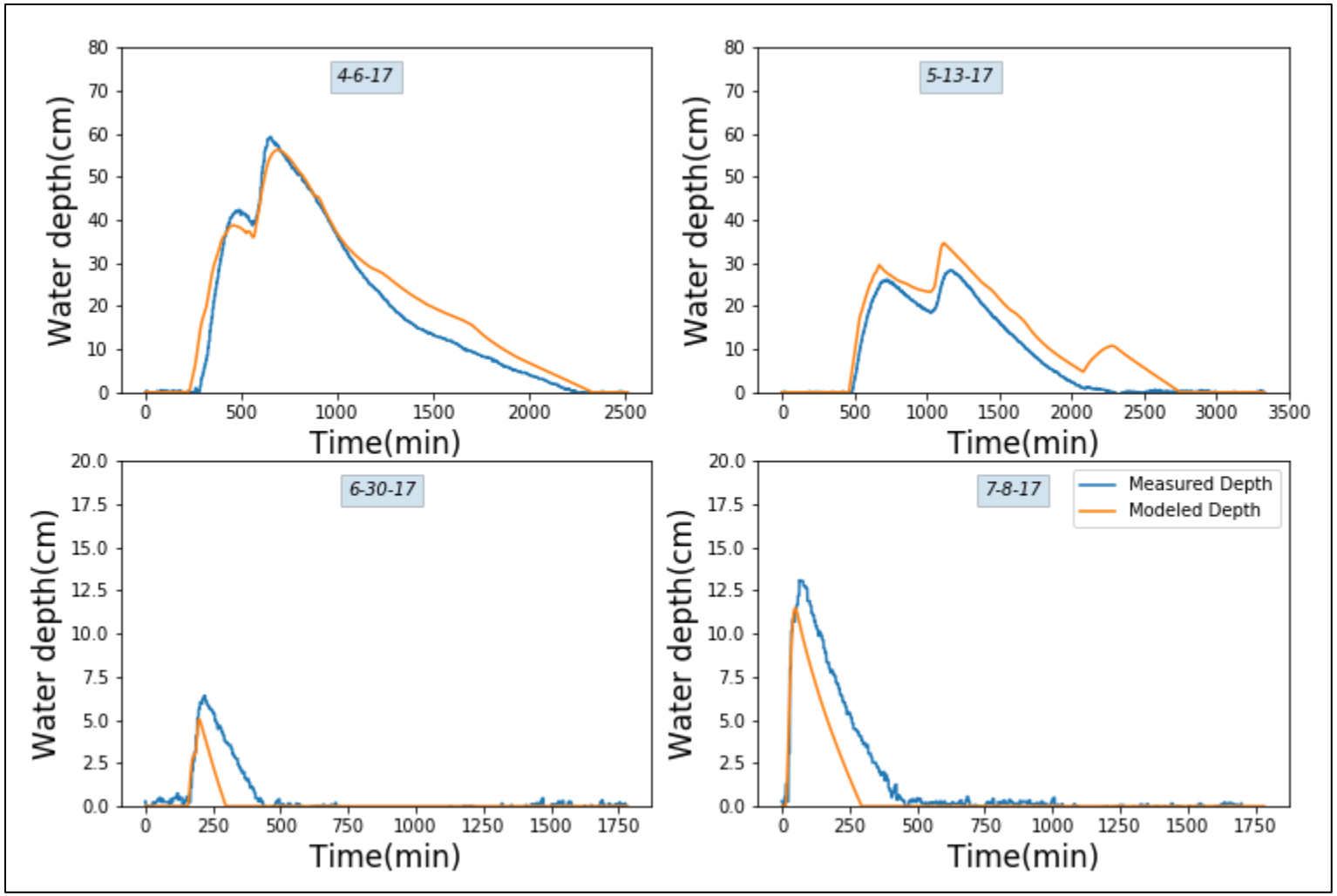

Figure 53: Comparison of measured water depths in the Grove St system to those simulated using the modified Green-Ampt model with a piece-wise function for A_{eff}

The results of the modified Green-Ampt model were also analyzed using two-sided T-tests, presented in Table 19 and by calculating the RMSE between the modeled and measure values for peak water depth in the gravel filter, time to peak depth, and total infiltration volume (Table 20). Overall, the T-tests could not prove that there is a statistical difference between the modeled and measured mean values for the peak water depth in the system, time to peak, and total infiltration volume. This suggests that the model is accurately simulating the infiltration processes within the Grove St system. The storm events were also grouped into small and large storm events (i.e. those which produced ponded water depths <20 cm and those which produced large water depths, respectively) and then analyzed separately with the T-test. A statistical difference between peak water depths, time to peak, and total infiltration volumes for both the small and large events could not be established. The RMSE values for modified Green-Ampt model (Table 20) are lower than those calculated for the saturated/unsaturated model and the regular Green-Ampt model. This suggests that the modified Green-Ampt model may be more accurate than the models which did not account for sidewall infiltration.

While the model results show a relatively good fit to the monitoring data, one should keep in mind that the piece-wise function used to calculate effective infiltration area was parted developed from a calibrated horizontal K-value. Because the constant is system specific, it would need to be redeveloped for other sites. Parameter calibration is not advantageous for design purposes. A method of accurately estimating horizontal hydraulic conductivity would be needed to implement the modified Green-Ampt model for system design. Additionally, the A_{eff} term cannot account for the decrease in infiltration which occurs as the soil moisture along the system's sidewalls increases.

Table 19: T-tests for the results of the modified Green-Ampt model

	Data set	n	t	α	± $t_{\alpha/2}$	Reject null hypothesis?
Peak Water Depths (cm)	Full Data Set	27	-0.01	0.05	±2.056	Cannot Reject
	Small Storm Events	18	-1.52	0.05	±2.11	Cannot Reject
	Large Storm Events	9	0.77	0.05	±2.306	Cannot Reject
Total Infiltration Volume (ft^3)	Full Data Set	27	-0.01	0.05	±2.056	Cannot Reject
	Small Storm Events	18	0.00	0.05	±2.11	Cannot Reject
	Large Storm Events	9	-0.02	0.05	±2.306	Cannot Reject
Time to Peak (hr)	Full Data Set	14	0.14	0.05	±2.056	Cannot Reject
	Small Storm Events	5	-0.20	0.05	±2.776	Cannot Reject
	Large Storm Events	9	0.32	0.05	±2.306	Cannot Reject

Table 20: SSE, MSE, and RMSE for the results of the modified Green-Ampt model

	Modified Green-Ampt Model		
	Peak Water Depth (cm)	**Total Infiltration Volume (ft^3)**	**Time to Peak (hr)**
SSE	839	5099	93577
MSE	31	189	6684
RMSE	6	14	82

4.4.5 Unit-gradient flow model

The unit-gradient model was initially run using the K_{fs} estimate of 0.51 cm/hr, from the Guelph permeameter, for both the horizontal and vertical hydraulic conductivity values. Simulations were then performed using the calibrated K values presented in Section 4.1. The unit-gradient flow model was only used to simulate infiltration for the Grove St. system as the calibrated K-values could not be developed from the monitoring data from the Kettlebell system. Measured and simulated water depths in the system's storage layer were visually compared to

help determine the accuracy of the simulation. Figure 54 and Figure 55 present graphs of the modeled and measured water levels for 13 of the 27 rain events which were simulated. The accuracy of the model was also evaluated statistically through the use of two-sided T-tests and by calculating the RMSE between various modeled and measured values, including the peak storage depth, the time to peak depth, and the total infiltration volume for each storm event. Table 21 to Table 24 present the results of the statistical analyses for the unit gradient model.

Table 21: T-tests for the results of the unit-gradient model using the Guelph permeameter-based K-value

	Data set	n	t	α	± $t_{\alpha/2}$	Reject null hypothesis?
Peak Water Depths (cm)	Full Data Set	27	3.13	0.05	±2.056	Reject
	Small Storm Events	18	0.34	0.05	±2.11	Cannot Reject
	Large Storm Events	9	11.65	0.05	±2.306	Reject
Total Infiltration Volume (cf)	Full Data Set	27	-1.89	0.05	±2.056	Cannot Reject
	Small Storm Events	18	0.00	0.05	±2.11	Cannot Reject
	Large Storm Events	9	-4.10	0.05	±2.306	Reject
Time to Peak (hr)	Full Data Set	14	0.43	0.05	±2.056	Cannot Reject
	Small Storm Events	5	-0.08	0.05	±2.776	Cannot Reject
	Large Storm Events	9	0.76	0.05	±2.306	Cannot Reject

Table 22: SSE, MSE, and RMSE for the results of the unit-gradient model using the Guelph permeameter-based K-value

	Unit Gradient Model (Guelph-Based K-values)		
Statistical Parameters	**Peak Water Depth (cm)**	**Total Infiltration Volume (cf)**	**Time to Peak (hr)**
SSE	18121	36662765	302330
MSE	671	1357880	21595
RMSE	26	1165	147

Table 23: T-tests for the results of the unit-gradient model using the calibrated K-value

	Data set	n	t	α	± $t_{\alpha/2}$	Reject null hypothesis?
Peak Water Depths (cm)	Full Data Set	27	0.61	0.05	±2.056	Cannot Reject
	Small Storm Events	18	-0.15	0.05	±2.11	Cannot Reject
	Large Storm Events	9	1.44	0.05	±2.306	Cannot Reject
Total Infiltration Volume (cf)	Full Data Set	27	0.00	0.05	±2.056	Cannot Reject
	Small Storm Events	18	0.00	0.05	±2.11	Cannot Reject
	Large Storm Events	9	0.00	0.05	±2.306	Cannot Reject
Time to Peak (hr)	Full Data Set	14	-0.20	0.05	±2.056	Cannot Reject
	Small Storm Events	5	-0.20	0.05	±2.776	Cannot Reject
	Large Storm Events	9	-0.20	0.05	±2.306	Cannot Reject

Table 24: SSE, MSE, and RMSE for the results of the unit-gradient model using the calibrated K-value

	Unit Gradient Model (Calibrated K-values)		
Statistical Parameters	**Peak Water Depth (cm)**	**Total Infiltration Volume (cf)**	**Time to Peak (hr)**
SSE	917	0	30931
MSE	34	0	2209
RMSE	6	0	47

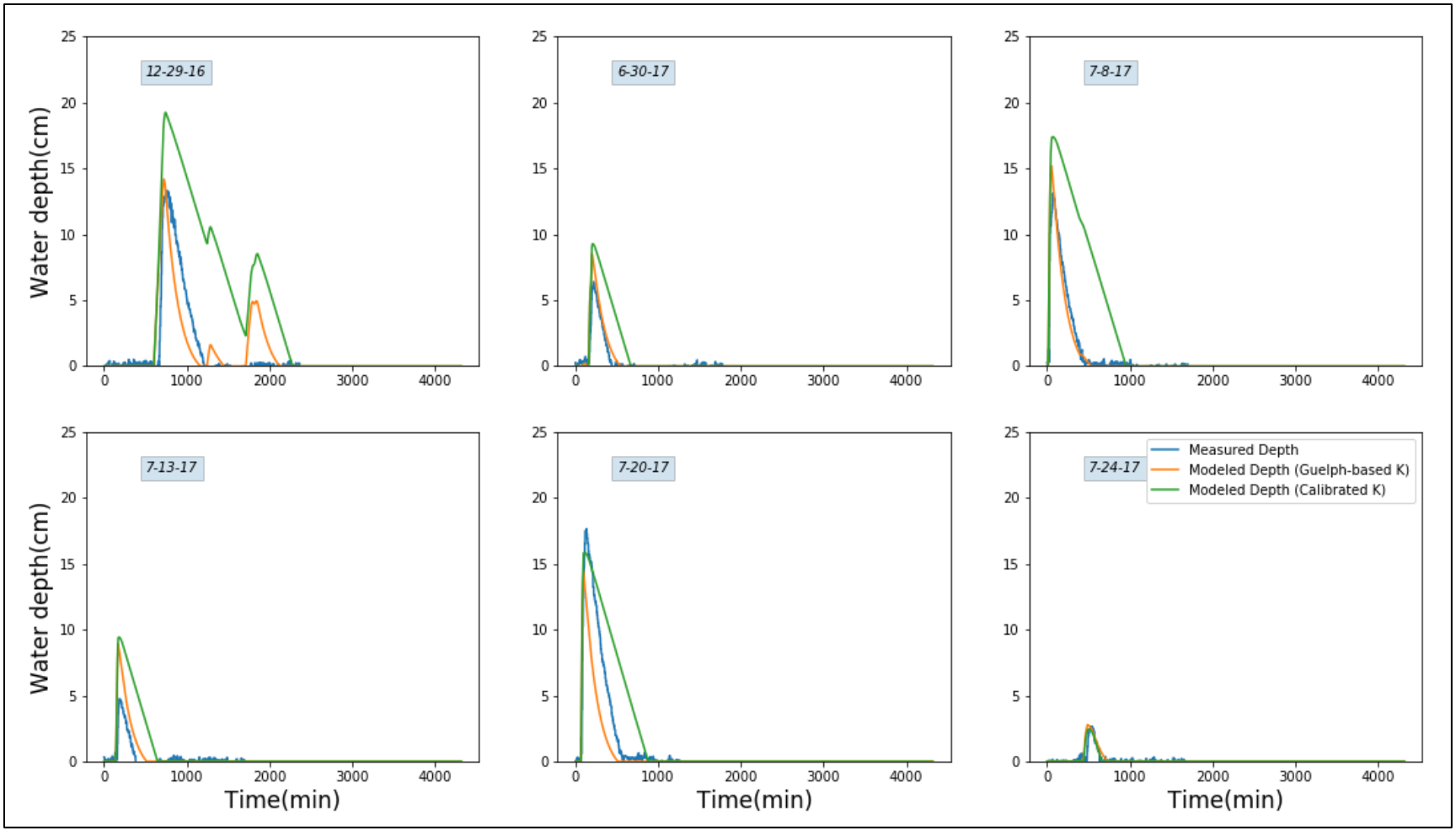

Figure 54: Comparison of simulated water depths from the unit-gradient flow model to the measured water depths in the Grove St system for various short-duration rainfall events

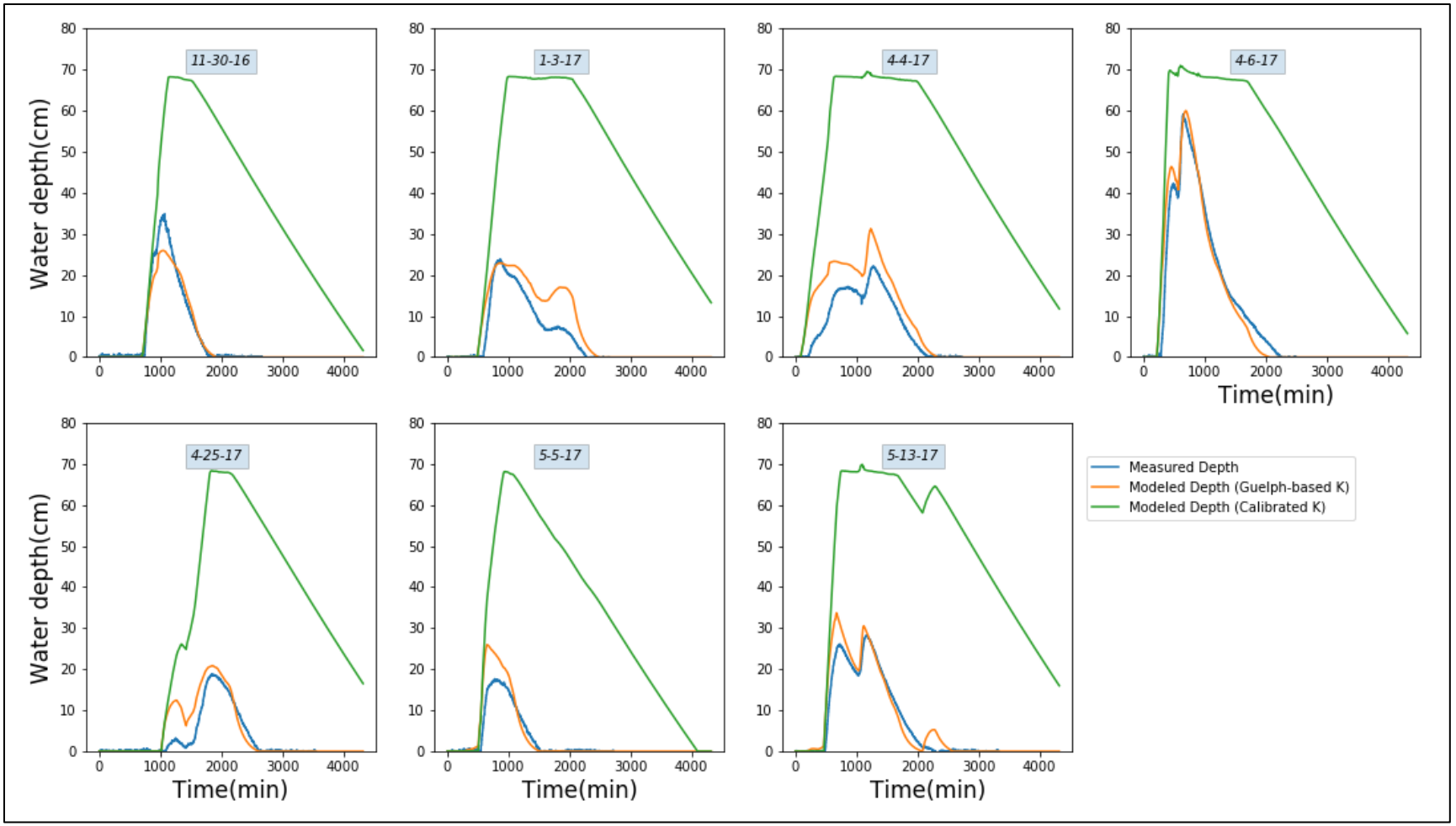

Figure 55: Comparison of simulated water depths from the unit-gradient flow model to the measured water depths in the Grove St system for various long-duration rainfall events

As with the saturated/unsaturated and Green-Ampt models, the unit-gradient model appears to overestimate the depth and period of ponding in the system for larger, longer-duration rain events (Figure 55) when the Guelph-based K_{fs} value is used as input. For the smaller, shorter-duration events (Figure 54), the model appears to more accurate simulate the measured water depths. The T-test for the model output suggest that there is a statistically significant difference between the peak water depths in the system for the measured and model results. The modeled peak water depths and total infiltration volumes for just the larger storm events are also statistically different from the measured values. However, based on the results of the 27 storms that were modeled, the T-test could did not show a significant difference between the total infiltration volumes and time to peak ponding from the modeled and measured results. The T-test for the full data set may not be detecting the differences in total infiltration volumes which occurred during the larger storm events due to the inclusion of twice as many small storm events for which the model produced the same infiltration volumes. All of the T-tests which were performed for the 18 smaller storm events show no statistical difference between the water depth output of the model and the monitoring data.

Based on the statistical analyses and visual comparison of the graphed water depths, the unit-gradient model appeared to underestimate infiltration for larger events when the Guelph-based K-value was used. While the unit-gradient model can account for horizontal infiltration, the area of the filter sidewalls is only a quarter of the basal area. Substantial horizontal infiltration can only occur if the sidewall K is higher than the vertical K. By using the same value for both horizontal and vertical hydraulic conductivity, sidewall infiltration can only contribute to a small portion of the total infiltration volume for the unit-gradient model and may have led to an underestimation of the infiltration rate. During smaller rain events, when inflows are low and

ponding remains minimal, vertical infiltration dominates due to the limited wetted sidewall area. Using K_{fs} may also lead to inaccuracy if the soils surround the system are anisotropic because K_{fs}-value developed from Guelph permeameter measurements is effectively an average of the horizontal and vertical K-values.

The results for the unit-gradient model were far more accurate when the calibrated K-values were used. For the majority of modeled storm events, the simulated water levels fluctuated in a similar manner to the measured ones, rising and falling at comparable rates and times throughout each event (see Figure 54 and Figure 55). Both the modeled and measured depths also peaked at similar maximum values. Table 25 provides the peak values for both the simulated and measured water levels, and the difference between the two. On average, the maximum water depths differed by only 1.7 cm. The model appears to be especially accurate in simulating the events on 4/6/2017, 5/13/2017, 7/8/2017, and 7/24/2017.

Table 25: Comparison of maximum water depths for the unit-gradient model and the monitoring data from 13 different rainfall events, Grove St system

Date of Event	Maximum Modeled Depth (cm)	Maximum Measured Depth (cm)	Difference (cm)
4/6/2017	60.0	59.2	0.8
5/13/2017	33.7	28.3	5.4
4/4/2017	31.3	22.2	9.1
1/3/2017	22.9	23.9	-1.0
1/10/2017	30.3	8.0	22.3
11/30/2016	26.0	34.9	-8.9
4/25/2017	20.9	18.8	2.1
5/5/2017	26.0	17.6	8.3
5/1/2017	19.7	9.4	10.3
7/8/2017	15.2	13.1	2.1
7/20/2017	14.4	17.7	-3.2
12/29/2016	14.2	13.3	0.9
7/13/2017	8.9	4.8	4.2
6/30/2017	8.5	6.4	2.1
7/24/2017	2.8	2.7	0.1
11/29/2016	0.7	2.4	-1.8
11/24/2016	0.0	0.3	-0.3
11/26/2016	0.0	0.4	-0.4
12/6/2016	0.0	0.9	-0.9
1/19/2017	0.0	0.6	-0.6
1/24/2017	0.0	0.7	-0.7
4/12/2017	0.1	0.4	-0.2
4/15/2017	0.0	0.9	-0.9
4/19/2017	0.0	1.0	-1.0
4/21/2017	0.2	0.9	-0.7
7/7/2017	0.0	0.6	-0.6
7/11/2017	0.0	0.7	-0.7
		Average:	**1.7**
		Standard Deviation:	**5.7**

The results of the T-tests (Table 22) could not prove that there is a statistical difference between modeled and measured mean values for the peak water depth in the system, time to peak, and total infiltration volume. For each storm event, the modeled peak water depths in the system and the time to peak were very similar to those which were measured at the Grove St site. The calculated value of the t-statistic for the total infiltration volume was zero because the modeled and measured total infiltration volumes were the same. Throughout the 1-year monitoring period, the ponded water depth in the gravel filter was never found to reach system

capacity. Therefore, all flows which entered the gravel filter theoretically should have infiltrated. Simulated water levels from the unit-gradient model using the calibrated K-values also did not entirely fill the system. Because both the simulation and actual SGF system did not bypass flows, the total infiltration volumes are the same. The RMSE values for the calibrated unit-gradient model (Table 24) were significantly lower than those calculated using the Guelph-based K_{fs} value or the other models previously discussed (Table 15 and Table 17). This suggests that the calibrated unit-gradient model is more accurately modeling infiltration for the Grove St SGF system.

One of the major differences between the unit-gradient model and the other models previously discussed is that the unit-gradient model includes horizontal infiltration, while the Green-Ampt and saturated/unsaturated models do not. If the soils surrounding an SGF are anisotropic, including horizontal infiltration may dramatically increase the overall infiltration rate from the system during ponding, causing the simulated water depths to better replicate the measured depths. However, the unit-gradient model is strongly affected by one's choice for K-values. Use of the Guelph-based K_{fs} value for both horizontal and vertical hydraulic conductivity appears to cause the model to inaccurately simulate infiltration for the system. Calibration of the K-values suggests that the horizontal K is actually substantially larger than the vertical K.

Table 26 and Table 27 present the division of horizontal and vertical infiltration volumes for each storm event from the unit-gradient model. When the Guelph-based hydraulic conductivity estimate is used (Table 26), the model produces a total infiltration volume of 18,900 ft^3 of which 88% is related to vertical infiltration and only 12% from sidewall infiltration. The division of infiltration switches when the horizontal and vertical K-values are calibrated (Table 27). Horizontal infiltration become the primary mechanism of runoff volume reduction in the

simulations. In the calibrated unit-gradient model, 32,700 ft^3 of water was infiltrated of which approximately 10% was related to vertical infiltration and 90% was from horizontal infiltration. One should note that during smaller storm events, such as that which occurred on 11/29/2017 and 4/12/2017, vertical infiltration contributed to over 80% of the total infiltration volume.

Table 26: Comparison of vertical and horizontal infiltration in the unit-gradient model when the Guelph-based hydraulic conductivity is used

Date	Rainfall Depth (in)	Horizontal Infiltration Volume		Vertical Infiltration Volume		Total Infiltration Volume
		Volume (ft^3)	% of total	Volume (ft^3)	% of total	Volume (ft^3)
11/30/2016	1.14	213	12%	1546	88%	1758
1/3/2017	0.66	283	15%	1623	85%	1906
4/4/2017	0.824	315	15%	1788	85%	2103
4/6/2017	1.22	296	15%	1738	85%	2035
4/25/2017	1.24	217	13%	1432	87%	1649
5/5/2017	0.98	203	11%	1591	89%	1794
5/13/2017	1.756	304	15%	1717	85%	2021
12/29/2016	1.44	23	3%	707	97%	730
6/30/2017	0.811	4	2%	235	98%	239
7/8/2017	0.891	14	3%	398	97%	412
7/13/2017	0.68	4	2%	216	98%	219
7/20/2017	0.674	11	3%	342	97%	353
7/24/2017	0.724	1	0%	112	100%	112
11/29/2016	0.728	0	0%	74	100%	74
11/24/2016	0.252	0	0%	4	100%	4
11/26/2016	0.06	0	0%	1	100%	1
12/6/2016	0.236	0	0%	1	100%	1
1/10/2017	0.128	214	12%	1569	88%	1783
1/19/2017	0.52	0	0%	2	100%	2
1/24/2017	0.652	0	0%	30	100%	30
4/12/2017	0.184	0	0%	31	100%	31
4/15/2017	0.056	0	0%	6	100%	6
4/19/2017	0.064	0	0%	12	100%	12
4/21/2017	0.756	0	0%	104	100%	104
5/1/2017	0.748	143	10%	1330	90%	1474
7/7/2017	0.124	0	0%	1	100%	1
7/11/2017	0.136	0	0%	2	100%	2

Table 27: Comparison of vertical and horizontal infiltration in the calibrated unit-gradient model

Date	Rainfall Depth (in)	Horizontal Infiltration Volume		Vertical Infiltration Volume		Total Infiltration Volume
		Volume (ft^3)	% of total	Volume (ft^3)	% of total	Volume (ft^3)
11/30/2016	1.14	2,153	91%	213	9%	2,365
1/3/2017	0.66	3,730	92%	316	8%	4,046
4/4/2017	0.824	4,654	93%	354	7%	5,008
4/6/2017	1.22	5,951	95%	305	5%	6,257
4/25/2017	1.24	2,298	89%	292	11%	2,590
5/5/2017	0.98	1,737	87%	262	13%	1,999
5/13/2017	1.756	3,785	91%	381	9%	4,166
12/29/2016	1.44	532	73%	198	27%	730
6/30/2017	0.811	163	68%	77	32%	239
7/8/2017	0.891	324	79%	88	21%	412
7/13/2017	0.68	159	72%	61	28%	219
7/20/2017	0.674	283	80%	70	20%	353
7/24/2017	0.724	55	49%	57	51%	112
11/29/2016	0.728	13	18%	61	82%	74
11/24/2016	0.252	0	0%	4	100%	4
11/26/2016	0.06	0	0%	1	100%	1
12/6/2016	0.236	0	0%	1	100%	1
1/10/2017	0.128	2,221	92%	198	8%	2,419
1/19/2017	0.52	0	0%	2	100%	2
1/24/2017	0.652	0	0%	30	100%	30
4/12/2017	0.184	1	2%	30	98%	31
4/15/2017	0.056	0	0%	6	100%	6
4/19/2017	0.064	0	0%	12	100%	12
4/21/2017	0.756	2	2%	102	98%	104
5/1/2017	0.748	1,286	87%	187	13%	1,474
7/7/2017	0.124	0	0%	1	100%	1
7/11/2017	0.136	0	0%	2	100%	2

The primary deficiency of the unit-gradient model is that it appears to slightly underestimate initial infiltration rates causing water to start ponding in the simulated system slightly earlier than what was recorded and the simulated depths to rise somewhat higher than the measured depth. The model's underestimation of the infiltration rate can be explained by the fact that the model does not account for the variation in K-values due to changes in soil moisture or the initially high matric potential of the soils at the start of infiltration. The unit-gradient model also neglects the additional hydraulic head provided by the ponded water in the system. All of

these factors cause the model to underestimate infiltration, especially at the beginning of rain events when infiltration is most likely occurring under unsaturated conditions. The K-values used in the model were developed from the receding water level data near the end of rain storms and most likely represent field saturated conditions.

4.5 Discussion

The primary objective for the modeling portion of this research was to determine how horizontal infiltration, soil moisture, and stormwater runoff dynamics affect system performance, in terms of runoff volume reduction, by comparing the results of various infiltration models to monitoring data from the SGF systems. The insight gained from this analysis was then be used to make recommendation on how GSI sizing methodologies could be improved. Model accuracy was evaluated by comparing the simulated water depths in the gravel layer, the timing of water depth fluctuations, and the volume of water infiltrated during a storm event to the measured values from the actual systems.

The simulated and measured water depths in the Grove St SGF for various storm events are presented in Figure 56 and Figure 57. One can see that for the larger, longer-duration rain events (Figure 56) the calibrated unit-gradient and modified Green-Ampt models appear to accurately replicate the measured water depth, while the Green-Ampt, saturated/unsaturated flow, and Guelph-based unit-gradient models significantly overestimate water depths. For the smaller, shorter-duration rain events, all of the models appear to do a fair job of simulated the water depths of the Grove St system. The model results can also be compared according to root mean square error (RMSE) and the results of the T-test. Table 28 and Table 29 summarize the RMSE and T-test results, respectively, for peak water depth, total infiltration volume, and time to peak water depth for each model.

Table 28: Summary of RMSE values for each model

Model	Peak Water Depth	Total Infiltration Volume	Time to Peak
Saturated/Unsaturated Model	26	1547	156
Green-Ampt Model	24	1203	209
Modified Green-Ampt Model	6	14	82
Unit Gradient Model (Guelph-Based K-Values)	26	1165	147
Calibrated Unit Gradient Model	6	0	47

Table 29: Summary of T-test results for each model

Model	Peak Water Depth	Total Infiltration Volume	Time to Peak
Saturated/Unsaturated Model	Reject	Reject	Cannot Reject
Green-Ampt Model	Reject	Cannot Reject	Cannot Reject
Modified Green-Ampt Model	Cannot Reject	Cannot Reject	Cannot Reject
Unit Gradient Model (Guelph-Based K-Values)	Reject	Cannot Reject	Cannot Reject
Calibrated Unit Gradient Model	Cannot Reject	Cannot Reject	Cannot Reject

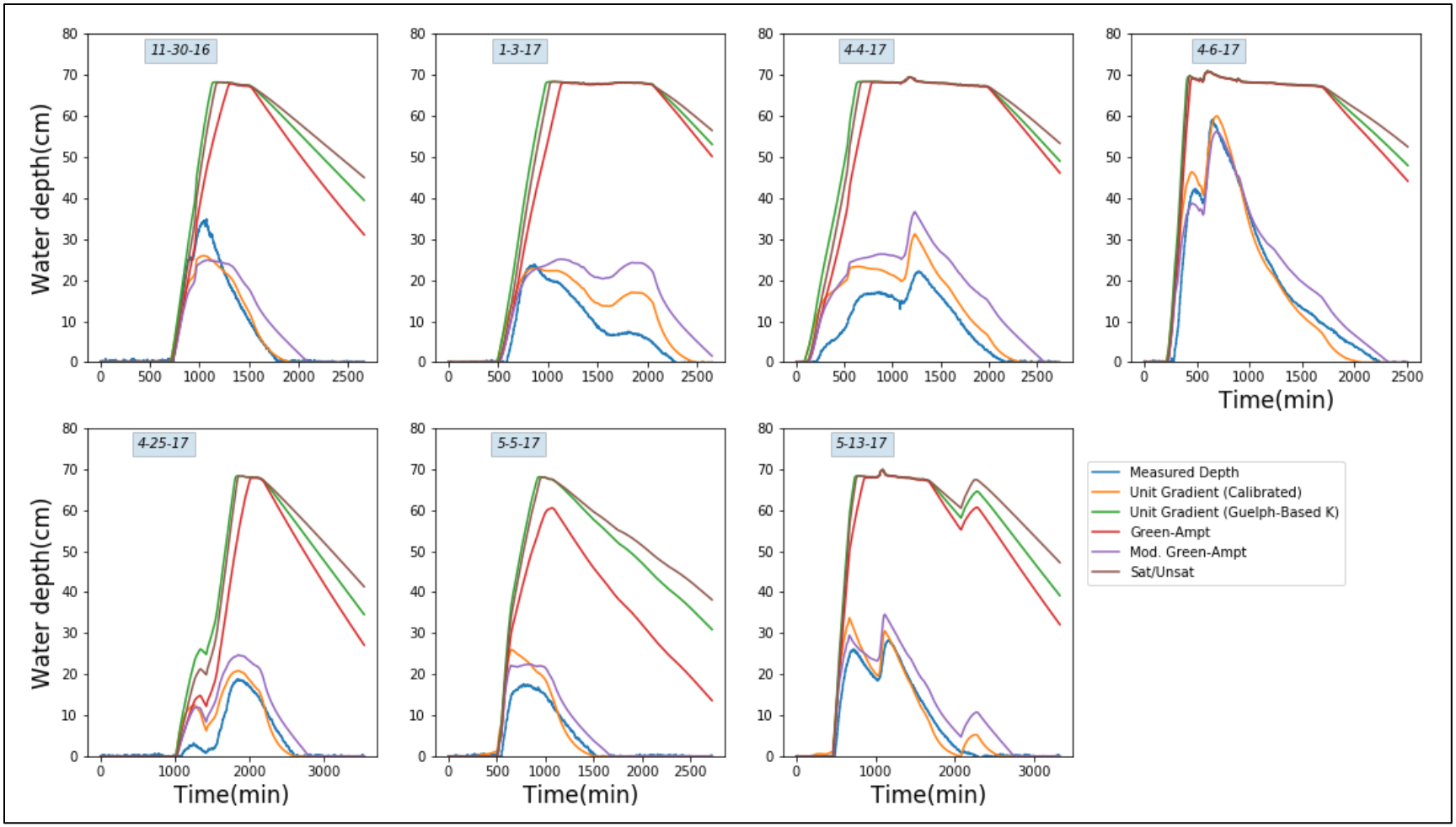

Figure 56: Comparison of simulated water depths from the infiltration models to the measured water depths in the Grove St system for various long-duration rainfall events

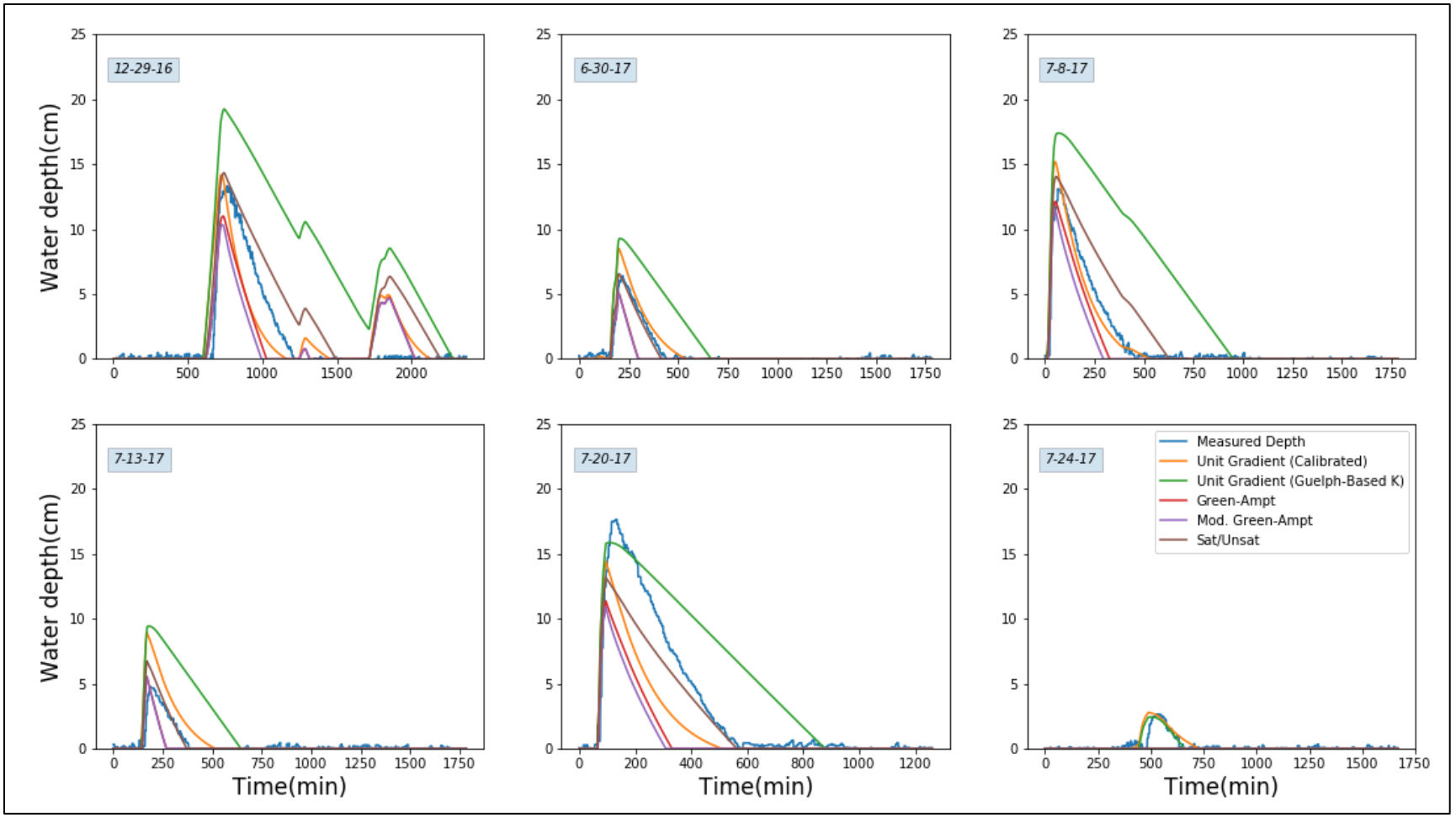

Figure 57: Comparison of simulated water depths from the four infiltration models to the measured water depths in the Grove St system for various short-duration rainfall events

Overall, the Guelph-based unit-gradient, saturated/unsaturated flow, and traditional Green-Ampt appear to be relatively similar according to RMSE values (see Table 28); although the Guelph-based unit-gradient model has slightly lower RMSE for total infiltration volume and time to peak ponding depth. The calibrated unit-gradient model produced the lowest RMSE for the three variables, suggesting that it is the most accurate model for simulating infiltration in SGF systems. The second lowest values were produced by the modified Green-Ampt model. These findings were supported by the T-test results (Table 29) which could not detect a statistically significant difference between the measured and modeled peak water depths, time to peak depth, or total infiltration volume for the modified Green-Ampt and calibrated unit-gradient models. Based on these results, it appears that accounting for horizontal infiltration is vital to the accuracy of the infiltration models for the Grove St system. The modified Green-Ampt method can, to some degree, account for horizontal infiltration and unsaturated conditions, by incorporating an effective infiltration area parameter. However, the model relies on calibrated input parameters and is therefore not advantageous for system design. The unit-gradient model assumes saturated conditions and a constant hydraulic gradient of one, but includes horizontal infiltration and can be used even when the soils surrounding a system are anisotropic.

Accounting for the effect of soil moisture and unsaturated conditions appears to have less of an impact on model accuracy. As demonstrated in Figure 44 and Figure 45, infiltration rates decrease rapidly after runoff begins to flow into the gravel filter. Once water starts to pond in the system, the unsaturated infiltration rates have already decreased to be essentially under saturated conditions. Therefore, water levels in the system are initially controlled by saturated vertical infiltration rates. The statistical analyses appear to support this theory as the T-tests could not detect a statistical difference between the measured and model time to peak water depth for any

of the models. All of the models appear to sufficiently estimate the time to the initiation of ponding and time to peak ponding depth; although the models which accounted for horizontal infiltration produced the lowest RMSE for time to peak. Insight into the effects of unsaturated conditions on horizontal infiltration could not be evaluated from the model analyses in this research because the only model which accounted for horizontal infiltration was the saturated flow, unit-gradient model.

The results of the infiltration models provide information about how the measured hydrologic performance of an SGF relates to infiltration processes within that system. However, it is difficult to compare these results to the original design performance because the Grove St and Kettlebell systems were sized to store the runoff from an amorphous 1-inch rain event. The dynamics of storm events is neglected when using static sizing techniques. To better compare the models from this research to current design practices, the models were run for synthetic runoff hydrograph for the Grove St system. The synthetic hydrograph was developed using the Curve Number method to calculate the runoff from a 1-inch, 24-hour rainfall event with an SCS Type III rainfall distribution (USDA-SCS 1986). HydroCAD, a hydrologic and hydraulic modeling program commonly used in the stormwater management industry (HydroCAD 2019), was also used to simulate SGF performance by assume a constant infiltration rate equal to the vertical hydraulic conductivity of the native soils at a site. The Guelph permeameter estimate for K was used in the HydroCAD model given that it was used as input for all of the other models except for the calibrated unit-gradient model. Results from the modeling exercise and a graph of the ponded water depths in the gravel filter produced by each model are presented in Table 30 and Figure 58, respectively.

Table 30: Comparison of model results for the Grove St SGF for a synthetic 1-inch rain event

Model	Peak water depth (cm)	Time to Peak Water Depth (min)	Cumulative Infiltration Volume (ft^3)	% Volume Reduction
Static Design	-	-	1320	67%
Constant Infiltration Rate (HydroCAD)	67.9	482	1630	83%
Saturated/ Unsaturated	67.6	815	1778	90%
Green-Ampt	58.4	815	1971	100%
Unit-Gradient (Calibrated)	29.3	241	1971	100%
Unit-Gradient (Guelph)	67.8	482	1696	86%
Modified Green-Ampt	23.5	288	1971	100%

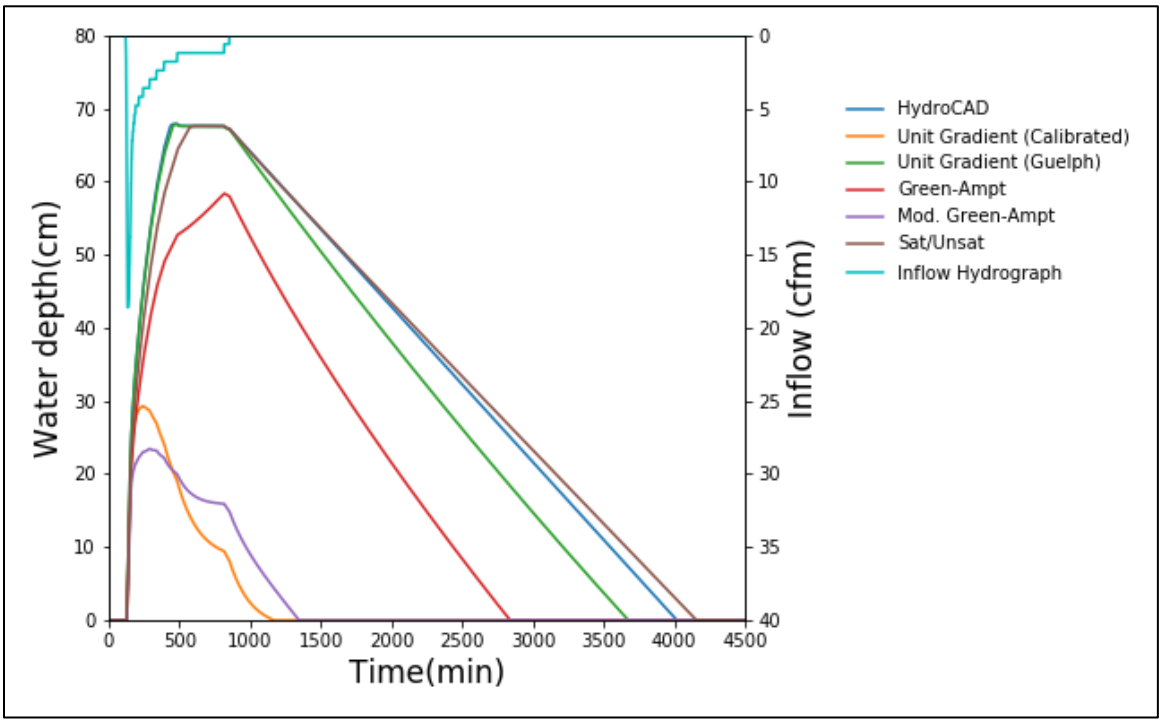

Figure 58: Comparison of simulation water depths in the Grove St SGF for a synthetic 1-inch rain event

By comparing the cumulative infiltration volumes from the models (Table 30) to the statically sized storage volume, one can see that the dynamics of runoff generation and infiltration affect perceived system performance. All of the models, including the HydroCAD

constant infiltration rate model, infiltrated larger volumes of runoff than the supposedly undersized, design storage volume of 1,320 ft^3, which constitutes approximately 67% of the total runoff volume. The HydroCAD model produced the lowest cumulative infiltration volume (i.e. 1,630 ft^3), but still reduced runoff volumes by 83%. The Green-Ampt, modified Green-Ampt, and calibrated unit-gradient models were all able to reduce runoff volumes by 100% for the 1-inch rain event. If the Grove St system had been fully sized to store its WQV of 4,910 ft^3, the system would be significantly oversized. By neglecting stormwater dynamics, the design methods for SGFs and other GSI systems produce oversized systems. The model results and simulated water depths in the filter (Figure 58) also show how horizontal infiltration and unsaturated soil conditions impact system performance. The unit-gradient model which used the Guelph-based K-value produced slightly high runoff volume reductions than the HydroCAD model, but lower reductions that the saturated/unsaturated and Green-Ampt models. By accounting for anisotropic conditions and the high horizontal hydraulic conductivity of native soils, the modified Green-Ampt and calibrated unit-gradient model produced much shallower ponded water depths than the other simulations. These two models also predict 100% reduction of the runoff volume. It appears that horizontal infiltration rates affect the hydrologic performance of a system, but only if the horizontal K-value is much large than the vertical K-value.

The results from the model simulations of the synthetic rain event and the 27 actual events highlight some of the deficiencies of the models. For example, accuracy of the models appears to be limited by the hydraulic conductivity values used as input. When the K_{fs} estimate from the Guelph permeameter measurements is used in the unit-gradient model for both horizontal and vertical K, the model underestimates total infiltration rates, especially during large

storm events. The Guelph-based unit-gradient model produces similar RMSE values to the Green-Ampt and saturated/unsaturated flow model which did not account for sidewall infiltration (see Table 28). However, when the calibrated K-values are used in the unit-gradient model, the results are statistically similar to the monitoring data (Table 23). The calibration process produced a much larger value for horizontal hydraulic conductivity, suggesting that the soils surround the system are highly anisotropic, with much high horizontal infiltration rates.

Several other assumptions about the soils surrounding the SGF system may influence the model results. One assumption is that the native soils below the system are freely draining and that the groundwater table is at an elevation where it will not influence exfiltration from the systems. If this assumption is violated, a model may overestimate infiltration causing simulated water levels to drop more rapidly than what was measured. For the Grove St. SGF, the simulated peak water levels were higher than those that were measured for most storm events and appeared to recede at similar rates to the monitoring data, suggesting that the water table is not limiting infiltration. However, the presence of a baseflow at the outlet provides some evidence that there may have been a shallow groundwater table. For the Kettlebell system, the monitoring data and modeling results both suggest that there was a high groundwater table at the site. The Green-Ampt model appeared to overestimate infiltration because the water level in the single-event simulations dropped faster than measured values. The modeled water levels only matched the monitoring data when the simulation was run for an extended time period and flows approached saturated conditions.

Another model assumption which may have influenced model results was that soils were assumed to be homogeneous in terms of texture, porosity, hydraulic conductivity, and, initially, soil moisture. Soils may be highly heterogeneous, especially in urban environments where

development and construction activities can lead to soil stratification. The presence of a more restrictive clay layer below one of the SGFs or a less restrictive sandy layer along the sidewalls could lead to significant differences between measured and modeled infiltration. Attempts were made to classify and measure the properties of the soils at the SGF sites in Dover. However, the systems and surrounding areas are covered by asphalt, limiting the number of soil samples and Guelph measurements which could be taken. The PSD results for two samples which were collect, in addition to site observations during system construction, support the assumption that the soils surrounding the Kettlebell system are a homogenous clayey material. Soil samples and Guelph permeameter measurements from Grove St showed a greater range of variability. The textural classes of soil samples from the site ranged from clays to sandy-clay loams, with the majority of samples falling into the clay-loam textural class. Infiltration rates measured along the sides of the system with the Guelph permeameter varied with depth by approximately 50%. This may be due to the presence of soil stratification or the influence of macropores.

CHAPTER 5: CONCLUSIONS

5.1 System Performance

Based on the water balance analyses for the Grove St. and Kettlebell subsurface gravel filters, the systems are not performing in accordance with their designs. The Grove St system is infiltrating much larger volumes of runoff (i.e. 84% of collected runoff) than would be expected for an undersized infiltration system constructed over an HGS type C soil. Most design standards assume zero infiltration and provide no runoff reduction credit for systems in type C soils (U.S. EPA, 2011). Even in highly permeable soils, many design standards use static sizing techniques which neglect infiltration and assume systems only begin to drain once they have been filled. These unrealistic sizing methods may lead to the construction of systems which are larger than they need to be to treat desired runoff volumes.

While the Grove St system performance exceeded design expectations, the Kettlebell system performed very poorly, providing negligible runoff volume and peak flow reductions during the monitoring period for this research. The system was constructed at a site with highly impermeable, clayey soils which essentially prevented infiltration. Additionally, the difference in elevation between the system and the water surface of Berry Brook is very small, making it difficult to incorporate an underdrain into the design. Without an underdrain to drain the system between storm events, and potentially due to the impacts of a shallow groundwater table, the system filled with runoff and remained full throughout the monitoring period.

These results emphasize the importance of including an underdrain or some other downgradient drain in systems situated in low permeability soils. Systems need to be able to empty in between rain events so that they can provide some measure of filtration and peak flow reduction for runoff, even if infiltration is limited. The failure of the Kettlebell system also

highlights the importance of performing pre-design site investigations. If infiltration testing had been performed prior to construction, the Kettlebell system would have most likely been redesigned or relocated to an area that is more favorable for infiltration. Unfortunately, soil testing was neglected because the Kettlebell site is completely paved, making it difficult to assess the soils. The proximity of Kettlebell to Berry Brook may also have led to the issue of a shallow water table. The negligible infiltration rates from the system may have been due, in part, to the location of the groundwater table below the gravel layer.

The monitoring results also show that SGF performance could potentially be improved through regular system maintenance, including removing collected sediment from the catch basins and cleaning out perforated inlet pipes. This would help reduce the amount of water that bypasses the gravel layer and does not have an opportunity to infiltrate. When the third catch basin (CB #3) in the Grove St system fills to its upper inlet pipe, water can either drain into the system through the slots in the pipe or flow directly to the system's outlet in the fourth catch basin (CB #4). The 6-inch slotted pipes have a maximum drainage rate of approximately 5 cfm per foot of pipe when flowing full (UNHSC 2015), which should be sufficient to drain all inflows into the gravel layer until it fills. Over several years of operation, a layer of fine sediment has settled out in the pipe and significantly reduced its effective drainage rate. Due to this layer of sediment, a significant portion of the water entering the upper inlet pipe flows directly to the outlet instead of draining into the system. This is one reason why the Grove St system never became entirely full, even during large rain events that were greater than the 1-inch design storm. The system could capture and infiltrate a larger volume of water if the inlet pipes were cleaned out and drainage rates were restored. Additional pretreatment could also help reduce the amount of sediment entering the pipes. Currently, the hoods on the openings to the inlet pipes help

prevent trash and larger sediments from entering. Extending the downward bends of the hoods may allow more sediment to settle before the runoff flows into the pipes.

5.2 Infiltration Analysis

Analysis of system performance using various infiltration models provided insight into why the Grove St system is outperforming predictions. The infiltration models used were the 1-D saturated/unsaturated model based on Richards' equation (Browne et al. 2008), the Green-Ampt and modified Green-Ampt models (Freni et al. 2009), and the unit-gradient model (Warnaars et al. 1999). The results of each model were compared to the monitoring data both graphically and through the use of statistical analyses, including two-sided T-tests and the root mean square error (RMSE). Comparison of the models showed that horizontal infiltration plays a key role in system performance for the Grove St system. Accounting for the high horizontal infiltration rates in the system with the unit-gradient model significantly improved model fit. The model results also showed that accounting for horizontal infiltration is more important for predicting system performance than accounting for unsaturated soil properties. The initially high unsaturated infiltration rates in the saturated/unsaturated flow and Green-Ampt models decreased so rapidly that their effect on the total infiltration volume and the water depth in the system were less substantial compared to the amount of water infiltrating through the sides of the system during ponding.

The Green-Ampt and the saturated/unsaturated flow models, both of which assume one-dimensional vertical infiltration, underestimated infiltration rates, especially for larger storm events and those which produced significant ponding depths (i.e. >20 cm) within the gravel filter. Due to the underestimation, the models were not able to accurately simulate the ponded water level in the Grove St. The T-tests confirmed, with a 95% confidence level, that the results

of the two models were statistically different from the monitoring data in terms of peak water depths and total infiltration volumes. However, the accuracy of the 1-D models improved when simulating system performance for smaller rain events, when ponding in the gravel layer was minimal. When the T-tests were performed for the results of only the smaller events, a statistically significant difference could not be detected between the modeled and measured values of peak water depth, time to peak, and total infiltration volume.

Simulations can more accurately replicate the monitoring data when horizontal infiltration through the sidewalls of a system is taken into account. The calibrated unit-gradient model accounts for both horizontal and vertical infiltration and was the most accurate of the models presented in this research. The RMSE values for the unit-gradient model were significantly lower than the RMSE values calculated for the other models. Additionally, the T-tests did not detect a statistically significant difference between the modeled and measured values of time to peak, total infiltration volume, and peak water depth in the system, suggesting that the model results were statistically similar to the monitoring data.

By comparing the total horizontal and vertical infiltration volumes from the calibrated unit-gradient model (Table 27), it becomes apparent that horizontal infiltration plays a significant role in the performance of SGF systems. For the 27 modeled rain events, horizontal infiltration accounted for approximately 90% of the total runoff volume reductions. This helps explain why the accuracy of the Green-Ampt and saturated/unsaturated models decreased substantially when simulating the larger storm events. If water levels in the gravel layer remained fairly low throughout a storm, the wetted area of the system's sides was fairly small and horizontal infiltration was minimal. During these scenarios, assuming entirely vertical infiltration does not substantially impact model results. However, during large storm events, water levels rose high

enough that horizontal infiltration surpassed vertical infiltration. The unit-gradient model was the only one which could accurately simulate the measured water depth during larger storms.

The accuracy of the unit-gradient model strongly depends on the hydraulic conductivity values used as input parameters. When the Guelph permeameter-based estimate for K_{fs} was used for both the horizontal and vertical K-values, the model underestimated infiltration and produced similar results to the Green-Ampt and saturated/unsaturated flow models. The RMSE calculated for the simulated peak water depth in the system, time to peak depth, and total infiltration volume for the unit-gradient model were found to be similar, if not slightly lower, than those from the 1-D models. The Guelph permeameter K_{fs} estimate of 0.51 cm/hr is much smaller than the calibrated value of 41.9 cm/hr for horizontal hydraulic conductivity. Horizontal and vertical infiltration rates are significantly different according to these results.

The infiltration models were also used to simulated system performance for a synthetic, 1-inch, 24-hour rain event developed according to the methods outline in TR-55 (USDA-SCS, 1986). A comparison of volume reductions from the model results to those predicted by static sizing methods (Table 30) highlights the importance of account for runoff and infiltration dynamics. All of the models estimated large runoff volume reductions between 86 and 100%, which are significantly larger than the statically sized storage volume.

One can conclude from the monitoring and modeling results presented in this research, that the design methodology for subsurface gravel filters could be improved through the use of dynamic sizing techniques that account for both vertical and horizontal infiltration. While static sizing is simple, user-friendly, and requires limited input data, it neglects the dynamic nature of runoff generation and infiltration, leading to the construction of stormwater infiltration systems that are unnecessarily large and expensive. Dynamic design techniques that incorporate some

measure of the infiltration that occurs throughout a storm event produce smaller, more realistically sized systems, especially in soils with high hydraulic conductivities. Some states, such as Massachusetts, have already started to incorporate dynamic techniques, which give designers the choice of using one of three approved sizing methods: static, simple dynamic, and dynamic field methods (MassDEP 2008). The simple dynamic and dynamic field methods produce system designs with smaller footprints because they consider that vertical infiltration occurs under saturated conditions during some portion of the design storm event. For example, using the semi-dynamic and dynamic-field methods to size the Grove St SGF produces storage volumes around 1% and 10% smaller, respectively, than the statically sized storage volume of 4910ft^3 (see Table 31). If the native soils at the Grove St site were less restrictive, the calculated storage volumes from the dynamic methods would been even smaller.

Table 31: Comparison of system sizing methods

Parameters	**NH Static Sizing Method**	**MA Dynamic Sizing Methods**		**Unit Gradient Model (SCS 24-hr storm)**	
		Simple Dynamic Method	**Dynamic Field Method**	**Calibrated K-values**	**Guelph-Based K-values**
Drainage Area (acres)	4.10	4.10	4.10	4.10	4.10
Impervious Area (%)	31%	31%	31%	31%	31%
Rv (-)	0.33	0.33	0.33	0.33	0.33
WQV (ft^3)	4910	4910	4910	4910	4910
Storage Depth (ft)	-	2.2	2.2	2.2	2.2
Filter porosity (-)	0.4	0.4	0.4	0.4	0.4
K (cm/hr)	-	0.1*	0.51**	-	0.51**
T (hr)	-	2	12	24	24
Basal Area (ft^2)	-	5540	5010	2050	4400
Storage Volume (ft^3)	**4910**	**4870**	**4410**	**1800**	**3870**
% of WQV	**100%**	**99%**	**90%**	**37%**	**79%**

*Value for clay-loam obtain from Rawls et al., 1983
**Hydraulic conductivity calculated from Guelph permeameter measurements

Accounting for both vertical and horizontal infiltration would further increase the accuracy of system sizing, allowing systems to be designed to meet specific runoff reduction goals, and helping reduce space requirements for subsurface infiltration. In some locations, such as at the site of the Grove St SGF, state stormwater regulations would advise against installing an infiltration system due to low vertical K-values, which are less than 0.5 in/hr. However, the current system has been shown to provide substantial runoff volume reductions due to horizontal infiltration. If sizing techniques considered horizontal infiltration, the size of SGF systems could potentially be reduced for areas with hydrologically favorable soils (i.e. HGS type A and B soils) and system designs could be developed for a larger variety of soil types, such as urban fill.

The results of this study show that the unit-gradient model can accurately account for both horizontal and vertical infiltration in subsurface gravel filters. This model could be effectively implemented to design SGF systems if the horizontal and vertical hydraulic conductivity values can be accurately estimated. One strategy could be to develop a synthetic hydrograph with a total runoff volume equal to the WQV. The SCS Curve Number method, described in TR-55, requires limited input information and could be used to develop the hydrograph. The unit-gradient model would then be used to simulate the infiltration processes within a proposed SGF system for the synthetic runoff hydrograph. Sizing an SGF would then involve adjusting the dimensions of the proposed filter until the peak water depth just reaches the maximum storage capacity of the system during the modeled time period.

This method was implemented to size the Grove St system using a 24-hour, synthetic hydrograph based on the SCS Type III rainfall distribution. Infiltration was simulated with unit-gradient model using both the calibrated hydraulic conductivity values and the Guelph permeameter K_{fs} estimated. For simplicity, the gravel filter thickness was kept constant at 2.2 ft

(i.e. the same thickness as the existing filter), while the bottom area of the system was adjusted until simulated peak water depth just filled the system. The results of the design method are presented in Table 31. For the unit-gradient model with the Guelph-based K-values, the method produced a minimum storage volume of 3,870 ft^3, which is approximately 79% of the statically sized system. For the calibrated K-values, a storage volume of only 1800 ft^3, or 22% of the statically sized storage volume, would be needed to contain and infiltrate the WQV. This design strategy produces significantly smaller systems than the static, simple dynamic, and dynamic field methods because the method accounts for horizontal infiltration and the dynamics of system performance. Note that this design method assumes all runoff flows are entering the gravel filter, which is not the case for the existing Grove St SGF. The primary challenge of implementing the unit-gradient model for design is obtaining accurate estimates of horizontal and vertical hydraulic conductivity. Using the Guelph-based K_{fs} estimate as input to the unit-gradient model helps reduce the design volume compared to the other design methods, but still underestimated infiltration rates compared to the calibrated model where horizontal K is significantly larger than the vertical K.

As mentioned previously, hydraulic conductivity is one of the most important properties affecting infiltration. Vertical K-values can be measured using a variety of different techniques, but horizontal K-values can be more difficult to determine. The Guelph permeameter was evaluated as a potential tool to determine horizontal K-values because the device measures hydraulic conductivity as an average of both horizontal and vertical infiltration. However, when used at the Grove St and Kettlebell sites, the device had varying success. This may have been due to the low conductivity of the native soils, the presence of macropores, the development of a clayey smear with the test holes, or the relatively high moisture level of the soils prior to testing.

While the Guelph permeameter can be a useful device for measuring hydraulic conductivity, it may not be ideal for silty or clayey soils which are prone to producing a smear layer during test hole excavation and require long time periods to run tests. The method used to determine the horizontal K-values from the Guelph measurements appeared to have potential, but requires further investigations as the technique produced significantly lower horizontal K-values than those which were calibrated from the receding water level in the Grove St SGF system. The higher horizontal hydraulic conductivity for the system may be due to the effects of macropores in the surrounding soils.

The determination of soil properties based on soil texture and particle size distributions was also evaluated. Numerous publications provide average values for soil properties based on soil texture, making the information readily available for the design of stormwater systems. Additionally, the techniques for estimating soil properties from soil texture and PSD data require far less time and resources than in situ or laboratory measurements. However, site specific soil properties can vary significantly from the published averages due to compaction and the presence of macropores. The values can also be inaccurate for sites, such as the Grove St system, which have anisotropic soils. In situ measurements of hydrologic soil properties are advantageous for SGF design computations.

5.3 Future Research

This research identifies some of the factors which affect the performance of subsurface gravel filters and presents various improvements that can be made to current design techniques. However, there are still several gaps in our understanding of system performance and design which should be addressed in future research initiatives. For example, there is a need for research on measurement methods for horizontal hydraulic conductivity and anisotropic soil. Current

measurement techniques either focus on vertical infiltration or are time and effort intensive. A rapid yet reliable method is needed so that horizontal infiltration estimates can be incorporated into the design methodology of stormwater infiltration systems. The Guelph permeameter has potential for this purpose, but further testing is needed to determine how horizontal hydraulic conductivity can be extracted from the averaged K_{fs}-value it provides.

REFERENCES

Assouline, A., J.S. Selker, and J.Y. Parlange. 2007. A simple accurate method to predict time of ponding under variable intensity rainfall. Water Resources Research, 43, W03426.

ASTM Standard D7928. 2016 (2017). Standard Test Method for Particle-Size Distribution (Gradation) of Fine-Grained Soils Using the Sedimentation (Hydrometer) Analysis. ASTM International.

ASTM Standard D5126/D5126M. 1990 (2010). Standard Guide for Comparison of Field Methods for Determining Hydraulic Conductivity in Vadose Zone. ASTM International.

Bergman, M., M.R. Hedegaard, M.F. Petersen, P. Binning, O. Mark, and P.S. Mikkelsen. 2011. Evaluation of two stormwater infiltration trenches in central Copenhagen after 15 years of operation. Water Science Technology, 63(10): 2279-2286.

Bouwer, H. 1966. Rapid Field Measurement of Air Entry Value and Hydraulic Conductivity of Soil as Significant Parameters in Flow System Analysis. *Water resources Research*, 2(4): 729-738.

Bower, H. 1969. Infiltration of Water into Nonuniform Soil. Journal of Irrigation and Drainage, Division of ASCE, 95(IR4): 451-462.

Browne, D., A. Deletic, G.M. Mudd, and T.D. Fletcher. 2008. A new saturated/unsaturated model for stormwater infiltration systems. Hydrological Processes, 22: 4838-4849.

Campisano, A., E. Creaco, and C. Modica. 2011. A simplified approach for the design of infiltration trenches. Water Science & Technology, 64(6): 1362-1367.

Celia, M.A., E.T. Bouloutas, and R.L. Zarba. 1990. A general mass-conservative numerical solution for the unsaturated flow equation. Water Resources Research, 26(7): 1483-1496.

Claytor, R.A. and T.R. Schueler. 1996. Design of Stormwater Filtering Systems. The Center of Watershed Protection. Silver Springs, MD.

Dempsey, B.A., and D.M. Swisher. 2003. Evaluation of porous pavement and infiltration in Centre County, PA. World Water & Environmental Resources Congress, ASCE, Reston, VA.

Dussaillant, A. R., C.H. Wu, A.M. ASCE, and K.W. Potter. 2004. Richards equation model of raingardens. *Journal of Hydrologic Engineering*, 9(3): 219-225.

Elliott, A.H. and S.A. Trowsdale. 2007. A review of models for low impact urban stormwater drainage. *Environmental Modelling & Software*, 22: 394-405.Finch, S.D., D.E. Radcliffe, and L.T. West. 2008. Modeling Trench Sidewall and Bottom Flow in On-Site Wastewater Systems. Journal of Hydrologic Engineering, 13(8): 692-701.

Elrick, D.E., W.D. Reynolds, and K.A. Tan. 1989. Hydraulic Conductivity Measurements in the Unsaturated Zone Using Improved Well Analyses. Groundwater Monitoring & Remediation, 9(3): 184-193.

Evans, Mary Anna. 2015. "Flushing the Toilet Has Never Been Riskier." *The Atlantic*. https://www.theatlantic.com/technology/archive/2015/09/americas-sewage-crisis-public-health/405541/

Finch, S.D., D.E. Radcliffe, and L.T. West. 2008. Modeling Trench Sidewall and Bottom Flow in On-Site Wastewater Systems. Journal of Hydrologic Engineering, 13(8): 692-701.

Flerchinger, G.N., F.J. Watts, and G.L. Bloomsburg. 1988. Explicit Solution to Green-Ampt Equation for Nonuniform Soils. Journal of Irrigation and Drainage, Division of ASCE, 114(3): 561-565.

Freni, G., G. Mannina, and G. Viviani. 2009. Stormwater infiltration trenches: a conceptual modelling approach. Water Science & Technology, 60(1): 185-199.

Gallichand, J., C.A. Madramootoo, P. Enright, S.F. Barrington. 1990. An Evaluation of the Guelph Permeameter for Measuring Saturated Hydraulic Conductivity. *American Society of Agricultural Engineers*, 33(4): 1179-1184.

Graham, P., L. Maclean, D. Medina, A. Patwardhan, and G. Vasarhelyi. 2004. The role of water balance modelling in the transition to low impact development. Water Quality Resources Journal of Canada, 39(4): 331-342.

Green, W. H and C.A. Ampt. 1911. Studies on Soil Physics I. The Flow of Air and Water through Soils. Journal of Agricultural Science IV (Part I 1911): 1-24.

Heasom, W., R.G. Traver, A. Welker. 2006. Hydrologic modeling of a biofiltration best management practice. Journal of the American Water Resources Association (JAWRA) 42(5): 1329-1347.

Horton, R.E. 1940. An approach towards a physical interpretation of infiltration capacity. Soil Science Society of America Proceedings 5: 399-417.

Houle, J.J., T.P Ballestero, and T.A. Puls. 2017. The performance analysis of two relatively small capacity urban retrofit stormwater controls. Journal of Water Management Modeling, 25:C417.

Huang, R.Q. and L.Z. Wu. 2012. Analytical solutions to 1-D horizontal and vertical water infiltration in saturated/unsaturated soils considering time-varying rainfall. Computers and Geotechnics, 39: 66-72.

HydroCAD Stormwater Modeling System. 2019. HydroCAD Software Solutions LLC. https://www.hydrocad.net/index.htm

Jagai, J.S., Q. Li, S. Wang, K.P. Messier, T.J. Wade, and E.D. Hilborn. 2015. Extreme Precipitation and Emergency Room Visits for Gastrointestinal Illness in areas with and without Combined Sewer Systems: An Analysis of Massachusetts Data, 2003-2007. Environmental Health Perspective, 123:873–879.

Konrad, C.P. 2016. Effects of Urban Development on Floods. Fact Sheet 076-03. U.S. Geological Survey. https://pubs.usgs.gov/fs/fs07603/.

Kwiatkowski, M., A.L. Welker, R.G. Traver, M. Vanacore, and T. Ladd. 2007. Evaluation of an infiltration best management practice utilizing pervious concrete. Journal of the American Water Resources Association (JAWRA), 43(5):1208-1222. DOI: 10.1111 / j.1752-1688.2007.00104.x

Lee, D.M., W.D. Reynolds, D.E. Elrick, and B.E. Clothier. 1985. A comparison of three field methods for measuring saturated hydraulic conductivity. *Canadian Journal of Soil Science*, 65: 563-573.

Legret, M., and V. Colandini. 1999. Effects of a porous pavement with reservoir structure on runoff water: water quality and fate of heavy metals. Water Sci. Technol., 39(2): 111-117.

Luell, S.K., W.F. Hunter, and R.J. Winston. 2011. Evaluation of undersized bioretention stormwater control measures for treatment of highway bridge deck runoff. Water Science & Technology, 64(4): 974-979.

Kwiatkowski, M., A.L. Welker, R.G. Traver, M. Vanacore, and T. Ladd. 2007. Evaluation of an infiltration best management practice utilizing pervious concrete. Journal of the American Water Resource Association, 43(5): 1208-1222

Massachusetts Department of Environmental Protection (MassDEP). 2008. Massachusetts Stormwater Handbook. Vol. 1, Ch. 1: Overview of Massachusetts Stormwater Standards. https://www.mass.gov/guides/massachusetts-stormwater-handbook-and-stormwater-standards

McCuen, R.H., W.J. Rawls, and D.L. Brakensiek. 1981. Statistical Analysis of the Brooks-Corey and the Green-Ampt Parameters Across Soil Textures. *Water Resources Research*, 17(4): 1005-1013.

Mikkelsen, P.S. 1995. Hydrological and pollutional aspects of urban stormwater infiltration. Ph. D. thesis. Department of Environmental Science and Engineering, Technical University of Denmark.

Mishra, S., J.C. Parker, and N. Singhal. 1989. Estimation of soil hydraulic properties and their uncertainty from particle size distribution data. *Journal of Hydrology*, 108: 1-18.

New Hampshire Department of Environmental Services (NHDES). 2008. NH Stormwater Manual, Vol. 1: Stormwater and Antidegradation.

https://www.des.nh.gov/organization/commissioner/pip/publications/wd/documents/wd-08-20a.pdf

New Hampshire Department of Environmental Services (NHDES). 2008. NH Stormwater Manual, Vol. 2: Post-Construction Best Management Practices Selection & Design. https://www.des.nh.gov/organization/commissioner/pip/publications/wd/documents/wd-08-20b.pdf

Philip, J.R. 1957. The Theory of Infiltration: 4. Sorptivity and Algebraic Infiltration Equations. Soil Science 84: 257-264.

Philip, J.R. 1969. Theory of Infiltration. Advances in Hydroscience 5: 215-296. Academic Press, New York, NY.

Philip, J.R. 1972. Steady Infiltration from Buried, Surface, and Perched Point and Line Sources in Heterogenous Soils: I. Analysis. Soil Science Society of America Proceedings, 36: 268-273.

Ragab, R. and J.D. Cooper. 1993. Variability of unsaturated zone water transport parameters: implications for hydrological modelling 2. Predicted vs. in situ measurements and evaluation of methods. Journal of Hydrology, 148: 133-147.

Ravi, V. (Dynamac Corporation) and J.R. Williams (U.S. EPA). 1998. Estimation of Infiltration Rate in the Vadose Zone: Compilation of Simple Mathematical Models, Volume I. National Risk Management Research Laboratory, U.S. EPA. EPA/600/R-97/128a.

Rawls, W.J., D.L. Brakensiek, and K.E. Saxton. 1982. Estimation of Soil Water Properties. Transactions American Society of Agricultural Engineers, 25(5): 1316-1320.

Rawls, W.J., M. ASCE, D.L. Brakensiek, and N. Miller. 1983. Green-Ampt Infiltration Parameters from Soils Data. Journal of Hydraulic Engineering 109(1): 62-70.

Rawl et al. 1992

Reeve, R.C. and D. Kirkham. 1951. Soil anisotropy and some field methods for measuring permeability. American Geophysical Union, 32(4): 582-590.

Region 1: EPA New England. *What are Combined Sewer Overflows (CSOs)*. Urban Environmental Program. https://www3.epa.gov/region1/eco/uep/cso.html.

Reynolds, W.D. and D.E. Elrick. 1985. In Situ Measurement of Field-Saturated Hydraulic Conductivity, Sorptivity and the α-Parameter using the Guelph Permeameter. Soil Science, 140(4): 292-302.

Reynolds, W.D. and D.E. Elrick. 1986. A Method for Simultaneous In Situ Measurement in the Vadose Zone of Field-Saturated Hydraulic Conductivity, Sorptivity, and the Conductivity-Pressure Head Relationship. Ground Water Monitoring & Remediation, 6 (1): 84–95.

Richards, L.A. 1931. Capillary conduction of liquids through porous mediums. Physics, 1(5): 318-333.

Roseen, R.M., T.P. Ballestero, J.J. Houle, P. Avellenda, R. Wildey, J. Briggs. 2006. Storm water low-impact development, conventional structural, and manufactured treatment strategies for parking lot runoff: Performance evaluation under varied mass loading conditions. *Transportation Research Record*, 1984: 135-147.

Roseen, R.M., T.P. Ballestero, J.J. Houle, J.F. Briggs, and K.M. Houle. 2012. Water quality and hydrologic performance of a porous asphalt pavement as a storm-water treatment strategy in a cold climate. ASCE Journal of Environmental Engineering, 138(1): 81-89.

Stenmark, C. 1995. An alternative road construction for stormwater management in cold climates. Water Sci. Technol., 32(1): 79–84.

Sørup, H.J.D., S.M. Lerer, K. Arnbjerg-Nielsen, P.S. Mikkelsen, and M. Rygaard. 2016. Efficiency of stormwater control measures for combined sewer retrofitting under varying rain conditions: Quantifying the Three Points Approach (3PA). Environmental Science & Policy, 63: 19-26.

Taebi, A. and R.L Droste. 2004. First flush pollution load of urban stormwater runoff. Journal of Environmental Engineering and Science, 3(4): 301-309.

Todd, D.K. and L.W. Mays. 2005. Groundwater Hydrology. 3rd edition. John Wiley & Sons, Inc. Hoboken, NJ.

UNH Stormwater Center (UNHSC) and Vanasse Hangen Brustlin (VHB), Inc. 2015. Modeling the Effect of Local Stormwater Regulations on Future Pollutant Loads in the Oyster River Watershed.

UNH Stormwater Center (UNHSC). 2010. 2009 Biannual Report. https://www.unh.edu/unhsc/sites/unh.edu.unhsc/files/pubs_specs_info/2009_unhsc_report.pdf

UNH Stormwater Center (UNHSC). 2015. Laboratory measurements of drain rate for slotted pipes.

U.S. Census Bureau. 2012. *Growth in Urban Population Outpaces Rest of Nation, Census Bureau Reports.* 2010 Census. Newsroom Archive. https://www.census.gov/newsroom/releases/archives/2010_census/cb12-50.html.

U.S. Department of Agriculture, Soil Conservation Service (USDA-SCS). 1957. Hydrology. National Engineering Handbook. Section 4. Supplement A.

U.S. Department of Agriculture, Soil Conservation Service (USDA-SCS). 1991. Measurement and Estimation of Permeability of Soils for Animal Waste Storage Facility Design. Technical Note 717.

U.S. Department of Agriculture, Soil Conservation Service (USDA-SCS). 1986. Urban Hydrology for Small Watersheds. Technical Release No. 55 (TR-55).

U.S. EPA. 1996. *Nonpoint Source Pollution: The Nation's Largest Water Quality Problem.* EPA-841-F-96-004A. https://nepis.epa.gov/Exe/ZyPDF.cgi/20004PZG.PDF?Dockey=20004PZG.PDF.

U.S. EPA. 2004. Report to Congress: Impacts and Control of CSOs and SSOs. EPA 833-R-04-001. https://www.epa.gov/sites/production/files/2015-10/documents/csossortc2004_chapter02.pdf

U.S. EPA. 2008. Combined Sewer Overflows (CSO) Home: Overview. Available: http://water.epa. gov/polwaste/npdes/cso/index.cfm.

U.S. EPA. 2011. Summary of State Stormwater Standards. https://www3.epa.gov/npdes/pubs/sw_state_summary_standards.pdf

U.S. EPA. 2017. What are Combined Sewer Overflows (CSOs)? https://www3.epa.gov/region1/eco/uep/cso.html

Van Genuchten, M.T. 1980. A closed-form equation for predicting the hydraulic conductivity of unsaturated soils. Soil Science Society of America Journal, 44(5): 892-898.

Wang, J.P., B. Francois, and P. Lambert. 2017. Equations for hydraulic conductivity estimation from particle size distribution: A dimensional analysis. Water Resources Research, 53: 8127-8134.

Warnaars, E., A.V. Larsen, P. Jacobsen, and P.S. Mikkelsen. 1999. Hydrologic behavior of stormwater infiltration trenches in a central urban area during 2 ¾ years of operation. Water Science Technology: 39(2): 217-224.

Warrick, A.W., A. Islas, and D.O. Lomen. 1991. An analytical solution to richards equation for time-varying infiltration. Water Resources Research 27(5): 763-766.

Williams, J.R. (U.S. EPA), Y. Ouyang (ManTech Environmental Technologies, Inc.), J.S. Chen, V.Ravi (Dynamac Corporation). 1998. Estimation of Infiltration Rate in the Vadose Zone: Compilation of Simple Mathematical Models, Volume II. National Risk Management Research Laboratory, U.S. EPA. EPA/600/R-97/128b.

APPENDICES

Sizing Calculations for SGF Systems

Grove St System:

A = 1.44 acres
I = 22%
P = 1.0 inch
φ_g = 0.4
L = 60ft
W = 25ft

$$R_v = 0.05 + 0.9(I) = 0.05 + 0.9(0.22) = 0.252$$

$$WQV = (P)(R_v)(A) = (1\ inch)(0.252)(1.44\ acres) = 0.36\ acre * inches = 1320ft^3$$

$$V = \frac{WQV}{\varphi_g} = \frac{1320ft^3}{0.4} = 3290ft^3$$

$$A_f = L * W = 60ft * 25ft = 1500ft^2$$

$$D = \frac{3290ft^3}{1500ft^2} = 2.2ft$$

The finalized dimensions of the filter bed were 60ft long by 25ft wide by 2.2ft deep. With these dimensions, the system should be able to store the entire WQV of 1320ft^3. However, after review of the local topography, the watershed area draining to the system was increased to 4.10 acres, with 31% IC. This means that the actual WQV is larger than what was originally calculate and that the system is technically undersized because was only designed for a percentage of the total WQV. The amount of water storage that the filter provides, in terms of the percentage of the total WQV, is calculated below.

$$R_v = 0.05 + 0.9(I) = 0.05 + 0.9(0.31) = 0.329$$

$$Updated\ WQV = (P)(R_v)(A) = (1\ inch)(0.329)(4.10\ acres) = 1.36\ acre * inches = 4926ft^3$$

$$\%\ of\ WQV = \frac{1320ft^3}{4926ft^3} = 26.8\%$$

The system can only store approximately 26.8% of the WQV.

Seacoast Kettlebell System:

Note – The size of the system was limited by various constraints such as the size of the parking lot and the elevation of Berry Brook, to which the system outlets.

A = 2.09 acres
I = 72%
P = 1.0 inch
$\varphi_g = 0.4$
L = 60ft
W = 30ft

$$R_v = 0.05 + 0.9(I) = 0.05 + 0.9(0.72) = 0.70$$

$$WQV = (P)(R_v)(A) = (1\ inch)(0.252)(1.44\ acres) = 1.46\ acre * inches = 5310ft^3$$

$$V = \frac{WQV}{\varphi_g} = \frac{5310ft^3}{0.4} = 13{,}300ft^3$$

$$A_f = L * W = 60ft * 30ft = 1800ft^2$$

$$D = \frac{13{,}300ft^3}{1800ft^2} = 7.4ft$$

Due to elevation constraints, the depth of the filter was reduced to 2.5ft. The final dimensions of the filter bed are 60ft long by 30ft wide by 2.5ft deep.

$$V = 60ft * 30ft * 2.5ft = 4500ft^3$$

$$V_s = 4500ft^3 * 0.4 = 1800ft^3$$

$$\%\ of\ WQV = \frac{1800ft^3}{5310ft^3} = 34\%$$

The system is undersized and can only hold approximately 1/3 of the WQV. However, after review of the local topography, the watershed area draining to the system was increased to 2.75 acres, with 72% IC. This means that the actual WQV is larger than what was originally calculate and that the system is technically undersized because was only designed for a percentage of the total WQV. The amount of water storage that the filter provides, in terms of the percentage of the total WQV, is calculated below.

$$R_v = 0.05 + 0.9(I) = 0.05 + 0.9(0.61) = 0.60$$

$$Updated\ WQV = (P)(R_v)(A) = (1\ inch)(0.60)(2.67\ acres) = 1.59\ acre * inches$$
$$= 5770 ft^3$$

$$\%\ of\ WQV = \frac{1800 ft^3}{5770 ft^3} = 31.2\%$$

The system can only store approximately 31.2% of the WQV.

Variables:
WQV = water quality volume (acre-inches)
P = design precipitation depth (inches)
R_v = runoff coefficient (unitless)
A = watershed area (acres)
A_f = filter surface area (ft^2)
V = total filter volume (ft)
V_s = volume of system storage (ft)
L = filter length (ft)
W = filter width (ft)
D = filter depth (ft)
I = fraction of drainage area that is IC
φ_g = porosity of gravel

Design Diagrams

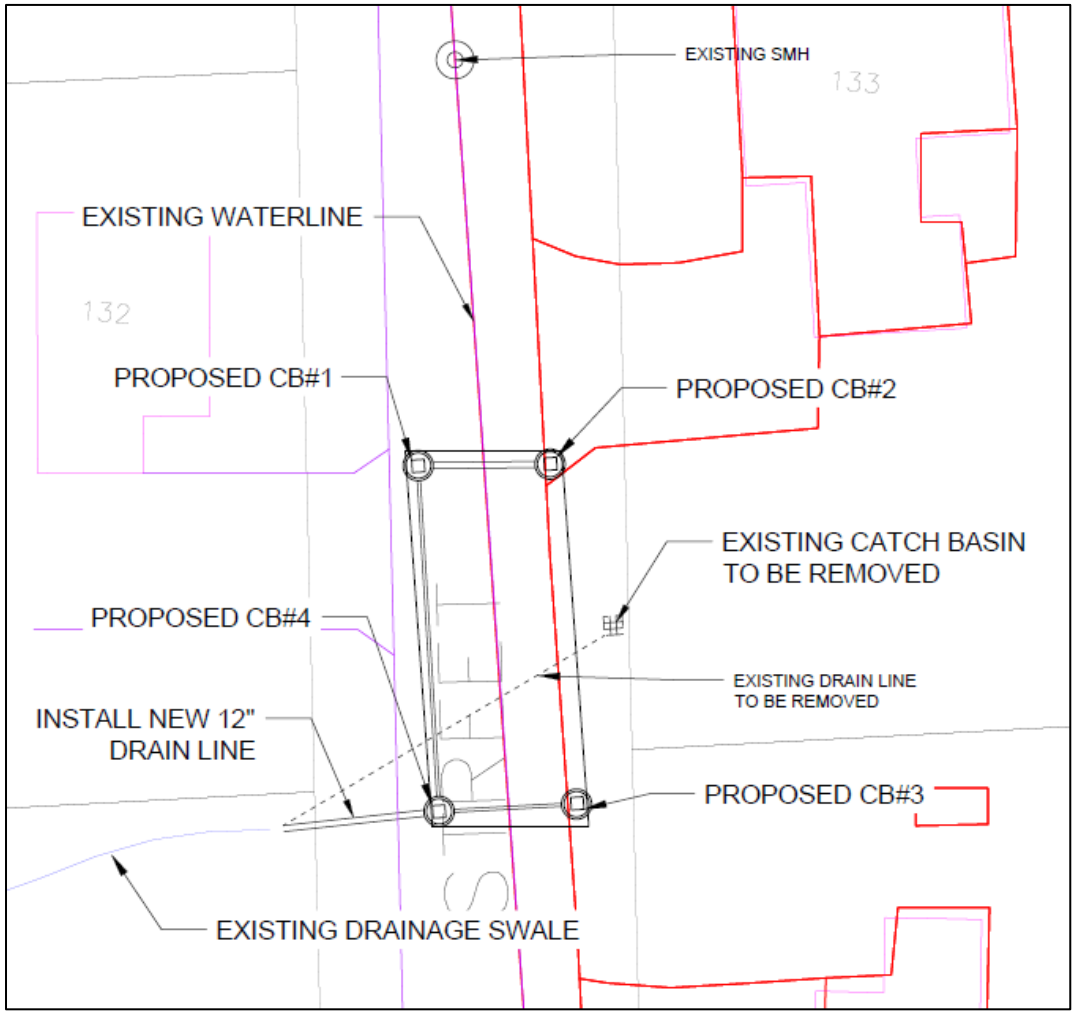

Figure 59: Plan view of the Grove St SGF

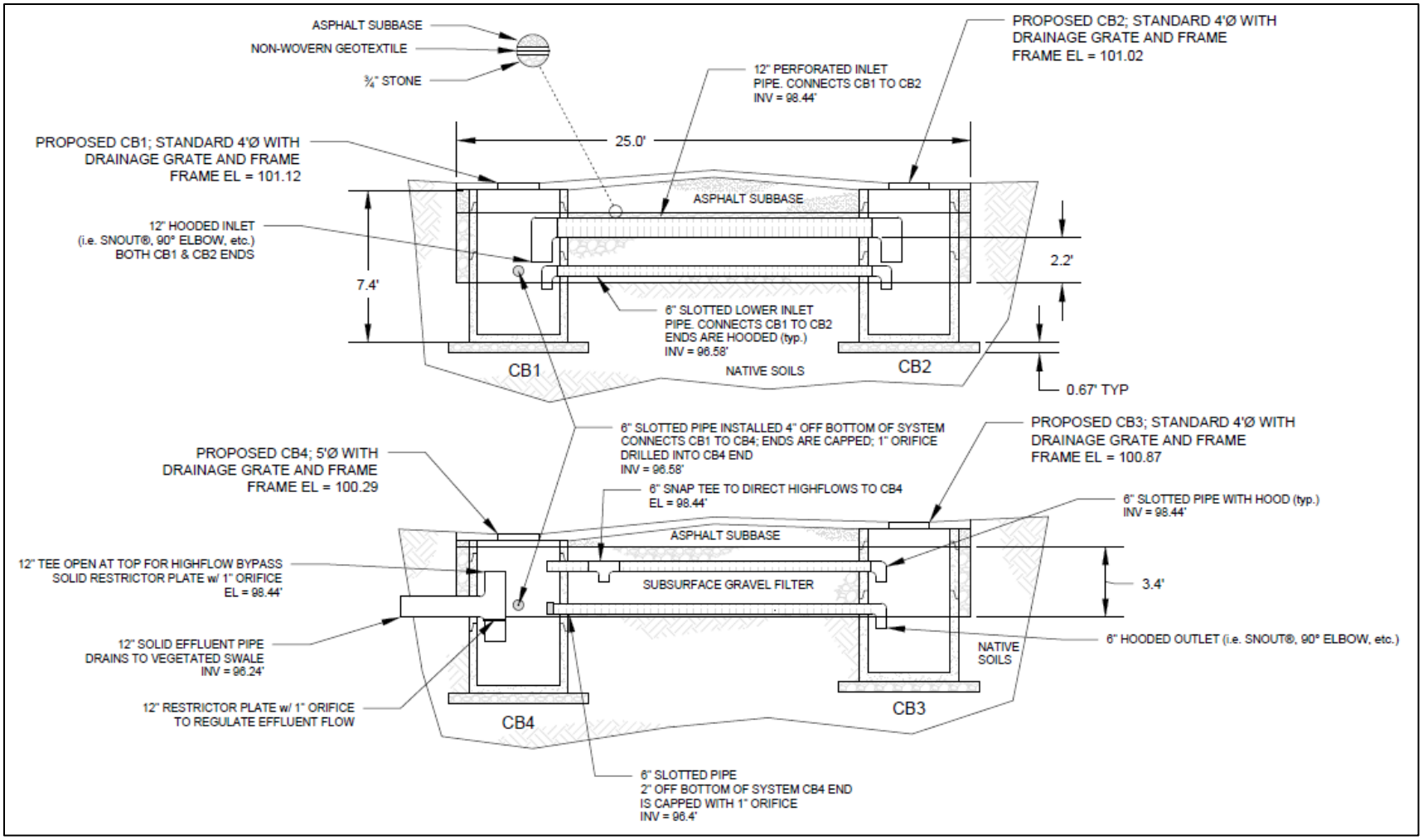

Figure 60: Design diagram showing the cross-sectional view of the Grove St SGF

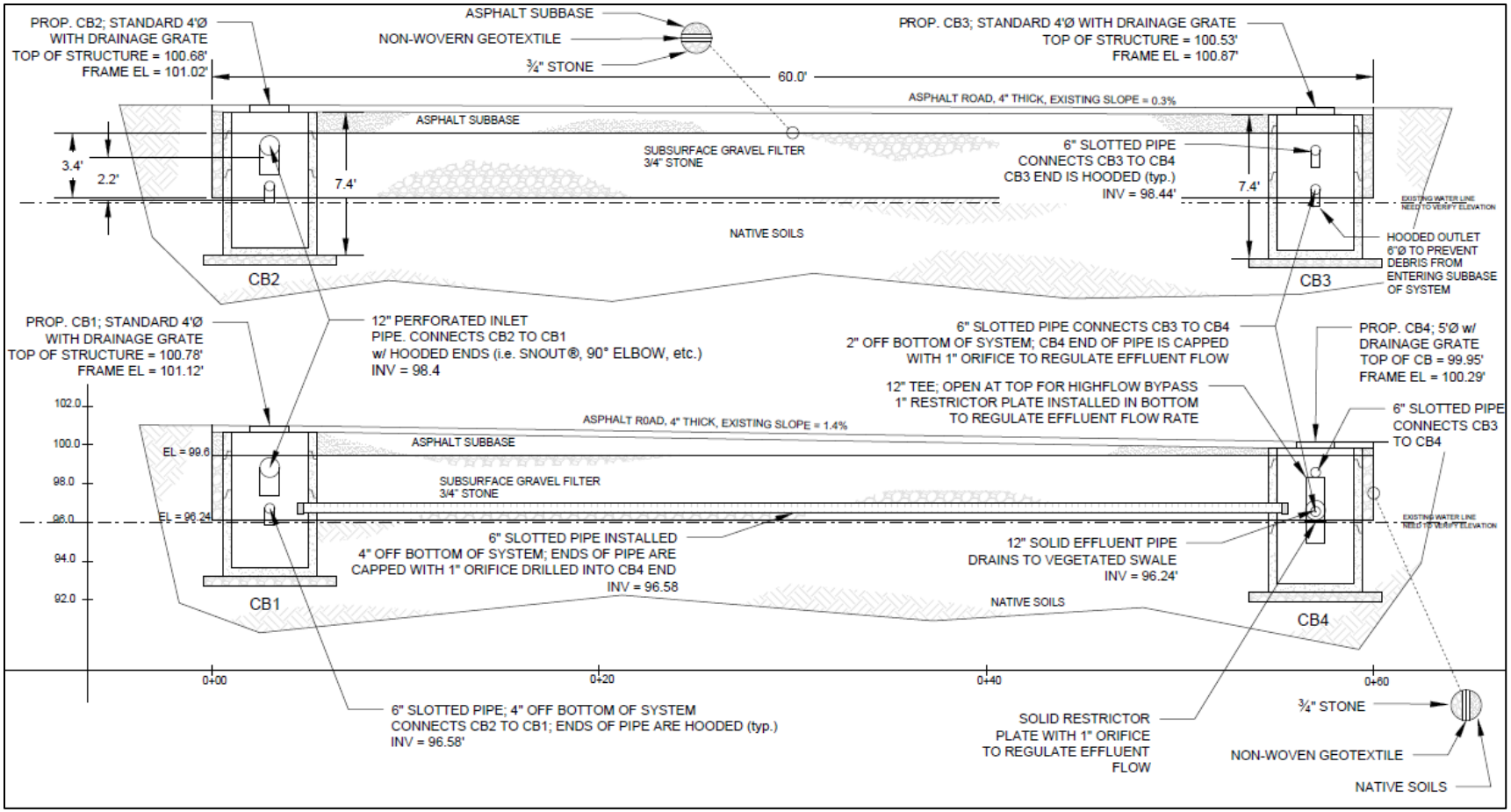

Figure 61: Design diagram showing the profile view of the Grove St SGF

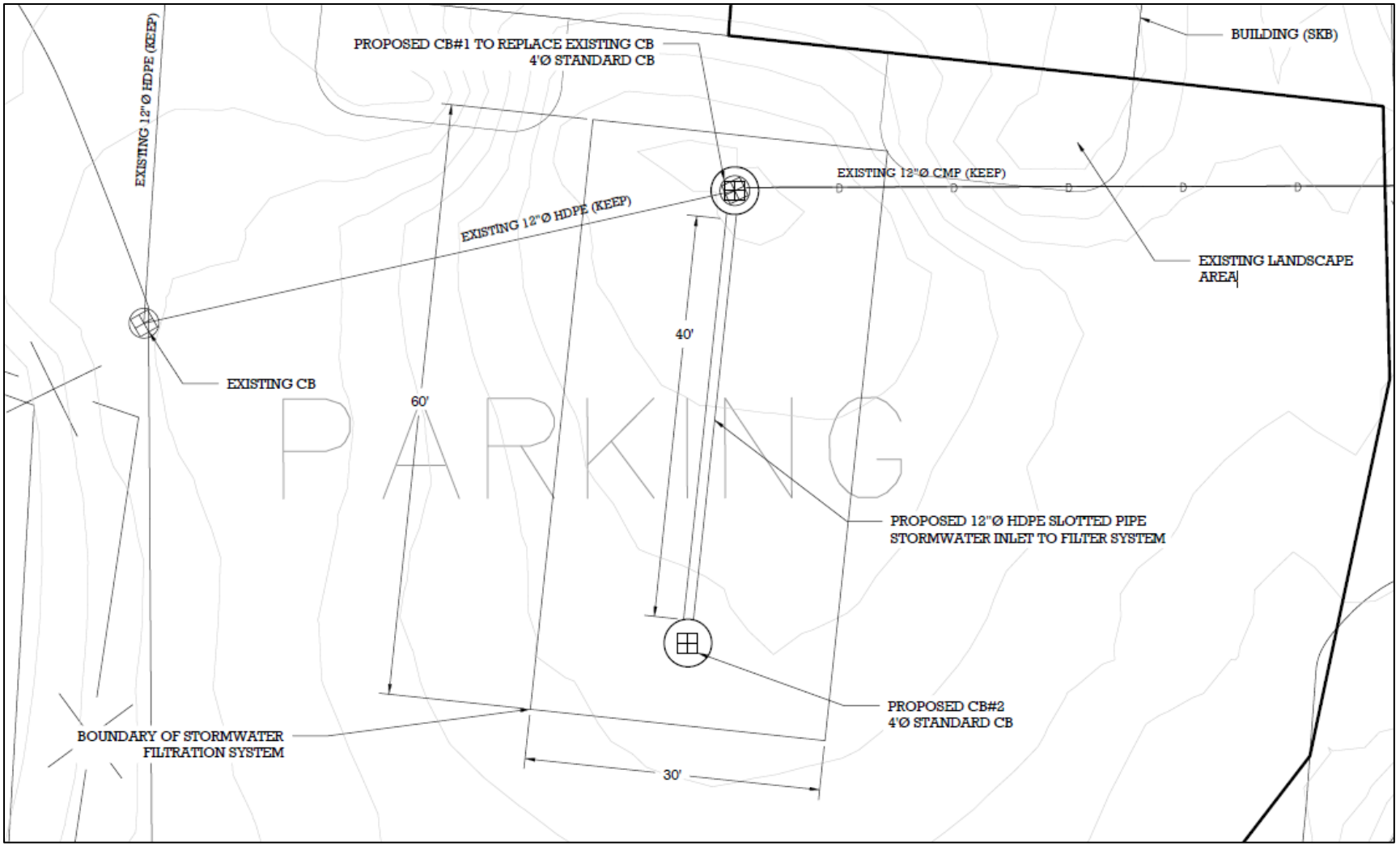

Figure 62: Plan view of Kettlebell SGF

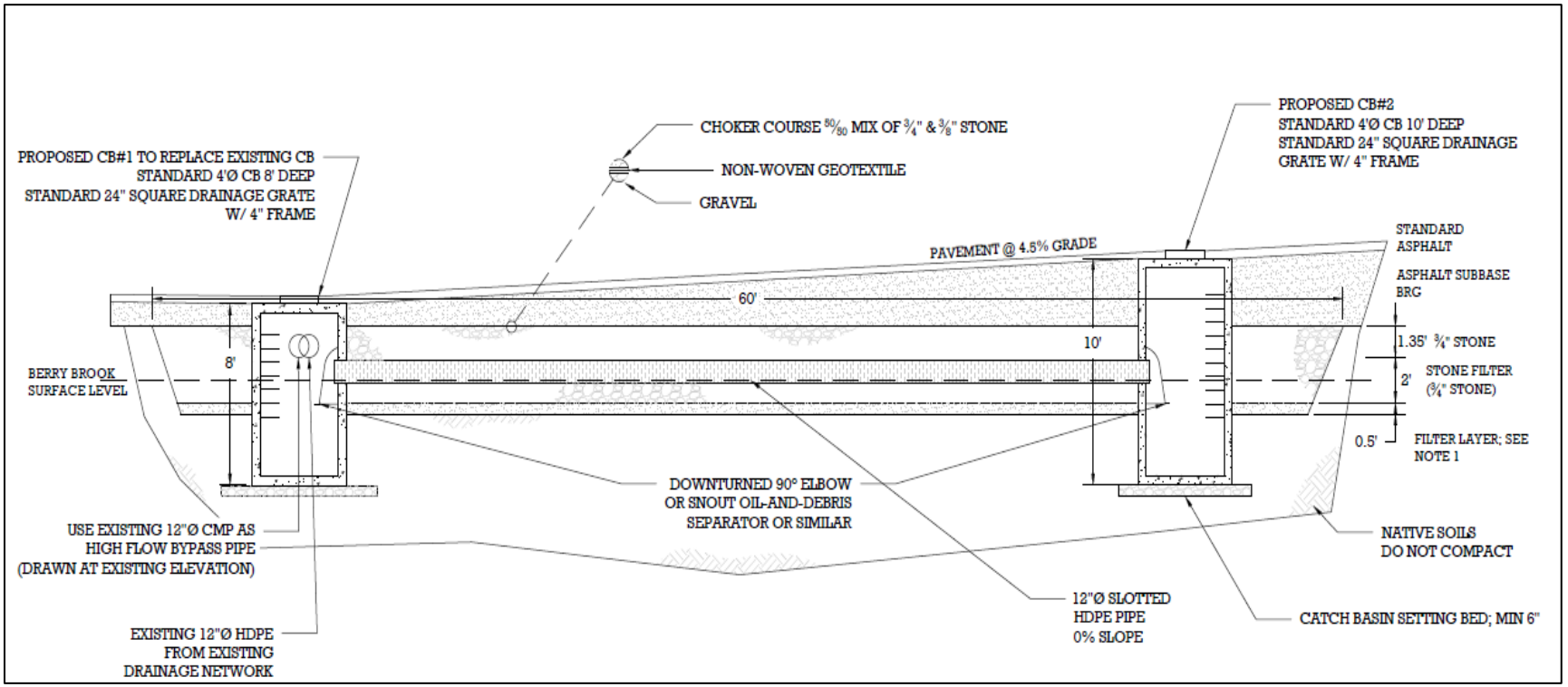

Figure 63: Design diagram showing the profile view of the Kettlebell SGF

Guelph Permeameter Analyses

Laplace analysis (Reynolds and Elrick 1986):

Determine α* based on soil structures (see Table 32) and use corresponding m-constants to calculated C_1:

$$K_{fs}^1 = B_1 Q_1 \quad Q_1 = A\bar{R}_1$$

$$B_1 = \frac{C_1}{2\pi H_1^2 \left[1 + \left(\frac{C_1}{2}\right)\left(\frac{a}{H_1}\right)^2\right]}$$

$$C_1 = \left(\frac{\frac{H_1}{a}}{m_1 + m_2\left(\frac{H_1}{a}\right)}\right)^{m_3}$$

Gardner analysis (Reynolds and Elrick 1986):

$$\phi_m^1 = T_1 Q_1$$

$$T_1 = \frac{C_1}{2\pi H_1}$$

One-ponded head analysis (Elrick et al. 1989):

$$K_{fs} = B_1 Q_1 \quad \phi_m = T_1 Q_1 \quad Q_1 = A\bar{R}_1$$

$$B_1 = \frac{C_1}{2\pi H_1^2 + \pi a^2 C_1 + 2\pi\left(\frac{H_1}{a^*}\right)}$$

$$T_1 = \frac{C_1}{(2\pi H_1^2 + \pi a^2 C_1)a^* + 2\pi H_1}$$

Richards analysis (Reynolds and Elrick 1986):

$$Q_1 = A\bar{R}_1 \qquad Q_2 = A\bar{R}_2$$

$$K_{fs} = G_2 Q_2 - G_1 Q_1 \qquad \phi_m = J_1 Q_1 - J_2 Q_2$$

$$\alpha^* = \frac{K_{fs}}{\phi_m}$$

$$G_1 = \frac{H_2 C_1}{\pi\left(2H_1H_2(H_2 - H_1) + a(H_1C_2 - H_2C_1)\right)}$$

$$G_2 = \frac{H_1 C_2}{\pi\left(2H_1H_2(H_2 - H_1) + a(H_1C_2 - H_2C_1)\right)}$$

$$J_1 = \frac{(2H_2^2 + a^2C_2)C_1}{2\pi\left(2H_1H_2(H_2 - H_1) + a(H_1C_2 - H_2C_1)\right)}$$

$$J_2 = \frac{(2H_1^2 + a^2C_1)C_2}{2\pi\left(2H_1H_2(H_2 - H_1) + a(H_1C_2 - H_2C_1)\right)}$$

$$C_1 = \left(\frac{\frac{H_1}{a}}{m_1 + m_2\left(\frac{H_1}{a}\right)}\right)^{m_3}$$

$$C_2 = \left(\frac{\frac{H_2}{a}}{m_1 + m_2\left(\frac{H_2}{a}\right)}\right)^{m_3}$$

Least squares analysis (Reynolds and Elrick 1986):

$$K_{fs} = \frac{\left(\sum_{i=1}^{n} H_i^2 \sum_{i=1}^{n} C_i Q_i \left(\frac{C_i a_i^2}{2} + H_i^2\right) - \sum_{i=1}^{n} H_i C_i Q_i \sum_{i=1}^{n} H_i \left(\frac{C_i a_i^2}{2} + H_i^2\right)\right)}{\left(2\pi\left\{\sum_{i=1}^{n} H_i^2 \sum_{i=1}^{n} \left(\frac{C_i a_i^2}{2} + H_i^2\right)^2 - \left[\sum_{i=1}^{n} H_i \left(\frac{C_i a_i^2}{2} + H_i^2\right)\right]^2\right\}\right)}$$

$$\phi_m = \frac{\left(\sum_{i=1}^{n} C_i Q_i \left(\frac{C_i a_i^2}{2} + H_i^2\right) \sum_{i=1}^{n} H_i \left(\frac{C_i a_i^2}{2} + H_i^2\right) - \sum_{i=1}^{n} H_i C_i Q_i \sum_{i=1}^{n} \left(\frac{C_i a_i^2}{2} + H_i^2\right)^2\right)}{\left(2\pi\left\{\left[\sum_{i=1}^{n} H_i \left(\frac{C_i a_i^2}{2} + H_i^2\right)\right]^2 - \sum_{i=1}^{n} H_i^2 \sum_{i=1}^{n} \left(\frac{C_i a_i^2}{2} + H_i^2\right)^2\right\}\right)}$$

$$C_i = \left(\frac{\frac{H_i}{a}}{m_1 + m_2\left(\frac{H_i}{a}\right)}\right)^{m_3}$$

$$\alpha^* = \frac{K_{fs}}{\phi_m}$$

Where:
K_{fs}^{1} = field saturated hydraulic conductivity for Laplace analysis (L/T)
K_{fs} = field saturated hydraulic conductivity (L/T)
Φ_m = matric flux potential (L^2/T)
$\overline{R_1}$ = single measurement of average steady exfiltration rate (L/T)
$\overline{R_2}$ = second measurement of average steady exfiltration rate (L/T)
$\overline{R_i}$ = i^{th} measurement of average steady exfiltration rate (L/T)
Q_1 = single measurement of exfiltration flow rate (L^3/T)
Q_2 = second measurement of exfiltration flow rate (L^3/T)
Q_i = i^{th} measurement of exfiltration flow rate (L^3/T)
A = cross-sectional area between reservoir tube and air-inlet tube in Guelph permeameter (L^2) = 2.13cm^2 if only the inner reservoir was used or 35.19cm^2 if both reservoirs were used
C_1 = proportionality constant for a single infiltration rate measurement
C_2 = proportionality constant for second infiltration rate measurement
C_i = proportionality constant for i^{th} infiltration rate measurement
H_1 = water head height for a single infiltration rate measurement (L)
H_2 = water head height for second infiltration rate measurement (L)
H_i = water head height for i^{th} infiltration rate measurement (L)
a = radius of borehole
α^* = ratio field saturated hydraulic conductivity to matric flux potential (L^{-1})

Values for m_1, m_2, and m_3 depend on soil texture and structure according to the Table 32 below (Elrick et al. 1989):

Table 32: α and m-values for specific soil structure categories*

Soil texture/structure category	**α* (cm^{-1})**	**m-values in proportionality constant equation**
Compacted, structure-less, clayey or silty materials such as landfill caps and liners, lacustrine or marine sediments, etc.	0.01	m_1 = 2.081 m_2 = 0.121 m_3 = 0.672
Soil which are both fine textured (clayey or silty) and unstructured; may also include some fine sands	0.04	m_1 = 1.992 m_2 = 0.091 m_3 = 0.683
Most structured soils from clays through loams; also includes unstructured medium and fine sands. The category most frequently applicable for agricultural soils	0.12	m_1 = 2.074 m_2 = 0.093 m_3 = 0.754
Coarse and gravely sands; may also include some highly structured soils with large and/or numerous cracks, macropores, etc.	0.36	m_1 = 2.074 m_2 = 0.093 m_3 = 0.754

Example calculations:

	Time		Δ Time	WSL	Δ WSL	Rate
	Min	**Sec**	**Min**	**cm**	**cm**	**cm/min**
Head #1	0	0		12.4		
	1	60	1	12.8	0.4	0.40
	2	120	1	13.5	0.7	0.70
	3	180	1	14.4	0.9	0.90
	4	240	1	15.2	0.8	0.80
	5	300	1	15.9	0.7	0.70
	6	360	1	16.6	0.7	0.70
	7	420	1	17.2	0.6	0.60
	8	480	1	17.9	0.7	0.70
	9	540	1	18.6	0.7	0.70
	10	600	1	19.3	0.7	0.70
	11	660	1	20	0.7	0.70

	Time		Δ Time	WSL	Δ WSL	Rate
	Min	**Sec**	**Min**	**cm**	**cm**	**cm/min**
Head #2	0	0		23.8		
	1.5	90	1.5	24.9	1.1	0.73
	3	180	1.5	26.5	1.6	1.07
	4.5	270	1.5	28.2	1.7	1.13
	6	360	1.5	29.8	1.6	1.07
	7.75	465	1.75	31.5	1.7	0.97
	9.25	555	1.5	33	1.5	1.00
	10.75	645	1.5	34.7	1.7	1.13
	12.25	735	1.5	36	1.3	0.87

	Time		Δ Time	WSL	Δ WSL	Rate
	Min	**Sec**	**Min**	**cm**	**cm**	**cm/min**
Head #3	0	0		4.8		
	1	60	1	6	1.2	1.20
	2	120	1	7.1	1.1	1.10
	3	180	1	8.1	1	1.00
	4.25	255	1.25	9.4	1.3	1.04
	5.25	315	1	10.4	1	1.00
	6.25	375	1	11.4	1	1.00
	7.25	435	1	12.4	1	1.00
	8.25	495	1	13.4	1	1.00

	Time		Δ Time	WSL	Δ WSL	Rate
	Min	**Sec**	**Min**	**cm**	**cm**	**cm/min**
Head #4	0	0		17		
	1	60	1	17.8	0.8	0.80
	2.5	150	1.5	19.7	1.9	1.27
	3.5	210	1	21	1.3	1.30
	4.5	270	1	22.3	1.3	1.30
	5.5	330	1	23.5	1.2	1.20
	6.5	390	1	24.7	1.2	1.20
	7.5	450	1	25.9	1.2	1.20
	8.5	510	1	27	1.1	1.10
	9.5	570	1	28.2	1.2	1.20

Note: An α* of 0.04 was selected due to the structural characteristics of the soil being evaluated.

H_1 (cm)	5	**H_2 (cm)**	8
Reservoir	Combined	**Reservoir**	Combined
Hole depth (ft)	4.2	**Hole depth (ft)**	4.2
Hole diameter (cm)	8	**Hole diameter (cm)**	8
Elevation (ft)	96.17	**Elevation (ft)**	96.17
R1 (cm/min)	0.70	**R2 (cm/min)**	1.00
a (cm)	4	**a (cm)**	4
a* (cm^{-1})	0.04	**a* (cm^{-1})**	0.04
a/H	0.80	**a/H**	0.50

H_3 (cm)	10	**H_4 (cm)**	13
Reservoir	Combined	**Reservoir**	Combined
Hole depth (ft)	4.2	**Hole depth (ft)**	4.2
Hole diameter (cm)	8	**Hole diameter (cm)**	8
Elevation (ft)	96.17	**Elevation (ft)**	96.17
R3 (cm/min)	1.00	**R4 (cm/min)**	1.20
a (cm)	4	**a (cm)**	4
a* (cm^{-1})	0.04	**a* (cm^{-1})**	0.04
a/H	0.40	**a/H**	0.31

Single Head Method						
H #	**C_1**	**B_1 (cm^{-2})**	**Q_1 (cm/s)**	**T_1 (cm^{-1})**	**K_{fs} (cm/s)**	**Φ_m (cm^2/s)**
H1	0.700	0.000716	0.411	0.0179	**2.94×10^{-4}**	**7.35×10^{-3}**
H2	0.945	0.000554	0.587	0.0138	**3.25×10^{-4}**	**8.12×10^{-3}**
H3	1.085	0.000481	0.587	0.0120	**2.82×10^{-4}**	**7.06×10^{-3}**
H4	1.271	0.000401	0.704	0.0100	**2.82×10^{-4}**	**7.06×10^{-3}**

Laplace and Gardner Methods						
H #	**C_1**	**B_1 (cm^{-2})**	**Q_1 (cm/s)**	**T_1 (cm^{-1})**	**K_{fs}^1 (cm/s)**	**Φ_m^1 (cm^2/s)**
H1	0.700	0.00364	0.411	0.0223	**1.50×10^{-3}**	**9.15×10^{-3}**
H2	0.945	0.00210	0.587	0.0188	**1.23×10^{-3}**	**1.10×10^{-2}**
H3	1.085	0.00159	0.587	0.0173	**9.32×10^{-4}**	**1.01×10^{-2}**
H4	1.271	0.00113	0.704	0.0156	**7.95×10^{-4}**	**1.10×10^{-2}**

Richards Method									
Calculation #	**H (cm)**	**C**	**a (cm)**	**G (cm^{-2})**	**J (cm^{-1})**	**Q (cm^3/sec)**	**K_{fs} (cm/s)**	**Φ_m (cm^2/s)**	**α* (cm^{-1})**
1	5	0.700	4	0.0073	0.0706	0.41	**6.62×10^{-4}**	**5.10×10^{-3}**	**0.130**
	8	0.945	4	0.0063	0.0407	0.59			
2	5	0.700	4	0.0043	0.0510	0.41	**2.05×10^{-4}**	**7.90×10^{-3}**	**0.026**
	10	1.085	4	0.0035	0.0223	0.59			
3	5	0.700	4	0.0027	0.0401	0.41	**2.35×10^{-4}**	**7.71×10^{-3}**	**0.030**
	13	1.271	4	0.0020	0.0124	0.70			
4	8	0.945	4	0.0094	0.106	0.59	**-4.66×10^{-4}**	**1.52×10^{-2}**	**-0.031**
	10	1.085	4	0.0087	0.0803	0.59			
5	8	0.945	4	0.0037	0.0535	0.59	**-1.46×10^{-5}**	**1.12×10^{-2}**	**-0.001**
	13	1.271	4	0.0032	0.0288	0.70			
6	10	1.085	4	0.0058	0.0816	0.59	**2.84×10^{-4}**	**7.04×10^{-3}**	**0.040**
	13	1.271	4	0.0053	0.0580	0.70			

Note: The values in red above indicate those which are invalid due to their negative sign.

Least Squares Method							
	H^2	$CQ(C a^2/2 + H^2)$	HCQ	$H(C a^2/2 + H^2)$	H^2	$(C a^2/2 + H^2)^2$	$H(C a^2/2 + H^2)$
	25	8.80	1.44	153.01	25	936.52	153.01
	64	39.64	4.43	572.46	64	5120.39	572.46
	100	69.14	6.36	1086.77	100	11810.78	1086.77
	169	160.27	11.63	2329.18	169	32101.13	2329.18
Sum:	**358**	**277.85**	**23.86**	**4135.28**	**358**	**49968.83**	**4141.43**

K_{fs} (cm/sec) = 1.41×10^{-4}
Φ_m (cm^2/s) = 8.97×10^{-3}
α^* (cm^{-1}) = 0.016

Particle Size Distribution Analyses

Sedimentation test measurements:

	Specific Gravity Measurements								
	t_m (min)	1	2	5	15	30	60	240	1440
Soil Sample	GSt #3	1.013	1.013	1.012	1.0107	1.01	1.0085	1.0075	1.006
	GSt #4	1.0235	1.023	1.02	1.0198	1.018	1.0165	1.0135	1.011
	GSt #2	1.019	1.0175	1.016	1.0143	1.013	1.0115	1.0092	1.0073
	KB #2	1.028	1.0275	1.0265	1.025	1.0235	1.0215	1.019	1.015
	GSt #5	1.0185	1.018	1.0165	1.0145	1.0135	1.012	1.0095	1.0075
	GSt #1	1.035	1.032	1.03	1.0255	1.0235	1.0215	1.0175	1.0142
	KB #1	1.028	1.0265	1.0245	1.0215	1.0195	1.018	1.0145	1.0113

Sample	D_c (cm)	A_c (cm^2)	M_d (g)
GSt #1	6.2	30.19	58.8
GSt #2	6.5	33.18	59.2
GSt #5	6.15	29.71	49.6
KB #2	6	28.27	49.35
GSt #4	6.6	34.21	49.9
GSt #3	6.25	30.68	56.2
KB #1	6.1	29.22	53.5

Where:
t_m = time elapse (min)
D_c = diameter of the graduated cylinder (cm)
A_c = cross-sectional area of the graduated cylinder (cm^2)
M_d = total dry mass of the soil sample (g)

Sedimentation test example calculations for soil sample GSt #3:

- Notes:
  - Calculations were performed in a spreadsheet and in the same manner for all of the soil samples.
  - A control solution was measured throughout the tests. The solution contained 5g of sodium hexametaphosphate dissolved in distilled water.
  - Specific gravity of the soil samples was measured by measuring the density of soil and dividing this value by the density of water (see calculation below). The soil density was calculated by dividing the mass of a small sample of soil (Msoil) by the volume it displaced in a graduated cylinder of water

$$G_s = \frac{\rho_s}{\rho_w} = \frac{\left(\frac{M_{soil}}{V_{displaced}}\right)}{\rho_w}$$

$$G_s\ of\ first\ soil\ sample = \frac{\left(\frac{9.9g}{4cm^3}\right)}{0.998} = 2.47$$

$$G_s\ of\ second\ soil\ sample = \frac{\left(\frac{7.4g}{2.6cm^3}\right)}{0.998} = 2.85$$

$$\overline{G_s} = average\ soil\ specific\ gravity = 2.66$$

$$N_m = \left(\frac{G_s}{G_s - 1}\right)\left(\frac{V_{sp}}{M_d}\right)\rho_c(r_m - r_{d,m}) \times 100$$

$$H_m = H_{r2} + \left(\left(\frac{H_{r1} - H_{r2}}{r_2 - r_1}\right) \times (r_2 - r_m - C_m)\right) - \left(\frac{V_{hb}}{2A_c}\right)$$

$$D_m = \left(\sqrt{\frac{10\mu H_m}{\rho_w g t_m (G_s - 1)}}\right) \times 10$$

Where:
m = reading #
N_m = mass % finer at reading m
G_s = specific gravity of the soil sample
V_{sp} = volume of suspension (cm^3)
M_d = dry soil mass of sample (g)
ρ_c = density of water at the temperature of the manufacturer calibration (20°C) (g/cm^3)
ρ_w = density of water at 20°C (g/cm^3)
ρ_s = density of soil (g/cm^3)
r_m = hydrometer reading (i.e. specific gravity) of soil-dispersant suspension at reading m
$r_{d,m}$ = hydrometer reading (i.e. specific gravity) of control solutions at reading m
M_{soil} = mass of soil sample used for specific gravity calculation (g)
$V_{displaced}$ = volume of water displaced by soil sample for specific gravity calculation (cm^3)
H_{r2} = distance between the center of buoyancy and the minimum hydrometer reading (cm)
H_{r1} = distance between the center of buoyancy and the maximum hydrometer reading (cm)
r_2 = minimum hydrometer reading = 1.000
r_1 = maximum hydrometer reading = 1.050
C_m = meniscus correction = 0.001
V_{hb} = volume of hydrometer bulb = $70cm^3$
A_c = cross-sectional area of graduated cylinder (cm^3)
H_m = distance particles fall at reading m
μ = viscosity of water at 20°C (g/cm*s)
t_m = time elapsed for reading m (s)
D_m = soil particle diameter (mm)

m	t_m (min)	r_m	$r_{d,m}$	G_s	V_{sp} (cm^3)	ρ_c (g/cm^3)	M_d (g)	N_m (% finer)	A_c (cm^2)
1	1	1.035	1.000	2.66	1000	0.998	56.2	**100%**	30.68
2	2	1.032	1.000	2.66	1000	0.998	56.2	**91%**	30.68
3	5	1.03	1.000	2.66	1000	0.998	56.2	**85%**	30.68
4	15	1.0255	1.000	2.66	1000	0.998	56.2	**73%**	30.68
5	30	1.0235	1.000	2.66	1000	0.998	56.2	**67%**	30.68
6	60	1.0215	1.000	2.66	1000	0.998	56.2	**61%**	30.68
7	240	1.0175	1.000	2.66	1000	0.998	56.2	**50%**	30.68
8	1440	1.0142	1.000	2.66	1000	0.998	56.2	**40%**	30.68

m	H_{r1} (cm)	H_{r2} (cm)	V_{hb} (cm^3)	H_m (cm)	μ (g/cm*s)	ρ_w (g/cm^3)	g (cm/s^2)	D_m (mm)
1	7.5	19.2	70	10.10	0.01	0.998	980.7	**0.0432**
2	7.5	19.2	70	10.81	0.01	0.998	980.7	**0.0316**
3	7.5	19.2	70	11.27	0.01	0.998	980.7	**0.0204**
4	7.5	19.2	70	12.33	0.01	0.998	980.7	**0.0123**
5	7.5	19.2	70	12.79	0.01	0.998	980.7	**0.0089**
6	7.5	19.2	70	13.26	0.01	0.998	980.7	**0.0064**
7	7.5	19.2	70	14.20	0.01	0.998	980.7	**0.0033**
8	7.5	19.2	70	14.97	0.01	0.998	980.7	**0.0014**

Sieve Test Results for GSt. Sample #3						
Sieve #	**Sieve size (mm)**	**Sieve mass (g)**	**Sieve + soil mass (g)**	**Soil mass (g)**	**Cum. Mass (g)**	**% Finer**
Pan		487.6	487.9	0.3	51.25	
200	0.075	507.4	508.9	1.5	52.75	91.2%
100	0.15	522.4	522.7	0.3	53.05	93.9%
80	0.18	350.6	351.4	0.8	53.85	94.4%
60	0.25	540.2	540.6	0.4	54.25	95.8%
50	0.3	550.8	551.5	0.7	54.95	96.5%
40	0.425	356.6	357.2	0.6	55.55	97.8%
25	0.701	441.2	441.4	0.2	55.75	98.8%
20	0.833	442.8	443.05	0.25	56	99.2%
10	2	472.9	473.1	0.2	56.2	99.6%
			Total:	5.25		

The sieve results and sedimentation results were combined to develop the full PSDs for each soil sample (see Table 33). Figure 40 and Figure 41, in the Section 4.3, present graphs of the PSD results.

Table 33: PSD results for Grove St soil samples

Grove St. Soil Sample PSD Results									
Sample #1		**Sample #2**		**Sample #3**		**Sample #4**		**Sample #5**	
D (mm)	**% Finer**	**D (mm)**	**% Finer**	**D (mm)**	**% Finer**	**D (mm)**	**% Finer**	**D (mm)**	**% Finer**
0.001	16.2%	0.001	29.9%	0.001	40.4%	0.001	24.3%	0.001	23.3%
0.004	20.3%	0.003	36.7%	0.003	49.8%	0.004	30.8%	0.004	29.3%
0.007	23.0%	0.007	44.8%	0.006	61.2%	0.007	38.9%	0.007	36.7%
0.010	27.1%	0.009	48.9%	0.009	66.9%	0.010	43.7%	0.010	41.4%
0.014	29.0%	0.013	53.8%	0.012	72.6%	0.014	47.0%	0.014	45.6%
0.024	32.5%	0.023	54.3%	0.020	85.4%	0.023	53.4%	0.023	51.0%
0.038	35.2%	0.035	62.5%	0.032	91.1%	0.036	58.3%	0.036	55.8%
0.053	35.2%	0.049	63.9%	0.075	91.2%	0.051	59.9%	0.051	61.2%
0.075	41.2%	0.075	70.7%	0.150	93.9%	0.075	64.4%	0.075	79.9%
0.150	51.4%	0.150	74.1%	0.180	94.4%	0.150	68.9%	0.150	80.7%
0.180	54.7%	0.180	75.3%	0.250	95.8%	0.180	70.1%	0.250	83.3%
0.250	62.3%	0.250	77.6%	0.300	96.5%	0.250	72.9%	0.425	87.8%
0.300	66.7%	0.300	79.0%	0.425	97.8%	0.300	74.9%	0.833	93.0%
0.425	75.0%	0.425	82.5%	0.701	98.8%	0.425	79.4%	2.000	96.4%
0.701	84.1%	0.701	87.3%	0.833	99.2%	0.701	86.5%		
0.833	86.0%	0.833	88.5%	2.000	99.6%	0.833	88.1%		
2.000	92.7%	2.000	94.1%			2.000	94.3%		

Table 34: PSD results for Kettlebel soil samples

Kettlebell Soil Sample PSD Results			
Sample #1		**Sample #2**	
D (mm)	**% Finer**	**D (mm)**	**% Finer**
0.001	34.1%	0.001	48.4%
0.003	43.7%	0.003	61.3%
0.007	54.3%	0.006	69.4%
0.009	58.8%	0.009	75.8%
0.013	64.9%	0.012	80.6%
0.022	73.9%	0.021	85.5%
0.033	79.9%	0.033	88.7%
0.047	84.5%	0.047	90.3%
0.075	98.7%	0.075	93.4%
0.150	99.4%	0.150	97.2%
0.250	99.4%	0.180	98.0%
0.425	99.6%	0.250	98.6%
0.833	99.8%	0.300	99.0%
2.000	99.8%	0.425	99.6%
		0.701	99.8%
		0.833	99.8%
		2.000	100.0%

Figure 64: USDA textural classification chart

AquaTROLL Rating Curve

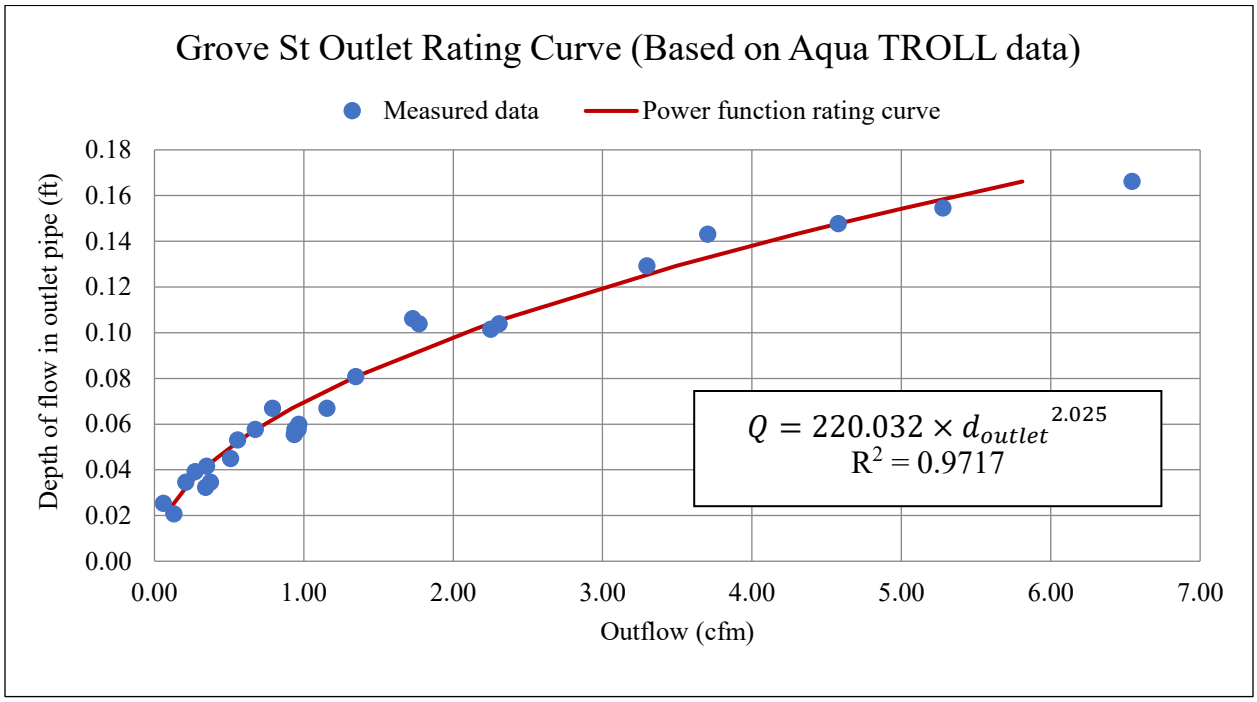

Figure 65: Outflow rating curve for the Grove St system, based on Aqua TROLL sensor measurements

Model Input Parameters

Table 35: Parameters for saturated/unsaturated infiltration model

	Grove St			
Parameters	**Regression**	**Brakensiek et al. 1981**	**Rawls et al. 1992**	**Guelph**
Δt (min)	0.5	0.5	0.5	0.5
Δz (cm)	2.0	2.0	2.0	2.0
Soil depth (cm)	200	200	200	200
K_s or K_{fs} (cm/hr)	0.12	0.099	0.23	0.51
θ_s (cm^3/cm^3)	0.47	0.48	0.46	0.47*
θ_r (cm^3/cm^3)	0.11	0.19	0.08	0.1*
θ_i (cm^3/cm^3)	0.32	0.32	0.32	0.32
ψ_b (cm)	42.99	42.28	25.89	55.37***
ψ_f (cm)	30.21	32.63	18.37	38.5**
λ (-)	0.23	0.28	0.19	0.28*

Footnotes:
*Parameter is based on median value from Table 11 for clay-loams
**Parameter is estimated by raising the measure α-value to the power of -1 as described by Elrick et al. 1989
***Parameter is based on ψ_f according to equation from Rawls et al. 1983

Table 36: Parameters for modified Green-Ampt infiltration model

Parameter	**Grove St**				**Kettlebell**		
	Regression	**Rawls et al. 1983**	**McCuen et al. 1981**	**Guelph**	**Regression**	**Rawls et al. 1983**	**McCuen et al. 1981**
Δt (min)	0.5	0.5	0.5	0.5	0.5	0.5	0.5
K_s or K_{fs} (cm/hr)	0.13	0.2	0.28	0.51	0.005	0.06	0.042
θ_s (cm^3/cm^3)	0.47	0.46	0.48	0.47*	0.48	0.48	0.48
θ_i (cm^3/cm^3)	0.32	0.32	0.32	0.32	0.40	0.40	0.40
ψ_f (cm)	29.55	20.88	21.41	38.5**	90.39	31.63	27.11
A (cm^3)	1393546	1393546	1393546	1393546	1672255	1672255	1672255

Footnotes:
*Parameter is based on median value from Table 11 for clay-loams
**Parameter is estimated by raising the measure α-value to the power of -1 as described by Elrick et al. 1989

Statistical Comparison of Soil Input Parameters for Infiltration Models

Table 37: SSE, MSE, and RMSE between the results of the Saturated/Unsaturated Model and the measured data

Soil Parameters	Saturated/Unsaturated Model								
	Peak Water Depths (cm)			Total Infiltration Volume (cf)			Time to Peak (hr)		
	SSE	MSE	RMSE	SSE	MSE	RMSE	SSE	MSE	RMSE
Regression	12448	957.5	30.9	93753900	7211838	2685	93809	7216	85
Brakensiek et al 1981	12526	963.6	31.0	95757985	7365999	2714	94068	7236	85
Rawls et al 1992	12361	950.9	30.8	86127864	6625220	2574	89523	6886	83
Guelph	12231	940.8	30.7	61637689	4741361	2177	130184	10014	100

Table 38: SSE, MSE, and RMSE between the results of the Green-Ampt Model and the measured data

Soil Parameters	Green-Ampt Model								
	Maximum Water Depths (cm)			Total Infiltration Volume (ft^3)			Time to Peak (hr)		
	SSE	MSE	RMSE	SSE	MSE	RMSE	SSE	MSE	RMSE
Regression	12289	945.3	30.7	76794311	5907255	2430	99770	7675	88
Rawls et al 1983	12256	942.8	30.7	69173049	5321004	2307	108035	8310	91
McCuen et al 1981	12195	938.1	30.6	58593837	4507218	2123	134316	10332	102
Guelph	11434	879.5	29.7	37594272	2891867	1701	338514	26040	161

Monitoring Data

Table 39, Table 40, Table 41, and Table 42 present various values from the monitoring data for the Grove St SGF. The flows and flow volumes present in the tables are designated as either 'total' or 'system' flows/volumes. This designation references the fact that not all of the runoff collected by the SGF's catch basins was able to enter the gravel filter. The outlet pipe in the fourth catch basin (CB #4) was position at such an elevation that all of the runoff collected by CB #4 flowed directly to the outlet swale. When performing calculation of hydrologic performance, only the runoff which was collected in the other three catch basins (CB #1-3) was included. Therefore, inflows and outflows which did not include the runoff collected by CB #4 are referred to below as 'system' flows, while 'total' flows refer to all of the runoff which was collected by the system's catch basins. A list of table variables is provided below.

Table variables:
$V_{tot,in}$ = total inflow volume (ft^3)
$V_{tot,out}$ = total outflow volume (ft^3)
$V_{sys,in}$ = system inflow volume (ft^3)
$V_{sys,out}$ = system outflow volume (ft^3)
V_{inf} = infiltration volume (ft^3)

Table 39: Grove St flow data for which system water depths were also measured

Date	Precipitation Depth (in)	Max. System Depth (ft)	$V_{tot,in}$ (ft^3)	$V_{tot,out}$ (ft^3)	$V_{sys,in}$ (ft^3)	$V_{sys,out}$ (ft^3)	V_{inf} (ft^3)
11/24/2016	0.252	0.009	3.84*	0*	3.84	0	3.84
11/26/2016	0.06	0.015	1.23*	0*	1.23	0	1.23
11/29/2016	0.728	0.081	148	75	73.22	0	73.2
11/30/2016	1.14	1.150	5,053	2,686	3,099	749	2,350
12/6/2016	0.236	0.029	6.58	5.81	0.78	0	0.78
12/29/2016	1.44	0.440	1,160	340	974	249	725
1/3/2017	0.66**	0.784	5,943	1,864	4,520	501	4,019
1/10/2017	0.128**	0.263	2,681	264	2,471	67	2,404
1/19/2017	0.52**	0.020	14.3	12.1	2.25	0	2.25
1/24/2017	0.652**	0.022	33.8	4.12	30	0	30

4/4/2017	0.824	0.727	6,480	1,505	5,334	359	4,975
4/6/2017	1.22	1.944	12,274	6,032	7,874	1,658	6,216
4/12/2017	0.184	0.012	54	23	31	0	31
4/15/2017	0.056	0.029	18	13	5.59	0	5.59
4/19/2017	0.064	0.033	55	9	12	0	12
4/21/2017	0.756	0.017	398	289	108	0	108
4/25/2017	1.24	0.618	5,436	2,863	2,011	125	1,886
5/1/2001	0.748	0.310	2,175	1,513	1,513	49	1,464
5/5/2017	0.98	0.579	3,582	1,597	2,173	188	1,985
5/13/2017	1.756	0.928	7,676	3,537	4,681	542	4,139
6/30/2017	0.811	0.210	530	287	257	19	238
7/7/2017	0.124	0.021	2.16	1.2	0.96	0	0.96
7/8/2017	0.891	0.430	1,040	631	552	143	409
7/11/2017	0.136	0.022	5.12	3.55	1.57	0	1.57
7/13/2017	0.68	0.156	513	295	240	22	218
7/20/2017	0.674	0.579	1,076	722	698	335	350
7/24/2017	0.724	0.087	256	144	111	0	111
		Totals:	56,615	24,716	36,779	5,005	31,773

* Total inflow and outflows do not include flow into/out of CB #4 because WSE in the catch basin did not rise above the invert of the outlet pipe

**Rainfall depth is not reflective of actual runoff flows because snowmelt also occurred

Table 40: Rainfall Data for Monitoring Sites in Dover, NH

Event #	Start of Rainfall Event	Total Depth (in.)	Antecedent Dry Period (days)	Length of Event (days)	SCS-Based Runoff Volume (ft^3)
1	7/23/2016 17:46	0.954	3.2	0.3	1701
2	7/25/2016 19:16	1.212	2.0	0.7	3361
3	7/28/2016 18:01	0.024	2.5	0.3	0
4	7/29/2016 8:01	0.052	0.6	0.3	0
5	7/31/2016 3:31	0.309	1.8	0.7	0
6	8/1/2016 0:46	0.017	0.4	0.3	0
7	8/1/2016 13:01	0.060	0.4	0.4	0
8	8/12/2016 18:35	0.052	11.1	0.3	0
9	8/13/2016 20:16	0.416	1.0	0.5	0.3
10	8/18/2016 19:15	0.012	4.7	0.3	0
11	8/22/2016 0:05	0.852	3.2	0.5	1169
12	9/11/2016 10:16	0.325	20.2	0.3	0
13	9/14/2016 16:52	0.056	3.3	0.3	0
14	9/18/2016 9:45	0.020	3.7	0.3	0
15	9/19/2016 3:17	1.310	0.7	0.4	4092

16	9/23/2016 9:28	0.030	4.1	0.3	0
17	9/27/2016 5:14	0.224	3.8	0.4	0
18	10/1/2016 7:11	0.484	3.9	1.2	39
19	10/3/2016 15:14	0.008	1.3	0.3	0
20	10/6/2016 6:26	0.004	2.6	0.2	0
21	10/9/2016 3:34	0.920	2.9	0.9	1515
22	10/13/2016 18:20	0.044	3.9	0.4	0
23	10/18/2016 2:18	0.004	4.2	0.2	0
24	10/18/2016 22:29	0.004	0.8	0.2	0
25	10/19/2016 15:15	0.004	0.7	0.2	0
26	10/21/2016 0:49	0.132	1.4	0.6	0
27	10/21/2016 19:07	2.707	0.4	1.1	18076
28	10/23/2016 3:39	0.020	0.5	0.5	0
29	10/27/2016 14:05	1.876	4.2	1.3	9105
30	10/29/2016 12:02	0.028	0.8	0.4	0
31	10/30/2016 18:29	0.080	1.1	0.6	0
32	11/3/2016 6:12	0.352	3.2	0.7	0
33	11/6/2016 3:24	0.084	2.4	0.4	0
34	11/15/2016 16:30	1.292	9.4	0.8	3954
35	11/20/2016 1:11	0.196	3.8	0.7	0
36	11/21/2016 9:06	0.036	0.9	0.4	0
37	11/24/2016 22:30	0.252	3.4	1.1	0
38	11/26/2016 17:29	0.060	0.9	0.4	0
39	11/29/2016 10:11	0.728	2.5	0.8	637
40	11/30/2016 13:38	1.144	0.6	1.1	2884
41	12/5/2016 12:17	0.008	4.1	0.3	0
42	12/6/2016 10:18	0.236	0.9	0.4	0
43	12/7/2016 11:03	0.052	0.9	0.3	0
44	12/12/2016 9:31	0.408	4.9	0.5	0
45	12/13/2016 10:51	0.056	0.8	0.5	0
46	12/14/2016 11:16	0.052	0.8	0.4	0
47	12/18/2016 8:20	0.972	3.7	0.6	1803
48	12/23/2016 10:23	0.140	4.7	0.4	0
49	12/24/2016 10:43	0.208	0.9	0.5	0
50	12/25/2016 9:34	0.004	0.7	0.2	0
51	12/26/2016 22:03	0.088	1.5	0.7	0
52	12/29/2016 8:34	1.440	2.0	0.9	5132
53	12/31/2016 22:19	0.040	1.9	0.4	0
54	1/3/2017 10:53	0.660	2.4	0.9	406
55	1/7/2017 14:06	0.080	3.5	0.6	0
56	1/8/2017 9:29	0.010	0.4	0.2	0
57	1/10/2017 11:59	0.004	2.1	0.2	0
58	1/11/2017 0:45	0.128	0.5	0.5	0
59	1/12/2017 2:10	0.044	0.8	0.5	0
60	1/12/2017 15:56	0.044	0.3	0.6	0
61	1/13/2017 7:16	0.004	0.3	0.2	0
62	1/17/2017 22:03	0.004	4.6	0.2	0
63	1/19/2017 10:22	0.520	1.5	0.9	84
64	1/20/2017 10:19	0.012	0.4	0.3	0

65	1/24/2017 20:23	0.652	4.4	1.2	382
66	1/26/2017 5:30	0.148	0.5	0.6	0
67	2/1/2017 12:54	0.144	6.0	0.4	0
68	2/8/2017 12:21	0.436	6.9	0.4	5
69	2/13/2017 13:55	0.012	4.9	0.3	0
70	2/14/2017 10:09	0.148	0.8	0.6	0
71	2/15/2017 10:50	0.380	0.7	0.6	0
72	2/16/2017 14:20	0.092	0.8	0.4	0
73	2/17/2017 11:57	0.004	0.8	0.2	0
74	2/18/2017 10:33	0.244	0.9	0.5	0
75	2/24/2017 9:37	0.028	5.7	0.3	0
76	2/25/2017 11:09	0.004	1.0	0.2	0
77	2/25/2017 20:07	0.374	0.4	0.4	0
78	3/1/2017 2:05	0.080	3.1	0.5	0
79	3/2/2017 4:49	0.004	0.8	0.2	0
80	3/7/2017 13:47	0.188	5.4	1.2	0
81	3/13/2017 11:06	0.008	4.9	0.3	0
82	3/15/2017 9:36	0.012	1.9	0.3	0
83	3/16/2017 10:13	0.016	1.0	0.5	0
84	3/17/2017 10:54	0.192	0.8	0.5	0
85	3/18/2017 10:21	0.144	0.7	0.4	0
86	3/24/2017 11:48	0.224	5.9	0.8	0
87	3/25/2017 12:29	0.080	0.4	0.4	0
88	3/26/2017 9:17	0.004	0.7	0.2	0
89	3/27/2017 6:56	0.748	0.9	0.6	714
90	3/29/2017 15:47	0.004	2.0	0.2	0
91	4/1/2017 14:21	1.092	2.9	1.2	2538
92	4/4/2017 5:17	0.824	1.7	1.1	1038
93	4/6/2017 10:40	1.220	1.4	0.9	3419
94	4/7/2017 17:39	0.028	0.6	0.3	0
95	4/8/2017 8:16	0.004	0.6	0.2	0
96	4/12/2017 14:10	0.184	4.2	0.3	0
97	4/15/2017 22:42	0.056	3.3	0.4	0
98	4/19/2017 20:29	0.064	3.7	0.3	0
99	4/21/2017 3:46	0.756	1.2	1.4	746
100	4/25/2017 6:57	1.240	3.0	2.2	3565
101	4/28/2017 9:21	0.004	1.1	0.2	0
102	4/30/2017 17:02	0.044	2.3	0.4	0
103	5/1/2017 18:04	0.748	0.8	1.4	714
104	5/3/2017 16:00	0.032	0.8	0.3	0
105	5/5/2017 9:06	0.980	1.7	1.8	1849
106	5/7/2017 7:26	0.004	0.3	0.2	0
107	5/8/2017 3:36	0.004	0.8	0.2	0
108	5/12/2017 5:48	0.028	4.1	0.3	0
109	5/13/2017 22:31	1.756	1.6	1.7	7948
110	5/18/2017 23:31	0.020	3.6	0.3	0
111	5/22/2017 1:58	0.136	3.1	0.5	0
112	5/22/2017 15:44	0.296	0.3	0.7	0
113	5/25/2017 15:52	1.687	2.6	1.2	7302

114	5/29/2017 13:00	0.024	2.9	0.7	0
115	5/31/2017 1:37	0.024	1.1	0.4	0
116	5/31/2017 21:06	0.336	0.7	0.6	0
117	6/5/2017 3:11	1.356	3.9	2.4	4451
118	6/16/2017 14:56	0.732	9.4	0.8	652
119	6/19/2017 19:26	0.240	2.7	0.4	0
120	6/20/2017 12:50	0.172	0.5	0.3	0
121	6/24/2017 4:25	0.008	3.6	0.4	0
122	6/25/2017 21:53	0.004	1.6	0.2	0
123	6/27/2017 20:21	0.064	1.9	0.7	0
124	6/28/2017 16:20	0.020	0.4	0.3	0
125	6/29/2017 14:44	0.004	0.9	0.2	0
126	6/30/2017 11:33	0.004	0.9	0.2	0
127	6/30/2017 18:58	0.811	0.3	0.6	979
128	7/2/2017 1:41	0.008	1.0	0.3	0
129	7/7/2017 10:02	0.124	5.3	0.6	0
130	7/8/2017 13:41	0.891	0.8	0.6	1363
131	7/11/2017 3:06	0.136	2.2	0.5	0
132	7/13/2017 7:40	0.680	1.9	0.5	469
133	7/20/2017 16:00	0.674	7.1	0.3	450
134	7/24/2017 8:12	0.724	3.7	0.7	623

Note: Yellow highlighted rows correspond to rain events for which flow data was not collected while blue highlighted rows correspond to event for which the flow data was used to determine infiltration rates.

Table 41: Water balance data for the Grove St System

Event #	$V_{tot,in}$ (ft^3)	$V_{tot,out}$ (ft^3)	$V_{sys,in}$ (ft^3)	$V_{sys,out}$ (ft^3)	V_{inf} (ft^3)	% Infiltrated of $V_{tot,in}$	% Infiltrated of $V_{sys,in}$
1	4123	3631	1021	529	492	12%	48%
2	2053	1480	734	161	573	28%	78%
3	44	41	3	0	3	7%	100%
4	12	0	12	0	12	100%	100%
5	132	120	12	0	12	9%	100%
6	5	0	5	0	5	100%	100%
7	10	0	10	0	10	100%	100%
8	4	0	4	0	4	100%	100%
9	28	17	11	0	11	41%	100%
10	3	0	3	0	3	100%	100%
11	1136	817	377	58	319	28%	85%
12	324	126	260	62	198	61%	76%
13	8	0	8	0	8	100%	100%
14	5	0	5	0	5	100%	100%
15	2303	1316	1308	321	987	43%	75%
16	7	0	7	0	7	100%	100%

17	9	0	9	0	9	100%	100%
18	13	3	10	0	10	80%	100%
19	0	0	0	0	0	0%	0%
20	0	0	0	0	0	0%	0%
21	0	0	0	0	0	0%	0%
22	3	0	3	0	3	100%	100%
23	1	0	1	0	1	100%	100%
24	0	0	0	0	0	100%	100%
25	0	0	0	0	0	100%	100%
26	3	0	3	0	3	100%	100%
27	9494	7200	4550	2257	2294	24%	50%
28	13	0	12	0	12	99%	100%
29	5081	3378	2056	352	1703	34%	83%
30	14	0	14	0	14	100%	100%
31	20	0	20	0	20	100%	100%
32	153	113	40	0	40	26%	100%
33	15	1	14	0	14	92%	100%
34	2815	1584	1347	115	1231	44%	91%
35	43	34	10	0	10	23%	100%
36	101	62	39	0	39	38%	100%
37	7	0	7	0	7	100%	100%
38	4	0	4	0	4	100%	100%
39	569	493	76	0	76	49%	100%
40	5296	2927	3118	749	2369	47%	76%
41	4	1	2	0	2	67%	100%
42	99	97	3	0	3	12%	100%
43	19	16	3	0	3	17%	100%
44	23	16	7	0	7	30%	100%
45	12	8	4	0	4	31%	100%
46	4	2	2	0	2	49%	100%
47	776	714	62	0	62	8%	100%
48	22	15	7	0	7	33%	100%
49	126	84	42	0	42	33%	100%
50	11	3	8	0	8	72%	100%
51	1349	401	985	36	949	70%	96%
52	2231	1472	1008	249	759	63%	74%
53	48	29	19	0	19	39%	100%
54	7402	3364	4539	501	4038	68%	89%
55	5	0	5	0	5	98%	100%
56	8	0	8	0	8	100%	100%
57	30	6	24	0	24	79%	100%
58	3539	994	2612	67	2545	90%	97%
59	93	0	93	0	93	100%	100%
60	52	0	52	0	52	100%	100%
61	10	0	10	0	10	97%	100%
62	67	52	16	0	16	23%	100%
63	26	17	10	0	10	16%	100%
64	16	0	16	0	16	97%	100%
65	48	0	48	0	48	89%	100%

66	38	9	29	0	29	76%	100%
67	57	46	11	0	11	19%	100%
68	0	0	0	0	0	0%	0%
69	0	0	0	0	0	0%	0%
70	0	0	0	0	0	0%	0%
71	0	0	0	0	0	0%	0%
72	0	0	0	0	0	0%	0%
73	0	0	0	0	0	0%	0%
74	0	0	0	0	0	0%	0%
75	3824	959	2997	132	2865	75%	96%
76	2673	968	2226	520	1705	64%	77%
77	3858	0	4762	905	3858	100%	81%
78	1705	153	1551	0	1551	91%	100%
79	183	0	183	0	183	100%	100%
80	150	67	83	0	83	55%	100%
81	0	0	0	0	0	0%	0%
82	0	0	0	0	0	0%	0%
83	0	0	0	0	0	0%	0%
84	0	0	0	0	0	0%	0%
85	0	0	0	0	0	0%	0%
86	0	0	0	0	0	0%	0%
87	0	0	0	0	0	0%	0%
88	91	69	23	0	23	25%	100%
89	6560	2502	4513	456	4057	62%	90%
90	2146	0	2204	58	2146	100%	97%
91	5098	1524	3881	307	3574	70%	92%
92	8389	3336	5411	359	5053	77%	93%
93	16739	10490	7908	1658	6250	51%	79%
94	65	0	65	0	65	100%	100%
95	58	0	58	0	58	100%	100%
96	78	0	78	0	78	57%	100%
97	56	0	56	0	56	31%	100%
98	121	73	47	0	47	22%	100%
99	393	215	177	0	177	27%	100%
100	6271	3624	2772	125	2647	35%	94%
101	11	0	11	0	11	100%	100%
102	167	159	8	0	8	5%	100%
103	2730	1219	1560	49	1511	67%	97%
104	71	17	54	0	54	76%	100%
105	4057	1975	2269	188	2082	55%	91%
106	34	0	34	0	34	100%	100%
107	46	6	40	0	40	87%	100%
108	35	0	35	0	35	100%	100%
109	8364	4130	4777	542	4234	54%	88%
110	79	41	38	0	38	48%	100%
111	131	109	22	0	22	17%	100%
112	101	34	68	0	68	67%	100%
113	7255	4943	3265	953	2312	32%	71%
114	34	2	32	0	32	95%	100%

115	17	0	17	0	17	100%	100%
116	389	0	433	44	389	100%	90%
117	0	0	0	0	0	0%	0%
118	0	0	0	0	0	0%	0%
119	0	0	0	0	0	0%	0%
120	0	0	0	0	0	0%	0%
121	0	0	0	0	0	0%	0%
122	0	0	0	0	0	0%	0%
123	0	0	0	0	0	0%	0%
124	0	0	0	0	0	0%	0%
125	0	0	0	0	0	0%	0%
126	0	0	0	0	0	15%	100%
127	828	591	257	19	238	45%	92%
128	0	0	0	0	0	100%	100%
129	2	1	1	0	1	44%	100%
130	1177	768	552	143	409	39%	74%
131	5	4	2	0	2	31%	100%
132	1167	948	240	22	218	42%	91%
133	1294	943	685	335	351	34%	52%
134	524	412	111	0	111	43%	100%

Note: Yellow highlighted rows correspond to rain events for which flow data was not collected while blue highlighted rows correspond to event for which the flow data was used to determine infiltration rates.

Table 42: Peak flow and peak flow reductions for the Grove St SGF

Event #	Maximum System Flows (cfm)			Maximum Total Flows (cfm)		
	Inflow	Outflow	% Reduction	Inflow	Outflow	% Reduction
1	59.98	41.60	31%	133.65	115.26	14%
2	21.29	8.71	59%	30.52	17.95	41%
3	0.00	0.00		0.16	0.16	3%
4	0.01	0.00	100%	0.17	0.16	5%
5	0.04	0.00	100%	0.57	0.55	2%
6	0.01	0.00	100%	0.12	0.11	6%
7	0.01	0.00	100%	0.03	0.02	22%
8	0.01	0.00	100%	0.01	0.00	100%
9	0.11	0.00	100%	0.14	0.13	4%
10	0.00	0.00		0.00	0.00	
11	11.99	3.67	69%	17.24	8.92	48%
12	19.09	7.69	60%	24.64	13.24	46%
13	0.02	0.00	100%	0.02	0.00	100%
14	0.01	0.00	100%	0.01	0.00	100%
15	53.58	34.95	35%	81.82	64.44	21%
16	0.07	0.00	100%	0.07	0.00	100%
17	0.05	0.00	100%	0.05	0.00	100%
18	0.07	0.00	100%	0.30	0.26	14%

19	0.00	0.00		0.00	0.00	
20	0.00	0.00		0.00	0.00	
21	0.00	0.00		0.00	0.00	
22	0.01	0.00	100%	0.01	0.00	100%
23	0.00	0.00		0.00	0.00	
24	0.00	0.00		0.00	0.00	
25	0.00	0.00		0.00	0.00	
26	0.02	0.00	100%	0.02	0.00	100%
27	82.30	59.06	28%	126.42	107.70	15%
28	0.01	0.00	100%	0.02	0.01	59%
29	12.28	3.47	72%	16.88	10.75	36%
30	0.01	0.00	100%	0.03	0.02	35%
31	0.01	0.00	100%	0.06	0.05	19%
32	0.23	0.00	100%	0.73	0.67	8%
33	0.03	0.00	100%	0.05	0.03	50%
34	8.69	2.18	75%	10.48	4.66	56%
35	0.11	0.00	100%	0.37	0.35	6%
36	3.23	0.00	100%	3.34	0.88	74%
37	0.01	0.00	100%	0.01	0.00	100%
38	0.01	0.00	100%	0.01	0.00	100%
39	0.74	0.00	100%	1.43	1.20	16%
40	10.85	3.29	70%	13.14	9.15	30%
41	0.00	0.00		0.16	0.16	1%
42	0.00	0.00		0.30	0.29	1%
43	0.00	0.00		0.28	0.28	1%
44	0.02	0.00	100%	0.43	0.42	2%
45	0.00	0.00		0.16	0.15	3%
46	0.00	0.00		0.14	0.13	2%
47	0.16	0.00	100%	2.40	2.24	7%
48	0.01	0.00	100%	0.11	0.10	7%
49	1.52	0.00	100%	1.78	0.34	81%
50	0.01	0.00	100%	0.09	0.09	4%
51	3.60	0.66	82%	4.71	1.85	61%
52	8.92	4.73	47%	9.29	5.11	45%
53	0.03	0.00	100%	0.62	0.60	2%
54	6.54	2.66	59%	8.32	5.10	39%
55	0.01	0.00	100%	0.02	0.02	28%
56	0.01	0.00	100%	0.01	0.00	80%
57	0.29	0.00	100%	0.36	0.13	66%
58	8.54	0.77	91%	8.84	2.11	76%
59	1.32	0.00	100%	1.55	0.38	75%
60	0.38	0.00	100%	0.74	0.50	33%
61	0.01	0.00	100%	0.36	0.35	3%
62	0.02	0.00	100%	0.23	0.22	8%
63	0.01	0.00	100%	0.08	0.07	11%
64	0.05	0.00	100%	0.19	0.14	27%
65	0.10	0.00	100%	0.62	0.54	14%
66	0.07	0.00	100%	0.19	0.17	11%
67	0.01	0.00	100%	0.21	0.20	4%

68	0.00	0.00		0.00	0.00	
69	0.00	0.00		0.00	0.00	
70	0.00	0.00		0.00	0.00	
71	0.00	0.00		0.00	0.00	
72	0.00	0.00		0.00	0.00	
73	0.00	0.00		0.00	0.00	
74	0.00	0.00		0.00	0.00	
75	3.68	0.66	82%	5.30	2.37	55%
76	5.92	2.20	63%	7.97	4.51	43%
77	27.87	12.77	54%	51.74	36.93	29%
78	2.66	0.00	100%	3.46	0.80	77%
79	1.42	0.00	100%	1.98	1.09	45%
80	0.05	0.00	100%	0.40	0.37	7%
81	0.00	0.00		0.00	0.00	
82	0.00	0.00		0.00	0.00	
83	0.00	0.00		0.00	0.00	
84	0.00	0.00		0.00	0.00	
85	0.00	0.00		0.00	0.00	
86	0.00	0.00		0.00	0.00	
87	0.00	0.00		0.00	0.00	
88	0.04	0.00	100%	0.27	0.24	12%
89	7.35	2.08	72%	8.70	3.80	56%
90	11.04	6.74	39%	8.99	8.48	6%
91	5.23	1.65	69%	7.64	4.15	46%
92	8.21	1.31	84%	12.29	6.18	50%
93	25.69	12.55	51%	54.66	44.20	19%
94	0.13	0.00	100%	1.54	1.41	8%
95	0.04	0.00	100%	0.37	0.33	10%
96	0.30	0.00	100%	0.83	0.53	36%
97	0.03	0.00	100%	0.30	0.27	8%
98	0.03	0.00	100%	0.35	0.33	7%
99	0.42	0.00	100%	0.98	0.80	19%
100	4.70	1.23	74%	7.23	4.15	43%
101	0.01	0.00	100%	0.22	0.21	4%
102	0.01	0.00	100%	0.40	0.39	2%
103	8.84	1.32	85%	9.81	3.96	60%
104	0.10	0.00	100%	0.70	0.66	7%
105	9.96	2.41	76%	11.29	4.18	63%
106	0.04	0.00	100%	0.26	0.23	12%
107	0.03	0.00	100%	0.08	0.05	33%
108	0.02	0.00	100%	0.15	0.13	15%
109	10.20	2.66	74%	14.55	6.67	54%
110	0.02	0.00	100%	0.26	0.24	9%
111	0.04	0.00	100%	0.53	0.50	6%
112	0.05	0.00	100%	0.71	0.68	5%
113	13.63	8.79	36%	22.46	17.65	21%
114	0.02	0.00	100%	0.14	0.12	12%
115	0.02	0.00	100%	0.22	0.21	7%
116	12.06	7.39	39%	23.08	18.52	20%

117	0.00	0.00		0.00	0.00	
118	0.00	0.00		0.00	0.00	
119	0.00	0.00		0.00	0.00	
120	0.00	0.00		0.00	0.00	
121	0.00	0.00		0.00	0.00	
122	0.00	0.00		0.00	0.00	
123	0.00	0.00		0.00	0.00	
124	0.00	0.00		0.00	0.00	
125	0.00	0.00		0.00	0.00	
126	0.00	0.00		0.01	0.01	8%
127	9.32	2.16	77%	9.03	2.67	70%
128	0.00	0.00		0.03	0.03	2%
129	0.01	0.00	100%	0.02	0.02	7%
130	25.79	11.71	55%	35.70	21.62	39%
131	0.00	0.00		0.03	0.03	4%
132	10.56	1.93	82%	14.45	5.71	61%
133	52.85	31.74	40%	96.68	75.57	22%
134	2.18	0.00	100%	3.65	2.30	37%

Note: Yellow highlighted rows correspond to rain events for which flow data was not collected while blue highlighted rows correspond to event for which the flow data was used to determine infiltration rates.